

# **ICESA 2017**

2017 Tokyo International Conference on  
Engineering, Science, and Applications

<http://icesa2017.globalconf.org>

## **Conference Organizers**

Global Academic-Industrial Cooperation Society

## **Proceedings Editors**

Ta-Wei Hung, Shih Chien University  
Chian-Son Yu, Shih Chien University

Toshi Center Hotel, Tokyo, Japan  
16-18, August, 2017

Proceedings of the International Conference on Engineering, Science and Applications,  
ISSN 2521-3814, Vol.1, No.1, August 2017  
Published by Global Academic-Industrial Cooperation Society

# Table of Contents

Message from the ICESA Conference Chair .....	4
<b>Strain induced bandgap-engineering of Silicon clathrates: Towards a direct bandgap silicon for future solar cells.</b>	
Nassim Ahmed Mahammedi, Marhoun Ferhat, Toyohiro Chikyow.....	1
<b>Joint Estimation of CFO and Channel in Multi-Antenna OFDM-based Two-Way Relaying Communications</b>	
Yi-Ru Lin, Tsui-Tsai Lin.....	2
<b>Novel Blind Image Watermarking via Exploitation of Interval Location Block with Support Vector Regression and Just-noticeable Difference</b>	
Ling-Yuan Hsu, Hwai-Tsu Hu, Hsien-Hsin Chou .....	4
<b>Harmonics Mitigation in Grid-Connected Wind–Photovoltaic Hybrid Generation System</b>	
Maged N. F. Nashed, Mona Eskander .....	17
<b>Upconversion Emission of Tm<sup>3+</sup> / Yb<sup>3+</sup> co-doped Na<sub>0.5</sub>Gd<sub>0.5</sub>MoO<sub>4</sub> Phosphor for Optical Devices</b>	
Yu Jin Lee, Joo Hyun Lee, Hyun Kyoung Yang .....	29
<b>Synthesis of Sr<sub>2</sub>SiO<sub>4</sub>:Eu<sup>2+</sup> Phosphor via Microwave-assisted Sintering</b>	
Woo Cheol Lee, Ju Young Mun, Hyun Kyoung Yang .....	30
<b>Facile Synthesis of Graphene Quantum Dots Derived from Vinegar</b>	
Woo Tae Hong, Sung Jae Lee, Sung Jun Park, Jin Young Park, Hyun Kyoung Yang.....	31
<b>The Use of Virtual Reality Technology to Enhance E-learning</b>	
Mak Kai-Long.....	32
<b>Effect of Time-Dependent Extraction Flow Rates on a Radially Convergent Fingering flow</b>	
Chih-Ang Chung, Jui-Hsiang Chiu.....	42
<b>Decellularized Porcine Corneal Scaffold for Cultivating Fibroblasts and Corneal Endothelial Cells in Vitro</b>	
Hung-Jun Lin, Ling-Chi Hsiao, Ping-Lun Jiang, Yun-An Chen, Chun-Han Lin, Yi-You Huang, Der-Zen Liu.....	44
<b>Design principles for stiffness adjustment in soft material robotics using layer jamming</b>	
Sebastian Blankemeyer, Jenna Losensky, Jan Peters, Annika Raatz .....	45
<b>Creation of Web Learning Environment Intended to Learning Motivation on Mechanical Design</b>	
Yuya Nakamura, Tsutomu Sekine, Atsushi Okuyama .....	63

<b>Economical Interpretation of Volume Flexibility in Production Systems</b> Maurice Schmidt, Peter Nyhuis .....	72
<b>Production and Characterization of Biodegradable Plastic from Nigeria Cassava Starch</b> Elizabeth J. Eterigho, T. S. Farrow, Ejejigbe Silver E, Ene C. Onaivi .....	84
<b>Isolation and Identification of Jellyfish Alkaloid (<i>Bougainvillia</i> sp) As Immunostimulan to Protein Profile and Histopathology of Tiger Grouper Liver (<i>Epinephelus fuscoguttatus</i>)</b> Sri Andayani, M.Fadjar, M.Farid Rahman.....	91
<b>Bacteria Amount, Protease Enzyme Activity, and Protein Energy Retention of Catfish (<i>Clarias Gariepinus</i>) on Red Water System in Different Density</b> Mohamad Fadjar, Arning W. Ekawaty, Dhiannita Siskharini, Sherly S.T. Merdekawati, Arif Udin	96
<b>Simulation Research on Speed Control of Permanent Magnet Direct-driven System for Mining Scraper Conveyor</b> En Lu, Wei Li, Xuefeng Yang.....	103
<b>Position Sensorless Control for Short Range Cutting Interior Permanent Magnet Synchronous Motor of Shearer Based on a New Sliding Mode Observer</b> Lianchao Sheng, Wei Li.....	104
<b>Stepwise Regression Model and Prediction of Retardance in Citric Acid Coated Ferrofluids</b> Jing-Fung Lin, Xin-Rong Qiu.....	105
<b>A Design of Inter-vehicle Communication System Using Software-defined Radio</b> Wen-Tzu Chen, Jen-Yu Wu.....	118
<b>Energy Planning Framework Based on a Multi-objective Optimization Approach for University Campus Buildings</b> Aumnad Phdungsilp.....	119
<b>A Novel Q-Learning Approach for Early-Termination Algorithm for HEVC Coding Unit Partition</b> Yih-Chuan Lin, Yi-Sheng Lin.....	129
<b>Development of surface assembly of Immunostimulatory Gelatin Nanoparticle Carriers for Mucosal Antigen Delivery</b> Shen-Fu Lin, Jeng-Shiang Tsai, I-Hsiu Liu, Yun-Huan Liu, Shyr-Yi Lin, Der-Zen Liu .....	130
<b>The Synthesis of Sex Steroid Hormones Is Dysregulated in the Placenta of Preeclampsia Women</b> Min Jae Kim, Ye Young Shin, Mee-Na Park, Jae-Eon Lee, Beum-Soo An.....	131
<b>Hospital Wastewater Treatment Using Aerated Fixed Film Biofilter (AF2B)</b> Prayitno, Hadi Saroso, Sri Rulianah, Hardjono .....	132

**Auranofin, a Thioredoxin Reductase Inhibitor, Induces ER stress and PI3K/Akt pathways-mediated Apoptosis in Human Breast Carcinoma Cells**

Hyun HwangBo, Jin Woo Jeong, Cheol Park, Su Hyun Hong, Jae-Hun Cheong, Yung Hyun Choi  
139

**Baicalein Protects the Schwannoma Cells against Hydrogen Peroxide-induced Cellular Damage and Apoptosis via Activation of the Nrf2 Signaling Pathway**

Eun Ok Choi, Jin-Woo Jeong, Cheol Park, Su Hyun Hong, Hye-Jin Hwang, Yung Hyun Choi.. 140

**Electrochemistry Evaluation of Ferrocene in Organic Solvents for High-performance Non-aqueous Organic Redox Flow Electrolyte**

Yongbeom Kim, Joonhyeon Jeon ..... 141

**Greenhouse Monitoring system using Arduino Yún and Blynk Framework**

Meena Momand, Chika Yoshida..... 143

**Study on New Control System Design of Pv Cell Emulating System in the Stand Alone Mode**

Kirian Guiller, Vu Minh Phap, N. Yamamura, M. Ishida, J. Hirai..... 153

**The Viscoelastic Behavior of Alginate Hydrogels for Cartilage applications**

Hussein Mishbak, Dhurgham A. Kadhim, Roberto Donno, Paulo Bartolo ..... 162

**Heat Conduction Analysis of Wall Materials**

Sirikul Siriteerakul, Teera Siriteerakul..... 171

**Text Localization based on Multiple Features and Recognition Techniques**

Teera Siriteerakul, Sirikul Siriteerakul..... 183

**The Shift in Generations of Computing Platforms and the Impact on Information Technology Solutions**

Mehdi Asgarkhani, Eduardo Correia, Bernard Otinpong ..... 188

**Co-doping Effect on Structural, Morphological and Optical Properties of ZnO Thin Films**

Ahmed Maache, Mokhtar Boudissa..... 198

**Spatial Relationship Between Hydro-oceanography Parameters and Phytoplankton Potentially Habs in Bali Strait**

Endang Yuli Herawati, Mohammad Mahmudi, Fani Fariedah, Ruly Isfatul Khasanah ..... 208

## **Message from the ICESA Conference Chair**

On behalf of the Organizing Committee, I would like to take this opportunity to welcome all attendees and participants to the 2017 International Joint Conference held in Tokyo, Japan on August 16-18, 2017. The 2017 International Joint Conference is a prestigious gathering of researchers to share and strengthen interdisciplinary research. Therefore, the conference offers a great opportunity for all people present here to share new findings and research results as well as to seek collaborative research opportunities across disciplines. This year the International Joint Conference includes the International Conference on Education and Learning (ICEL), the International Conference on Engineering, Science, and Applications (ICESA), the International Conference on Hospitality, Tourism, and Sports Management (HTSM), and the International Conference on Business, Internet, and Social Media (BISM).

The total number of paper submissions is 416 from 45 countries, with an acceptance rate of approximately 75.72%, and around 85.08% of the accepted papers have been registered. About 70% of registrants have completed the payment processes, which yields 182 papers to be presented in 37 parallel sessions and three poster sessions. There are about 200 delegates from 43 countries participating in this event. We welcome delegates from Bangladesh, Brazil, Canada, China, Ecuador, Ghana, Hong Kong, India, Indonesia, Iran, Iraq, Israel, Ivory Coast, Japan, Korea, Kuwait, Lesotho, Malaysia, Mexico, Mongolia, Mozambique, Netherlands, New Zealand, Nigeria, Pakistan, Poland, Palestine, Romania, Russia, Rwanda, Saudi Arabia, Singapore, South Africa, Spain, Sri Lanka, Swaziland, Taiwan, Thailand, Turkey, Tuvalu, Uganda, United Kingdom, and USA.

This year ICESA received 64 submissions with an acceptance rate of about 69%. 37 of the accepted papers have been registered and 23 were arranged into the session program. The successful organization of such an international conference fully depends on the integrated effort of many volunteers. Therefore, I would like to thank all researchers who submitted their manuscripts and will participate in the conference, and to all the reviewers for their great and timely assistance and support. Thanks also go to the Conference Co-Chairs, Local Committee Chair, Program Chair, and International Committee Members for their full support and great enthusiasm to make such a large-scale international conference possible. I would also like to thank the secretaries and staff of the Organizing Committee and Local staff for their hard work and indispensable contributions to the conference.

Finally, I hope this conference will be a successful and memorable conference, and will be fruitful to all participants both academically and socially. I hope you will all enjoy the conference and your stay in Tokyo.

Professor Kassem Saleh  
Conference Chair of ICESA 2017  
August 16, 2017

## Strain induced bandgap-engineering of silicon clathrates: Towards a direct bandgap silicon for future solar cells.

Nassim Ahmed MAHAMMEDI <sup>a, b</sup>, Marhoun FERHAT <sup>b, c</sup> Toyohiro CHIKYOW <sup>d</sup>

<sup>a</sup>Laboratoire de physique des matériaux LPM, Amar Têlidji University of Laghouat, BP37G, Laghouat 03000, ALGERIA.

<sup>b</sup>Semiconductors and Functional Materials Laboratory SFML, Amar Têlidji University of Laghouat, BP37G, Laghouat 03000, ALGERIA.

<sup>c</sup>Department of physics, The University of the West Indies, Mona, Kingston 07, JAMAICA.

<sup>d</sup>National Institute for Materials Science (WPI-MANA), 1-1 Namiki, Tsukuba, Ibaraki, 305-0044, JAPAN

\*Corresponding Author: n.mahammedi@lagh-univ.dz

### Abstract

Through first-principles calculations, and by means of tensile and compressive biaxial strain through lattice mismatch technique, we have successfully engineered the bandgap of two types of guest-free silicon clathrates Si<sub>46</sub> in the type-I and type-VIII systems. Initial equilibrium lattice parameters for type-I and type-VIII Si<sub>46</sub> are obtained after structural optimization as  $a=10.22$  Å and  $10.12$  Å respectively. The electronic structures and densities of states DOS were computed by means of GGA-PBE approximation in the frame of the DFT as implemented in the CASTEP package. At zero pressure fundamental bandgaps by GGA-PBE are 1.364 eV (1.359 eV) for type-I (type-VIII) Si<sub>46</sub>. Under tensile strains of +2% and +4%, type-I and type-VIII clathrates become respectively direct-bandgap semiconductors, with optimal magnitudes within the visible range of the electromagnetic spectrum. Such findings play in the favor of further exploration and exploitation of silicon clathrates (that could be integrated in silicon based industries) to design thin film silicon based photovoltaic and photonic devices with higher efficiencies.

### Keywords

Silicon, Clathrates, Bandgap engineering, Biaxial strain, Direct bandgap.

## Joint Estimation of CFO and Channel in Multi-Antenna OFDM-based Two-Way Relaying Communications

Yi-Ru Lin and Tsui-Tsai Lin\*

Department of Electronics Engineering, National United University,  
No. 2, Lien-Da Rd., Miaoli, Taiwan, R.O.C.

\*Corresponding Author: [ttlincs@nuu.edu.tw](mailto:ttlincs@nuu.edu.tw)

### ABSTRACT

Nowadays, wireless multimedia service is growing rapidly, and thus the applicable radio frequency spectrum becomes especially valuable. A particularly important issue is to find the solution for effective promotion of spectrum efficiency as well as link quality. The multiple-input multiple-output (MIMO) technique not only improves the link quality but also increases the system capacity by exploiting the spatial resource without sacrificing the transmission bandwidth. However, the implementation of MIMO is inevitably limited by the equipment size and hardware cost of the end-user. Recently, the cooperative relay network has been proposed to substitute for the MIMO technique. It can be regarded as a distributed virtual multi-antenna transmission system, which utilizes diversity/relay transmission without using additional antennas at the receiver end while providing a performance similar to that of a MIMO system. Among the protocols, single-antenna one-way relaying orthogonal frequency division multiplexing (OFDM) has gained much more increasing attentions recently when incorporated with space time block coding. However, one-way relay network using half-duplex communications gives rise to spectrum inefficiency due to requirement of orthogonal channel for relay transmission. As a remedy, half-duplex two-way relay (TWR) protocol has been developed. Specifically, in the half-duplex TWR network, as shown in Fig. 1, two terminal nodes transmit the information signals simultaneously to the relay in the first time slot, and then the multi-antenna relay broadcasts the pre-processed data to two terminals in the second time slot. Study on multi-antenna relaying processing and the carrier frequency offset (CFO) effect on the performance of the TWR system has not been found in the literature so far. To deal with this problem, in this paper, we revisit the low-complexity multi-antenna relaying scheme, and try to design an efficient receiver for a high spectrum-efficient TWR OFDM-based system. The contributions of this paper provide two major objectives as follow: (1) A novel multi-antenna relaying scheme, as shown in Fig. 2, is designed for the TWR communications. (2) To alleviate the performance degradation introduced by CFO, joint estimation of CFO and channel estimation is proposed. Simulation results, as shown in Fig. 3, show that the expected advantage and confirm the efficacy of the proposed scheme.

**Keyword:** Two-way relay (TWR), orthogonal frequency division multiplexing (OFDM), multi-antenna relaying, carrier frequency offset (CFO), CFO and channel estimation.

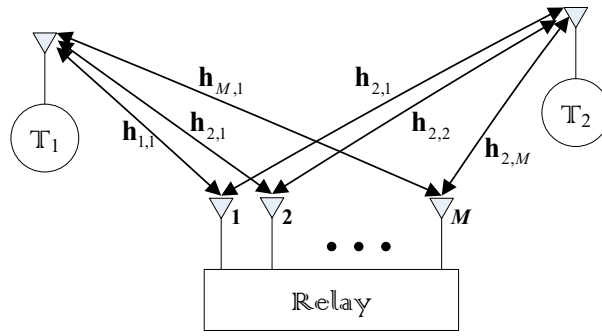


Fig. 1. Schematic diagram of the multi-antenna relaying scheme.

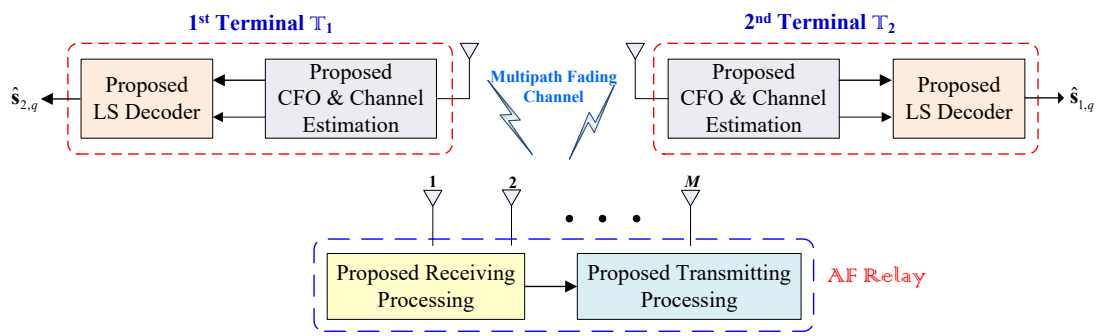


Fig. 2 Schematic diagram of the proposed TWR communication network.

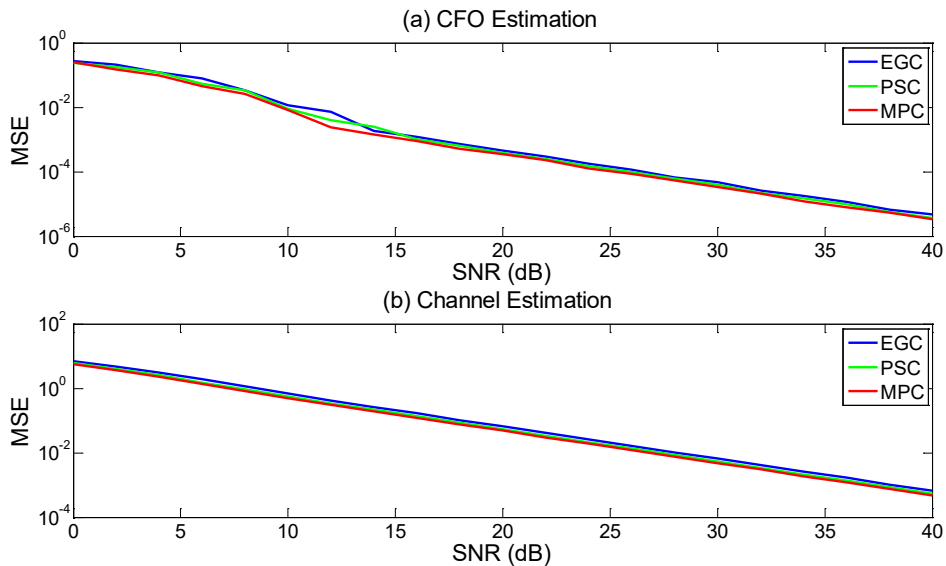


Fig. 3 Mean square error (MSE) performance of the proposed joint CFO and channel estimation. Number of antennas: 3. EGC: Equal gain combining; PSC: Power selection combining; MPC: Maximum power combining.



## Novel blind image watermarking via exploitation of interval location block with support vector regression and just-noticeable difference

Ling-Yuan Hsu<sup>a\*</sup>, Hwai-Tsu Hu<sup>b</sup> and Hsien-Hsin Chou<sup>b</sup>

<sup>a</sup> Department of Information Management, St. Mary's Junior College of Medicine,  
Nursing and Management,  
I-Lan, Taiwan

<sup>b</sup> Department of Electronic Engineering, National I-Lan University  
I-Lan Taiwan

\*Corresponding Author: [hsulingyuan@gmail.com](mailto:hsulingyuan@gmail.com)

### ABSTRACT

This study incorporates support vector regression (SVR) and the just-noticeable difference (JND) model within a scheme based on the lock-wise discrete cosine transform (DCT) to ensure robustness and imperceptibility without sacrificing sufficient payload capacity. Reference to particular DCT coefficients over a  $5 \times 5$  grid of blocks makes it possible for SVR to render a suitable prediction of a designated vector norm selected from specified coefficients in the central block. Watermarking is essentially a process of adjusting the relationship between the intended coefficients and their SVR predictions, in accordance with the norm-based JND. Experiment results demonstrate the robustness of visible watermarks embedded using the proposed algorithm against a range of attacks, particularly JPEG and JPEG2000 compression attacks. The proposed method exhibits robustness and imperceptibility superior to those of three other schemes that utilize inter-block correlation.

**Keyword:** blind image watermarking, discrete cosine transform, support vector regression, just-noticeable difference

### 1. Introduction

Digital watermarking, as a means of hiding data, has attracted considerable attention due to its widespread applicability in authentication, copyright protection, and secret communication. All digital image watermarking techniques must satisfy five requirements: imperceptibility, non-detectability, security, robustness, and capacity. In developing a watermarking method, there is a trade-off between imperceptibility and robustness. It is desirable to embed messages of appropriate length, thereby ensuring the imperceptibility of the embedded watermark without sacrificing robustness against common attacks.

In (Wang & Pearmain, 2004), Wang and Pearmain proposed a data hiding technique that self-references specific coefficients in the DCT domain. They divide the host image

into blocks of  $8 \times 8$  pixels, each of which is converted to a DCT representation. The DC coefficients are formulated in a  $3 \times 3$  grid of DCT blocks to render an estimate of an AC coefficient in the central block. The magnitude of the corresponding AC coefficient is adaptively increased or decreased according to whether the watermark bit is a '0' or '1' based on relative modulation (RM). The use of adaptive AC coefficient prediction for blind image watermarking can also be found in (Veerawamy & Kumar, 2008). This type of reference scheme is efficient; however, it tends to lower the image quality due to inaccuracies in estimation. In (Das, Panigrahi, Sharma, & Mahapatra, 2014), Das et al. explored the correlation between DCT coefficients drawn from adjacent DCT blocks. They selected a pair of DCT coefficients from two neighboring blocks and adjusted one coefficient according to these other. This approach improves imperceptibility due to the fact that the DCT coefficients are modified only slightly; however, the resulting watermark is unable to withstand strong attacks.

In this study, we used support vector regression (SVR) to exploit coefficient correlations to facilitate the description of binary information according to distinct criteria. SVR is a popular tool for problems of regression. The fact that it has a sparse representation of solutions means it is relatively fast in training/testing. The basic architecture of an SVR involves hyperplanes passing through normal vectors and biases. Assigning the SVR a set of training data makes it possible to tune the biases and normal vectors in order to attain the optimal match between inputs and desired outputs. This study is based on the assumption that SVR could be used to search for suitable relationships among DCT coefficients in different locations for use in formulating watermarks. Many perceptual properties can be explored in the DCT domain; therefore, we adopted a just-noticeable difference (JND) model to act as a guide in image watermarking. The JND model removes redundancies associated with statistical correlation while maintaining the perceptual quality of the resulting watermarked images (Chou & Li, 1995).

## 2. Relevant Works

In this study, we employed three techniques to serve as the basis for the development of a watermarking scheme.

### 1.1 Discrete cosine transform (DCT)

Discrete cosine transform (DCT) is a technique used to convert image pixels into elementary frequency components. DCT-based techniques are generally implemented using spatially local with a block size of  $8 \times 8$ . The DCT block represents an image as the sum of sinusoids of various magnitudes and frequencies (Lam & Goodman, 2000).

## 1.2 Support vector regression (SVR)

Support vector regression (SVR) is one of the fundamental techniques used with support vector machines (SVMs). SVR uses a learning algorithm to enable the recognition of fine patterns within complex data sets. SVR algorithms use examples to perform discriminative classification learning in order to predict the classifications of previously unseen data. Given training data  $\{(x_1, y_1), (x_2, y_2), \dots, (x_l, y_l)\} \subset \mathbf{R}^d \times \mathbf{R}$ , the goal of  $\varepsilon$ -SVR (Vapnik, 1995) is to find function  $f(x)$  that deviates no more than  $\varepsilon$  from the obtained targets  $y_i$  in all training data, while remaining as flat as possible (Chang & Lin, 2011). The case of linear functions  $f(x)$ , taking the form as follows:

$$f(x) = \langle w, x \rangle + b, \quad \text{with } w \in \mathbf{R}^d, b \in \mathbf{R} \quad (1)$$

where  $\langle \cdot, \cdot \rangle$  denotes the dot product in  $\mathbf{R}^d$ . One way to ensure this is to minimize the norm; i.e.,  $\|w\|^2 = \langle w, w \rangle$ . The constraints for violating the tube constraint from above and below can thus be formulated as follows:

$$\begin{aligned} & \text{minimize} \quad \frac{1}{2} \|w\|^2 + a \sum_{i=1}^l (\zeta_i^+ + \zeta_i^-) \\ & \text{subject to} \quad \begin{cases} y_i - (\langle w, x_i \rangle + b) \leq \varepsilon + \zeta_i^+ \\ (\langle w, x_i \rangle + b) - y_i \leq \varepsilon + \zeta_i^- \end{cases} \end{aligned} \quad (2)$$

where  $a$  is positive constant value that determines the degree of penalized loss.  $\zeta_i^+$  and  $\zeta_i^-$  ( $\zeta_i^+ \geq 0$ ,  $\zeta_i^- \geq 0$ ) are slack variables that specify the upper and the lower training errors subject to error tolerance. The Lagrangian and dual maximization problem are expressed as follows:

$$\begin{aligned} & \text{maximize}_{\alpha^+, \alpha^-} \quad -\frac{1}{2} \sum_{i,k} \{(\alpha_i^+ - \alpha_i^-)(\alpha_k^+ - \alpha_k^-)K(x_i, x_k)\} \\ & \quad \quad \quad - \varepsilon \sum_i (\alpha_i^+ + \alpha_i^-) + \sum_i y_i (\alpha_i^+ - \alpha_i^-) \\ & \text{subject to} \quad \begin{cases} \sum_i (\alpha_i^+ - \alpha_i^-) = 0 \\ 0 \leq \alpha_i^+, \alpha_i^- \leq a \end{cases} \end{aligned} \quad (3)$$

where  $K$  represents a kernel function.

## 1.3 Robust perceptual just-noticeable difference (JND)

Within the framework of watermarking, JND refers to the minimum perceptible visibility threshold incorporating the spatial contrast sensitivity function (CSF), the contrast masking effect, and the luminance adaptation effect; however, it remains

invariant with watermark embedding. JND is deduced from the psychophysical and physiological characteristics of the human visual system (HVS)(Bae & Kim, 2014; Bae & M., 2013).

The JND in the location of the  $(i, j)$ -th DCT coefficient in  $(x, y)$  block is expressed as  $J_{x,y}^{i,j}$ , which is a product function of base threshold  $J_{base}^{i,j}$  and two modulation

factors (i.e.,  $\hat{M}_{x,y}^{i,j}$  and  $\tilde{M}_{x,y}^{i,j}$ ).  $J_{base}^{i,j}$  is a base threshold for the spatial CSF effect.

$\hat{M}_{x,y}^{i,j}$  is the luminance adaptation modulation factor used to elevate  $J_{base}^{i,j}$  in accordance with local pixel intensity.  $\tilde{M}_{x,y}^{i,j}$  is a contrast masking modulation factor

used to boost  $J_{base}^{i,j}$  based on the complexity of the local spatial texture. The robust perceptual JND model (Wan, Liu, Sun, & Gao, 2015) is expressed as follows:

$$J_{x,y}^{i,j} = \tau \cdot N \cdot J_{base}^{i,j} \cdot \hat{M}_{x,y}^{i,j} \cdot \tilde{M}_{x,y}^{i,j} \quad (4)$$

where  $\tau$  is used to account for the summation effect of individual JND thresholds over a spatial neighborhood for the visual system with a recommended value of 0.14.

$N$  indicates the value of DCT (i.e.,  $N = 8$ )(Bae & M., 2013).  $J_{base}^{i,j}$  can be given by considering the oblique effect as follows:

$$J_{base}^{i,j} = (J_d(\omega^{i,j}) - J_v(\omega^{i,j})) \cdot \sin(\psi^{i,j})^2 + J_v(\omega^{i,j}) \quad (5)$$

where  $J_d(\omega^{i,j})$  and  $J_v(\omega^{i,j})$  are the diagonal and vertical directions of  $8 \times 8$  DCT basis functions,  $\omega^{i,j}$  indicates the cycles per degree (cpd), and  $\psi^{i,j}$  represents the directional angle of the corresponding DCT component. An improved luminance adaptation modulation factor  $M_{LA}^{i,j}$  employing the cycles per degree  $\omega^{i,j}$  as well as

the average intensity of the block  $\mu_p$  (Wan et al., 2015), can be represented as follows:

$$M_{LA}^{i,j} = \begin{cases} 1 + (M_{0.1}(\omega^{i,j}) - 1) \cdot \left| \frac{(\mu_p / 255) - 0.3}{0.2} \right|^{0.8}, & \text{if } \frac{\mu_p}{255} \leq 0.3 \\ 1 + (M_{0.9}(\omega^{i,j}) - 1) \cdot \left| \frac{(\mu_p / 255) - 0.3}{0.6} \right|^{0.6}, & \text{if } \frac{\mu_p}{255} > 0.3 \end{cases} \quad (6)$$

where  $M_{0.1}(\omega^{i,j})$  and  $M_{0.9}(\omega^{i,j})$  are the quadratic polynomial functions empirically set as using (Bae & M., 2013). The improved contrast-masking modulation factor  $M_{CM}^{i,j}$

based on the cycles per degree  $\omega^{i,j}$  and the edge pixel density  $\mu_e$  for texture complexities is given by the following:

$$M_{CM}^{i,j} = \begin{cases} 1 + (g_{0.15}(\omega^{i,j}) - 1)(\mu_e / 0.15), & \text{if } 0 \leq \mu_e < 0.15 \\ g_{0.15}(\omega^{i,j}), & \text{if } 0.15 \leq \mu_e < 0.2 \\ g_{0.15}(\omega^{i,j}) + (g_{0.2}(\omega^{i,j}) - g_{0.15}(\omega^{i,j}))(\mu_e - 0.2) / 0.1, & \text{if } 0.2 \leq \mu_e \end{cases} \quad (7)$$

where  $g_{0.15}(\omega^{i,j})$  and  $g_{0.2}(\omega^{i,j})$  are modeled in a gamma pdf form and expressed as (Bae & M., 2013).

### 3. Proposed blind watermarking scheme

The blind watermarking scheme presented in this paper exploits interval location blocks with support vector regression in the DCT domain (wmSVR). The relationships among DCT coefficients in neighboring blocks can be explored using the SVR prediction model. We obtain the vector norm of the DCT coefficient  $\varphi_{x',y'}$ 's as the input of the SVR prediction model from the twelve blocks in a  $5 \times 5$  grid, where

$(x', y') \in \left\{ \begin{array}{l} (x-1, y-2), (x+1, y-2), (x-2, y-1), (x, y-1), \\ (x+2, y-1), (x-1, y), (x+1, y), (x-2, y+1), \\ (x, y+1), (x+2, y+1), (x-1, y+2), (x+1, y+2) \end{array} \right\}$ . The vector norm  $\varphi_{x',y'}$  as follows:

$$\varphi_{x',y'} = \begin{cases} \sqrt{(C_{x',y'}^{2,1})^2 + (C_{x',y'}^{1,1})^2 + (C_{x',y'}^{1,2})^2}, & \text{if } (x' + y') \% 2 = 0, \\ \sqrt{(C_{x',y'}^{2,0})^2 + (C_{x',y'}^{2,2})^2 + (C_{x',y'}^{0,2})^2}, & \text{if } (x' + y') \% 2 = 1 \end{cases} \quad (8)$$

where % represents the modulus operator. Selecting two groups (i.e.,  $C_{x',y'}^{2,1}, C_{x',y'}^{1,1}, C_{x',y'}^{1,2}$

and  $C_{x',y'}^{2,0}, C_{x',y'}^{2,2}, C_{x',y'}^{0,2}$ ) makes available mutually different coefficients by which to

prevent interference. Two approaches to the selection of the two groups are as follows: reducing volatility on a single coefficient, and balancing high and low frequencies with frequencies in the vertical and horizontal directions.

Within the central block (in which the targeted coefficients are located), we add vector norm  $\varphi_{x,y}$  of the intra-block coefficients as an input of SVR prediction model. This

results in a total of twelve input vector norms  $\varphi_{x',y'}$  being fed into the SVR prediction model. The SVR prediction model is used to estimate the absolute value of vector norm

$\varphi_{x,y}$ , specified AC coefficients chosen from  $\left\{ C_{x,y}^{i',j'} \mid (i', j') \in \{(2,1), (1,1), (1,2)\} \right\}$  (for

$((x+y)\%2) = 0$ ) and  $\left\{ C_{x,y}^{i',j'} \mid (i', j') \in \{(2,0), (2,2), (0,2)\} \right\}$  (for  $((x+y)\%2) = 1$ ). When

obtaining these 12 vector norms from a  $5 \times 5$  grid of blocks, the DCT coefficients situated outside the border of the block array are assumed to be equal to those in the nearest block. In other words, we expand the block array by replicating the exterior blocks around the border.

The SVR prediction model must be created in the training stage before SVR can be used to estimate the absolute value of vector norm  $\varphi_{x,y}$ . We use k-means clustering

to reduce the amount of training data that is required. k-means clustering is a method of vector quantization in which the the data set is a vector. In the proposed method, the

12 vector norms  $\varphi_{x',y'}$  (where  $(x',y') \in \left\{ \begin{array}{l} (x-1,y-2), (x+1,y-2), (x-2,y-1), (x,y-1), \\ (x+2,y-1), (x-1,y), (x+1,y), (x-2,y+1), \\ (x,y+1), (x+2,y+1), (x-1,y+2), (x+1,y+2) \end{array} \right\}$ ) and a

vector norm  $\varphi_{x,y}$  are combined into a vector. The k-means clustering algorithm

partitions all vector norms in the DCT of the training images into 1024 clusters, in which each vector norm belongs to the cluster with the nearest mean. The 1024 center points (or vectors) then serve as delegates of these clusters, such that the SVR algorithm can be used to train the SVR prediction model. We then exploit the inequality relationship between the actual and predicted variables to enable the embedding and extraction of watermarks. After using the SVR prediction model to obtain an estimated absolute vector norm value of  $\varphi_{x,y}$ , termed  $\bar{\varphi}_{x,y}$ , its value is adjusted using Eq. (9)

to ensure that it is greater than zero.

$$\bar{\varphi}_{x,y} = \max(\bar{\varphi}_{x,y}, \delta) \quad (9)$$

where  $\delta$  is the minimum clearance distance between  $\bar{\varphi}_{x,y}$  and zero.

The procedural flow of the proposed watermarking scheme is presented in Figure 1, in which mixed modulation (MM) is used for binary embedding presented by Hu and Hsu (Hu & Hsu, 2016). Two vector values are respectively calculated using RM and QIM in MM. The MM can take merits of QIM to remedy the shortage of RM in imperceptibility but still partly holds the advantage of RM in robustness. One vector value of MM is  $\phi_1$  using RM, which can be expressed in mathematic form as follows:

$$\phi_1 = \begin{cases} \max\{\bar{\varphi}_{x,y} - \lambda, \min\{\varphi_{x,y}, \bar{\varphi}_{x,y} - g\}\}, & \text{if } w_{x,y} = 0; \\ \min\{\bar{\varphi}_{x,y} + \lambda, \max\{\varphi_{x,y}, \bar{\varphi}_{x,y} + g\}\}, & \text{if } w_{x,y} = 1. \end{cases} \quad (10)$$

$$g = \max\{\xi, \beta\sigma_{x,y}\}, \quad (11)$$

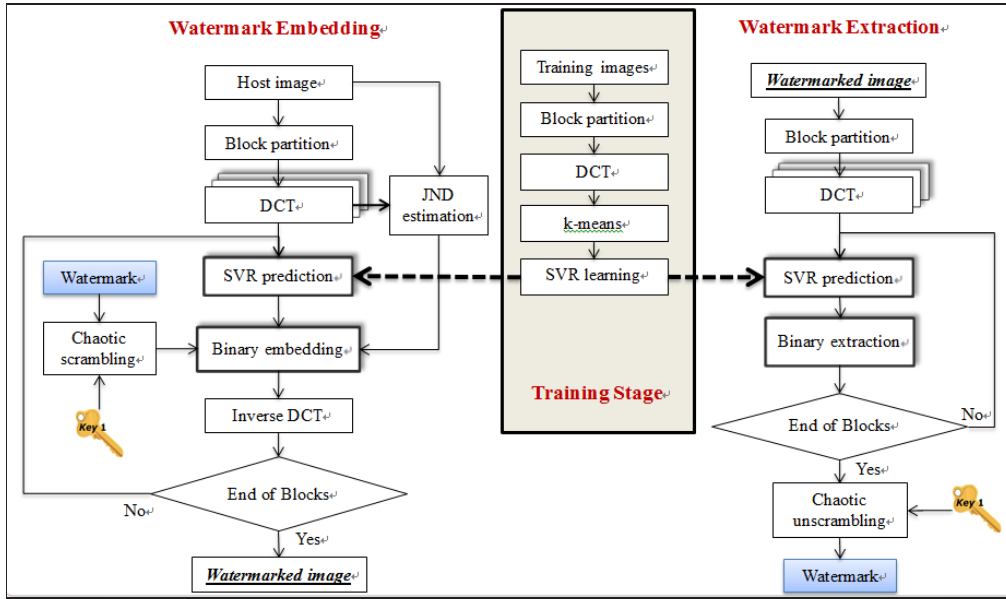


Figure 1. Embedding and extraction procedures of proposed watermarking scheme.

where  $\xi$  is set to  $0.55\Delta$  and  $\Delta$  is the quantization step. Symbol  $\beta$  denotes the adjustment factor for the embedding strength.  $\sigma_{x,y}$  is the norm-based JND estimated using the following formulae:

$$\sigma_{x,y} = \begin{cases} \sqrt{(\bar{J}_{x,y}^{2,1})^2 + (\bar{J}_{x,y}^{1,1})^2 + (\bar{J}_{x,y}^{1,2})^2}, & \text{if } (x+y) \% 2 = 0 \\ \sqrt{(\bar{J}_{x,y}^{2,0})^2 + (\bar{J}_{x,y}^{2,2})^2 + (\bar{J}_{x,y}^{0,2})^2}, & \text{if } (x+y) \% 2 = 1 \end{cases} \quad (12)$$

$$\bar{J}_{x,y}^{i,j} = \alpha \cdot q^{i,j} \cdot \hat{M}_{x,y}^{i,j} \cdot \tilde{M}_{x,y}^{i,j} \quad (13)$$

where  $\bar{J}_{x,y}^{i,j}$  is the JND value used in this paper and  $\alpha$  represents the adjustment factor for the embedding strength of relative modulation.  $\hat{M}_{x,y}^{i,j}$  is the modulation factor for luminance adaptation and  $\tilde{M}_{x,y}^{i,j}$  is the modulation factor for contrast masking.

$\hat{M}_{x,y}^{i,j}$  and  $\tilde{M}_{x,y}^{i,j}$  are the same as (Bae & M., 2013).  $q^{i,j}$  denotes the  $(i, j)$ -th value of the luminance quantization table.

And the other value of MM is  $\phi_2$ . Let  $d = \varphi_{x,y} - \bar{\varphi}_{x,y}$  denote the gap between  $\varphi_{x,y}$  and  $\bar{\varphi}_{x,y}$ . QIM is used to modulate the selected DCT coefficients as  $\phi_2$ . The entire formulation consists of three branches, which are expressed as a program equation in Figure 2.

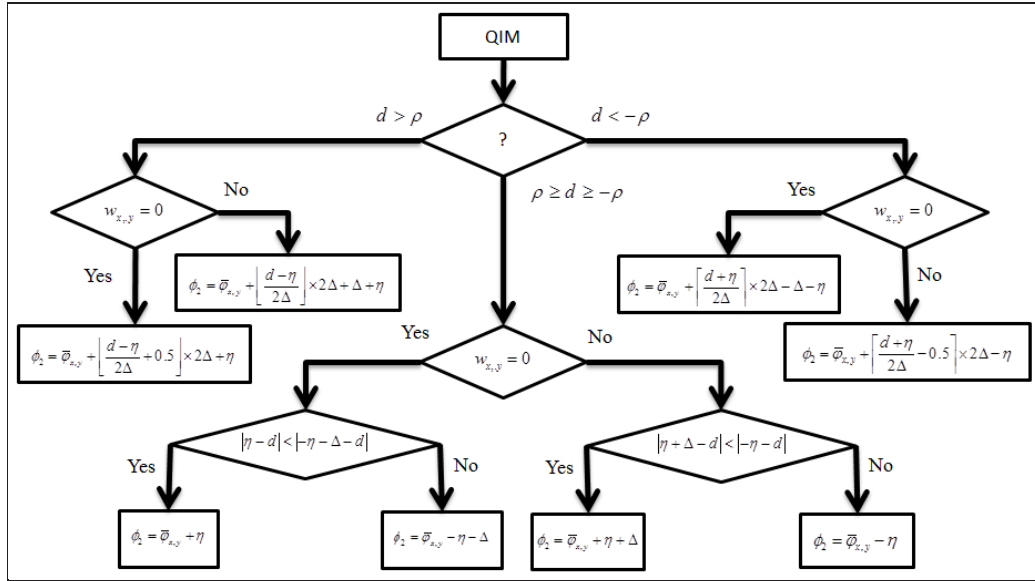


Figure 2. Embedding and extraction procedures in proposed watermarking scheme

Either  $\phi_1$  or  $\phi_2$  is negative. Equation (14) is used to modify it.

$$\bar{\phi} = \begin{cases} \phi, & \text{if } \phi \geq 0; \\ \phi + \xi, & \text{if } \phi < 0 \text{ and } w_{x,y} = 1; \\ \max(0, \phi - \xi), & \text{otherwise;} \end{cases} \quad (14)$$

Once  $\bar{\phi}_1$  and  $\bar{\phi}_2$  are both available, we must determine which one results in less alteration to the image.

$$\hat{\phi}_{x,y} = \begin{cases} \bar{\phi}_1, & \text{if } |\varphi_{x,y} - \bar{\phi}_1| < |\varphi_{x,y} - \bar{\phi}_2|; \\ \bar{\phi}_2, & \text{otherwise.} \end{cases} \quad (15)$$

The final step involves converting the estimated vector norm to specified AC coefficients. The alteration in magnitude subsequently reflects on the DCT coefficient via

$$\tilde{C}_{x,y}^{i',j'} = C_{x,y}^{i',j'} \times \sqrt{\frac{(\hat{\phi}_{x,y})^2}{\sum (C_{x,y}^{i',j'})^2}} \quad (16)$$

where  $(i', j') \in \{(2,1), (1,1), (1,2)\}$  when  $((x+y)\%2) = 0$ , and  $(i', j') \in \{(2,0), (2,2), (0,2)\}$  when  $((x+y)\%2) = 1$ .

In extracting the embedded watermark, we repeat the steps of block partition, DCT conversion, and vector norm estimation. We determine the watermark bit in each block based on the gap between the actual and estimated vector norms, respectively termed



$\varphi_{x,y}^{1,1}$  and  $\tilde{\varphi}_{x,y}^{1,1}$ , which are obtained from the watermarked image. Let  $d' = \varphi_{x,y}^{1,1} - \tilde{\varphi}_{x,y}^{1,1}$ .

We apply the RM rule when  $|d'| \leq \rho$  and otherwise the MM rule, as follows:

If  $d' > \rho$

$$\tilde{w}_{x,y} = \left\lfloor \frac{d' - \eta}{\Delta} + 0.5 \right\rfloor \% 2 \quad (17)$$

elseif  $d' < -\rho$

$$\tilde{w}_{x,y} = \left\lfloor \frac{d' + \eta}{\Delta} - 0.5 - 1 \right\rfloor \% 2 \quad (18)$$

elseif  $|d'| \leq \rho$

$$\tilde{w}_{x,y} = \begin{cases} 1, & \text{if } \varphi_{x,y}^{1,1} > \tilde{\varphi}_{x,y}^{1,1} \\ 0, & \text{otherwise.} \end{cases} \quad (19)$$

end

#### 4. Performance evaluation

A set of experiments was conducted to evaluate the performance of the proposed watermarking scheme. Test materials included 512×512 8-bit grayscale images obtained from image databases: “Jetplane”, “Lake”, “Lena”, “Livingroom”, “Mandrill”, “Peppers”, “Pirate”, and “Walkbridge” (Gonzalez, Woods, & Eddins), as shown in Figure 2. As a watermark, we used a binary image logo (64×64 px) in which the numbers of “1s” and “0s” were deliberately arranged to be equal. We also adopted the following parameters:  $\alpha = 0.68$ ,  $\beta = 0.50$ ,  $\delta = 16$  and  $\Delta = 34$ .

The metrics used to evaluate image distortion introduced by watermark casting included peak signal-to-noise ratio (PSNR) and bit error rate (BER). The definitions of PSNR and BER are given in (Hsu & Hu, 2015). The image attacks addressed in this study are listed in Table I.

Experiments aimed at determining robustness were conducted using three schemes: self-reference (SR) proposed by Wang and Pearmain (Wang & Pearmain, 2004), inter-block coefficient correlation (IBCC) proposed by Das et al. (Das et al., 2014) and a scheme based on Chinese remainder theorem (CRT) proposed by Patra et al. (Patra, Phua, & Bornand, 2010). We selected these three methods because they represent attempts to exploit correlation across blocks of DCT. Table 3 presents the average and standard deviation of PSNRs obtained from the eight images using the four schemes. The PSNR values obtained from the proposed wmSVR scheme are relatively high and the image quality after embedding appears more consistent.

TABLE I. TYPES OF ATTACK CONSIDERED IN THIS STUDY

a1	Apply JPEG compression to the image with the quality factor (QF) with 80 and 20.
a2	apply JPEG2000 compression to the image with the compression ratio (CR) with 2 and 8.
a3	Gaussian noise (0.001): add 0.001% Gaussian noise to the image.
a4	S&P noise (1%): add 1% salt-and-pepper noise to the image.
a5	Speckle noise (1%): add 1% speckle noise to the image.
a6	Median filter (3×3): apply a 3×3 median filter to the image.
a7	Gaussian low-pass filter (3×3): apply a 3×3 Gaussian low-pass filter to the image.
a8	Adaptive wiener filter (3×3): apply a 3×3 2-D adaptive noise-removal filter to the image.
a9	Scaling correction (25%): shrink the image from 512×512 to 256×256 pixels and then enlarge it back to 512×512 pixels.
a10	Rotation correction: rotate the image counterclockwise by and then back to the original direction
a11	Cropping I (25%): remove 25% of the image on the left side.
a12	Cropping II (25%): remove 25% of the image on the top left corner.
a13	Brighten (+20): add 20 to each pixel value of the image.
a14	Darken (-20): subtract 20 from each pixel value of the image.

Figure 3. Test images ( $512 \times 512$ ) obtained from image database (Gonzalez et al.):

From top left to bottom right are “Jetplane”, “Lake”, “Lena”, “Livingroom”, “Mandrill”, “Peppers”, “Pirate”, and “Walkbridge”.

In Table II, we assess the degree of distortion imposed by these four schemes, based on the measured PSNR from eight test images. As shown in Table II, wmSVR achieved image quality superior to that of the other three schemes. Furthermore, the PSNR values obtained after embedding watermark using wmSVR are more consistent. Table III presents the average BERs obtained from the four schemes addressed in this

comparison. As shown in Table III, all four of the schemes enable the extraction of watermarks without error. Furthermore, all four schemes were able to withstand a number of attacks, such as JPEG compression with QF equal to 80 (a1/QF80), JPEG2000 compression with CR equal to 2 (a2/CR2), Gaussian lowpass filter (a7) and luminance adjustment (a13 and a14). In this comparison, the proposed wmSVR achieved BER values below those of the other schemes. As shown in Table III, it is clear that the proposed wmSVR scheme is also able to render lucid watermarks (i.e., BER under 5%) even after undergoing attacks based on JPEG compression (a1), JPEG2000 compression (a2), Gaussian noise (a3), Gaussian low-pass filter (a7), scaling correction (a9), brightening (a13) and darkening (a14). CRT was also able to restore a good watermark; however, IBCC and SR suffered obvious deterioration. As mentioned in the previous section, the proposed scheme did not perform particularly well in a4, a5, or a10; however, it should be noted that the other three schemes did not perform well under these three types of attacks either. As for cropping attacks (i.e., a9 and a10), the results are based solely on guesswork; therefore, these results are inconsequential. Overall, we can conclude from the above discussion that the proposed wmSVR scheme outperforms the other watermarking schemes with regard to robustness against most attacks.

TABLE II. PSNR VALUES DERIVED FROM FOUR WATERMARKING SCHEMES

	CRT	IBCC	SR	wmSVR
mean	37.70	35.51	36.07	38.18
± standard deviation	0.17	0.65	1.24	0.38

TABLE III. AVERAGE BER VALUES FOR FOUR SCHEMES COMPARED IN THIS STUDY (IN PERCENTAGE)

Attack types	CRT	IBCC	SR	wmSVR
none	0.00	0.00	0.00	0.00
a1/QF20	34.43	23.86	32.37	1.62
a1/QF80	3.98	0.11	0.07	0.01
a2/CR2	3.43	0.11	0.06	0.01
a2/CR8	26.23	9.00	15.02	2.91
a3	20.03	10.51	11.87	4.91
a4	16.16	17.44	11.40	13.71
a5	24.94	18.30	19.41	16.26
a6	38.00	14.44	16.20	9.72

a7	21.61	1.75	2.37	0.08
a8	37.71	11.55	14.18	5.42
a9	33.67	10.00	11.64	4.97
a10	41.62	20.01	18.35	15.37
a11	12.48	12.38	12.42	12.83
a12	12.74	12.17	12.87	13.00
a13	17.85	0.22	0.24	0.11
a14	18.27	0.56	0.72	0.44

## 5. Conclusions

This paper presents a novel approach to the blind watermarking of images by combining the benefits of DCT, SVR, and JND. SVR is used to explore interval location block coefficient correlation in the DCT domain. Watermarks are adapted to the image based on the characteristics of JND of the HVS, to ensure that the watermark remains imperceptible without sacrificing resistance to attack. Experiment results demonstrate the stability and efficiency of the proposed wmSVR when used to draw a connection between coefficients interval located in blocks. Our results demonstrate that the proposed watermarking scheme provides excellent protection against a variety of attacks.

## Acknowledgment

This research work was supported by the Ministry of Science and Technology, Taiwan, ROC under Grants MOST 105-2221-E-562-003 and MOST 105-2221-E-197-020.

## References

- Bae, S. H., & Kim, M. 2014. A novel generalized DCT-based JND profile based on an elaborate CM-JND model for variable block-sized transforms in monochrome images. *IEEE Trans Image Process*, 23(8): 3227-3240.
- Bae, S. H., & M., K. 2013. A Novel DCT-Based JND Model for Luminance Adaptation Effect in DCT Frequency. *IEEE Signal Processing Letters*, 20(9): 893-896.
- Chang, C.-C., & Lin, C.-J. 2011. LIBSVM: A library for support vector machines. *ACM Trans. Intell. Syst. Technol.*, 2(3): 1-27.
- Chou, C. H., & Li, Y. C. 1995. A perceptually tuned subband image coder based on the measure of just-noticeable-distortion profile. *IEEE Trans. Circuits and Systems for Video Technology*, 5(6): 467-476.

- Das, C., Panigrahi, S., Sharma, V. K., & Mahapatra, K. K. 2014. A novel blind robust image watermarking in DCT domain using inter-block coefficient correlation. *AEU - International Journal of Electronics and Communications*, 68(3): 244-253.
- Gonzalez, Woods, & Eddins. Image Databases.
- Hsu, L.-Y., & Hu, H.-T. 2015. Blind image watermarking via exploitation of inter-block prediction and visibility threshold in DCT domain. *Journal of Visual Communication and Image Representation*, 32: 130-143.
- Hu, H.-T., & Hsu, L.-Y. 2016. A mixed modulation scheme for blind image watermarking. *AEU - International Journal of Electronics and Communications*, 70(2): 172-178.
- Lam, E. Y., & Goodman, J. W. 2000. A mathematical analysis of the DCT coefficient distributions for images. *IEEE Trans. Image Processing*, 9(10): 1661-1666.
- Patra, J. C., Phua, J. E., & Bornand, C. 2010. A novel DCT domain CRT-based watermarking scheme for image authentication surviving JPEG compression. *Digital Signal Processing*, 20(6): 1597-1611.
- Vapnik, V. N. 1995. *The nature of statistical learning theory*: Springer-Verlag New York, Inc.
- Veeraswamy, K., & Kumar, S. S. 2008. Adaptive AC-coefficient prediction for image compression and blind watermarking. *Journal of Multimedia*, 3(1): 16-22.
- Wan, W., Liu, J., Sun, J., & Gao, D. 2015. Improved logarithmic spread transform dither modulation using a robust perceptual model. *Multimedia Tools and Applications*: 1-22.
- Wang, Y., & Pearmain, A. 2004. Blind image data hiding based on self reference. *Pattern Recognition Letters*, 25(15): 1681-1689.

# Harmonics Mitigation in Grid-Connected Wind-Photovoltaic Hybrid Generation System

Maged N. F. Nashed<sup>a</sup> and Mona Eskander<sup>b\*</sup>

Electronics Research Institute,

Cairo, Egypt

\*Corresponding Author: eskander@eri.sci.eg

## ABSTRACT

Hybrid PV-wind generation systems have increased significantly due to the rapid improvement in power electronics techniques. In this paper, three switching techniques for mitigating the output harmonics of a PV-wind hybrid generation system are investigated. The proposed hybrid system consists of a PV panel connected to the grid via a DC/DC converter and a 3 phase two-level inverter. The wind generator is a DFIG, its stator connected to the grid through a 3-phase transformer, while its rotor is connected to the grid via two converters. The paper investigates the performance of PV system with two types of dc-dc converters interfacing the PV panel to the grid inverter, and the harmonics injected to the grid when using three types of switching techniques for the inverter interfacing the hybrid system to the grid. Comparing the THD of the two dc-dc converters' output voltage and of grid voltage and current at the point of common connection for each type of inverter switching technique is presented for high insolation level and wide range of wind speeds.

**Keyword:** Wind, PV, harmonics, DFIG, two level inverter.

## 1. Introduction

Electricity generation by photovoltaic (PV) or wind power (WP) has received considerable attention worldwide due to their advantages of being abundant in nature and nearly non-pollutant. Hybrid PV-wind generation systems have increased significantly due to the rapid improvement in power electronics techniques. Wind power is one of the most promising clean energy sources since it can be easily captured by wind generators with high power capacity. Photovoltaic (PV) power is another promising clean energy source since it is global and can be harnessed without using rotational generators. An important issue to be considered with grid-connected renewable energy generation is how to smooth power fluctuations and reduce current harmonics injected in the power grid. The application of an energy storage system such as battery or ultra-capacitor, have been proposed to reduce power fluctuations (Mendis and et 2014, Jayasinghe and et 2011, Khayyer and aaozguner, 2014). When using energy storage devices to control PV and wind power fluctuations, there is a trade-off

between battery effort and the degree of smoothness. That is, if one is willing to accept a less smooth output, the battery can be spared some effort. However, adding storage devices adds to the system cost and affects its reliability. Other harmonics mitigation techniques include active filters or Facts devices, such as STATCOM (Salmeron and et 2011, Badrzadeh and Gupta 2013). These devices add to the cost and complexity of control.

In this paper, switching techniques for decreasing the output harmonics of a PV-wind hybrid generation system are investigated. Also, the performance of the PV generation system with two types of dc-dc converters interfacing the PV panel to the grid-connected inverter is studied. The PV system consists of a PV panel connected to the grid via a DC/DC converter and an inverter. The wind generator is a DFIG, its stator connected to the grid through a 3-phase transformer, while its rotor is connected to the grid via two converters. The paper investigates the harmonics injected to the grid when different switching techniques are applied to the inverter interfacing the hybrid system to the grid. The compared switching techniques are; the offset addition carrier-based PWM (OAPWM), the flat top carrier-based PWM (FTPWM), and the space vector modulation (SVM) technique. These investigations are done for  $1000\text{w/m}^2$  insolation level and wide wind speed range (from sub- to super-synchronous speed). The proposed system, shown in Fig. (1), is modeled using practical data for the PV panel and the wind generator, given in the appendix. Simulation results are presented and conclusions, concerning the type of the dc-dc converter and the switching technique giving the better power quality, are drawn.

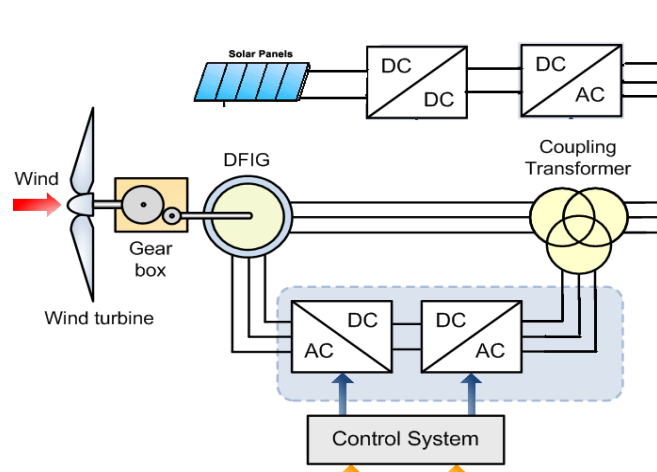


Fig. (1) The proposed grid-connected hybrid PV-Wind generation system.

## 2. System Description

### 2.1 PV generation System

The PV panel (its parameters given in (Nashed and Edwar 2015)) is connected to the grid via two types of converters as shown in Fig. (1). The dc-dc converter is either a

buck-boost or a Cuk converter, while the ac inverter is a 3 phase 2-level voltage source inverter. The buck-boost converter is characterized by:

- Pulsed input current, requires input filter.
- Pulsed output current increases output voltage ripple
- Inefficient use of input source

While the Cuk converter is characterized by:

- Continuous input and output current
- efficient use of input source
- bi-directional converter

The PV system is modeled using Matlab/Simulink and the voltage and current harmonics injected to the grid inverter at 1000w/m<sup>2</sup> insolation level when using a Buck-Boost converter are shown in Figure (2). The voltage THD is 10.66%, and the current THD is 15.32%.

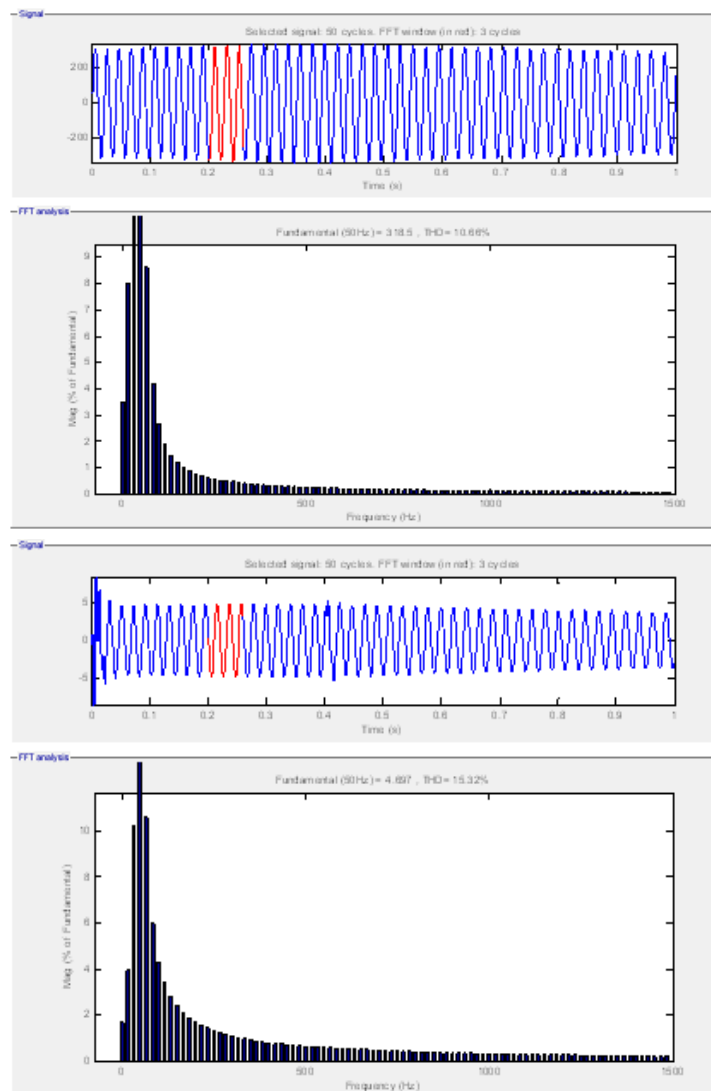


Fig. (2) THD for grid voltage and current with Buck-Boost Converter at insolation 1000 w/m.<sup>2</sup>



Then the PV system is modeled using a Cuk converter, and the voltage and current harmonics injected to the grid inverter are shown in Figure (3). The voltage THD decreased to 9.85%, and the current THD decreased to 10.66%. However it should be noted that the Buck-Boost converter has lower price, so a trade-off is to be done, since the decrease in harmonics content is moderate.

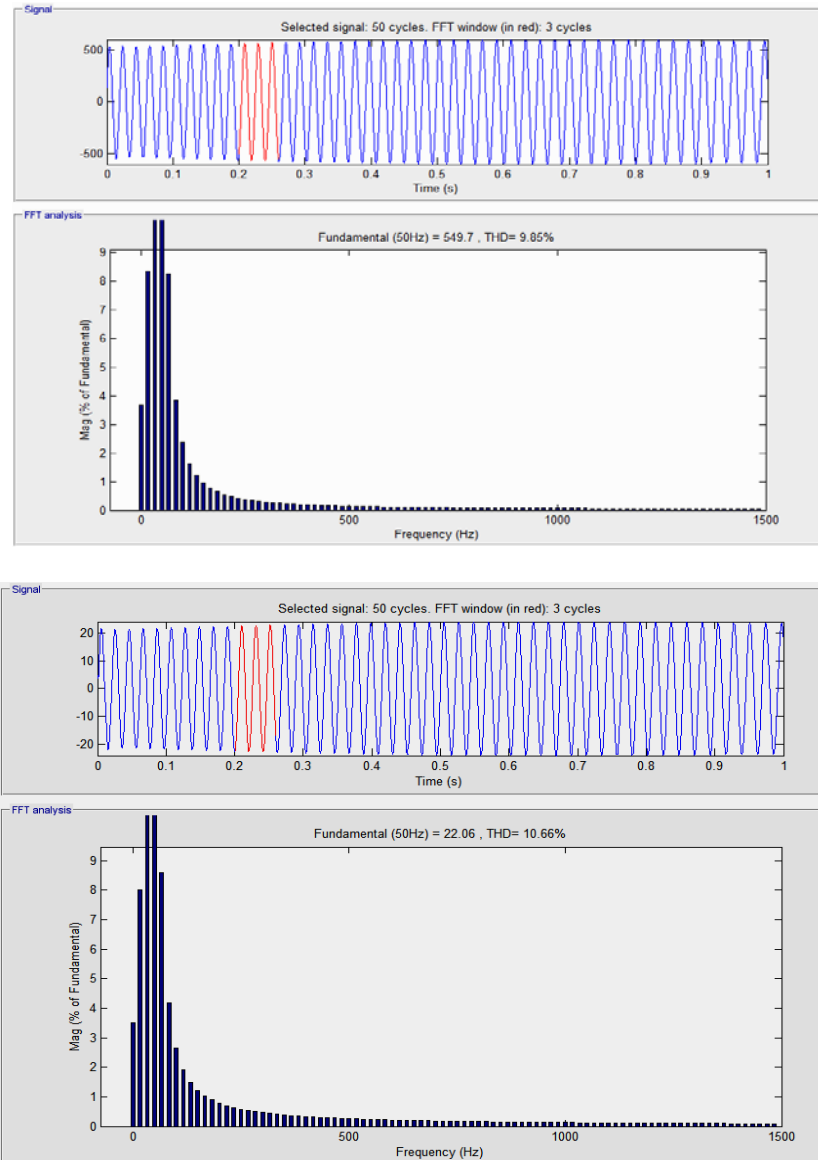


Fig. (3) THD for grid voltage and current with Cuk Converter at insolation 1000 w/m<sup>2</sup>

### 2.2 The wind energy generation system

A double-fed induction generator (DFIG) is employed in the wind energy conversion system due to its known merits as a commercial system. The rotor is connected to the grid via two controlled converters, the rotor side converter (RSC) and the grid side converter (GSC). Both converters can be operated as rectifier or inverter according to

the DFIG speed. Within the sub-synchronous speed range, the GSC operates as a rectifier and RSC operates as an inverter to supply the rotor with voltage at slip frequency. Within the super-synchronous speed range, the GSC operates as an inverter and RSC operates as rectifier to supply the grid with voltage at grid frequency. At synchronous speed the rotor circuit is supplied with DC current to operate as a synchronous generator. The generated harmonics are investigated from sub- to super-synchronous. Harmonics are investigated when applying three switching technique to the grid-connected converter. These are the Offset Addition carrier-based PWM (OAPWM), the Flat Top carrier-based PWM (FTPWM), and the Space Vector PWM (SVPWM) technique.

### 2.2.1 DFIG converter with OAPWM technique

The OAPWM is also called 60° PWM. The idea behind the 60° PWM technique is to “flat top” the waveform from 60° to 120° and 240° to 300°. The switching devices are held on for one third of the cycle (when full voltage) leading to reduced switching losses. All triple harmonics are absent in the three phase voltage. The 60° PWM

creates a larger fundamentals  $(2/\sqrt{3})$  and utilizes more of the available dc voltage (phase voltage  $V_{ph} = 0.57735V_{dc}$  and line voltage  $V_L = V_{dc}$ ) than does the sinusoidal PWM (Rashid 2004, Deethi and Saxena 2011, Mishra and Ramachandran 2011).

Fig. (4) a and b display grid current and its harmonic spectrum at wind speed 7 m/sec. (sub-synchronous speed), and 12 m/sec. (super-synchronous speed) respectively. Fig. (5) shows the grid voltage and its harmonic spectrum at 12 m/sec. wind speed.

### 2.2.2 DFIG converter with Carrier-based PWM with Offset Addition

The output voltage magnitude from a three-phase voltage source inverter can be enhanced by adding an offset to the sinusoidal modulating signal. The offset addition PWM scheme follows the same principle as that of the third-harmonic injection, reducing the peak of the modulating signal and hence increasing the modulation index, as presented in Fig. (5), (Salmern and et 2011). The offset is given as

$$\text{offset} = -\frac{\max\{V_a^*, V_b^*, V_c^*\} + \min\{V_a^*, V_b^*, V_c^*\}}{2}$$

Fig. (6) a and b display grid current and its harmonic spectrum at 7 m/sec, and 12 m/sec wind speed respectively. Also, Fig. (7) shows grid voltage and its harmonic spectrum at wind speed 12 m/sec.

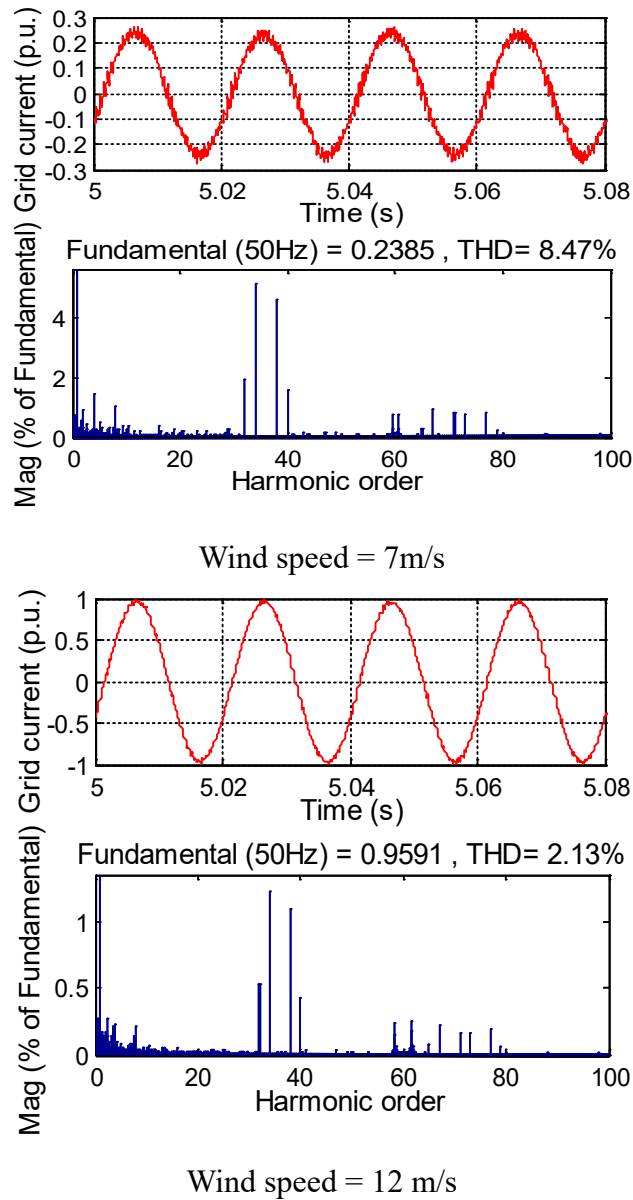


Fig. (4) Grid current and its harmonic spectrum for two-level FTPWM converter.

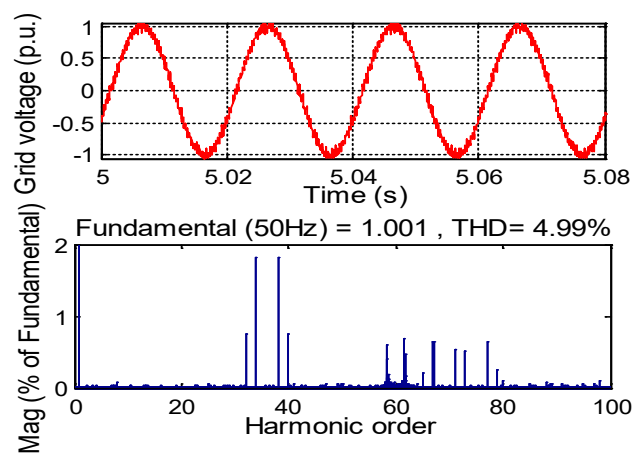


Fig. (5) Grid voltage and its harmonic spectrum for two-level FTPWM at wind speed 12 m/s.

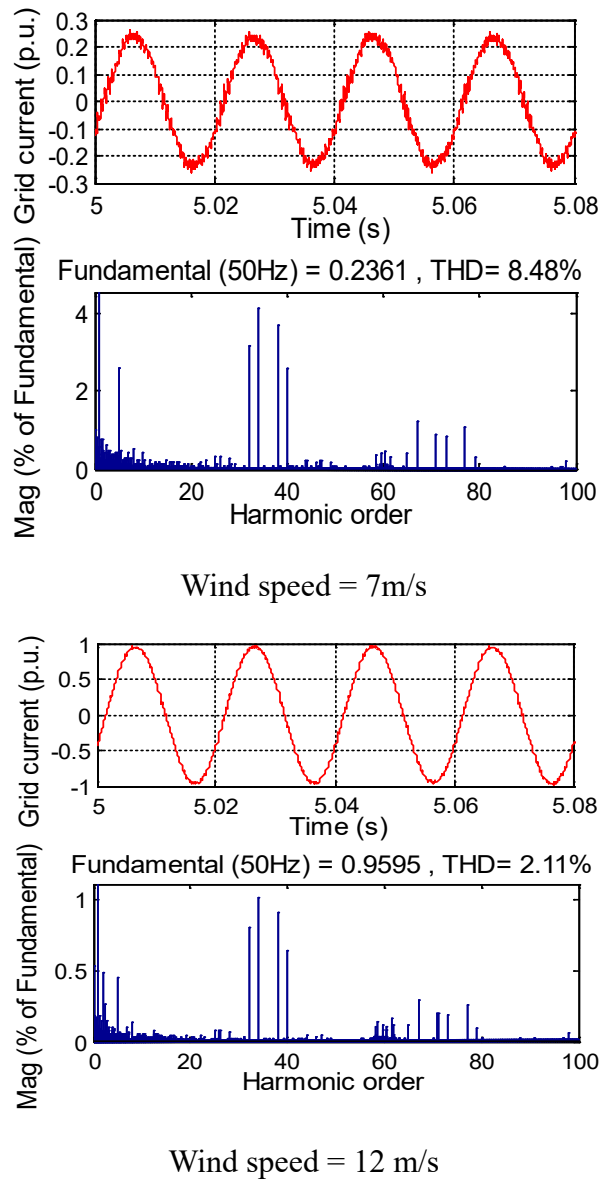


Fig. (6) Grid current and its harmonic spectrum for two-level OAPWM converter.

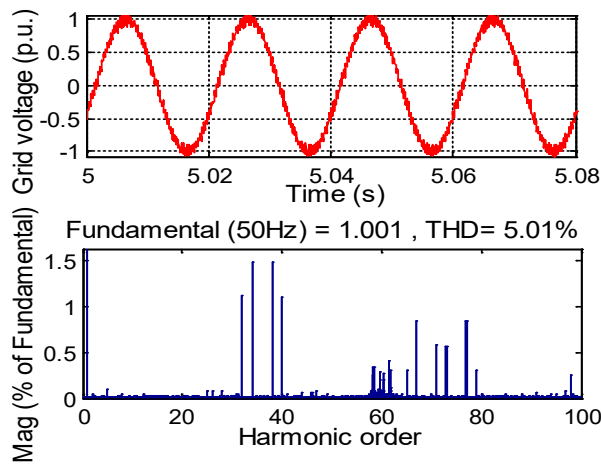


Fig. (7) Grid voltage and its harmonic spectrum for two-level OAPWM converter at wind speed 12 m/s

### 2.2.3 DFIG converter with Space Vector PWM technique

SVPWM refers to a special switching scheme of the six power semiconductor switches of a three phase power converter. Instead of using a separate modulator for each of the three phases (as in the previous techniques), the complex reference voltage vector is processed as a whole. Therefore, the interaction between the three motor phases is considered. It has been shown, that SVPWM generates less harmonic distortion in both output voltage and current applied to the phases of an ac motor and provides a more efficient use of the supply voltage in comparison with sinusoidal modulation techniques. SVPWM provides a constant switching frequency and therefore the switching frequency can be adjusted easily. The phase voltages corresponding to the eight combinations of switching patterns can be calculated and then converted into the stator two phase ( $\alpha, \beta$ ) reference frame. This transformation results in six non-zero voltage vectors and two zero vectors. The angle between any adjacent two non-zero vectors is 60 electrical degrees. The maximum output phase voltage and line-to-line voltage that can be achieved by applying SVPWM are:

$$V_{ph\ max} = V_{dc}/\sqrt{3} \qquad V_{ll\max} = V_{dc}$$

And r.m.s. output phase voltage and line-to-line voltage are:  $V_{ph\ rms} = V_{dc}/\sqrt{6}$   $V_{ll\max} = V_{dc}/\sqrt{2}$

Applying SVM switching technique to the inverter, the resulting grid current and its harmonic spectrum at 7m/sec. and 12 m/sec. wind speed are displayed in Fig. (8) a and b. The grid voltage and its harmonic spectrum at 12 m/sec. wind speed are displayed in Fig. (9). Comparing the THD resulting from SVM technique with those resulting from the two previous techniques show a decrease in the harmonic contents of the current and voltage at the grid side for both sub-and super-synchronous wind speeds.

### 2.3 Integrating the PV and WECS outputs

The DC-AC inverter interfacing the PV Cuk converter to the grid is controlled by the SVPWM technique. The insolation level is 1000 watt/m<sup>2</sup>. The resulting THD of the voltages and current injected to the grid from the PV inverter, the DFIG stator, and the DFIG rotor inverter for sub- and super-synchronous speeds are added and the results are shown in Figures (10) and (11) respectively. A slight increase in the THD of voltage injected to the grid took place; from 4.93% for wind system alone to 4.99% for the hybrid system. An increase in the THD of the current injected to the grid took place; from 1.98% for wind system alone to 2.37% for the hybrid system. These values are within the limits set by the grid standards.

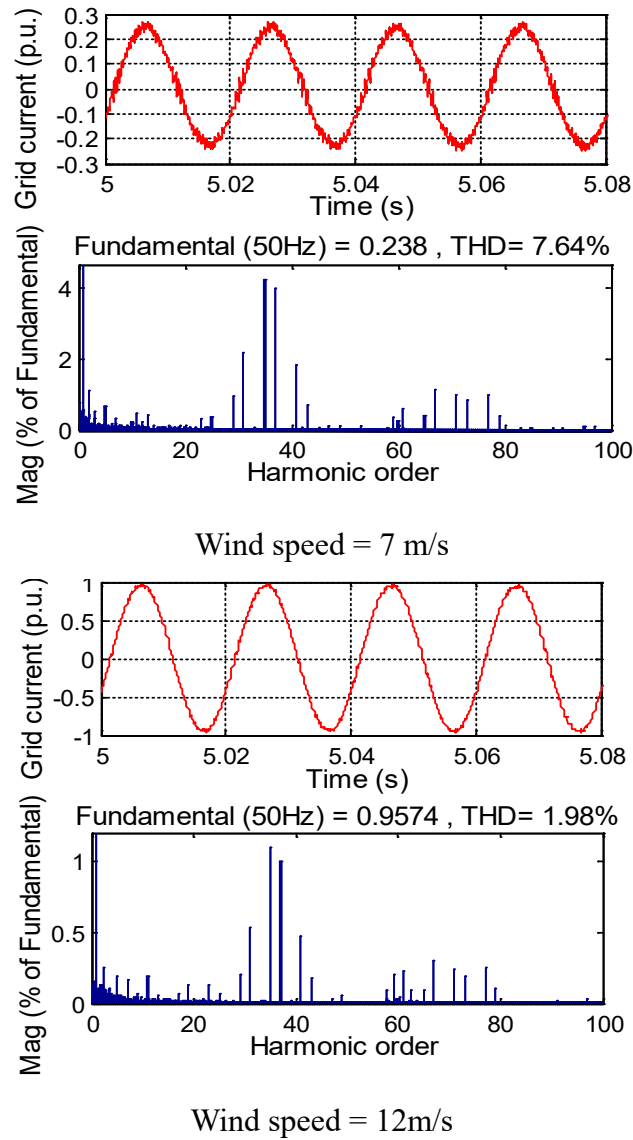


Fig. (8) Grid current and its harmonic spectrum for two-level SVPWM converter.

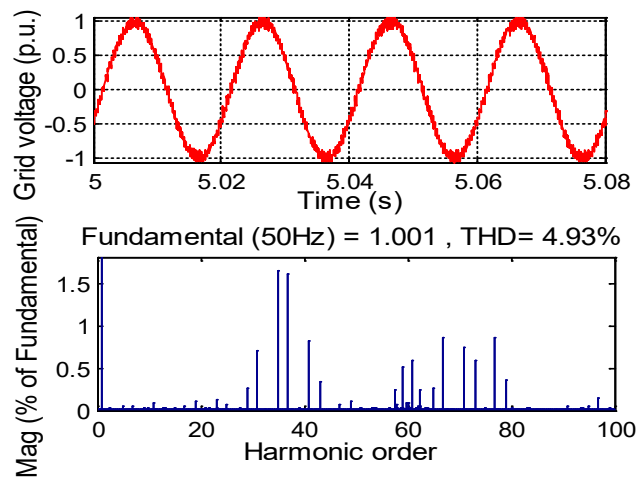


Fig. (9) Grid voltage and its harmonic spectrum for two-level SVPWM converter at wind speed 12 m/s.

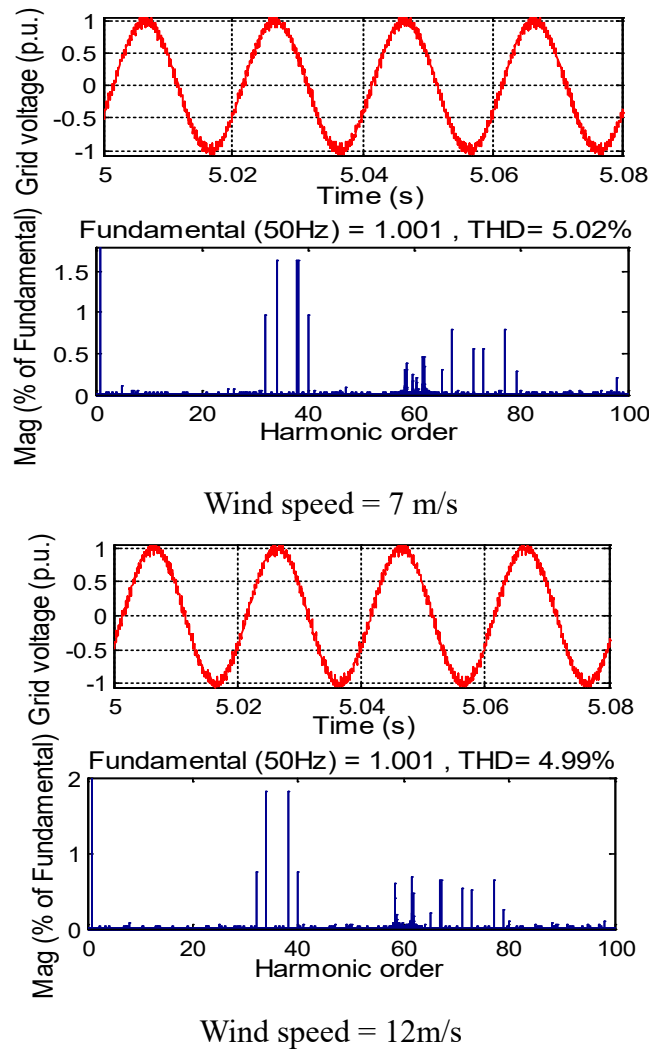


Fig. (10) Grid Voltage with harmonic spectrum for all system at insolation 1000 w/m<sup>2</sup>

#### 4. Conclusion

A grid-connected PV-Wind hybrid generation system is proposed. The PV system performance is presented when using two types of dc-dc converters, the buck-boost and the Cuk converter. Three types of PWM switching techniques for the inverter interfacing the DFIG rotor to the grid and for the inverter interfacing hybrid system to the grid are investigated and the resulting voltage and current THD are calculated using real system parameters. Comparing the THD of the grid voltage and current at the point of common connection for each switching technique is presented at 1000w/m<sup>2</sup> insolation level and wide range of wind speeds. It is concluded that the output voltage of the Cuk converter contains less harmonics which reduces the losses and the burden on the inverter interfacing it to the grid. It is also concluded that the SVPWM inverter switching technique minimized the THD of the voltage and current injected to the grid by the hybrid system.

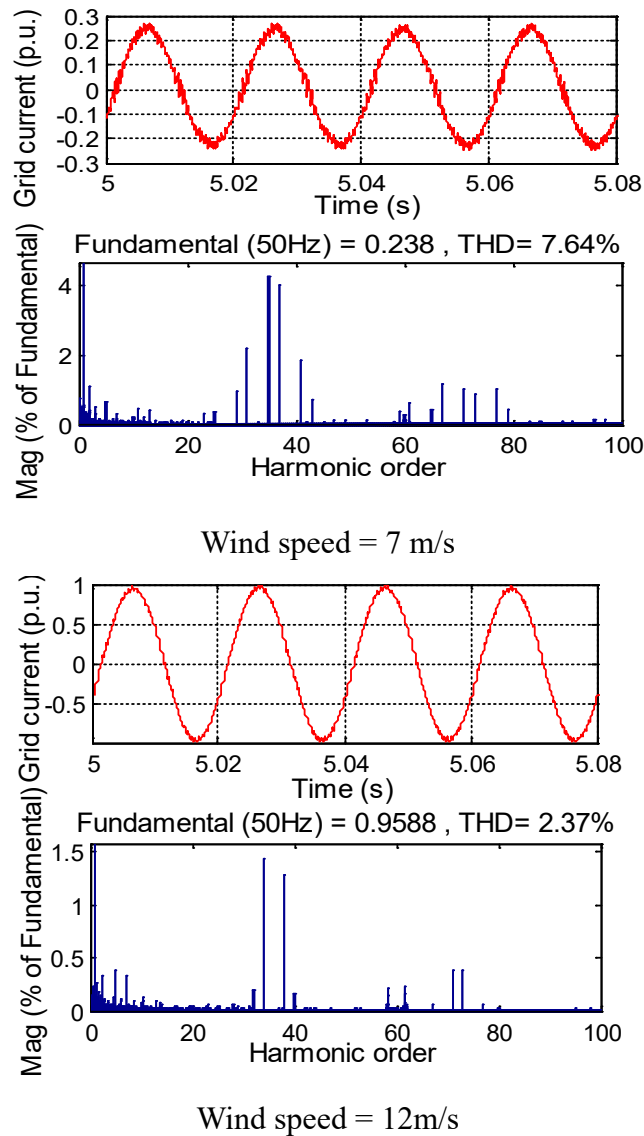


Fig. (11) Grid current with harmonic spectrum for all system at insolation  $1000 \text{ w/m}^2$

## REFERENCES

- Badrzadeh, B. and Gupta, M. 2013. Practical Experiences and Mitigation Methods of Harmonics in Wind Power Plants, *IEEE Trans. on Industry Applications*, 49 (5), 2279-2289.
- Deepthi, J. and Saxena, S N. Study of Variation of THD in a Diode Clamped Multilevel Inverter with respect to Modulation Index and Control Strategy, *2nd International Conference and workshop on Emerging Trends in Technology (ICWET)*, NY, USA, 2011, 1196-1200.
- Jayasinghe, S. D. G., Vilathgamuwa, D. M. and Madawala, U. K. 2011. Direct Integration of Battery Energy Storage Systems in Distributed Power Generation, *IEEE Trans. on Energy Conversion*, 26 (2), 677-675.



- Khayyer P. and Özgüner, Ü., 2014. Decentralized Control of Large-Scale Storage-Based Renewable Energy Systems, *IEEE Trans. on Smart Grid*, 5 (3), 1300-1308.
- Mendis, N., Muttaqi, K. M., and Perera, S. 2014. Management of Battery-Supercapacitor Hybrid Energy Storage and Synchronous Condenser for Isolated Operation of PMSG Based Variable-Speed Wind Turbine Generating Systems, *IEEE Trans. on Smart Grid*, 5 (2), 944-953.
- Mishra N. and Ramachandran V., Harmonics Reduction and Amplitude Boosting in Polyphase Inverter Using 60° PWM Technique, *Second International Conference, PEIE 2011*, Nagpur, Maharashtra, India, April 21-22, 2011.
- Nashed M. N. F. and Edwar I., 2015. Wind/PV Hybrid of DC Electric Vehicle Charging Station with Bi-directional Converter, *World Engineering conference and Convention (WEEC 2015)*, Kyoto, Japan, 29 Nov.-2 Dec. 2010.
- Rashid, M. H. Power Electronics Circuits, Devices and Applications, *Prentice Hall India, Pearson Education, Third Edition*, New Delhi 2004.
- Salmerón, P. Litrán, S. P. Herrera, R.S. and Vázquez, J. R. A Practical Assessment of Different Active Power Filter Configurations, *Proceedings of 2011 International Conference on Power Engineering, Energy and Electrical Drives*, Málaga, Spain. May 2011.

## APPENDIX

### Wind System

Parameter	Value
Rated mechanical power	2 MW
Rated stator line-to-line voltage	690 V(rms)
Rated stator phase voltage	398.37 V(rms)
Rated stator frequency	50 Hz
Synchronous speed	1500 rpm
Nominal rotor speed range	1050-1815 rpm
Number of pole pairs	2
Rated mechanical torque	10.5226 KN.m
Stator resistance	2.6 mΩ
Magnetizing inductance	2.5 mH
Rotor resistance referred to the stator	2.9 mΩ
Rotor leakage inductance referred to the stator	87 μH
Stator inductance	2.587 mH
Rotor inductance	2.587 mH

## Upconversion emission of $\text{Tm}^{3+}$ / $\text{Yb}^{3+}$ co-doped $\text{Na}_{0.5}\text{Gd}_{0.5}\text{MoO}_4$ phosphor for optical devices

Yu Jin Lee, Joo Hyun Lee and Hyun Kyoung Yang \*

Department of LED Convergence Engineering, Pukyong National University,

Busan 608-739, Republic of Korea

\*Corresponding Author: hkyang@pknu.ac.kr

### ABSTRACT

In recent, upconversion (UC) materials has attracted considerable attention. Because UC luminescence has unique optical properties and potential applications in fields such as volumetric displays, temperature sensors, UC lasers. In the UC phosphor, the emission intensity can be improved by selecting suitable host and sensitizer. Therefore, the properties of UC materials could be identified by various UC mechanisms involved between activators and sensitizers.

The host materials, oxide based phosphors have been prepared and characterized for various applications. Among these oxide based hosts, the molybdate based host materials have shown their important role because of good chemical, mechanical and thermal stability.

In this research, the  $\text{Na}_{0.5}\text{Gd}_{0.5}\text{MoO}_4:\text{Tm}^{3+}/\text{Yb}^{3+}$  phosphors were synthesized by the solid-state method. The crystal structure of materials was investigated by X-ray diffraction (XRD) The surface morphology and size of powders were observed by field emission scanning electron microscopy (FE-SEM). The optical properties of  $\text{Na}_{0.5}\text{Gd}_{0.5}\text{MoO}_4:\text{Tm}^{3+}/\text{Yb}^{3+}$  were characterized by analyzing the pump power-dependent UC emission spectra.

**Keyword:** Upconversion, luminescence, phosphor,  $\text{Na}_{0.5}\text{Gd}_{0.5}\text{MoO}_4$

## Synthesis of $\text{Sr}_2\text{SiO}_4:\text{Eu}^{2+}$ phosphor via microwave-assisted sintering

Woo Cheol Lee, Ju Young Mun and Hyun Kyoung Yang \*

Department of LED Convergence Engineering, Pukyong National University,  
Busan 608-739, Republic of Korea

\*Corresponding Author: hkyang@pknu.ac.kr

### ABSTRACT

Recently, white light-emitting diode (WLED) is excellent candidate for new generating light source instead of conventional incandescent and fluorescent lamp for next generation, due to the advantages such as high brightness, reliability, long life time, low environmental impact and energy efficiency.

There are two methods to generate white light. The one is the combination of three primary colors (red, green and blue) with three different LED chips. The second is to convert the blue emission to a longer emission by tallow emitting phosphors such as  $\text{Ce}^{3+}$  doped yttrium aluminum garnet ( $\text{YAG}:\text{Ce}^{3+}$ ). However, phosphors  $\text{YAG}:\text{Ce}^{3+}$  based on WLED show low color rendering index (CRI). To solve this problem, phosphors based on silicate are considered as replacement owing to strong absorption from blue to near UV region and  $\text{Eu}^{2+}$  ions shows wide emission range from near ultraviolet to red region due to energy level transition  $5d - 4f$ .

In this research, we synthesized  $\text{Eu}^{2+}$  doped  $\text{Sr}_2\text{SiO}_4$  phosphors via microwave-assisted sintering. Structural and thermal properties are investigated by X-ray diffraction analysis (XRD), thermogravimetric/differential thermal analysis (TG/DTA). The surface morphological study was observed with scanning electron microscope. The optical properties of phosphors were characterized by photoluminescence (PL).

**Keyword:** Luminescence, phosphor, microwave – assisted sintering,  $\text{Sr}_2\text{SiO}_4$

## Facile synthesis of graphene quantum dots derived from vinegar

Woo Tae Hong, Sung Jae Lee, Sung Jun Park, Jin Young Park and Hyun Kyoung Yang\*

Department of LED Convergence Engineering, Pukyong National University,  
365 Sinseon-ro, Busan, Republic of Korea

\*Corresponding Author: hkyang@pknu.ac.kr

### ABSTRACT

During the past decades, the inorganic quantum dots have an attention for promising candidate to replace the conventional phosphor materials due to their unique optical and electronic properties caused by the quantum confinement and edge effects. However, their toxicity, hydrophobicity and high fabrication cost limits their practical application.

For these reason, graphene quantum dots (GQDs) are recently discovered fluorescence nanomaterials. Benignity to the human bodies and the environment, abundance of materials on earth, and robust near-infrared to near-UV luminescence of GQDs can provide a great potential in biological labeling, bioimaging, drug delivery and optoelectronic device applications.

At present, the most popular synthesis of graphene oxide is Hummer's method. Through a thermal reduction, graphene oxide cutted to graphene quantum dots with high quality. However, these methods needs complex or post-treatment processes, or require expensive raw materials and severe synthetic conditions, which are disturb to be applied significantly in the near future.

To solve these problem, many researches were performed to synthesize GQDs from natural organic materials with facile synthetic method. Among them, the vinegar is familiar carbon materials. By using a hydrothermal synthesis, polysaccharides, acetic acid and citric acid in vinegar can be pyrolyzed and carbonized to GQDs.

In this study, fluorescent GQDs were synthesized from vinegar, through hydrothermal process. The fabricated CQDs showed good water solubility, blue luminescence at UV excitation.

**Keyword:** Graphene quantum dot, vinegar, hydrothermal synthesis.

## **The use of Virtual Reality technology to enhance e-learning**

MAK Kai-Long

Hong Kong Community College, The Hong Kong Polytechnic University,

\*Corresponding Author: ccklmak@hkcc-polyu.edu.hk

### **ABSTRACT**

Electronic Learning (e-learning) is the use of new multimedia technologies and the internet to improve the quality of learning by facilitating access to resources and services as well as remote exchanges and collaboration (European Commission, 2001). According to Arkorful and Abaidoo (2015), they agreed that despite different researchers has variety of definitions on the concept of e-learning, they however concluded that the fundamental of e-learning is to contain web-supplemented and web-dependent services for the provision of educational and support processes. Furthermore, Arkorful and Abaidoo (2015) concluded both advantages and disadvantage of adopting e-learning in tertiary education. E-learning however also facing some challenges, it require student to be self-motivated, require interpretation amount the learning process, have negative effect on students' communication skill as well as socialization skills, limit the role of instructors and unable to provide practical experiences.

In this research, we aimed to finding the way to enhance e-learning experience through new virtual reality technology.

**Keyword:** e-learning, Virtual Reality

### **1. Introduction**

As the new VR technology released in 2016, VR return to the focus of the people. As the pervious time, the computer technology and internet technology is not capable of support VR to visualize huge amount of information and graphics. Therefore, for the old kind of VR technology, the content is simple which have few of information included. Thus, there is a need to review the new virtual reality technology.

The use of multimedia technology is the fundamental of E-learning. However, we need to understand that multimedia has a huge variety of content. First, the basic of multimedia is the combination of text, audio, graphic and video (Lau et al., 2014). And then researcher suggesting that graphics and videos is having a broad definition which included textbook content, online animation and interactive simulation game(Mayer, 2002).

To conclude what E-learning is, it is a description of a learning process which associate with electronic device, such as computer and smartphone. With that premise, e-learning can also include online classroom, online learning resources and distance

learning.

Virtual Reality technology can simply classified as immersive Virtual Reality and non-immersive Virtual Reality (Merel, 2015). Immersive Virtual Reality referred to the view of users are completely surrounded by virtual world and the user's movement synchronize with the movement in the virtual world thus the users think they are immersed into the virtual world. The example of immersive Virtual Reality headset device included Oculus Rift and Sony PlayStation Virtual Reality. Non-immersive Virtual Reality referred to a Virtual Reality experience that user will not consider themselves as part of the virtual world where the user are simply viewing the virtual world as viewing a video. The example of non-immersive Virtual Reality included Google CardBoard and Samsung Gear Virtual Reality.

## 2. Literature Review

Electronic Learning (e-learning) are the use of new multimedia technologies and the internet to improve the quality of learning by facilitating access to resources and services as well as remote exchanges and collaboration (European Commission, 2001). According to Arkorful and Abaidoo (2015), they agreed that despite different researchers have variety of definitions on the concept of e-learning, they however concluded that the fundamental of e-learning is to contain web-supplemented and web-dependent services for the provision of educational and support processes. Furthermore, Arkorful and Abaidoo (2015) concluded both advantages and disadvantage of adopting e-learning in tertiary education. According to their report, e-learning increase the learning flexibility; enhances the efficacy of learning; improve interaction between students and teacher; cost effective; and help allocate academic resources. However, E-learning have the following disadvantages, it requires student to be self-motivated; require interpretation amount the learning process; has the negative effect on students' communication skill as well as socialisation skills; limit the role of instructors; and unable to provide practical experiences.

Researchers had suggested that how to make e-learning more effectiveness. According to Lau, Yen and Wah (2014), multimedia instruction and interactive learning activities are the key factors to improve e-learning effectiveness where multimedia instruction referred to the combination of text, audio, graphic and videos. Due to the student could formulate and visualise abstract concepts and interactivity allowed student to proactively discover new things. Also, Monahan, McArdle and Bertolotto (2008) indicated that a non-immersive 3-D learning environment can provide students with their social needs when learning, and able to engaging student and maintaining their interest.

Immersive Virtual Reality is a simulated 3-dimensional (3-D) environment which referred to a user using a headset device with software that allows the user to feel like he/she is inside the virtual environment. Apart from that, it should be able to provide real-time interaction between users and users or the virtual environment (Bailenson et al., 2008). Therefore, researchers also suggest the possibility of using Immersive Virtual Reality on e-learning as the related technology was still growing (Monahan et al., 2008). According to Merchant et al. (2014), today's Immersive Virtual Reality technology still facing problems such as heavy headset and simulator sickness where simulator sickness was known as physical and/or mental illness exposure to Virtual Reality environment (Kolasinski, 1995). However, with the better processing power of the computer, it could provide better graphic and thereby enhance learners' engagement. Furthermore, with the improvement of web technology, Immersive Virtual Reality technology is now able to allow more than one user to work collaboratively (Merchant et al., 2014).

For those researchers who study e-learning, most of them had mentioned about how the use of gaming to improve learning effectiveness or the role of the game on learning (Monahan et al., 2008; Bailenson et al., 2008; Lau et al., 2014; Merchant et al., 2014). According to Lau et al. (2014), the goal of game-based learning is to combine entertainment, visual-oriented and interaction-based tasks as the learning process. Merchant et al. (2014) pointed out the elements of how to make a game as an effective teaching tool. They mentioned that the game needs to provide users with the sense of autonomy, identity and interactivity so as to promote learning. If wanted the learners to keep learning, then the game need to be able to allow learners to strategise their decision, test hypotheses and finally solve the problems. Also, it is important to include goals or achievement, animated content and moderate difficulty. Lee, Wong and Fung (2010) had conducted a research about how virtual reality environment affects learning outcome. They used Virtual Reality software program, V-Frog as teaching material where the software is designed as a dissection simulator. They concluded that Virtual Reality learning environment is significantly and positively related to learning outcome. Based on the result that Virtual Reality learning environment can provide the sense of presence, increase learning motivation and improve reflective thinking.

Aside from educational purpose, Virtual Reality technology has been used on other aspect such as industrial training and demonstration. Cláudio et al.(2017) tried to apply Virtual Reality technology to ironmaking industry, they generated a fully

function realistic simulation of ironmaking plant then allow user to access the simulated environment via a third person perspective of the virtual character, also known as avatar. Within the virtual environment, it simulates the physics of real world and provide the corresponding feedback to the user, such as the gravity, the interaction when user “touch” an item in the simulation. But the value of apply Virtual Reality to industrial training is that the possibilities of simulate some critical situations such as on fire or critical injuries. Thus Virtual Reality technology make the training become more realistic and more memorable. Most importantly is that the simulation would affect the operation of the plant in real world such as an evacuation training will no longer need to pause the production in order to train. Also, researchers are now reviewing using immersive Virtual Reality technology on medical surgery training, particularly in neurosurgery(Panayiotis et.al, 2016). As they mentioned, neurosurgery required huge amount of medical knowledge, high technical skill and full preparation. Thus, the nature of neurosurgery makes Virtual Reality technology into a valuable tool for medical education. As the simulation is controlled by the computer, the training content could be so detailed and more realistic.

### **3. Recommendation**

#### **3.1 Using Immersive Virtual Reality as the e-learning medium**

As mention above, Arkorful and Abaidoo(2015) had listed the advantages and disadvantages of e-learning. However, the studies their used to conclude the disadvantages may be outdated as some of the studies released more than 10 years ago. As 2016 has several commercial Virtual Reality released which mean there is a need to review the disadvantages with a new perspective of Virtual Reality technology.

1. The remoteness of e-learning, i.e distance learning, which will cause lack of interaction and therefore decrease student’s communication skill. According to Merchant et al. (2014), today’s internet technology and is able to let multiple user to join the same Virtual Reality session and provide an instant interaction between users. However, today’s Virtual Reality industry has no Virtual Reality headset that could provide instant conversation.

2. Lack of interpretation during learning process and limit the role of instructors. This is actually depends on the quality of teaching material and whether there is an instructor or not. As above mentioned, the internet technology today is advanced enough to let multiple user join together from different place, the role of instructor in Virtual Reality environment could be the actual teacher themselves. Beside, Lau et.al(2014) indicated that, the role of instructors need to be transformed into a producer of the teaching material such that the learning process can fit the student



most.

3. Unable to provide practical experiences. Cláudio et.al.(2017) and Panayiotis et al.(2016) proved that the application of Virtual Reality technology on industrial and medical can provide practical experience to the trainer especially on dangerous and rare case, such as evacuation when the plant is on fire or a surgery of neuro system as the trainer could make mistake during the training and able to redo the training.

On the other hand, advantages will have less affect by the time. However, whether immersive Virtual Reality can fulfill the advantages of e-learning is worth mentioning.

1. The high flexibility of e-learning. As researchers consider that learner can choose the place and time that suitable for them to learn. Immersive Virtual Reality headset may restrict the place of learning as the headset required a connected computer to run the software. However, the time to learn is flexible as mention. But consider the need of instructor via learning. A scheduled online class is needed for the understanding of students.

2. Enhances the efficacy of learning. As the online content can also view by Virtual Reality headset. Using Virtual Reality headset will not affect online resources will affect the learning experience of the learner. With the use of Virtual Reality software, the learning efficiency could be further enhance(Merchant, 2014), because of the first person view of learning and the enhancement of interaction, learner can learn on hand knowledge and complicated concept via using immersive Virtual Reality to learn.

3. Cost effective. As immersive Virtual Reality can provide an enhanced learning content to learner, the cost of learning may be able to reduce. For example, frog dissection in biology is critical for understanding anatomy. Thus, there is a need to let every student try to learn how. However, there will be a high cost for purchasing frog for every student. Therefore, the immersive Virtual Reality can reduce the cost of physical consuming teaching material where the simulation of Virtual Reality technology can simulate practical learning content multiple time. Logically, the cost compare to actual learning material will be reduced by every single time of simulation.

### **3.2 Using Game as the learning content**

What game itself providing, is the entertainment of visual content and the game content. Thus using game-based learning can based on gaming experience, provide learners with teaching content. According to Lau et al.(2014), using game can significantly motivate students to learn where game-based learning combine interaction-based assignment, visual-oriented content and entertainment as the

learning process.

As mentioned above, immersive Virtual Reality can provide user with immersive experience and interaction within user to user or user to computer. Within game-based interaction, the interaction of the game itself is a critical factor to increase learner's interest and help the learning process into a fun experience. Also, with a game that could cooperate with other user will provide an opportunity of social interaction thus help users to feel their social presence.

In order to make game into an effective learning content. The game design and the actual academic knowledge in game need to pay attention to.

1. The game need to provide users a high level of customization such that they can customize the level of difficulty. However, the game itself should still be challenging in order to keep user trying, as people are tend to accept challenge in order to have more excitement(Gee, 2003).
2. The game need to make learner to strategise their decision and testing hypothesis. According to Squire and Barab(2004) research on strategy game Civilization III, student who played the game have showed deeper learning to which compared to those student who had not.
3. The game need to be online based but also available offline. By the definition of e-learning, the game is needed to be online such that the learner can perform distance learning. Also, the game becoming online could allow interaction between learner and the instructor. Besides, for the offline feature, the game should also ready for learner that who only want to review content for study purpose or quick check of some content.
4. The game need a clear goal and achievement system for learner to follow and keep playing the game in order to reach the end of the game which is the fundamental knowledge that developer want learner to learn. According to Swartout and van Lent(2003), goal within a game should diverse into three parts: short-term goal that last few second; medium-term goal that last few minutes; and long-term goal that last until the end of the game.
5. The game need to let user be part of the developer. Commercial game like The Elder Scrolls Franchise and Fallout Franchise, they allow player as a developer that make new content for the game, such as new story and new map. In the case for learning, teacher could change the role into a producer that make custom teaching material for their student and the goal of custom making is to fit the student level and the learning pace.
6. The game content need to be interesting and the story and background must be scientific and historical accurate. Beyond that, the presentation of the content could be more casual in order to maintain interest of learners.

## 4. Limitation

### 4.1 Limitation of immersive Virtual Reality application

As mentioned above, there are some properties of today's immersive Virtual Reality technology and products fit the principle of e-learning but however the technology itself has some limitations that could make it hard to apply.

1. The cost of immersive Virtual Reality headset is too high. Right now, immersive Virtual Reality headset device include the following, Oculus Rift, Sony PlayStation VR and HTC VIVE. The most expensive is HTC VIVE cost 799 US Dollar per set and the cheapest is Sony PlayStation VR which cost 598 US Dollar per set. The cost could be too high for the educational usage because of consider that the ownership should be one device per student in order to get the best education outcome and also to perform distance learning. However, if distance learning is not necessary to be done, the institute can alternately purchase the device at school for student to share. Thus the cost will be reduced but also reduce the mobility of e-learning.
2. The design of immersive Virtual Reality headset is not perfect for educational usage. As mentioned above, today's Virtual Reality headset has no microphone installed. Although immersive Virtual Reality technology could allow user to interact with other user which satisfied the e-learning disadvantages' of lack of interaction problem. But without an instant conversation, the interaction between user and user will be an incomplete intervention as the user may not understand the action of the other but no explanation could be received. Although user can additionally use external microphone and conversion software from third party software. But it is not a permanent solution for the long-term immersive Virtual Reality usage.
3. Lack of educational software. As the Virtual Reality industries right now are mainly focus on making profit from games. Thus Virtual Reality software for educational software would be lack of selection. Therefore, a custom Virtual Reality software would be a better solution that educator could include specific syllabus for their own school or groups of students. For existing educational software including but not limited to Unimersiv, a software that include space knowledge, human anatomy and British history; and Discover Labs, a Virtual Reality classroom that allowed academic personnel register as a tutor and start up a online tutorial for learner.
4. Simulator sickness is still a problem. According to Kolasinski(1995), the longer a user use a simulator, i.e. military Virtual Reality device, the higher possibilities that a user will suffer simulator sickness. However, based on today's Virtual Reality technology, simulator sickness is still has no way to avoid(Maraj et al.,2017).

#### **4.2 Limitation of educational game application**

1. It may be hard to develop an interesting game for educational purpose. As not every kind of knowledge will be fun for learner, such as mathematics concept, financial knowledge, etc. thus game developer need to conceal the academic knowledge within the detail of the game. Such as a game that have a society which contain a complete monetary system and financial system. But the main of the game should be much bigger, like a whole civilization that contain technology, religion, history, etc, which is alike to the real world.
2. The educator may be under qualified to make a custom teaching material. As game need knowledge on programming and logical calculation. Educators without corresponding knowledge may found difficulties on developing an educational game. Thus the cooperation of educators and game developers is needed for developing an educational game that are academic knowledge accurate content and a common commercial game setting.
3. Lack of developers developing Virtual Reality game.

#### **5. Conclusion**

This research studied the possibilities of applying of Immersive Virtual Reality technology corresponding with game on learning purpose. As mentioned above, immersive Virtual Reality technology is now capable but the development right now is not fully suitable to perform e-learning. As the price of the Virtual Reality headset is too high, the design of headset is not complete and the software support is not enough. Also, with the use of immersive Virtual Reality technology, educational game is also suitable for e-learning. But the game developers need to aware that an educational game required more academic knowledge so it would be better if the developers cooperate with academic personnel.

## REFERENCES

- Arkorful, V., & Abaidoo, N. (2015). The role of e-learning, advantages and disadvantages of its adoption in higher education. *International Journal of Instructional Technology and Distance Learning*, 12(1), 29-42.
- Ang, C. S., & Rao, G. R. K. (2008). Computer game theories for designing motivating educational software: A survey study. *International Journal on ELearning*, 7(2), 181.
- Bailenson, J. N., Yee, N., Blascovich, J., Beall, A. C., Lundblad, N., & Jin, M. (2008). The use of immersive virtual reality in the learning sciences: Digital transformations of teachers, students, and social context. *The Journal of the Learning Sciences*, 17(1), 102-141.
- Commission of the European Communities. (2001). *The E-learning Action Plan: Designing Tomorrow's Education*. Commission of the European Communities.
- Gee, J. P. (2003). What video games have to teach us about learning and literacy. *Computers in Entertainment ' (CIE)*, 1(1), 20-20.
- Kolasinski, E. M. (1995). *Simulator Sickness in Virtual Environments* (No. ARI-TR-1027). ARMY RESEARCH INST FOR THE BEHAVIORAL AND SOCIAL SCIENCES ALEXANDRIA VA.
- Lau, R. W., Yen, N. Y., Li, F., & Wah, B. (2014). Recent development in multimedia e-learning technologies. *World Wide Web*, 17(2), 189-198.
- Lee, E. A. L., Wong, K. W., & Fung, C. C. (2010). How does desktop virtual reality enhance learning outcomes? A structural equation modeling approach. *Computers & Education*, 55(4), 1424-1442.
- Mayer, R. E. (2002). Multimedia learning. *Psychology of learning and motivation*, 41, 85-139.
- Maraj, C. S., Badillo-Urquiola, K. A., Martinez, S. G., Stevens, J. A., & Maxwell, D. B. (2017). Exploring the Impact of Simulator Sickness on the Virtual World Experience. In *Advances in Human Factors, Business Management, Training and Education* (pp. 635-643). Springer International Publishing.
- Merchant, Z., Goetz, E. T., Cifuentes, L., Keeney-Kennicutt, W., & Davis, T. J. (2014). Effectiveness of virtual reality-based instruction on students' learning outcomes in K-12 and higher education: A meta-analysis. *Computers & Education*, 70, 29-40.
- Merel T. The 7 drivers of the \$150 billion AR/VR industry. *Aol Tech*; 2015.
- Monahan, T., McArdle, G., & Bertolotto, M. (2008). Virtual reality for collaborative e-learning. *Computers & Education*, 50(4), 1339-1353.
- Swartout, W., & van Lent, M. (2003). Making a game of system design. *Communications of the ACM*, 46(7), 32-39.
- Squire, K., & Barab, S. (2004, June). *Replaying history: Engaging urban underserved*

students in learning world history through computer simulation games. In Proceedings of the 6th international conference on Learning sciences (pp. 505-512). International Society of the Learning Sciences.

## Effect of Time-Dependent Extraction Flow Rates on a Radially Convergent Fingering flow

Chih-Ang Chung<sup>a,b\*</sup> and Jui-Hsiang Chiu<sup>a</sup>

<sup>a</sup>Department of Mechanical Engineering, National Central University,  
300 Zhongda Road, Zhongli District, Taoyuan City 32001, Taiwan

<sup>b</sup>Graduate Institute of Energy Engineering, National Central University,  
300 Zhongda Road, Zhongli District, Taoyuan City 32001, Taiwan

\*Corresponding Author: cachung@ncu.edu.tw

### ABSTRACT

Fluid displacement plays an important role in many industrial applications, including enhanced oil recovery, carbon capture and storage, fluid transport in fuel cells, and biological filtration. When the process involves a less viscous fluid displacing a more viscous fluid, the fluid interface may evolve from smooth into ramified patterns; this phenomenon is called viscous fingering. Viscous fingering reduces the spread of the displacing fluid, thus increasing the residual of the displaced one. To solve this problem, researchers have been using Hele-Shaw cells to study the fingering phenomenon. Previous literature has shown that a linearly time-dependent volumetric flow rate can suppress viscous fingering in a radially divergent flow, for which the fluid flows radially outwards from the cell center to the periphery. This is because the time-dependent flow rate can maintain the fluid interface velocity at a constant by changing the flow rate in accordance with the interfacial radius. In contrast, a constant flow rate will result in large interface velocities for the small radii. From the point of view of linear stability analysis, the optimized linearly time-dependent flow rate is able to suppress the interfacial instability for a radially convergent system, in which the fluids move from the periphery to the cell center. However, there have been no successful reports on using time-dependent flow rates to suppress fingering in the radially convergent flow system.

This paper presents an experimental study on applying the time-dependent extraction flow rates to the fluid displacement in a radially convergent Hele-Shaw flow, where the displacing water has less viscosity than does the displaced silicon oil. We investigated the displacements by extracting the silicon oil, which originally occupied the cell central region, through the exist hole at the cell center. The water surrounding the oil was then withdrawn inwards. The time history of the finger flow was recorded using a video camera. Experimental results were elucidated through a set of dimensionless parameters, including the capillary number which is the relative ratio of viscous force to interface tension, and the dimensionless time span which accounts for the flow rate. Comparisons of the result of constant flow rate with that of time-

dependent flow rate were conducted to investigate the effectiveness of changing flow rates.

The experimental results show that unlike the case of divergent flow in which the time-dependent flow rates can suppress the interface fingering virtually independent of the capillary number, the convergent fingering flow could be suppressed only if the capillary number was small. Even worse, the time-dependent flow rates in radially convergent flow could more easily induce interface stability. This is because of the following two facts in the convergent flow: (1) the interface velocity with time-dependent flow rate was larger in initial time than that with constant flow rate, (2) the interface velocity could be increased sensitively to the change in the flow thickness. The first point could then trigger interfacial ramification unless the capillary number was small enough. The second caused the interfacial velocity to increase quickly rather than keeping constant as the fluids flowed inwards. These two points, however, were found to play no important roles in the divergent flow.

**Keyword:** Fingering instability, Hele–Shaw cell flow, Time-dependent flow rate, Viscous finger.



## Decellularized porcine corneal scaffold for cultivating fibroblasts and corneal endothelial cells in vitro

Hung-Jun Lin<sup>a</sup>, Ling-Chi Hsiao<sup>b</sup>, Ping-Lun Jiang<sup>b</sup>, Yun-An Chen<sup>a</sup>, Chun-Han Lin<sup>b</sup>,  
Yi-You Huang<sup>a</sup> and Der-Zen Liu<sup>b,\*</sup>

<sup>a</sup> Institute of Biomedical Engineering, College of Medicine and College of Engineering, National Taiwan University, Taipei, Taiwan

<sup>b</sup> Graduate Institute of Biomedical Materials and Tissue Engineering, College of Biomedical Engineering, Taipei Medical University, Taipei, Taiwan

Email: <sup>a</sup>d02548004@ntu.edu.tw, <sup>b,\*</sup>tonyliu@tmu.edu.tw

### ABSTRACT

One of the main reasons caused human blindness is corneal diseases. Unfortunately, the demand of corneas evidently exceeds the available donor supplement. To solve these problems, decellularized cornea scaffolds were developed. This method preserves nature corneal ECM structure and original biologic factors which are critical for corneal keratocyte recellularization. In this study, we tested different acidic decellularized protocols on porcine corneas and examined the most efficient method for decellularization. Transmittance examination revealed there were no significant difference between native cornea and decellularized corneal scaffolds. The Qubit DNA assay showed over 90% porcine cells was eliminated after decellularized procedure. The SEM images confirmed the decellularized corneal scaffolds remained uniform parallel microstructure, and showed porous structure which might be beneficial for further keratocytes recellularization. After UV light sterilization, the decellularized corneal scaffolds were seeded with keratocytes, SIRC cells or bovine endothelial cells for 2 weeks. DAPI staining demonstrated keratocytes well distributed inside the decellular corneal scaffolds and bovine endothelial cells stable maintained on the scaffold. These results demonstrated that acidic decellularization for porcine corneas had favorable biological properties and suggested it could be a promising scaffold material for corneal tissue engineering applications.

**Keyword:** xenograft, tissue engineering, scaffold, decellularized cornea, recellularization

## Design principles for stiffness adjustment in soft material robotics using layer jamming

Sebastian Blankemeyer<sup>a</sup>, Jenna Losensky<sup>b</sup>, Jan Peters<sup>a</sup> and Annika Raatz<sup>a</sup>

<sup>a</sup>Leibniz Universität Hannover, Institute of Assembly Technology,

An der Universität, Garbsen, Germany

<sup>b</sup>Ohio State University, Columbus, Ohio 43210

\*Corresponding Author: blankemeyer@match.uni-hannover.de

### ABSTRACT

As companies increasingly face the consequences of an aging population and correspondingly a higher average age of the workforce, the need for support systems for workers is becoming more urgent. In order to allow an effective use of these systems, the worker must be able to integrate these into his daily work and therefore also accept it as an auxiliary system. To improve the safety of the worker and additionally the worker's acceptance of the support system, injury of the employee must be prevented. One approach is the use of soft material robotic systems. A problem that occurs is the trade-off between attainable softness and load-bearing capability. For support systems to exhibit soft behavior and to withstand process forces in other situations, they should be able to change their properties, e.g. the stiffness. This paper gives a short overview about different stiffness adjustment methods and tries to analyze the layer jamming technology as one approach to use in soft material robotic systems. For the technology to be used effectively, influencing factors must first be identified and investigated for the stiffening by means of layer jamming. Tests were carried out on a universal testing machine, which determined the required force for each measurement via a load cell and the corresponding deflection by means of a traverse system. The data determined with the measurement setup was then analyzed and evaluated. Finally, design principles were derived based on the knowledge gained from the experiments. The principles derived from our observations can be used as guidelines for the development of soft support systems.

**Keyword:** soft material robotic systems, stiffness adjustment, design principles, layer jamming.

### 1. Introduction

Producing companies are faced with an ever increasing number of challenges. In this context, companies must react flexibly to changing markets in order to secure their competitiveness. For this, well-trained specialists are needed to adapt and scale the production environment to the given conditions of the market. The growing demand for

skilled workers in many countries can therefore not necessarily be covered by new employees. In addition, a demographic change is taking place in many countries. The population is getting older and there is a limited number of younger people to fill these positions. As a consequence of these points, later retirement ages for employees are quite normal. In order to enable their employees to work longer, companies have to reduce or prevent their employees of heavy loads, un-ergonomic movements and long-lasting handling of objects during their day-to-day work. For this purpose, support systems can be used which assist the employee in the execution of tasks.

### **1.1 Support systems and stiffening mechanisms**

Support systems can be of many different shapes. There are first prototypes, which are built as exoskeletons of hard materials. Examples are the HAL-3 (Sankai 2011), Hercules (Bogue 2015) and the Chairless Chair (Schembera-Kneifel 2016), which was already tested in the production of Audi AG. Excluding of the last system, these structures are often very heavy and equipped with extra motors to allow movement. Therefore, the person in the system is positioned in a way that their mobility is constrained. Another approach could be support systems made of soft materials to reduce the mobility constraints of the worker using a hard support system. The difficulty in creating the support systems of soft materials is that stiffness-variable mechanisms are needed to be able to switch between the "hard" and "soft" states. This is necessary to solve the trade-off between attainable softness and load-bearing capabilities to withstand process forces. Approaches that make these ideas reality are enquired by research teams working in the field of "Soft Robotics". Here, concepts are investigated in which soft materials are used to build robot elements or structures. Frequently, "smart materials"—materials that undergo characteristic changes independently or by active stimulation—are also used in this context. Materials with which this is possible are, among others, magneto-rheological/electro-rheological fluids, shape memory polymers and novel fluids and gels, e.g. nanocomposite hydrogels and electro-active polymers. In addition to this, mechanisms exist that can change the behavior of materials like layer or granular jamming. Applications where they are already used include: STIFF-FLOP (Ranzani 2013), Snake-like manipulator (Kim 2013), Magnetic rheological fluid rubber for walking robot (Taniguchi 2014), Artificial rubber muscle using Shape memory polymer (Takashima 2011) and the hydrogel artificial muscles (Rogers 2013). Another approach is causing stiffness variability through a change of the geometry of objects. In the literature, examples are variable geometry structures, variable spring stiffness mechanisms and shape-locking mechanisms with the applications of variable stiffness cellular structures (Mc Knight 2010), stiffness-adjustable endoskeleton (Hu 2012) and "dragon skin" shape-locking mechanism (Zuo 2013).

## 1.2 Layer Jamming

A stiffening system that could provide support systems is layer jamming as it can be flexibly shaped and possibly integrated in the worker's clothes. Layer jamming works by compressing several layers of one or more materials with the help of a vacuum. For this purpose, the materials are stacked in an airtight envelope (e.g. polyethylene), and a vacuum is applied. With the negative pressure from the vacuum, the envelope moves toward one another and thus compresses the material layers. The compression results in a stiffening of the overall structure. Layer jamming mechanisms have already been implemented in various soft-robotic systems. Areas of application include minimal invasive surgery (Kim 2012), deformable furniture (Ou 2014) and a wheelchair positioning device (Veneman 2015). Ou et al. (Ou 2014) have carried out several tests with 32 different materials. For this purpose, 12 layers, each with the dimensions of 20x20cm<sup>2</sup>, were bent from 0° to 30° degree and the required torque was recorded. The focus in this investigation was on the material selection as a function of the weight and thickness. Bureau et al. (Bureau 2011) have carried out a limb attachment. To obtain the required forces, they performed three-point bending tests with a synthetic textile with various number of layers. According to their statements, the layers should exhibit high friction without electrical adhesion in order to obtain good stiffening results.

In this paper, further series of experiments are carried out in order to identify influencing parameters and thus make the stiffening result more predictable. Such investigations are necessary to formulate guidelines for designers to insure the components achieve the requirements and an appropriate stiffening result.

## 2. Test Preparation

At the beginning of the test series, possible influence parameters on the stiffening result need to be identified to obtain the right data. With regard to the stiffening result and to ensure predictability, the following parameters are first examined. As already noted by Bureau et al. the static coefficient of friction ( $\mu$ ) has a significant influence on the stiffening result. However, the number of layers ( $n$ ), the dimensions of the layers (length, width, height) and the applied air pressure ( $p$ ) also have a potential effect. Therefore, tests with different static coefficients of friction, the same number of layers and same height as well as the same cross-sectional area are tested in this paper. Furthermore, the air pressures are varied to make a prediction as well.

In addition, the test setup needs to be specified. Since in many applications bending loads are often required, a three-point bending test is used for the determination of the influencing variables in this test series. In order to obtain valid data pretests are made, e. g. the determination of the static coefficient of friction or tests to identify the appropriate dimensions of the samples (not content of this article).

## 2.1 Material selection

The main goal of the material selection is to identify materials that can be used to investigate the layer jamming process. The most important fact is that the material must be applicable for the layer jamming. This means materials need to be deliverable in sheets and flexible enough to bend with low forces. Furthermore, the materials must be acquirable with different parameters, cheap enough to execute various testing series and have a high and rapid availability. Since a single modification of parameters is needed in order to make statements on specific parameters, only one material was chosen opposed to the choice of using multiple materials. A material that fulfills many of the requirements is paper. There are many different types available with the opportunity to change only a few parameters simultaneously. It can be delivered in different shapes and sizes and is therefore applicable for the test series. Different types of paper are used in the test series and are as follows:

Table 1: materials for the testing series

paper		material properties		
		height of 40 layers (mm)	density (g/m <sup>2</sup> )	measured density (g/m <sup>2</sup> )
1	stiffer	5.10	100	105.82
2	weaker	4.16	80	82.57
3	enviromental	4.10	80	84.18
4	photo	8.15	210	199.62
5	painter	8.00	150	149.91
6	newspaper	2.52	45-48.8	46.13
7	sandpaper	13.48		236.11

At first, the different types of paper have been characterized relating to the height of the layers and the density. This is necessary to understand the basic conditions during the planning process of the testing series. In relation to the indicated density, deviations could be identified, e.g. for photo paper. Since the layers are meshed together at the surfaces, it is necessary to characterize them for the different types of material.

## 2.2 Determination of static coefficient of friction

As a key factor, the static coefficient of friction between the individual material layers was identified. Thus, it is assumed that the force for deformation also increases with increasing of the static coefficient. In order to check this assumption, friction tests are carried out at the beginning of the test series. For this purpose, two material layers are compressed by a defined force (see Figure 1). Subsequently, the force in the orthogonal plane is increased until the material layers slip relative to each other. The tests are made for the materials on itself and for the combination material on the shell (polyethylene).

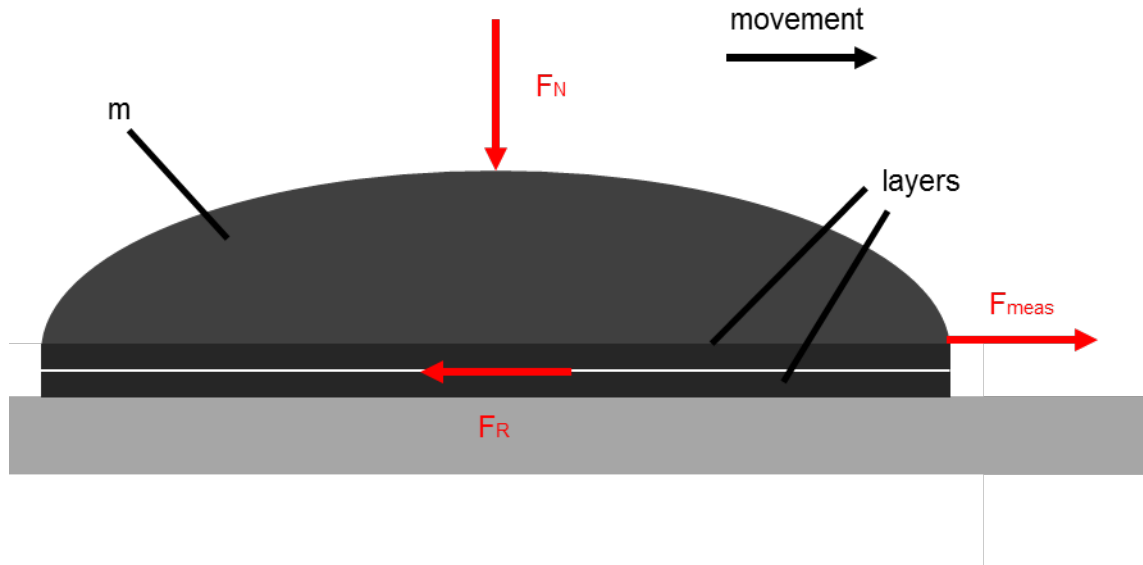


Figure 1: testing-setup for friction tests

For the test one layer is fixed at the ground and one layer at the bottom side of the block. The force  $F_{meas}$  results from pulling the block and can be measured by a force/displacement measuring device. When  $F_{meas}$  is as high as  $F_R$ , the block starts to slip and the static friction forces has been overcome. Since the mass of the block is known, the static coefficient of friction can be distinguished with the help of the following equation

$$F_{meas} = F_R = \mu F_N = \mu mg \rightarrow \mu = \frac{F_R}{mg}$$

- $F_{meas}$  – force measured
- $F_R$  – friction force
- $\mu$  – static coefficient of friction
- $F_N$  – normal force
- $m$  – mass
- $g$  – constant of gravitation

In order to get validated data, the tests were performed 20 times with one sample and the average was taken for the result.

The results are shown in Table 2.

Table 2: static coefficients of friction

	type of paper						
	stiffer (1)	weaker (2)	enviro-mental (3)	photo (4)	painter (5)	newspaper (6)	sandpaper (7)
$\mu$ , itself	0.114	0.144	0.122	0.160	0.222	0.220	0,35-0,63
$\mu$ , shell	0.127	0.101	0.086	0.267	0.124	0.078	0,40-0,48

The table shows that the static coefficient of friction between the different papers are in a range of 0.114 and 0.222. The coefficient between the material and the shell, with the exception of the stiffer paper, is always lower than to itself. During the tests it was

apparent that the static coefficient of friction of sandpaper decreases with every trial. The presumption is that the material is too abrasive and thus processed itself too much. Therefore, the longevity cannot be guaranteed which follows to the fact that not all tests can be executed with this material.

### 3. Three-point bending tests

The three-point bending tests are carried out on a universal testing machine named zwickiLine z0.5 from the Zwick Company. The load cell can measure forces up to 500 Newtons. The test method itself is based on DIN EN ISO 178 (DIN 2013), in which the determination of bending properties for synthetics are defined. The samples are prepared as shown in Figure 2.

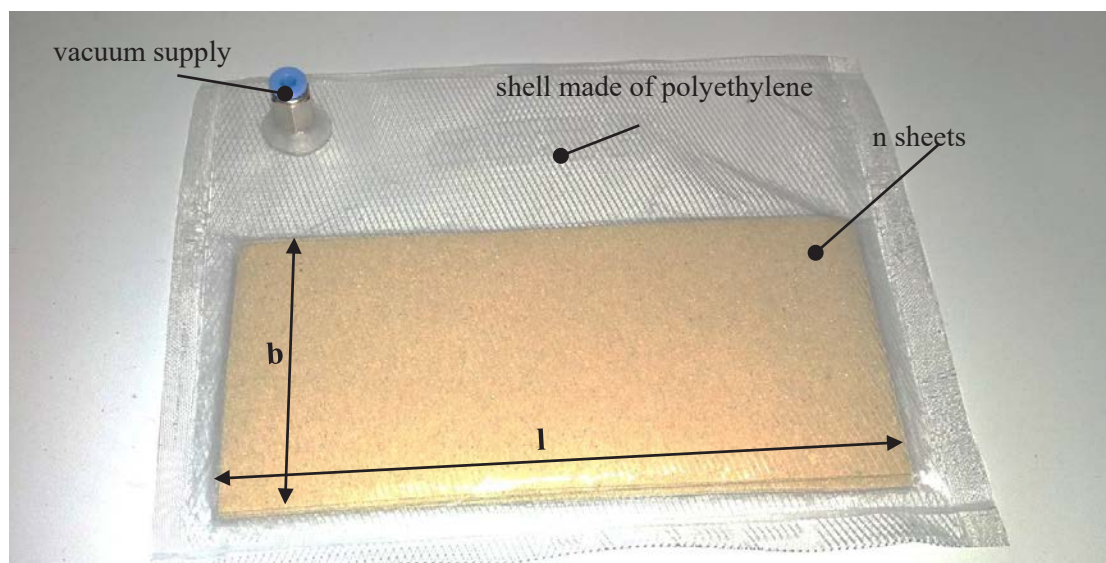


Figure 2: picture of one sample; shell with sandpaper (dimensions 70x160 mm) and a connector for the vacuum supply

The shell is made of polyethylene and is usually used for food vacuuming. The dimensions and the number of layers of the samples are determined according to the respective test. After the layers are placed in the bag and the vacuum connector is attached, the shell is welded air-tight. The shell is then placed on the test device as shown in Figure 3. In preliminary tests, it has been found that a width between the bearings of 100 mm is helpful in carrying out the tests. The traverse then travels centrally between the bars at a speed of 5 mm/min until the sample has reached a maximal bending strain of 4.5%. The vacuum can be adjusted via a valve according to the respective experiment. In order to make sure that the data is reliable, a test series with one sample was performed three times to validate the data.



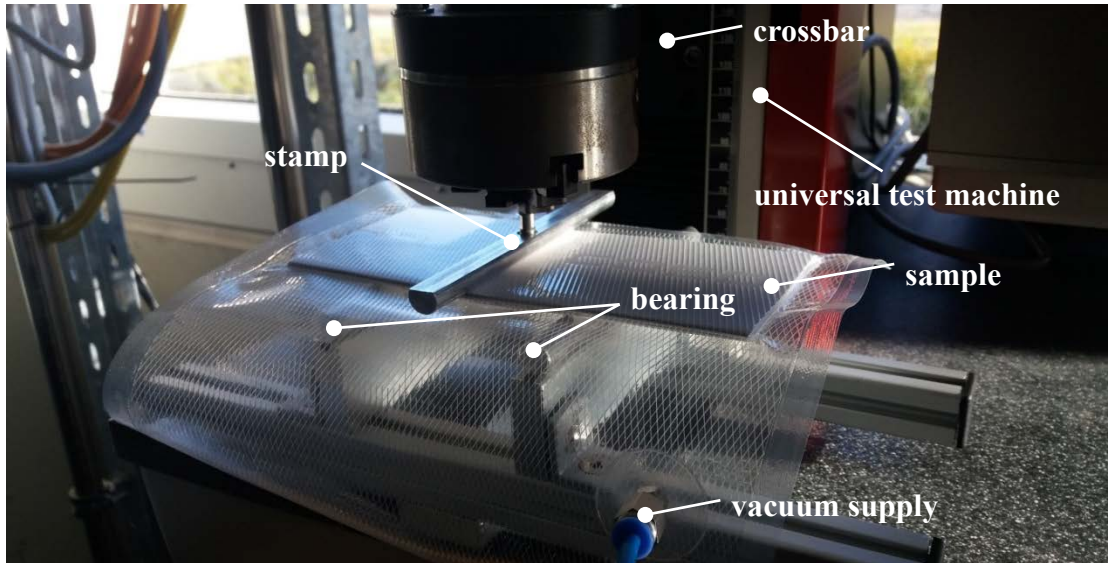


Figure 3: testing setup to investigate the bending stiffness by means of three-point bending tests

### 3.1 Influence of the pressure on the stiffening result

These tests are examined to identify how a change in the internal pressure influences the stiffness of the sample. Due to presentation reasons, only the results of weaker paper are shown in this paper, but the results of the other types of paper look similar. For this purpose, the sample is subjected to different pressures and is examined in the three-point bending test.

Table 3: testing parameters: different pressures

paper		testing parameters				
		length (mm)	width (mm)	height (mm)	pressure (bar)	Layers
2	weaker	160	70	4.16	0.0 - 0.9	40

For this test, the weaker paper was used. The pressure was raised in 0.2 bar increments up to 0.8. The maximum attainable vacuum in our testing setup was 0.9 bar.

The test results show that with increasing vacuum pressure, the forces which are necessary for the deformation increase as well (Figure 4). However, the proportion of the increase is nonlinear, since the amount decreased with increasing pressure. Thus, the jump between ambient pressure and 0.2 bar is higher than between 0.8 and 0.9 bar. Nevertheless, the increase between the ambient pressure and a negative pressure of 0.9 bar has a factor of approximate 41.



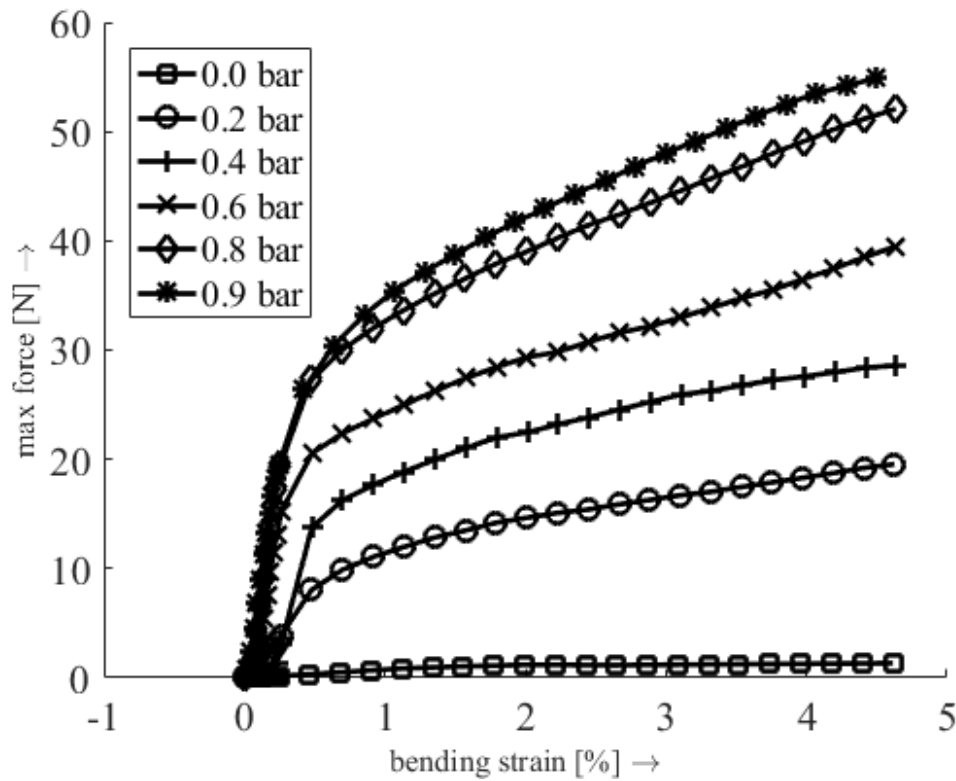


Figure 4: Influence of the pressure on the stiffening process for the weaker paper; proceed with pressures from 0.0 bar to 0.9 bar

### 3.2 Influence of the layers on the stiffening result

In the tests the influence of a changing number of layers is investigated. For this reason three samples of weaker paper were prepared with each 20, 40 and 80 layers. Consequently, the height of the samples increase as well. The test have been proceeded with a negative pressure of 0.9 bar. The deformation of the samples were in this case limited to 1 % of bending strain, since the sample with 20 layers is damaged at a bending strain of 4.5 %.

Table 4: testing parameters: same number of layers

paper		testing parameters				
		length (mm)	width (mm)	height (mm)	pressure (bar)	Layers
2	weaker	160	70	2.05	0.9	20
2	weaker	160	70	4.09	0.9	40
2	weaker	160	70	8.17	0.9	80

In figure 5 it is shown that the values of the force increases with an increasing bending strain. The values for 40 and 80 layers increase more rapidly than the force for 20 layers. The maximum value for 80 layers is at 62 N. It can be noted that with an increasing number of layers the attainable force rises as well. Unfortunately, the proportion is

nonlinear, as it was for the influence of the pressure, so a prediction of a precise value is very hard to implement.

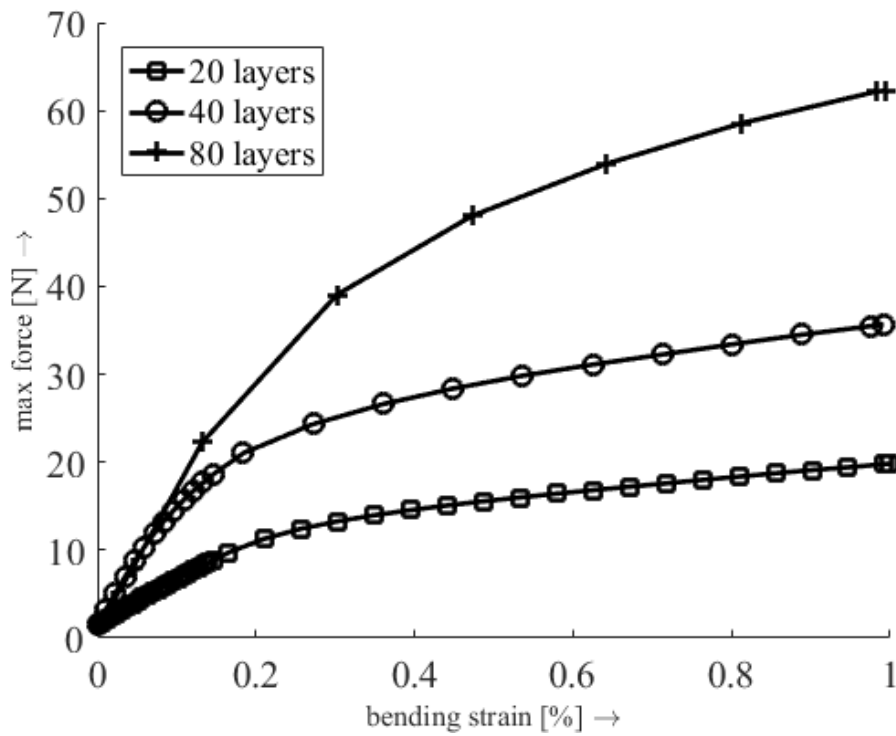


Figure 5: Influence of the amount of layers on the stiffening results at 0.9 bar vacuum

### 3.3 Influence of the height on the stiffening result

In the tests, the influence of the height on the stiffening result is investigated. For the test, the weaker paper was used. To identify the influence of the height, the cross-sectional area is left constant for all samples. That means that if the height will be doubled, the width of the sample is halved. The length is kept constant during the test series.

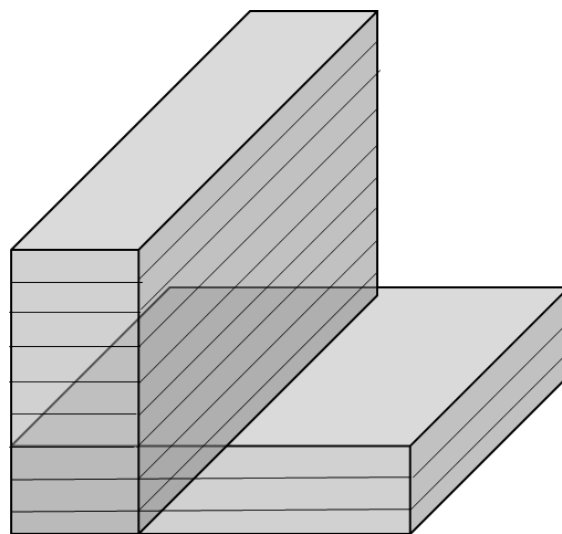


Figure 6: constant cross-section while changing the width and the number of layers

Therefore, the mass as well as the whole friction surface of the sample is kept constant.

The experimental parameters are:

Table 5: testing parameters: influence of the height on the stiffening result

paper		testing parameters				
		length (mm)	width (mm)	height (mm)	pressure (bar)	Layers
2	weaker	160	70	2.05	0.0	20
2	weaker	160	70	2.05	0.9	20
2	weaker	160	17.5	8.17	0.0	80
2	weaker	160	17.5	8.17	0.9	80

The results show that higher stiffness is achieved when the stack of layers are taller but not as wide. This can be attributed to the fact that the compressed layers behave more like a whole cross-section than as individual thin layers. Since the height in the calculation of the bending resistance moment for a rectangular cross-section according to equation

$$W_y = \frac{bh^3}{12z_{max}} = \frac{2bh^3}{12h} = \frac{bh^2}{6}$$

$W_y$  – bending resistance moment

b – width

h – height

$z_{max}$  – maximal distance to the neutral fiber –  $z_{max} = h/2$

is to the second power, this result can be expected. However, when considering the ratio, a wider sample shows a larger increase in stiffness than the taller sample. The ratio can be calculated by dividing the max force at 0.9 bar by the max force at 0.0 bar. In Table 6, it can be seen that a stack of 20 layers has a factor of 35 between ambient pressure and 0.9 bar vacuum, whereas the stack of 80 layers only has a factor of 25. Depending on the application and its general constraints, the designer can check which property is required.

Table 6: results for the influence of the height on the stiffening process

	20 layers		80 layers	
	0	0.9	0	0.9
negative pressure	0	0.9	0	0.9
max. force [N]	0.57	20.22	1.5	33.68
ratio	35.47		22.45	

### 3.4 Influence of the static coefficient of friction on the stiffening results

The test are examined to identify the influence of the static coefficient of friction on the stiffening result. For this study the number of layers and the width were kept constant for every sample. The tests were performed with a negative pressure of 0.9 bar

Table 7: testing parameters: influence of the static coefficient of friction (same number if layers)

paper		testing parameters				
		length (mm)	width (mm)	height (mm)	pressure (bar)	Layers
1	stiffer	160	70	5.1	0.9	40
2	weaker	160	70	4.16	0.9	40
3	enviromental	160	70	4.1	0.9	40
4	photo	160	70	8.15	0.9	40
5	painter	160	70	8	0.9	40
6	newspaper	160	70	2.52	0.9	40

As shown in Figure 7, every material behaves more or less in the same way. At the beginning of the test cycle, the force progression is rapidly raising. Depending on the material the charts flattens out between 0.2 % and 0.9 % bending strain. The newspaper shows a decrease of attainable force after 1.1 % of bending strain. At that point the sample wasn't stiff enough and a "set point" occurred through this overload. The test must be aborted after 2.5 % bending strain since the sample left the position.

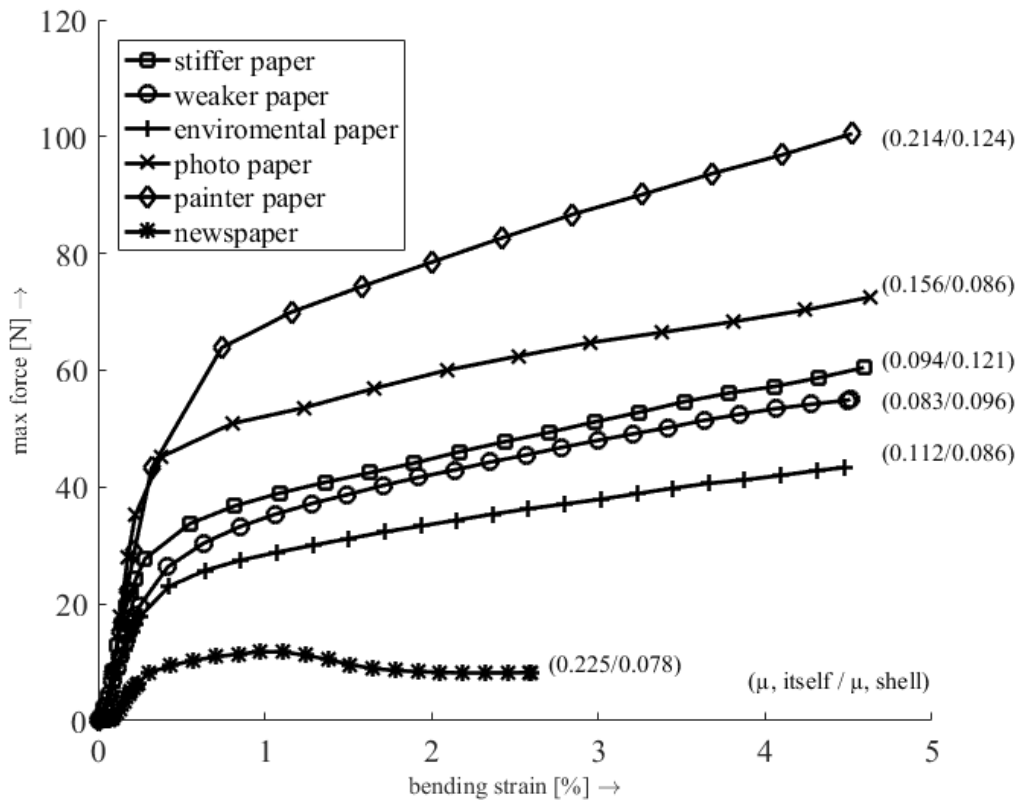


Figure 7: Influence of the coefficient of friction on the stiffening results using 40 Layers of each paper at 0.9 bar vacuum

The results show that no statement can be made when taking into account the static coefficient of friction between the layers. The presumption that higher values of the static coefficient of friction directly results in higher stiffness cannot be confirmed. If,

however, the static coefficient of friction between the layer material and the shell is observed, an increase in the static coefficient of friction results in an increase in stiffness of the sample. The assumption can be made for painter, environmental, weaker and stiffer paper as well as for newspaper. This result wasn't expected since only two out of all of the layers are interacting with the shell. However, the correlation of the stiffness and the coefficient is non-linear.

Photo paper represents an exception, since the force is very high in combination with the static coefficient of friction. An explanation could be that photo paper has different surfaces of each side of the sheet. Nevertheless, the fact of increasing forces through higher values of static coefficient of friction between material and shell, must be validated again in further experiments.

Regarding to the different heights using the same number of layers (Table 7) and the insight that the height has an influence on the result (Table 6), the study will be carried out again using similar heights for each sample. As it is shown in Table 7 the height differs between 2.52 mm and 8.15 mm. To get similar heights for every sample, the smallest stack of 40 layers that could bear a bending strain of 4.5 % was chosen as a starting point. Every other stack is reduced until a similar height is reached. The experimental parameters are as follows:

Table 8: testing parameters: influence of the static coefficient of friction (similar height)

paper		testing parameters				
		length (mm)	width (mm)	height (mm)	pressure (bar)	Layers
1	stiffer	160	70	4.1	0.9	32
2	weaker	160	70	4.08	0.9	39
3	enviromental	160	70	4.11	0.9	40
4	photo	160	70	4.08	0.9	20
5	painter	160	70	4.14	0.9	21
6	newspaper	160	70	4.09	0.9	65

Like it was for the test with the same amount of layers, the force progression rapidly rises at the beginning. At an approximate value of 0.3 the curves flatten. The newspaper failed early again, similar to the test before. The gradient of the other curves seem to correspond with their static coefficient of friction between shell and material. The curves of the materials with the larger static coefficient of friction rise quicker than the ones with small coefficients. Taking into account the conclusions of the test for the influence of the height, it can be recognized that the same height combined with a material with a larger coefficient could provide an increase of the attainable forces. A small exception is the curve of the weaker paper. The coefficient is higher than the ones of photo and environmental paper but smaller than the coefficients of painter and stiffer paper. This has to be investigated in further studies.

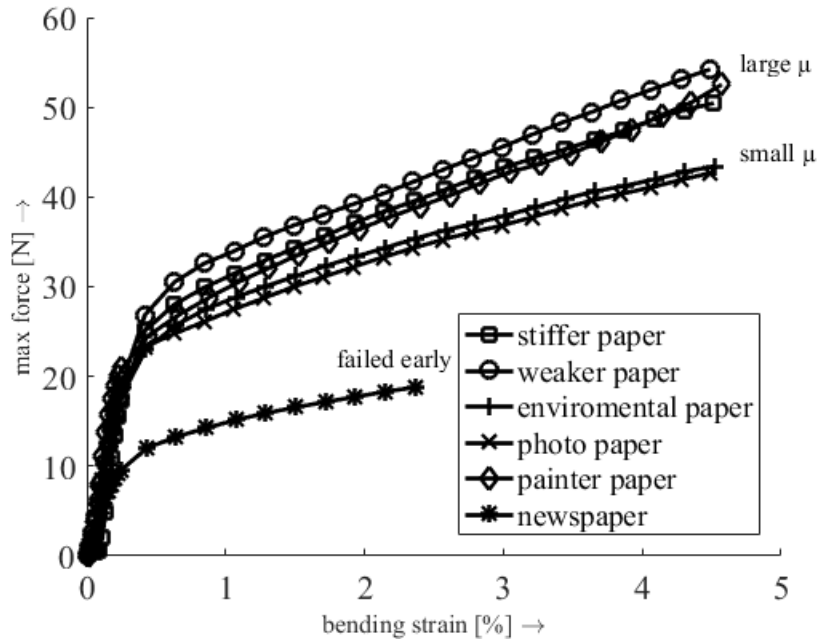


Figure 8: influence of the static coefficient of friction on the stiffening results with a similar height for every sample

### 3.5 Additional Observations

During the test series, some limitations could have been observed in relation to the selection process of materials. As it was already recognized during the determination of the static coefficient of friction tests, the surface of sandpaper changes its characteristics with nearly every relative movement. It was found that with a frequent repetition of the tests, the forces required for the deformation are constantly decreasing (Figure 9).

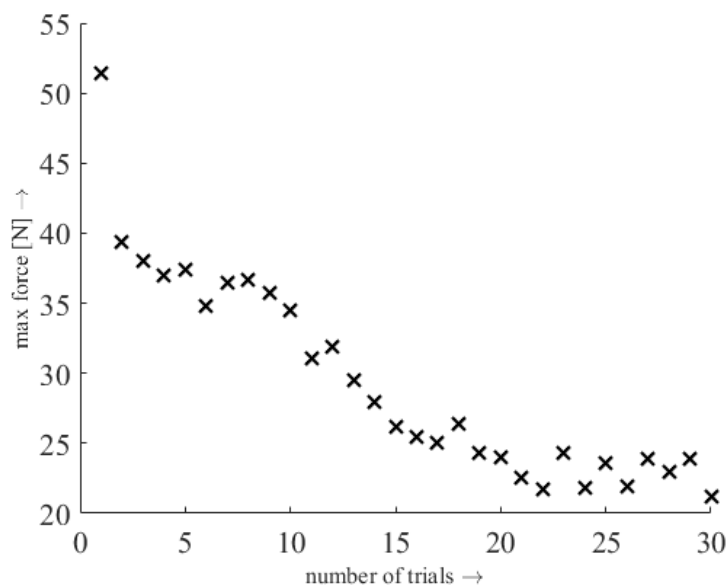


Figure 9: influence of the abrasive behavior of sandpaper on the maximum force

This can be explained by the fact that the material layers rub against one another, which makes the surface smoother and the layers interlock less. Unfortunately, such a behavior is hard to predict. It cannot be noted that the other types of paper don't have such a decreasing but in these testing series it wasn't recognizable. It is logical to assume that abrasive materials show this behavior more often.

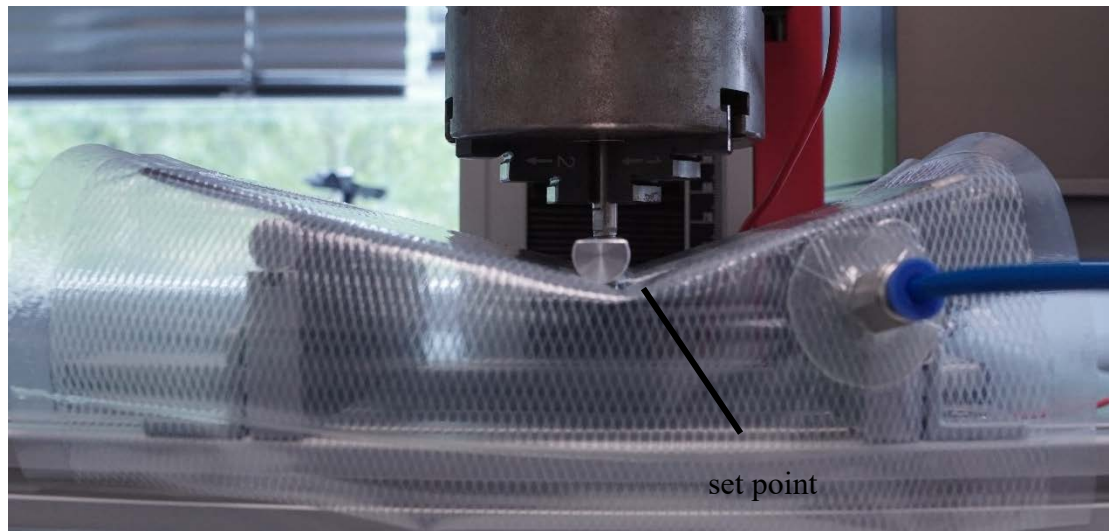


Figure 10: "set point" occurred through overload

Another point is the overloading of a test specimen towards a plastic deformation. If an overload occurs, a "set point" is established, where the required force for the deformation decreases (Figure 10). At this point, a faster bending occurs in the next tests so that the deformation in this area is carried out more quickly and with less force. This phenomenon appeared particularly in the newspaper, since the individual layers are very thin.

#### 4. Derivation of Design Principles

To give the designers ideas what properties influence the stiffening process the most, the given results are formulated as design principles. These can be used within the designing process of e.g. soft support systems for workers.

*The maximum possible negative pressure results in the greatest possible stiffness within the samples.*

For the different types of paper it was found that with a maximum adjustable vacuum of 0.9 bar, the maximum stiffness to this cross-section could be achieved. Depending on the material and the number of layers used, the increase in stiffness decreases with an increase of the vacuum. For this purpose the ratio between the different pressures were calculated (Figure 9). The "ratio to last" value describes the factor from one pressure value to the next one, e.g. 0.4 to 0.6 bar. The "ratio to first"-value represents the factor from ambient conditions to the given pressure level, e. g. 0.0 to 0.8 bar.



Table 9: development of pressure to max force

	pressure (bar)					
	0.0	0.2	0.4	0.6	0.8	0.9
max force	1.36	19.70	29.07	39.62	52.29	55.77
ratio to last		14.54	1.48	1.36	1.32	1.07
ratio to first	1	14.54	21.44	29.23	38.58	41.15

As shown in Table 9, the development decreases from a multiplier of 14.54 to almost 1. Although the maximum force is still at the highest vacuum, the designer has to think if it is really necessary to take the highest possible negative pressure. The results are qualitatively consistent with those of Ou et al. (2014) and Bureau et al. (2011).

*If the weight plays a subordinate role, the increase in stiffness can be achieved by a pure increase in the material thickness (= the number of layers).*

Depending on the application, it is possible that the weight and dimensions of the samples are of less relevance than the stiffening result. In this case, the stiffness can be increased by increasing the material layers. However, there is no proportional relationship and thus a doubling of the height does not automatically lead to a doubling of stiffness.

*A high stiffness at a low weight can be achieved by increasing the material thickness while reducing the material width.*

If the cross-sectional area must be kept constant because of weight, an increase in stiffness can be achieved by halving the layers and subsequent stacking. With this approach, the rigidity can be increased without having to gain weight. However, it can be disadvantageous to have a structure with this design because of the thickness. In the case that a high ratio between “soft” and “hard” state is required, a higher width is preferable.

*Using abrasively material can lead very fast to an impairment or at least a malfunction of the layer jamming process.*

As shown in Figure 9, the attainable forces of Sandpaper decrease with every trial. This is of course a disadvantage for the stiffening and leads to unpredictability of the whole process. Nevertheless, it can, for example, be used for processes where no relative movement between the layers is needed. One example can be a safety mechanism in which the forces should be limited.

*Exceeding the elastic-linear limit should be avoided as this can lead to irreversible damage to the material.*

In the case of Newspaper, deformation of the individual layers was found when the deformation was too large in the vacuumed state. From here, irreversible damage to



the material occurs. How large the deformation must be cannot be quantified and is material-dependent. However, a deformation of the specimens beyond the linear-elastic range is not to be attempted in any case since shifts occur between the individual material layers and the specimen is plastically deformed. To restore the desired shape, the normal pressure (ambient pressure) must be established within the sample and the whole sample must be vacuumed again in the desired position.

## 5. Conclusion

Design principles for stiffness in soft robotics using layer jamming have been proposed. Based on support systems for use in production areas, a distinction was made between hard and soft systems. In order to make soft systems usable, stiffness-variable mechanisms are required which are able to relieve the employee at desired times. Layer jamming is presented as one possibility and is discussed in more detail. The principle of stiffening several layers of materials by introducing a vacuum has already been shown in some demonstrators in research. The aim is to identify parameters which influence the stiffening result and thus make it predictable if necessary.

The static coefficients of the test specimens were first determined by experiments. Three-point bending tests were then carried out with the specimens in order to determine the achievable forces as a function of the deformation, which can be seen as a measure of the stiffness. In the experiments with different paper types, the value of the negative pressure has a great influence on the stiffening result. The higher the value, the greater the achievable forces. The static coefficient of friction between the individual layers does not have as much influence as the static coefficient of friction of the sample with the shell. Furthermore, the tests have shown that, in the case of a strongly abrasive material, such as sandpaper, the forces which can be reached are greatly reduced after a few test runs. In addition, overloading the sample leads to a set point, whereby the achievable forces are also reduced and the material thus behaves differently than previously predicted.

Further series of experiments will show how the material behavior of the shell influences the stiffening result in order to confirm the assumptions. Further parameters—such as force application, compressibility of the sample material, material combinations or sample geometries—are to be investigated in order to make the prediction of stiffness easier and more precise. On the basis of this, it is possible to make applications using layer jamming mechanisms easier. This would also benefit the design of soft-robotic support systems which can relieve the employees of their day-to-day work.

## ACKNOWLEDGEMENTS

We thank Tobias Koch for the building of the testing setup as well as the execution of testing series.

## REFERENCES

- Bogue, R. 2015. Robotic exoskeletons. A review of recent progress. *Industrial Robot: An International Journal* (42), S. 5–10.
- Bureau, M.; Keller, T.; Perry, J.; Velik, R.; Veneman, J. F. 2011. Variable Stiffness Structure for Limb Attachment. *2011 IEEE International Conference on Rehabilitation Robotics*.
- DIN EN ISO 178. 2013. 2013-09: Kunststoffe – Bestimmung der Biegeeigenschaften (ISO 178:2010 + Amd.1:2013).
- Hu T M, Park Y-J, Cho K-J 2012. Design and Analysis of a Stiffness Adjustable Structure Using an Endoskeleton. *Precision Engineering and Manufacturing* 13(7): 1255-1258.
- Kim Y. J., Cheng S., Kim S. and Iagnemma K., 2012. Design of a tubular snake-like manipulator with stiffening capability by layer jamming *2012 IEEE/RSJ International Conference on Intelligent Robots and Systems*, Vilamoura, 2012, pp. 4251-4256.
- Kim Y, Cheng S, Kim S, Iagnemma K 2013. A Novel Layer Jamming Mechanism with Tunable Stiffness Capability for Minimally Invasive Surgery. *IEEE Transactions on Robotics* 29(4): 1031-1042.
- Mc Knight G P, Henry C P 2010. Deformable variable-stiffness cellular structures. *US Patent* 7,678,440.
- Ou, J.; Yao, L.; Tauber, D.; Steimle, J.; Niiyama, R.; Ishii, H. 2014. jamSheets: Thin Interfaces with Tunable Stiffness Enabled by Layer Jamming. *Proceedings of the 8th International Conference on Tangible, Embedded and Embodied Interaction (TEI '14)*, S. 65–72.
- Ranzani T, Cianchetti M, Gerboni G, et al. 2013. A modular soft manipulator with variable stiffness. *3rd Joint Workshop on New Technologies for Computer/Robot Assisted Surgery*.
- Rogers J A 2013. A Clear Advance in Soft Actuators. *Material Science* 341:968-969.
- Sankai, Y. 2011. HAL: Hybrid Assistive Limb Based on Cybernetics. In: *Robotics Research. The 13th International Symposium ISRR*, Bd. 66. Berlin, Heidelberg: Springer Berlin Heidelberg (Springer Tracts in Advanced Robotics), S. 25–34.
- Schembera-Kneifel T., Keil M. 2016. Future ergonomics tools – From the prototype to the serial product by comprehensive product optimization. *Bargende M., Reuss HC., Wiedemann J. (eds) 16. Internationales Stuttgarter Symposium. Proceedings*.

Springer, Wiesbaden

Takashima K, Noritsugu T, Rossiter J, et al. 2011. Development of Curved Type Pneumatic Artificial Rubber Muscle Using Shape-memory Polymer. *SICE Annual Conference*, Tokyo, Japan: 1691 – 1695.

Taniguchi H, Miyake M, Suzumori K 2010. Development of New Soft Actuator Using Magnetic Intelligent Fluids for Flexible Walking Robot. *Int. Conf. on Control, Automation and Systems*, Oct., 2010: 1797-1801.

Veneman, J.; Manterola, I.; Bureau, M.; Jung, J. H. 2015. *Varstiff, an innovative variable stiffness material*, applied in a Wheelchair Positioning.

Zuo S, Iijima K, Tokumiya T, Masamune K 2013. *Variable stiffness outer sheath with “Dragon skin” structure and negative pneumatic shape-locking mechanism*. *Computer Assisted Radiology and Surgery* 2014: 1-9.

## Creation of web learning environment intended to learning motivation on mechanical design

Yuya Nakamura<sup>a\*</sup>, Tsutomu Sekine<sup>b</sup> and Atsushi Okuyama<sup>a</sup>

<sup>a</sup>Course of Mechanical Engineering, Graduate School of Engineering,

Tokai University, 4-1-1 Kitakaname, Hiratsuka, Kanagawa 259-1292, Japan

<sup>b</sup>Department of Systems Design Engineering, Faculty of Science and Technology,

Seikei University, 3-3-1 Kichijoji-kitamachi, Musashino, Tokyo 180-8633, Japan

\*Corresponding Author: [6bemm061@mail.u-tokai.ac.jp](mailto:6bemm061@mail.u-tokai.ac.jp)

### ABSTRACT

In mechanical design, it is a problem that a lecturer has students get a wide range of knowledge and skills in a class whose time and place are limited. Then, the level of students' understanding has scarcely shown some signs of improvement so far. It is also desired to establish an efficient learning environment in mechanical design. In this study, a web learning environment was created on the basis of motivation-oriented teaching method. Then, the learning environment was introduced to the "basic drafting" classes held in our university. In a drafting class, we carried out an evaluation test over the last two years using a comparison of paper-based and web-based answers' results. It is understandable that correct answer rate in current year is higher than that in previous year. Moreover, learning motivation was also assessed using ARCS evaluation sheet. As a result, there existed favorable effectiveness to enhance learning motivation. Especially, Attention-related factors contributed the enhancement of learning motivation in web learning.

**Keyword:** Drafting education, E-learning, ARCS model, Gagne's 9 events of instruction, Learning motivation.

### 1. Introduction

Among various subjects with respect to mechanical engineering, students can obtain especially important knowledge and skills in mechanical design and drawing. The knowledge and skills are also essential from a viewpoint of machine production. However, the education for design drafting is being given in insufficient time since its environment is inevitably limited due to drafting equipment. The fact has negative effect on improving the students' understanding. In addition, it is a considerable factor that students have to learn a wide range of knowledge and skills in mechanical design and drawing. From the backgrounds, the efficient learning environment has been desired to avoid a lack of knowledge and skills.

Meanwhile, various information technologies for education are being used to enhance the learning quality. Especially, e-learning has several merits. To name a few, we can learn what we want to know without any lecturer; the ubiquitous learning environment can be established using mobile devices; and a wide variety of learning contents can give us individual-oriented instructions. In creating a web learning environment, web design based on learning theory is expected for advancement of both learning motivation and efficiency.

In this study, a web environment to learn third angle projection method was created based on motivation-oriented teaching method. Then, it was introduced to the "basic drafting" classes held in our university. Subsequently, effectiveness of web learning was evaluated using a comparison of paper-based and web-based answers' results; moreover, the effect on learning motivation was quantitatively evaluated using the environment created in this study.

### 2. Construction of Web learning environment

ARCS model proposed by John Keller is one of the methods for instructional design improvable directly in learning motivation, and it has attracted the educational attention in recent years. Here, ARCS is an acronym standing for Attention, Relevance, Confidence, and Satisfaction. In the each factor, a motivation-oriented instruction and design procedure are proposed from a problem-solving perspective of learning motivation<sup>(1)</sup>.

On the other hand, Gagne's 9 events of instruction is well known as a beneficial method in instructional design. A learning process is classified into 9 events in the method, and learning effectiveness has been revealed using the method<sup>(2)</sup>.

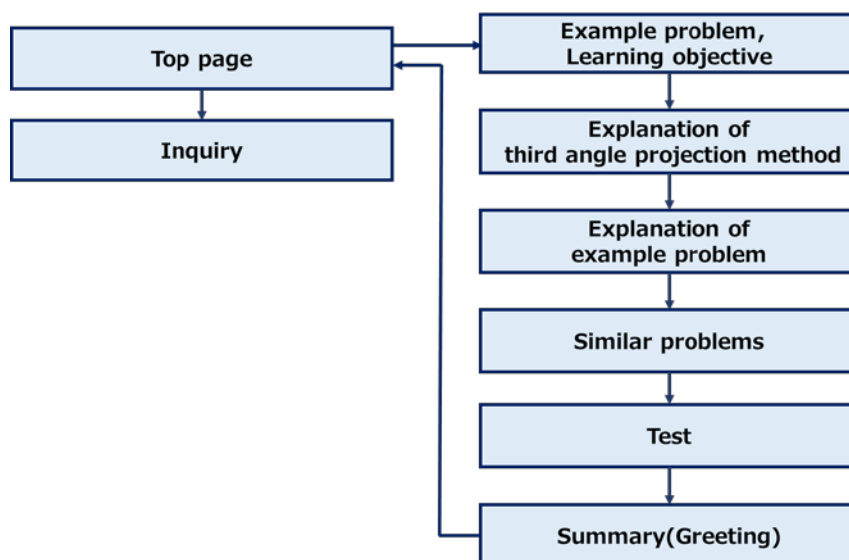


Fig. 1 The architecture of website

Figure 1 shows the architecture of website created in this study. This website is organized on the basis of both ARCS model and Gagne's 9 events of instruction<sup>(3)</sup>. Although this website was created in Japanese, the detailed explanation of web learning environment can be described as follows.

When a user access the website, top page is displayed as shown in Fig. 2. In the top page, we can check the overall structure of website with several hyperlinks. As helpful guidelines, the brief explanations are accompanied by each hyperlink. Example problem and learning objective are given as illustrated in Fig. 3. In this web page, we can specifically understand learning achievement points; moreover, next hyperlink is emerged at the bottom of this web page. When a user click the hyperlink, useful knowledge to solve the example problem is obtainable as shown in Fig. 4. With reference to a guideline on this page, we can go to the next web page. As expressed in

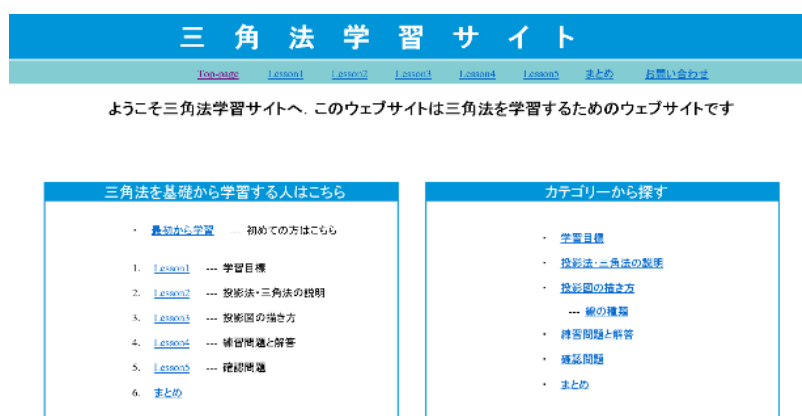


Fig. 2 Top page

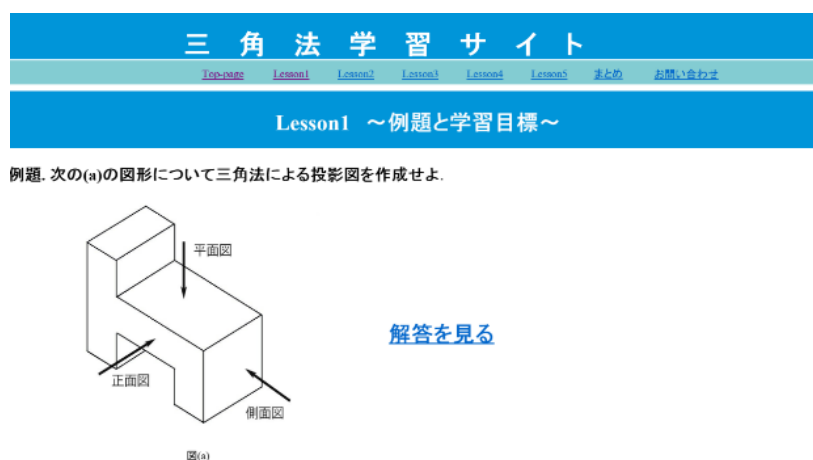


Fig. 3 Example problem and learning objective

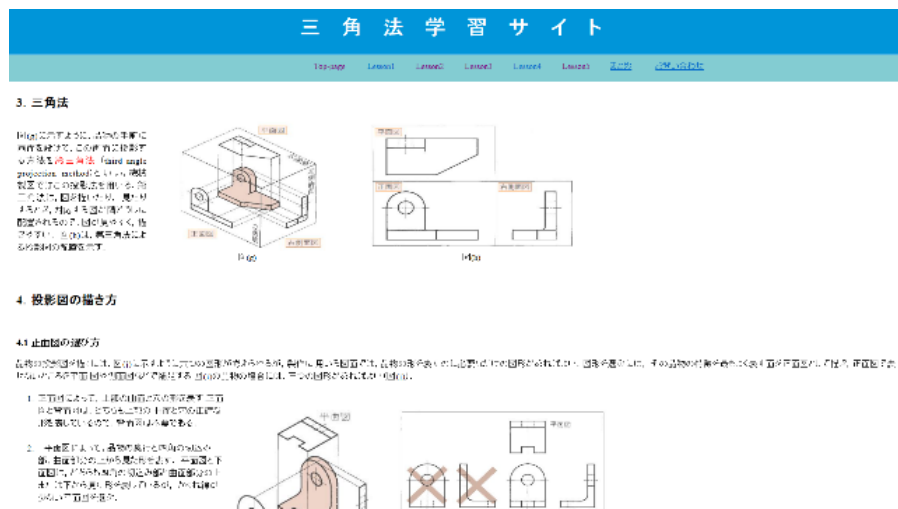


Fig. 4 Knowledge related to third angle projection method

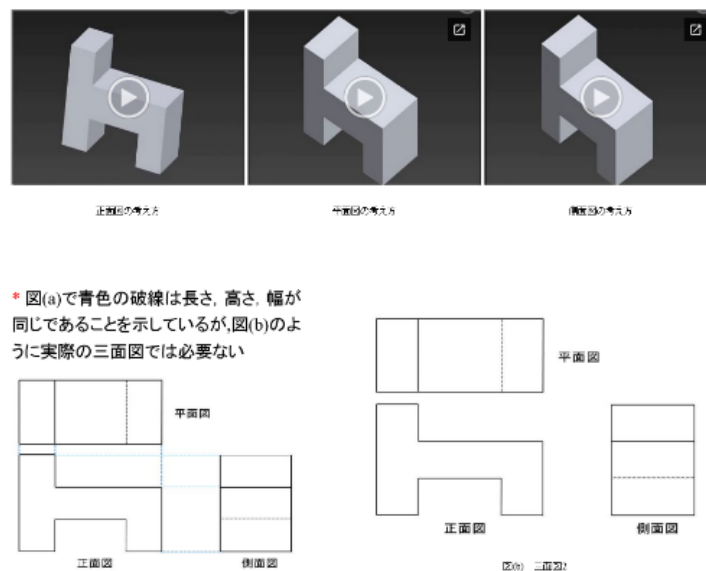


Fig. 5 Explanation of example problem

Fig. 5, this page explains example problems using suitable movies. Accordingly, a user can intuitively interpret essentials for problem-solving approach.

Then, the next page provides similar problems as shown in Fig. 6. For 3-view drawing based on third angle projection method, repetitive learning is practicable using this page. Finally, evaluation test explained in the following section is indicated on the next page. Figure 7 gives the visual image. In this page, the depth of understanding for third angle projection method can be verified after learning of the other pages. This evaluation test was used as a verification of web learning in a drafting class.

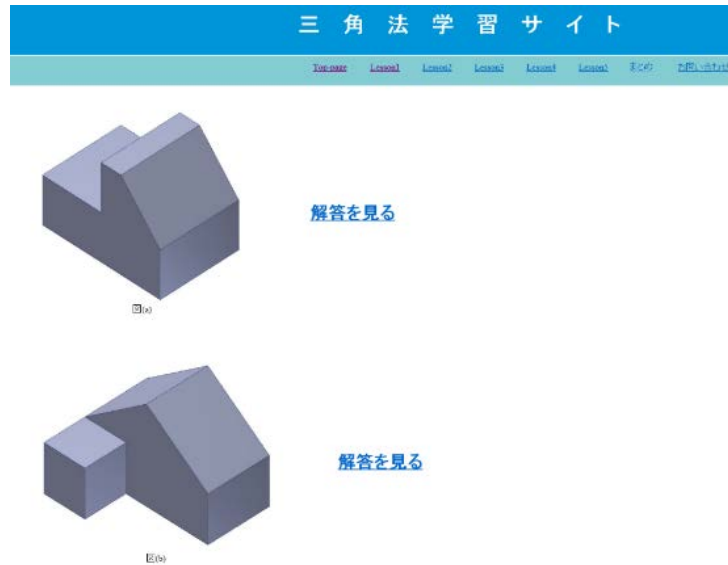


Fig. 6 Similar problems

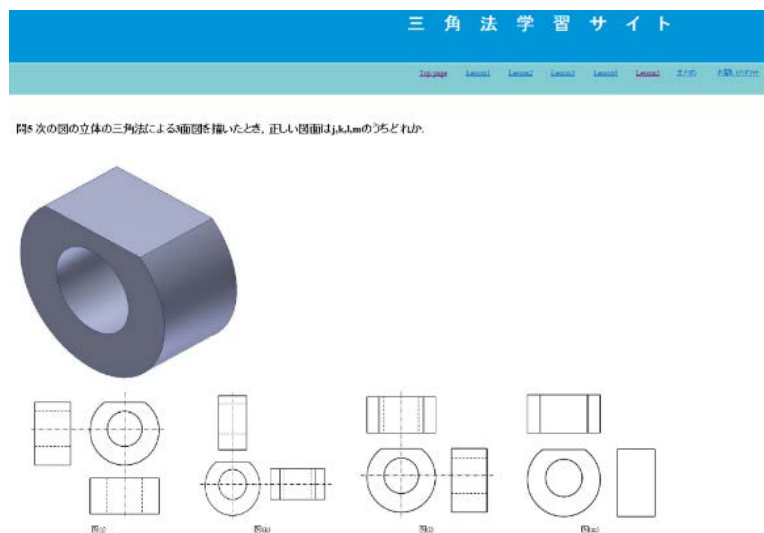


Fig. 7 Example test

### 3. Evaluation methodology

#### 3.1 Verification of web learning in a drafting class

In a drafting class, we carried out an evaluation test over the last two years. In the previous year, students took a paper-based evaluation test as shown in Fig. 8. In the test, students drafted a 3-view drawing based on third angle projection method. The handwriting drawings were used to evaluate the depth of understanding in third angle projection method.

In the current year, completely different students took an evaluation test through web learning environment. Figure 9 indicates an example of the test available anytime



and anywhere within a school term. In the current year, the answers for web test were also used to evaluate the depth of understanding in third angle projection method.

In the both years, we had students answer each test after the learning of third angle projection method in a drafting class. In the current year, students could additionally learn third angle projection method through web learning environment.

### 3.2 Evaluation of learning motivation

The influence of web learning environment on learning motivation was quantitatively investigated in this study. The evaluation test was performed for 10 students belonging to school of engineering in Tokai University. Their age was from 21 to 22 years old. In this test, university students were classified into two groups. One group can use web learning environment. After that, they take an evaluation test. In contrast, the other group take the same test without using web learning environment. In the evaluation test, the collaborators dealt with two types of problems regarding knowledge of third angle projection and drawing of three orthographic views. The drawing was expressed on a paper.

After the test, learning motivation was quantitatively investigated using ARCS evaluation sheet including 14 questions based on 4 ARCS factors. The questions were answered with rating on a scale of one to five. We had test collaborators answer the

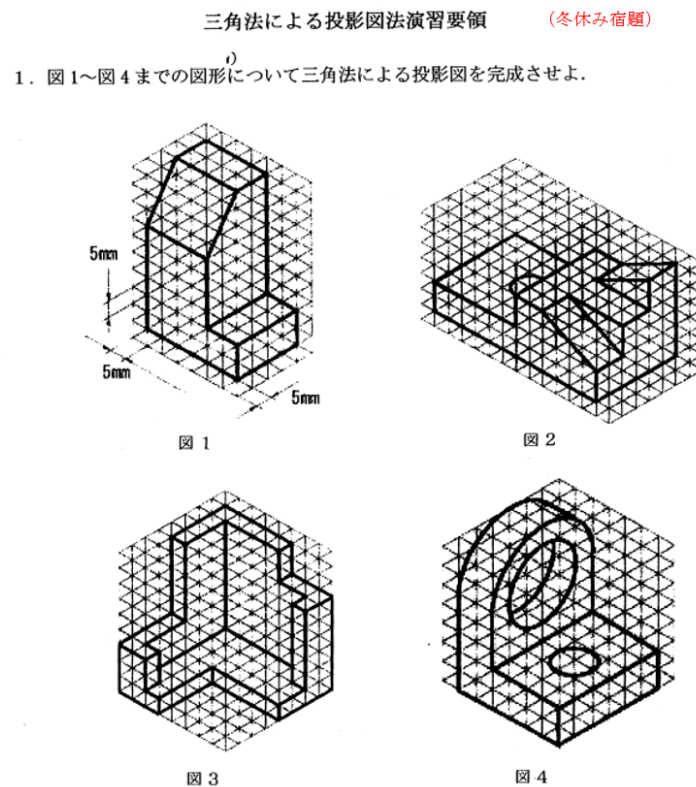


Fig. 8 Problems of evaluation test in previous year

問7 次の図の立体の三角法による面図を描いたとき、正しい図面はJ,K,L,mのうちどれか。

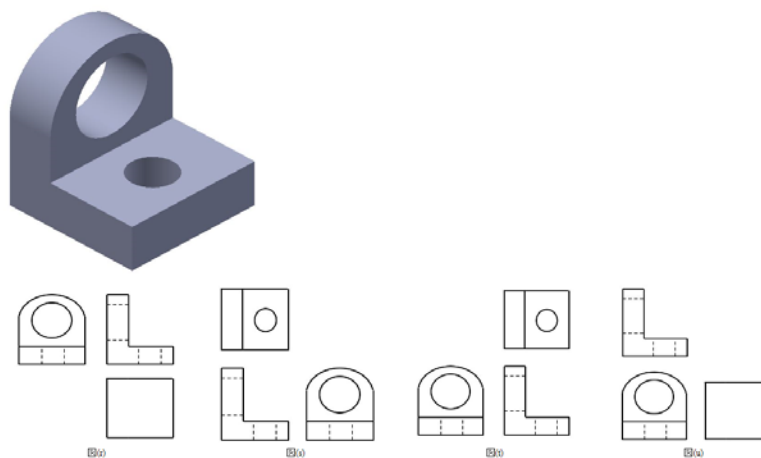


Fig. 9 Problems of evaluation test in current year

questions according to their impressions. Then, learning motivation was evaluated using average scores in each question<sup>(4)</sup>.

#### 4. Evaluation results and discussion

##### 4.1 Effectiveness of web learning in a drafting class

Table 1 shows a comparison of previous and current year's evaluation results. It is understandable that correct answer rate in current year is higher than that in previous year. This result suggests that there exists favorable effectiveness of web learning. However, it is conceivable that the difference may be caused from a change of answer format: paper-based or web-based answer format. We attempted to reveal the particular cause, and another evaluation test was carried out to investigate influence of web learning on learning motivation.

##### 4.2 Influence of web learning on learning motivation

Table 2 shows average scores resulted in the test using ARCS evaluation sheet. In table 2, the average score in all questions was 3.89 for the group using web learning environment. The standard deviation was 0.51. In contrast, the average score was 3.03 for the other group. The standard deviation was 0.59. The results indicated that the average score for the group using web learning environment was larger than that for the other group; moreover, the standard deviation for the former group had a smaller variation than that for the latter. From the results, web learning environment shows an effect on the enhancement of learning motivation. We can obviously interpret significant difference in three Attention-related factors. Accordingly, it was remarkable

Table 1 Correct answer rates of evaluation test

	Previous year	Current year
Correct answer rate	53.8%	87.6%
Number of subjects	146	108

Table 2 An itemized evaluation of learning motivation

Question	ARCS classification	Without web learning environment	With web learning environment
Q1	A : Attention	2.80	3.80
Q2	A : Perceptual evocation	4.40	4.60
Q3	A : Evocation of inquisitive mind	3.20	4.20
Q4	A : Variability	3.00	3.80
Q5	R : Relevance	3.00	4.20
Q6	R : Familiarity	2.40	3.40
Q7	R : conform with motivation	3.25	4.00
Q8	R : Purpose directivity	2.75	3.60
Q9	C : Confidence	1.75	3.00
Q10	C : Learning desire	3.25	4.60
Q11	C : Opportunity of success	3.50	4.00
Q12	C : Personalization of control	3.25	3.00
Q13	S : Satisfaction	2.75	4.40
Q14	S : Natural results	3.00	3.80

that Attention-related factors greatly contributed the enhancement of learning motivation. The several causes are considered as follows: web learning environment enables us to learn at their own pace; and the up-to-date way to learn mechanical design and drawing attracted the attentions of test collaborators. In addition, motivation-oriented teaching method provides a proper example in each problem. The way tends to activate collaborators' attention.

## 5. Summary

In this study, web learning environment was created on the basis of both ARCS model and Gagne's 9 events of instruction. The web learning was introduced in drafting class, and effectiveness of web learning was evaluated using a comparison of paper-based and web-based answers' results. Then, learning motivation was also assessed using ARCS evaluation sheet. As a result, there existed favorable effectiveness of web learning. In addition, it was remarkable that Attention-related factors greatly contributed the enhancement of learning motivation in web learning.

In the future work, an influence of web usability on drafting education will be investigated in detail since web usability is well known as one of the influential factors for learning motivation

## REFERENCES

- [1] Katsuaki Suzuki, 1995, On the Framework of Designing and Developing “appealing instruction” – The ARCS Motivational Model –, *The Japan Association for Educational Media Study*, 1(1), 55-61.
- [2] Katsuaki Suzuki, 2000, Gagne's 9 events of instruction, *Encyclopedia of educational technology*, Jikkyo Shuppan Co., Ltd., 221.
- [3] Wenyong Wang, Mitsuru Ikeda and Fengrong Li, 2007, Proposal and Evaluation of the “Motivational-Oriented” Teaching Method in Programming Education, *Japan Society for Educational Technology*, 31 (3), 221.
- [4] Chiharu KoGo and Katsuaki Suzuki, 1994, Making an Evaluation Sheet for Courses

## **A production-logistical evaluation approach for the planning and control of demand fluctuations**

Maurice Schmidt<sup>a\*</sup>, Peter Nyhuis<sup>a</sup>

<sup>a</sup>Institution of Production Systems and Logistics, Leibniz Universität Hannover,  
An der Universität 2, 30823 Garbsen, Germany

\*Corresponding Author: maurice.schmidt@ifa.uni-hannover.de

### **ABSTRACT**

Modern production companies are facing increasingly volatile markets and therefore fluctuating demand. In order to master these fluctuations, measures of production planning and control are usually used. However, the usage often takes place without established clarity about effect and contexts of these measures. This paper presents fundamentally relevant company characteristics as well as distinguishing marks in dealing with demand fluctuations. Subsequently, an approach for timed, performance-oriented and monetary evaluation is derived, which can be used to promote the selection of appropriate combinations of measures for the strategic compensation of these fluctuations.

**Keyword:** production planning, production control, demand fluctuation, measures

### **1. Current Situation and Challenges**

Due to short delivery times and flexible quantities required from production companies, production planning and control faces uncertainties in the prediction of customer demand. Therefore, the risks apply to the order situation of the company's own production as well as to the allocation of available capacities. Depending on the characteristics of a company, this challenge can be exacerbated. Companies whose product concept is characterized by product families have a higher ability to compensate than a one-off manufacturer. Furthermore, the position of the customer decoupling point in the value stream is of great importance. A company with a make-to-stock concept can dampen the fluctuation amplitude with its finished goods. This means, on the other hand, that companies with a make-to-order concept lack this possibility of damping and must directly counteract a fluctuating demand. Equally important is the process structure of machining and/or assembling of a the company. In productions, which are structured according to the flow principle, fluctuations often effect all interconnected capacities. In this respect, the manufacture with a workshop structure can be considered more robust, since the activities as well as their capacities are subject to a less fixed sequence. However, this distinction does not imply that the ability to react and respond adequately to demand fluctuations is of great importance

for all companies (Kersten, Seiter, von See, Hackius, & Maurer, 2017).

In theory, strategies can be found for the successful managing of demand fluctuations (cf. Wiendahl, 2006; Milberg, & Reinhart, 1999). There are approaches, which influence the purchasing behavior by incentive systems or self-induced fluctuations, for example by machine failures, with the help of operational measures. The focus of this paper is the planning and control of foreign-induced demand fluctuations in production. In practice, only a small part of possible measures is taken into account, and mainly those from the area of capacity adaption are used in a reactive manner. However, the possibility of a capacity adaption, for example by introducing weekend shifts or overtime, is limited. If the quantity of demand exceeds the capacity limits of the production system, companies miss significant potentials in terms of logistics performance and costs. If a strategic and process-oriented transformation of the production systems is not taken into account at an early stage, there is an additional risk. The adaptations that are progressing in small steps will solidify existing structures even more (Schmidt, & Nyhuis, 2017). Therefore, the goal in planning and control must be to use measures and combinations of measures that support the strategic orientation of the company and thus its positioning between the logistical goals of productivity and delivery reliability. For this purpose, a suitable evaluation approach is currently missing.

## 2. Basic Differentiations

While seasonal fluctuations can be relatively well-anticipated, intelligent decision-making mechanisms are required for more irregular fluctuations. Companies are confronted with the decision to cut loose their operating capacities from the characteristic of demand or to adjust continuously to fluctuating demand (see Figure 1) (cf. Gutenberg, 1971).

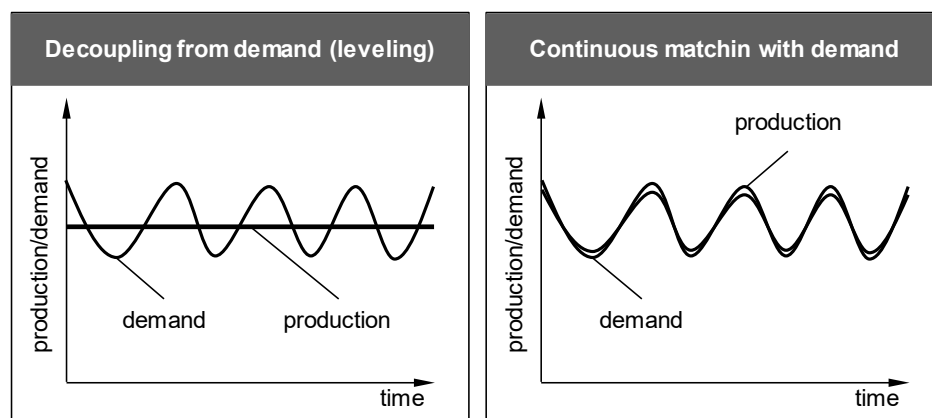


**Figure 1: Basic options for responding to demand fluctuations**

Two separate distinctions are necessary. The first differentiation has to be carried out with regard to the effect of the adaption: One possibility is the coordination of the load, more precisely the demand-induced volume fluctuation, by adapting it to the existing

capacities. This ability can be described as *load flexibility*. The alternative is the use of *capacity flexibility*, which describes the coordination of capacities aligned to a quantity demand (Lödding, 2013).

The second fundamental distinction is made with regard to the timing of the adaption. A change to a fixed date, which is compensated for at an earlier or later point in time within the same period of consideration, may be designated as a *levelling*. The average load or average capacity remains the same over the entire period under consideration. On the other hand, an *adjustment* is a quantitatively effective change, which can remain effective beyond the period considered (Schmidt, & Nyhuis, 2017).

In addition to these differentiations, a large number of measures can be identified. The *design areas of the production system* provide suitable support. *Organization, logistics, personnel* and *technology* can be used to deduce measures that are particularly suitable for the planning and control of demand fluctuations (see Table 1, Schmidt, & Nyhuis, 2017). Whether the acquisition of a facility, the hiring-up of an employee or the construction of working hours or stocks, these exemplary measures from the respective design fields provide opportunities to achieve the required capacity and/or comply the time requirements.

### 3. Approach of a timed evaluation of measures

In the context of demand fluctuations, the attainment of a high-level logistics performance is one of the essential challenges and at the same time one of the objectives that must be taken into account in a production-logistic evaluation approach. The logistics performance describes the ability to fulfill orders within the agreed (short) *delivery time* and with a high *delivery reliability* (Wiendahl, Lödding, & Schneider, 2002).

The delivery time corresponds to the time duration between order receipt and delivery (Wiendahl, Nyhuis, & Helms, 1997). In particular, short delivery times are of great strategic importance for SMEs, as they enable to increase prices and thus sales, but especially to ensure competitiveness. The effects are all the more serious if delivery times are prolonged due to strong demand fluctuations.

Delivery reliability corresponds in turn to the relative proportion of orders delivered to a pre-agreed delivery date or within an agreed delivery period (calendar week e.g.). The following formula can be used for determination:

$$LT = \frac{Auf_m - Auf_n}{Auf_m} * 100 \quad (1)$$

with

LT            delivery reliability [%]

Auf <sub>m</sub>	numbers of all orders [-]
Auf <sub>n</sub>	numbers of all orders with unacceptable LTA [-]
LTA	delivery deviation [TU]

The term delivery date itself is differentiated between the customer's desired delivery date, the customer's agreed delivery date, and the scheduled delivery schedule for the production (Lödding, 2013). A fluctuating demand can have a negative impact on these dates. Assuming rigid capacities, existing capacity limits can be reached (or exceeded) easily by strongly positive fluctuating demand. After exceeding the performance maximum, the orders accumulate in a queue, which means that the actual output deviate from the assigned or planned output and thus the delivery dates are missed. Known approaches have deeply illuminated this in the past (Nyhuis, & Wiendahl, 2009).

A known approach to estimate the necessary capacity beforehand is the determination of the planning backlog. The backlog is determined from the difference between the desired and planned output, and is suitable for the planned and actual output as well. The following formulas can be used to describe this connectedness:

$$RS_{planning}(t) = AB_{Wunsch}(t) - AB_{Plan}(t) \quad \wedge \quad RS_{control}(t) = AB_{Plan}(t) - AB_{Ist}(t) \quad (2)$$

with

RS	backlog [TU]
AB <sub>Wunsch</sub>	desired output [TU]
AB <sub>Plan</sub>	planned output [TU]
AB <sub>Ist</sub>	actual output [TU]

Suitable measures should allow adequate compensation for this planning backlog in the case of described fluctuations. In this context, adequate compensation means that there is no long-term backlog in production due to a fluctuating planned or actual output (see Figure 2).

For this purpose, it is necessary to identify the influence of the measures on the planned and actual output in production. Therefore, measures can be assigned to the functions of the Hanoverian supply chain model (see Table 1).



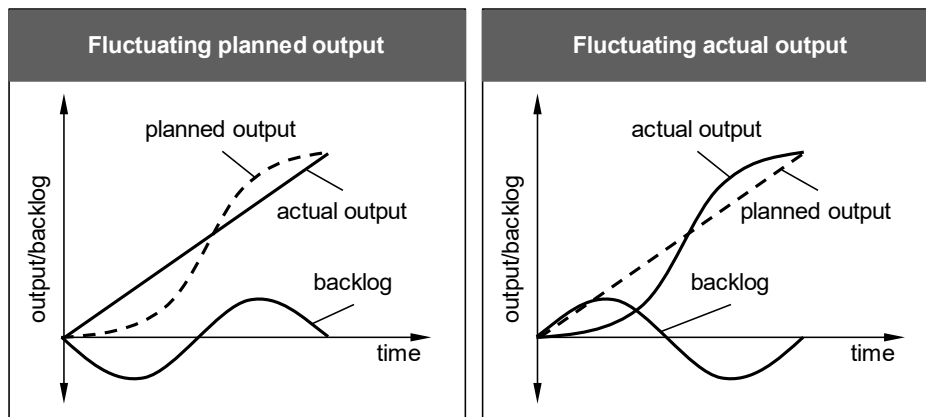


**Figure 2: Situations of fluctuating exits as a cause of residue in production**

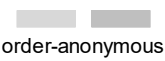

The Hanoverian supply chain model addresses the production planning processes; more precisely with production program planning, production requirements planning, as well as production planning and control (Schmidt, & Schäfers, 2017). Within these functions, the prerequisites are created for a (customer) order fulfilling the customer's request according to the deadline. In general, this also applies if there are no (customer-specific) orders in the stock.

In the long term, the *production program planning* deals with the definition of the order-anonymous planned output of work systems and thus with the anticipated capacity requirements. In this context, it is a rough feasibility check and the basis for any investment decisions, which are may be necessary in terms of new facilities (e.g.). At an early stage, it also shows whether an *up- or downsizing of permanent personnel*<sup>1</sup> is required. In order to dampen the fluctuations in demand, the strategic positioning and design of stocks is another way of levelling loads and thus mitigating the effects on production. The extended form of load levelling is the load adjustment, in which demand options can be outsourced or insourced in order to level the production program on an anonymous basis.

Within the scope of *production requirements planning*, capacity planning is carried out based on ascertained and scheduled production orders. At this time, there is still the possibility to make long- to medium-term decisions regarding capacities, for example by using temporary staff or short-time work. The alternative is also a load levelling. Thereto, demands can be merged to lots and/or demand dates can be moved. This can lead to the result that the internal planning backlog (planned to actual output) is reduced to the detriment of the external planning backlog (desired to planned output). At the same time, it is also possible to consider the purchase of certain shares of an order in terms of an operational load adjustment.

<sup>1</sup> see Table 1

**Table 1: Measures of planning and control to manage demand fluctuations**

Function	Capacity synchronization		Load synchronization	
	Capacity adjustment	Capacity levelling	Load levelling	Load adjustment
<b>Production program planning</b>	<ul style="list-style-type: none"> <li>• Purchase or dispose of manual to fully-automated systems</li> <li>• Modular expansion or demolition of scalable systems</li> <li>• Mechanization to full automation of processes</li> <li>• Up- or downsizing of permanent staff</li> </ul>	Currently no measures	Build-up or -down of raw material-, semi-finished- and finished goods stock	Outsourcing or insourcing of demand quantities (order-anonymous)
<b>Production requirements planning</b>	<ul style="list-style-type: none"> <li>• Increase or decrease the operating days</li> <li>• Leasing or rental of manual to fully-automated systems</li> <li>• Upsizing of temporary staff</li> <li>• Use of temporary or short-time work</li> </ul>	Currently no measures	<ul style="list-style-type: none"> <li>• Division or merging of required demand quantities</li> <li>• Advance or deferment of demand quantities</li> </ul>	Outsourcing or insourcing of demand quantities (order-related)
<b>Production planning</b>	<ul style="list-style-type: none"> <li>• Commissioning or decommissioning of facilities</li> <li>• Extension or reduction of the number of shifts</li> </ul>	<ul style="list-style-type: none"> <li>• Internal exchange of staff</li> <li>• Internal deployment of personnel (medium-term)</li> </ul>	<ul style="list-style-type: none"> <li>• Relocation of demand quantities to alternative facilities</li> <li>• Relocation of demand quantities to alternative personnel</li> </ul>	<b>Order reference:</b>  order-anonymous  order-related
<b>Production control</b>	<ul style="list-style-type: none"> <li>• Extension or shortening of shifts</li> <li>• Set-up of paid overtime</li> </ul>	<ul style="list-style-type: none"> <li>• Internal deployment of personnel (short-term)</li> <li>• Up- or downsizing flexible overtime</li> </ul>	<ul style="list-style-type: none"> <li>• Shortening or extending of occupancy time</li> <li>• Shortening or extending execution time</li> </ul>	

The *production planning* deals with the requirements that are effectively passed on to the company's own production. At this point, demand fluctuations can be mitigated by organizational measures in the medium to short term. This means that existing, unused capacities (personnel and technology) are available but limited. In this case, facilities can be commissioned and thus a capacity adjustment can be achieved. However, a levelling of capacities or loads can be reached by its (temporal) reallocation.

The task of *production control* is actually to achieve the described planned output. This is done by defining the date of the order release (actual input) as well as the capacity control. In the short term the control decides on the use of capacities and thus on the actual output of orders. Thus, measures such as *paid* or *flexible overtime*<sup>2</sup>, use of stand-in<sup>3</sup>, as well as the change in intensity by *shortening the equipment scheduling time*<sup>2</sup> may directly affect a possible backlog and thus the delivery reliability. On a majority this measures work on the order-specific basis and can be seen as a reactive influence on demand fluctuations. Above all planning and control levels, the interaction of the measures has to ensure that the strategically important delivery times and/or their deviations are also at a low level, even with an above-average demand.

<sup>2</sup> see Table 1

<sup>3</sup> see Table 1: *Internal deployment of personnel (short-term)*

### 4. Approach for performance-oriented assessment of measures

In addition to the consideration of the logistics performance, the logistics costs are also crucial. Logistics costs are defined by the company's internal keys *work-in-process level* and *utilization*. It should be borne in mind that a terminated interpretation of the capacities at the maximum demand in periods of lower capacity requirements can lead to utilization losses and thus costs. If, on the other hand, the interpretation is based on the average value of the capacity requirement, the capacities are not sufficient to meet the demand in a timely manner, which can be sanctioned with penalties. In order to make it possible to determine the most effective measures and combinations of measures, it is necessary to assess the performance of those measures. It should be noted that, unlike the simplest assumption, capacities do not behave rigidly but depending on the time. Therefore, measures can only be used in a targeted manner if this temporal dependency is not neglected in the performance determination.

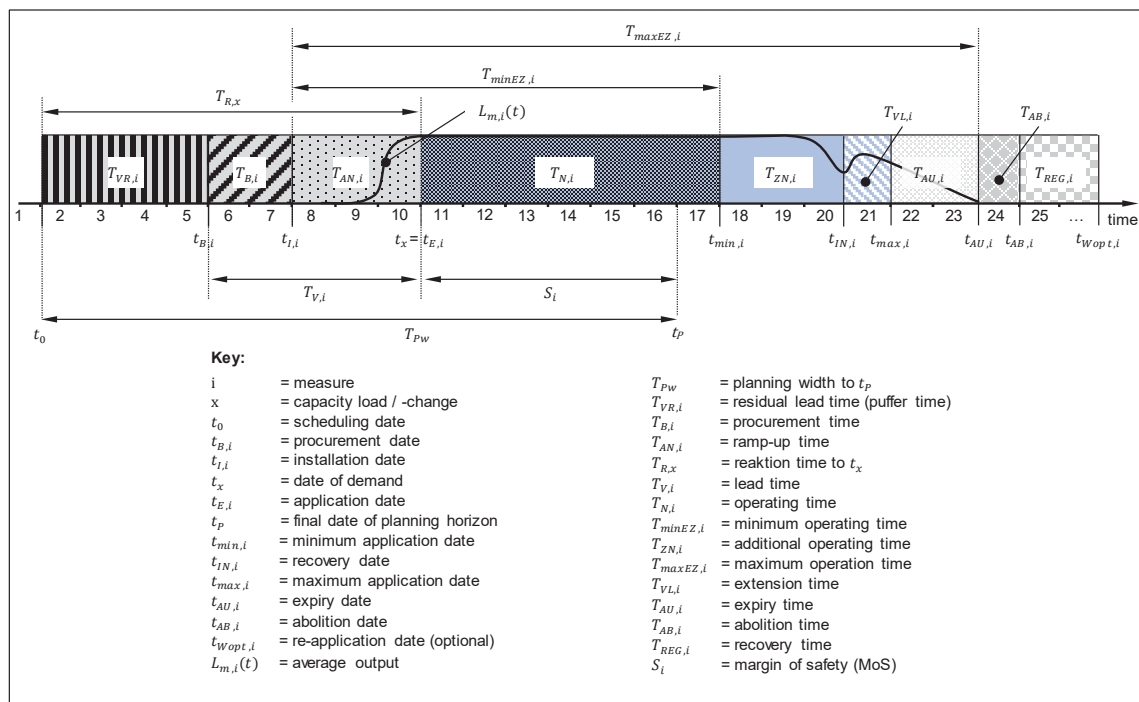


**Figure 3: Temporal approach to assess the performance of a measure**

With the help of the parameterization approach of a measure shown in Figure 3, it is possible to subdivide it into individual phases. This is particularly relevant for calculating its running time. Overall, all measures can be allot a lead-, ramp-up, operating, expiry, abolition and a regeneration time. Within the lead-time  $T_V$ , the procurement of a facility can be arranged. In this selected example, the ramp-up phase  $T_{AN}$  is necessary to install and commission the facility and thus decisive for the overall reaction time  $T_R$ , which is required to meet the demand fluctuation adequately.

In the ideal case, the measure act fully at the time of the load change and thus initialize its operating time  $T_N$ . By implication to the lead-time  $T_V$  and the ramp-up time  $T_{AN}$ ,

each measure has an expiry and abolish phase ( $T_{AU}$  and  $T_{AB}$ ), which sequences do not always have to proceed successively. At this time, it is already known that the use of the measure is not required anymore. In the example, it can be described by decommissioning and disposal of the facility. In addition, it is possible that certain measures require a regeneration time  $T_{REG}$  after use. This means that the reuse of the measure is correspondingly delayed and thus has to be included in the reaction time  $T_R$  already mentioned. Resting times for employees can exemplify that.

In addition to the determination of this temporal availability, this approach is a prerequisite for the determination of the average performance  $L_m$  of a measure. The performance of a measure is based on a quantity-time ratio. In practice, performance is often referred to as throughput or output (Lödding, 2013). However, the quantity data is often not sufficiently effective, since product concepts with product families in particular have a high variance in the resulting load. Therefore, the loads on the working systems are appropriately determined in the form of order hours and evaluated per time unit (operating calendar day e.g.).

As already mentioned in the introduction, the performance of a measure is dependent on the time phases shown. During the ramp-up time, it can be simplified to half of the performance maximum. On the assumption that a quantity-appropriate response to the demand fluctuation occurs, the performance of a measure in its operating phase corresponds to the maximum and leads to 100% utilization. In the expiry phase, the performance level falls correspondingly again. In principle, the assessment of the average utilization of each measure is possible as follows (cf. Nyhuis, & Wiendahl, 2009):

$$A_m(t) = \frac{L_m(t)}{L_{max}(t)} * 100 \quad (3)$$

with

$A_m(t)$  average utilization [%]

$L_m(t)$  average output rate [TU/TU]

$L_{max}(t)$  maximum possible output rate [TU/TU]

As in the ramp-up time, the speed of the performance change depends on the measure. For example, an installed machine can be decommissioned easily and thus the performance as well as the expiry phase can be reduced to a minimum. In this regard, measures from the design fields of organization or logistics can be considered as less quick-response.

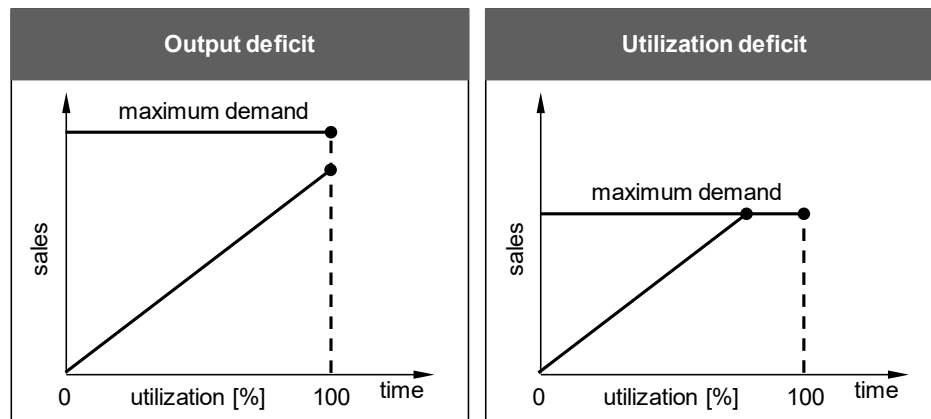


**Figure 4: Situations of fluctuating demand as a cause of output/utilization deficit**

### 5. Approach extension in terms of measure costs

To provide a practical decision-making aid, the utilization alone is not sufficient for the economic evaluation of measure actions. Therefore, an expansion of the performance-oriented approach is necessary. In dealing with demand fluctuations, the monetary expenditure is on the one hand for the performance cover, on the other hand for the adjustment and levelling of capacities or loads. The objective of cost modeling is to provide expected measure-specific costs. In terms of a general cost calculation, these can be shown as budget costs. In order to make budget accounting as effective as possible; the decision-relevant cost information must be limited. Therefore, both variable and fixed operating costs are taken into account by cost unit accounting and in the form of a full cost calculation. Since the construction of capacities is generally dependent on the strategic handling of demand fluctuations, a differentiation of direct and indirect costs is not relevant. The measures can be defined as individual cost centers. Since the frequency of their use can differ, the operating costs are allocated to individual demand situations. A performance allocation between two demand situations, for example by an internal deployment of personnel, is not required in the context of a holistic comparison.

Capacity adjustment or levelling with an organizational or logistical character can be taken into account as secondary costs and offset as extended operating costs. Monetary expenditures, which result from an under-compensation of the demand, such as the mentioned contractual penalties for delayed delivery delays, are added as a general cost charge proportional by the cost-by-cause-principle. In the end, a utilization-induced capacity deficiency can turn out as the more uneconomical result by additions, as a corresponding oversupply. Depending on the measure, this approach can be used to derive the step-fixed charge out rates over the expected demand.

In addition to the operating costs, necessary investments are also important when selecting the measures. For an evaluation over the entire planning horizon, the capital

value method with a uniform calculation interest rate is considered as suitable for the dynamic investment. The payment flows (for example, initial payments for the purchase of a facility<sup>4</sup>) are assessed over various periods until the end of the defined planning horizon. Together with the described charge out rates, the profitability of the use of measures can thus be determined and taken into account when identifying a suitable selection.

## 6. Conclusion and Outlook

Today's increasing volatility of the markets and the need of increasing flexibility, the consolidated consideration of production planning and control results in optimization potentials in production in terms of logistical performance and logistic costs. At the Institution of Production Systems and Logistics, a research project develops a decision-making aid for manufacturing companies to design and prepare production systems for the case of fluctuating demand. The approach shown for the timed, performance and monetary assessment of measures allows for a more accurate estimation of their effect and thus facilitates the selection of suitable combinations of measures. In order to provide an optimum combination, the measures will be interlinked in a decision tree in the near future. Only if the dependencies and restrictions of each measure are also considered, it will be possible to use them in a targeted way. On the one hand, this evaluation approach then offers a high potential to mitigate the target conflict between productivity and delivery reliability. On the other hand, it enables companies to counteract demand fluctuations strategically and thus economically as well.

## REFERENCES

- Gutenberg, E. 1971. Grundlagen der Betriebswirtschaftslehre. Band 2. Der Absatz. 12. Auflage. Berlin: Springer Verlag
- Kersten W., Seiter, M., von See, B., Hackius, N., Maurer, T. 2017. Trends und Strategien in Logistik und Supply Chain Management – Chancen der digitalen Transformation, Studie der Bundesvereinigung Logistik, Bremen
- Lödding, H. 2013. Handbook of manufacturing control - fundamentals, description, configuration. Springer, Heidelberg
- Milberg, J., Reinhart, G. 1999. Stückzahlflexible Montagesysteme: Lösungen für eine bedarfsgerechte Montage. München, München: Utz Verlag
- Nyhuis, P. 2006. Logistic production operating curves – basic model of the theory of logistic operating curves. CIRP Ann. Manuf. Technol. 55 (1), 441–444
- Nyhuis, P. 2007. Practical applications of logistic operating curves. CIRP Ann. Manuf. Technol. 56 (1), 483–486
- Nyhuis, P., Wiendahl, H.-P. 2009. Fundamentals of Production Logistics Theory, Tools

---

<sup>4</sup> see Table 1

and Applications, Berlin, Heidelberg: Springer Verlag

Schmidt, M., Nyhuis, P. 2016. Identification of Influencing Variables of Demand-oriented Measures for Volume Flexibility, *Universal Journal of Management* 4 (11), 601-606

Schmidt, M., Nyhuis, P. 2017. Wirtschaftliche Beherrschung von Nachfragemengenschwankungen in der Produktion, *ZWF Zeitschrift für wirtschaftlichen Fabrikbetrieb* Jahrg. 112 (5), 293-296

Schmidt, M., Schäfers, P. 2017. The Hanoverian Supply Chain Model: modelling the impact of production planning and control on a supply chain's logistic objectives, *Production Engineering*

Wiendahl, H.-P., Lödding, H., Schneider, M. (2002). Selected Strategies and Methods for Production Planning and Control, in: Prof. Pham (Ed.): *Springer Manufacturing Engineering Handbook* Springer Verlag

Wiendahl, H.-P., Nyhuis, P., Helms, K. (1997). Performance Measurement of the Procurement Process on the Basis of a New Characteristic Curve of Stock on Hand, in: *Production Engineering (Ann. of the German Academic Society for Production Engineering (WGP))*

## Synthesis of PA6 copolymer containing cyclohexane and aromatic group and their influence of properties

Chiu Chun Lai<sup>1\*</sup>, Shih You Chen<sup>2</sup>

<sup>1</sup>Department of Textile Engineering, Chinese Culture University, 55, Hwa Kang Road, Yang Ming Shan, Taipei, Taiwan, Republic of China

<sup>2</sup>Department of Chemical & Materials Engineering and Graduate Institute of Nanomaterials Chinese Culture University, 55, Hwa Kang Road, Yang Ming Shan, Taipei, Taiwan, Republic of China

\*Corresponding Author: lqj2@ulive.pccu.edu.tw

### ABSTRACT

This study investigates the physical properties of nylon 6 copolymerized with different types of diamines and acids. The polymer structured as different cyclohexane group, aromatic group, side chain, long aliphatic chain, para-benzoic group. The effects related to thermal property, mechanical property, water absorption and transparency were discussed. The alkyl chain length of diacid affected the crystallization, tensile strength and water absorption greatly. The number of cyclohexane group and benzoic group number had more influence than para-structure. The PA6 containing long alkyl chain and double cyclohexane structure had lower crystallization,  $T_m$ ,  $\Delta H$ , water absorption, tensile strength and transparency as enhancing composition ratio. It had great Transparency and tensile strength balance at copolymerization ratio of 5% and 7%.

**Keyword:** nylon 6, diamines, thermal property, mechanical property, crystallization.



## Production and Characterization of Biodegradable Plastic from Nigeria Cassava Starch

**Elizabeth J. Eterigho<sup>a\*</sup>, T. S. Farrow<sup>b</sup>, Ejejigbe Silver E<sup>c</sup>, and Ene C. Onaivi<sup>a</sup>**

<sup>a</sup> Chemical Engineering Department, Federal University of Technology,  
Minna, Niger State, Nigeria

<sup>c</sup> Chemical and Petroleum Engineering, Niger Delta University  
Wilberforce Island, Bayelsa State, Nigeria

<sup>e</sup> 8 Elem close off Rumuibekwe Road, Rumurolu Port Harcourt  
River State, Nigeria

*\*Corresponding author. Email: [jummyeterigho@futminna.edu.ng](mailto:jummyeterigho@futminna.edu.ng)*

### ABSTRACT

The use of synthetic polymer in the industries and household packaging for various purposes has increased, however, it possesses environmental challenge due to its non-degradability. This research therefore focused on the production of a biodegradable plastic by blending various composition of poly vinyl alcohol (PVA), additives and cassava starch. The product produced (plastic) were extruded, analysed and tested for biodegradability under natural conditions. The results obtained were compared with the conventional polymer. The density of the produced plastic was 0.83 Kg/m<sup>3</sup>, melting temperature was 200°C and its water adsorption rate was 1.3% per day. The tensile strength was 23.63N/mm<sup>2</sup> compared to 10.86N/mm<sup>2</sup> and 8.29N/mm<sup>2</sup> for polyethene and paper respectively. The results showed excellent retention of physical, thermal, structural and mechanical property required in plastics. Thus, indicating the possibility of universal application of Nigeria cassava starch as a source of biodegradable agent in plastic films production.

**Keywords:** biodegradability, cassava starch, plastics films, plasticizers.

### 1.0 Introduction

Packaging using plastic materials has rapidly increased in recent times. Its use covers a wide area of application from automobile parts, food, drinks, water, snacks, cloths, fresh and sea foods, farm products, medicals and pharmaceuticals, to mention but a few. The use of such bombastic amount of schematic plastics and its advantage over other packaging materials is due to its diverse and advance properties of longevity. The properties include resistance to chemical reaction, thermal strength, mechanical and its tensile strength, especially enzymatic reactions (Ezeoha and Ezenwanne, 2013.). For example, it will take a very long time say a hundred years to degrade just a piece of plastic film (polyethene) used to package snacks (gala) at standard environmental conditions. There is basically, two problems associated with the use of synthetic polymer plastics for packaging since its invention in the 1930s: They are: dependence on petroleum and the problem of waste disposal. Most of today's conventional synthetic polymers are produced from petrochemicals and are not biodegradable. These stable polymers are a significant source of environmental pollution, harmful to organic nature when they are dispersed in the environment. The raw materials such as fossil fuel and gas could be replaced by greener agricultural sources, which contribute to the reduction

of CO<sub>2</sub> emissions (Narayan, 2001). Based on the above it becomes of value to produce plastics that are biodegradable. Over the past few years packaging suppliers have been introducing various forms of biodegradable plastics. Synthetic polymers cause changes to the carbon dioxide cycle, and are associated with increased toxic emission. The sources of synthetic polymers such as fossil fuel and gas are now of environmental concern. Researches on different methods of improving plastics that can be used more efficiently are on-going, such that they could be recycled, reused and possibly degrade after use. According to the Biodegradable Products Institute (BPI), a biodegradable plastic is one in which degradation results from the action of naturally occurring microorganisms such as bacteria, fungi or algae. Attention is towards greener agricultural sources, which also would lead to the reduction of CO<sub>2</sub> emissions (Narayan, 2001). Degradable plastics are classified by American Society for Testing and Materials (ASTM) into four categories, these are: - Photodegradable, Oxidative degradable, Hydrolytically degradable and Biodegradable Plastics. Biodegradable Plastics are degradable plastics in which the long chain polymer molecule breakdown into smaller or shorter lengths. It undergoes oxidation which is triggered by heat, ultraviolet light (UV light), and mechanical stress. It occurs in the presence of moisture and actions from naturally occurring microorganisms such as bacterial, fungi and algae. (ASTM Standards, 1998)

Starch has been discovered amongst all biopolymers as a high potential material for biodegradable films. Starch consists of two types of polysaccharides, amylose (10-20%) and amylopectin (80-90%) depending on the sucrose. The hydrophlicity of starch can be used to increase the biodegradability of starch-based plastics. Amylose is a linear molecule with a few branches, whereas amylopectin is a highly branched molecule. Therefore, amylose content is an important factor to biodegradable plastic film strength. Branched structure of amylopectin generally leads to film with low mechanical properties. To improve the flexibility of plastics, plasticizers are added to reduce internal hydrogen bond between polymer chains while increasing molecular space. The most commonly used starch plasticizers are polyols, sorbitol and glycerol. The main focus in biodegradability is that biopolymer materials breakdown into smaller compounds, either chemically or by organisms sooner than synthetic plastics (Bastioli, 2005.). Biodegradable packaging materials are materials that degrades back to the earth surface harmlessly when disposed. This helps largely in reducing the amount of packaging materials that goes back into landfills and in addition saves energy, as the biodegradable process does not require external energy. Biodegradable polymer sources are from agricultural feed stocks, animal sources, marine food processing industries waste, or microbial sources which are replaceable. In addition to its replaceability, biodegradable materials breakdown into environmental friendly products such; as carbon dioxide, water and quality compost. The market of biodegradable polymers at present is growing based on considerations that consumers and recycling regulations will drive demand for environmentally-friendly packaging. Some of the biodegradable polymers are already competitive alternatives to conventional food packaging. Polylactate (PLA) being one of the most important of such (Haugard and Martensen, 2003).

Biodegradation takes place in two-steps: degradation/defragmentation initiated by heat, moisture, or microbial enzymes, and second step – biodegradation – where the shorter carbon chains pass through the cell walls of the microbes and are used as an energy source. Biodegradable plastics are made from cellulose-based starch. Starch-based biopolymer, swells and deform when exposed to moisture, include amylose, hydroxyalkanoate (PHA), polyhydroxybuterate (PHB), and a copolymer of PHB and

valeric acid (PHB/V). These are made from lactic acid formed from microbial fermentation of starch derivatives, polylactide does not degrade when exposed to moisture (Auras *et al.*, 2007). Hydroxyalkanoate (PHA), polyhydroxybuterate (PHB), and a copolymer of PHB /valeric acid (PHB/V) are formed by bacterial actions on starch (Krochta, 1997). In addition, biodegradable films can also be produced from chitosan, which is derived from chitin of crustacean and insect exoskeletons. Chitin is a biopolymer similar to cellulose structure. There are various ways starch can be used for biodegradable polymer production; Starch content being more than half by mass of the plasticizers, Biodegradable polymers preparation using the extrusion process of mixtures of granular starch, Composition of starch with other plastics of low amount of starch to enhance the biodegradability of traditional based polymer materials. Synthetic polymers can also be made partially degradable by blending with biopolymers, incorporating biodegradable components such as starch, or by adding bioactive compounds. In this research corn starch was used as an agent of biodegradability. Starch is inexpensive and abundant in nature, Nigeria being the world largest producer of cassava (FAO, 2009) and being a root crop that can be grown in every part of the nation, Starch is totally biodegradable in a wide range of environments and can be used in the development of biodegradable packaging products for various market uses.

The aim of this research is to produce biodegradable plastic films from cassava starch used in food packaging, using various additives and plasticizers.

## 2.0 Methodology

Cassava tubers were obtained from local market in Nigeria. They were peeled and washed, followed by mechanical grating. The grated cassava was mixed with water in a ratio of 1:10. The mixture was sieved and filtered using a coarse sieve and filter cloth respectively. Thereafter, the filtrate was allowed to settle for eight hours. The resulting starch was mixed with water again and allowed to settle for twelve hours. This is called starch washing. The wet starch was dewatered and oven-dried (tray drying), at a temperature range of 80-150°C for 6 hours. The dried starch was sieved using sieve of mesh size "8". A mixture of 1kg powdered cassava starch, 2kg polyvinyl alcohol liquid (PVA), 100g talc powder, and 100g urea was prepared. The resulting mixture was stirred with 500ml of glycerin. The whole mixture was stirred to yield a semi dry powder. This mixture was prepared in two batches to aid effective mixing, each batch was manually stirred for four (4) hours, heated for three (3) minutes at temperature of 50°C. Then applied force in rolling little amount of the film to have a good surface area for drying and dried for five (5) hours in an oven of 80-150° range. The dried film was pelletized by reducing the size to a range of 2-5mm using an electronic crusher, to suite global specification of pelletized ethylene used in industries. The pelletized biodegradable film was tested in an extruder at 200°C. The following characterization were carried out: tensile strength, biodegradability, density, water adsorption and thermal property. Comparison of the biodegradable film was made with two other materials, namely paper and synthetic polythene films.

## 3.0 Results and Discussion

The moisture content of the cassava was reduced to 13% of the original moisture which is the universally acceptable value according to Ezenwane (2013). It was noticed that drying the film above 80°C, the film would become charred, noting that the glass transition temperature is greater than room temperature, and it is an indication that the plastic film produced was an elastomer (Akula, 2015). The tensile strength of the film

produced was compared with paper (its biodegrades) and polyethene (non-biodegradable). Tables 1 to 3 showed the result of the tensile strength of the biodegradable plastic, polyethene and paper respectively, presenting the forces applied and their extensions with the corresponding stress and strain calculated.

Table 1: Results of Tensile Strength for the Produced Biodegradable Plastic

Force, F (N)	Extension, Ext(mm)	Stress, $\delta = F/A$ (N/mm <sup>2</sup> )	Strain, $\epsilon = \text{Ext}/L(\text{m/m})$
0.00	0.00	0.00	0.00
5.00	0.20	12.50	2.00exp-3
6.30	0.26	15.75	2.60exp-3
7.88	2.14	19.70	2.14exp-2
9.45	5.02	23.63	5.02exp-2
9.45	8.33	23.63	8.33exp-2
9.45	11.85	23.63	1.19exp-1
9.45	16.61	23.63	1.66exp-1
9.45	22.45	23.63	2.25exp-1

Table 2: Results of Tensile Strength for Polyethene

Force, F (N)	Extension (mm)	Stress, $\delta = F/A$ (N/mm <sup>2</sup> )	Strain, $\epsilon = \text{Ext}/L(\text{mm/mm})$
0.00	0.00	0.00	0.00
1.58	0.78	5.45	7.80exp-3
3.15	2.75	10.86	2.80exp-2
3.15	6.25	10.86	6.30exp-2
3.15	8.00	10.86	8.00exp-2
3.15	10.75	10.86	1.08exp-1
3.15	16.50	10.86	1.65exp-1
3.15	20.50	10.86	2.05exp-1

Table 3: Results of Tensile for Paper

Force, F (N)	Extension, (mm)	Stress, $\delta = F/A$ (N/mm <sup>2</sup> )	Strain, $\epsilon = \text{Ext}/L(\text{m/m})$
0.00	0.00	0.00	0.00
3.15	1.00	8.29	1.0exp-2
3.15	2.00	8.29	2.00exp-2
3.15	2.88	8.29	2.88exp-2

From the tensile strength result it can be deduced that the biodegradable plastic produced has the highest tensile strength of 23.63 N/mm<sup>2</sup> and this could be as a result of the plasticiser used (glycerol) in the production of the plastic. This was added to improve the workability/mechanical property of the polymer (Akula, 2015). The strength was much higher than that of the paper (8.29 N/mm<sup>2</sup>) and the polyethene (10.86 N/mm<sup>2</sup>) materials. Paper which has the least tensile strength failed the force applied within a very short time. Figure 1 shows a comparative chart of the tensile strength of biodegradable plastic, polyethene, and paper. From the graph, the tensile

strength (i.e. stress- strain ratio “young modulus”) of the biodegradable plastic is higher than that of conventional polyethene and paper. The gap between the two materials are very dissimilar, although the strain is approximately same for polyethene and bio plastic but the stress is not. Paper has the least stress- strain ratio. This is the point at which the material can no longer retain its plastic property. Any point at which there is a constant stress the material has the tendency of breaking.

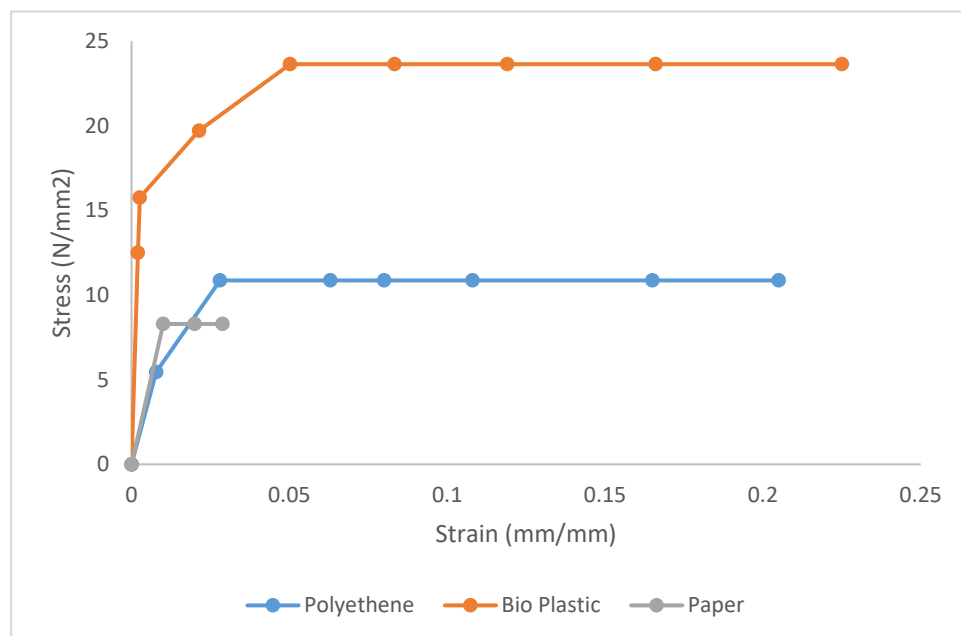


Figure 1: comparative chart of the tensile strength of the three materials (biodegradable plastic, polyethene, and paper)

In the case of water absorption, the produced biodegradable plastic absorbed 1.3% of its original weight after 24 hours which is the acceptable maximum water adsorption for plastic materials ([www.scientificamerican.com](http://www.scientificamerican.com)). This is yet another prove that the produced biodegradable plastic has good moisture resistance. The density of the produced biodegradable plastic was found to be 0.833g/ml indicating a low-density polyethene (LDPE). The scanning electron microscope (SEM) of the produced biodegradable plastic revealed a polymer material, fibre-like structure bounded around amorphous structure. The SEM also showed spaces in-between the polymer produced; meaning it was not totally compact. This would give room for actions of microorganisms to act on them at any chance of interaction with microorganisms. From the organic matter content, paper had the highest organic carbon content of 82.55% no wonder its biodegradation is within 2-5months in accordance to Mobley (1994). It was followed by the produced biodegradable plastic with 61% organic matter content. This showed a good tendency for microorganisms to mineralise and fragmentise the plastic which is the target of biodegradability. The conventional polyethene material had the least organic matter content of 18.22%. This makes polyethene material non-biodegradable. The results of the burying test of the materials are given in Table 4. It was observed that after 7 days, the produced biodegradable plastics had increased form 5.20g to 6.10g.

Table 4. Biodegradable Test Result of the Materials Used

Sample (g)	Initial sample weight (g)	Weight after 7 days (g)	Weight after 14 days (g)	Weight after 21 days (g)
Plastic	11.30	-	-	
A	5.20	6.10	-	
B	5.40	-	5.32	
C	15.30	-	-	15.28

This is one of the actions of the microorganisms on the biodegradable plastic and created pore spaces for the plastic to adsorb moisture from the compost soil and resulted to the increase in weight. The colour still remained unchanged however, the plastic had swollen and little deformation was noticed in the structure of the biodegradable plastic. One of the proves of biodegradability is the swelling of the material (Hans, 2009). After 14 days, the sample showed little green colour, an effect of algae on the biodegradable plastic, reduction in the compatibility of the material.

#### 4.0 Conclusion

Without question, the challenges surrounding plastics waste treatment are multifaceted and complex as numerous studies have indicated, and are further being compounded as time progresses. It could be concluded from the results obtained in the research that the production of biodegradable plastic from cassava starch is viable as revealed in the various biodegradability tests. The total carbon content was found to be 61% against 18.22% of conventional synthetic plastic. The introduction of biodegradable plastic into the world market would over time, replace the conventional polymers, and eradicate the world environmental challenge generated from the use of conventional synthetic polymers. The properties; strength, strain, elongation and toughness of the biodegradable plastic produced were excellent in comparison with synthetic polymers. Hence, the production of biodegradable plastic product is as useful as the conventional plastic with lesser menace to the environment.

#### REFERENCES

- Bastilo E. R., Tuzlakoglu K., Marques A. P., Azevedo H. S., Reis R. L. (2008). A novel enzymatically-mediated drug delivery carrier for bone tissue engineering applications: Combining biodegradable starch-based microparticles and differentiation agents. *Journal of Material Science: Materials in Medicine*, 19, 1617–1623.
- Cao X., Chen Y., Chang P. R., Cerede Muir A. D., Falk G. (2008). Starch-based nanocomposites reinforced with flax cellulose nanocrystals. *Express Polymer Letters*, 2, 502–510.
- Ezeoha S. L. And Ezenwanne J. N. (2013) Production of Biodegradable Plastic Packaging Film from Cassava Starch. *IOSR Journal of Engineering*
- Hans, G.B. (2002). Biodegradable Plastics – Developments and Environmental Impacts. Australia: Nolan-ITU Pty Ltd, Prepared in association with Excel Plas Australia, Department of Environment and Heritage.
- Haugard G, Martensen, Zhan F., Wu L. (2005). Preparation and properties of a slow-release membrane-encapsulated urea fertilizer with superabsorbent and moisture preservation. *Industrial and Engineering Chemistry Research*, 44, 4206–4211
- Krochta R.A., Harayama S. (2000). Biodegradation of High-Molecular-Weight Polycyclic Aromatic Hydrocarbons by Bacteria. *Journal of Bacteriology*. 8, 2059

Mendes S. C., Reis R. L., Bovell Y. P., Cunha A. M., van Blitterswijk C. A., de Bruijn J. D. (2001). Biocompatibility testing of novel starch-based materials with potential application in orthopaedic surgery: A preliminary study. *Biomaterials*, 22, 2057–2064.

Narayan, R. (1997). *Commercialising Technology: From Laboratory to the Marketplace – A Case Study of Starch-based Biodegradable Plastics Technology*. Department of Chemical Engineering, Michigan State University.

Robert, O. Ebewele (2000) *Polymer Science and Technology*, University of Benin, CRC. BOCA, Network, pp. 14- 243.

[www.scientificamerican.com](http://www.scientificamerican.com) accessed 15<sup>th</sup> March, 2017



ISOLATION AND IDENTIFICATION OF JELLYFISH ALKALOID (*Bougainvillia sp*) AS IMUNOSTIMULANT TO PROTEIN PROFILE AND HISTOPATHOLOGY OF TIGER GROUPER LIVER (*Epinephelus fuscoguttatus*)

Sri Andayani<sup>1)</sup>, M.Fadjar<sup>1)</sup>, M.Farid Rahman<sup>2)</sup>

<sup>1)</sup> Faculty of Fisheries and Marine Sciences, UB Malang Indonesia.

<sup>2)</sup> Laboratory of Organic Chemistry from Science Faculty, University of Brawijaya  
Veteran street, Malang -Indonesia

Corresponding author : srianday\_08@yahoo.com

### Abstract

The study was aimed to (1) isolate and identify jellyfish alkaloids using Thin Layer Chromatography (TLC), Ultraviolet (UV) spectroscopy, Infrared (IR) and Hydrogen-Nuclear Magnetic Resonance (<sup>1</sup>H-NMR) methods (2) protein profiles and (3) the histopathology of tiger grouper (*Epinephelus fuscoguttatus*) liver. This research was experimental method with Completely Randomized Design (RAL). Using alkaloid on 1 and 7 days with bath immersion for 1 hour, then it was challenging test with *Vibrio harveyi* of 10<sup>5</sup> cfu/ml bathing for 7 days. There were 5 treatments and 2 replications as follows: A = 6.4 ppm: B = 8.4 ppm: C = 10.4 ppm, D = 12.4 ppm and Control = 0 ppm. Blood plasma taking for protein profile and liver for histopathology was performed after giving immunostimulants and after infection. The results of the study were: (1) alkaloid characteristic was N-1 Benzylalcohol, 4-Ocilli Piperidine) (2) protein profile after immunostimulant addition resulted in 8 bands and sample after infection, it appeared 10 protein bands (3) Result of the best alkaloids in the treatment of C dose 10.4 ppm alkaloids, was a minor damage to liver tissue including inflammation, *Hemorrhagic* and necrosis. It is suggested for the future researchers to use dose of 10.4 ppm alkaloid through the immersion because it can increase non-specific immunity through protein profile and minor damage to liver histopathology.

Key words : isolation and identification of jellyfish alkaloid, immunostimulant, protein profile, liver histopathology, *Vibrio harveyi* infected

## 1.INTRODUCTION

The intensification of grouper culture has led to a number of disease outbreaks with an increasing range of pathogens causing them. Vibriosis, a common disease caused by *Vibrio carchariae*, *Vibrio alginolyticus*, *Vibrio parahaemolyticus*, *Vibrio harveyi* and is one of the most serious problems in various stages of grouper culture. fish farming is the mortality rate of the seeds up to 99% which mainly caused by pathogenic bacteria infection (Hariskrishnan *et al.*, 2011) .

The Rate of *Vibrio harveyi* outbreak in tiger grouper hatchery fish can be calculated within a few hours. *Vibrio sp* attack can lead to the destruction of organs in fish, and the wounds on the skin (Moriarty, 1997). To control the disease, particularly bacterial diseases, various types of antibiotics have been used such as chloramphenicol, and erythromycin and oxytracycline. But apparently a lot of antibiotics raise the resistance of new bacteria strains in the response to disease (Hariskrisnan *et al.*, 2010 ; Hameed, *et al.*, 2003). Thus it is necessary to control the disease using natural



materials, which are still limited to saponins and rotenon, so it needs a new break through in the utilization of jellyfish that are environmentally friendly as immunostimulants (Hariskrisnan *et al.*, 2010 ; Sakai, 1999).

Based on previous findings, it is necessary to explore unconventional natural resources in order to get the benefits of bioactive compounds from the jellyfish as immunostimulant, particularly for tiger grouper seed. it can increase non-specific immunity through protein profile and minor damage to liver histopathology.

## 2 METHOD

Extraction of jellyfish (*Bougainvilliasp*) alkaloids using the modified method of Maldoni (1991). The extract was centrifuged and the supernatant was analyzed Thin Layer Chromatography (TLC), UV Spectrophotometer, Irradiated Red (IR) and Hydrogen Nuclear Magnetic Resonance (<sup>1</sup>H-NMR).

The method used in this research was experimental method with Completely Randomized Design (RAL). Using alkaloid on 1 and 7 days with bath immersion for 1 hour, then it was challenging test with *Vibrio harveyi* of 10<sup>5</sup> cfu/ml bathing for 7 days. There were 5 treatments and 2 replications as follows: A = 6.4 ppm: B = 8.4 ppm: C = 10.4 ppm, D = 12.4 ppm and Control = 0 ppm, The tested fish used were Tiger grouper (*Epinephelus fuscoguttatus*) 7-8 cm in size at the age of D 90. The fish was kept in a glass tank with a volume of 15 liters (5 levels of treatment), with the density of 10 fish per tank. Blood plasma taking for protein profile was performed after giving immunostimulant on Day 7 and after Day 9 of infection, then it was analyzed using electrophoresis method (SDS-PAGE). The liver sample for histopathology was taken after day 8 of immunostimulant and after infection bacterial on Day 15. The preparation of liver histology used Lightner (1996) methods.

## 3.RESULTS

### 3.1. Characterization of alkaloids *Bougainvillia sp*

The result of analysis with a spectrophotometer H<sup>1</sup>-NMR spectrum supported by ultraviolet (UV) and infra-red spectrum (IR), the molecular structure of the alkaloid contained in the chloroform extract ( is shown in Figure 1.

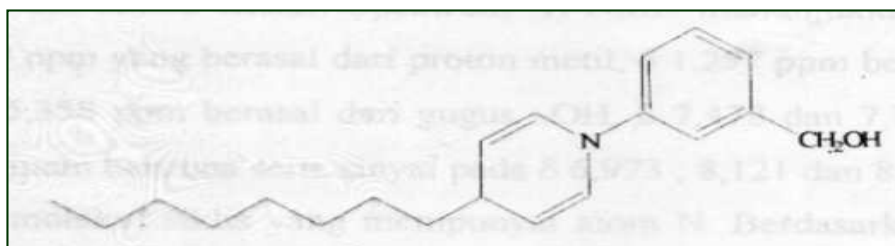


Figure 1. Chemical Structure of alkaloid substance from *Bougainvillia sp*. (N-1 – Benzilalkohol, 4 – Oktil Piperidin)

### 3.2 Electrophoresis of Plasma protein

Result of electrophoresis of plasma protein of tiger grouper is described in figure 2.

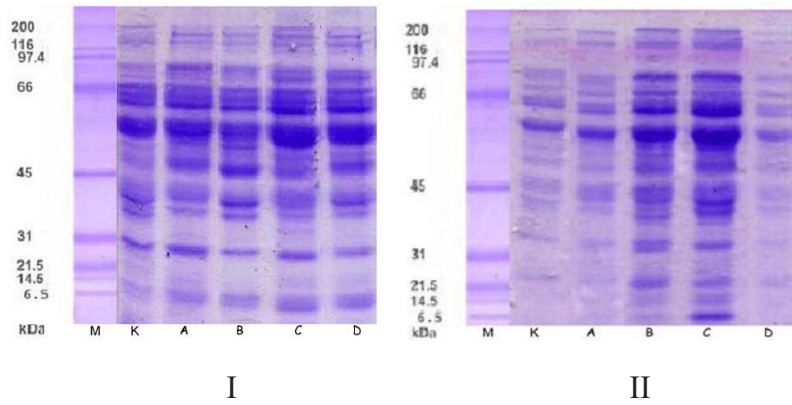


Fig.2. Profiles of plasma proteins of Grouper by SDS PAGE electrophoresis methods: (I) given immunostimulan (II) after infection, treatment with different doses of immunostimulant comprised: control K, treatment A, B, C and D in columns (2,3,4,5, 6), and (M = 1) kDa molecular weight marker.

### 3.3 Liver histopathology

Based on the results of the study, the condition of the tiger grouper's liver after being given an alkaloid immunostimulant showed a normal histological form with the appearance of the cell nucleus, hepatocyte cells, and sinusoids in the liver based on Setyowati *et al.*, (2010), After tested challenge with *Vibrio* liver damage liver damage such as inflammation, Hemorrhagic and Necrosis as Figure 3.

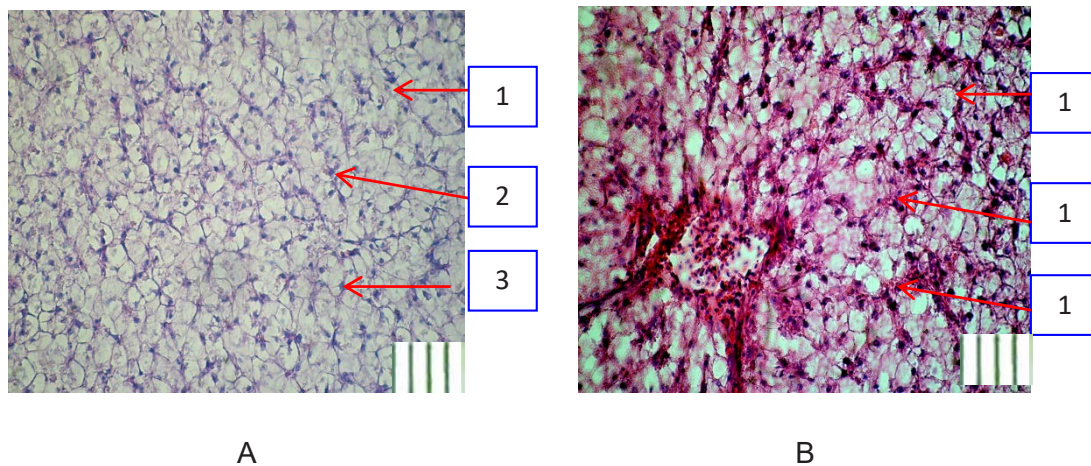


Figure 3. Normal cross section of the liver after an alkaloid immunostimulant consisting of (1) hepatocytes (2) Sinusoid (3) Cell nucleus, 400x HE (bar = 100 µm). (B) After tested challenge with *Vibrio* liver damage liver damage such as (1) Inflammation; (2) Hemorrhagic; (3) Necrosis 400 x HE, (bar = 100 µm).

## 4. DISCUSSION

The result of analysis with a spectrophotometer H'-NMR spectrum supported by ultraviolet (UV) and infra-red spectrum (IR), the molecular structure of the alkaloid contained in the chloroform extract from *Bougainvillia* sp. Is N-1 – Benzilalkohol, 4 – Oktil Piperidin. The alkaloid as immunostimulants are chemicals may increase the production of hydroxyl radicals which are supposed to kill *Vibrio harveyi*. Sahan and Duman, (2010) mentioned that as immunostimulants can activate fish

leukocytes cells to be more resistant to fungal, viruses and bacteria. microbial pathogens is a very important process in the mechanism of disease prevention. In addition, one of humoral defense mechanism indicator is the number of protein found in fish blood plasma increased by administering extracts of plants / animals (Dugency *et al.*, 2003). Plasma protein-containing alkaloids showed 8 bands including 149.28 kDa, 103.51 kDa, 83.95 kDa, 61.37 kDa, 44.87 kDa, 29.58 kDa, 19.50 kDa and 11.56 kDa. And after infected with *Vibrio harveyi* formed 10 bands of protein that is 154.52 kDa, 103.04 kDa, 84.33 kDa, 66.22 kDa, 49.88 kDa, 37.67 kDa, 25.18 kDa, 16.78 kDa, 14, 89 kDa, 12.67 kDa. Presumably the missing protein is a protein after infection of 12.67 kDa and 14.89 kDa protein and 37.67 kDa. Apparently these changes are caused by bacterial activity in the fish's body post-infection, which affects the damage of certain proteins so that the protein is to be lost, also the presence of new proteins are synthesized which may function in helping the immune system of fish during bacteria attacks. This finding is supported by Bullock, Conroy and Snieszko (1985) ; Andayani (2007) who stated that the thinner bands of plasma protein appeared in Infected fish.

In addition, alkaloids as immunostimulants can inhibit bacteria as seen in normal liver histology (Fig. 3A). Because Alkaloid compounds can damage nucleic acids (DNA and RNA) of bacteria as the basic structure of these alkaloids are alkylating agents and other substances that react covalently with purine and pyrimidine bases so that they can join to DNA / RNA as well as cut its hydrogen bonding (Bullock *et al.*, 1985; Jawetz *et al.*, 1987). These toxins can damage cell membranes by interfering with the transport of compounds in and out of cells, capable of penetrating cell walls and also destroy the existing system in cells. But fish infected with bacteria damage to the liver inflammation, Hemorrhagic and necrosis. And on treatment C is reduced damage.

## 5. CONCLUSION

- Chemical Structure of alkaloid substance from *Bougainvillia* sp. (N-1 – Benzilalkohol, 4 – Oktil Piperidin)
- Plasma protein electrophoresis results of SDS PAGE after being given the alkaloid 8 bands and after infected by *Vibrio harveyi* 10 bands.
- it can increase non-specific immunity through protein profile and minor damage to liver histopathology. And on treatment C is reduced damage

## 6. ACKNOWLEDGMENTS

This research was supported by the project of DP2M PHB X-XV. The author would like to thank Afifah, Ninis, Indri, Nafis, Dina, Anggi, Merry, Firdi, Kartika and afriandini at the Faculty of Fisheries and Marine sciences, UB, Malang, East Java, Indonesia.

## 7. REFERENCES

- Andayani, S. 2007. Effect of bioactive alkaloids jellyfish (*Bougainvillia* sp) as immunostimulant toward bactericidal activity, non-specific immune responses and survival (RPS) of tiger grouper (*Ephinephelus fuscoguttatus*). Dissertation. Graduate Program in University of Brawijaya. 155p

- Bullock, G.L., Conroy, D.A. and Snieszko, S.F. 1985. Bacterial diseases of fishes. Research fellow, Fish pathology. The Zoological Society of London. 41 p.
- Dugenci, S.K., Arda, N and Candan, A. 2003. Some medicinal plants as immunostimulant for fish. J of Ethnopharmacology (88): p. 99-106
- Hamed, A.S., Rahaman, K.H., Alagan, A dan Yoganandhan, K. 2003. Antibiotic resistance in bacteria isolated from hatchery reared larvae and post larvae of *Macrobrachium rosenbergii*. J. Aquaculture, (217) : 39-48 p
- Harikrishnan R, Balasundaram C., and Heo, M.S. 2010. Molecular studies, disease status and prophylactic measures in grouper aquaculture: economic importance, diseases and immunology. Aquaculture. 30(9), 1-14.
- Harikrishnan R, Balasundaram C, and Heo, M.S. 2011. Diet enriched with mushrooms *Phellinus linteus* extract enhances the growth, innate immune response, and disease resistance of kelp grouper, *Epinephelus bruneus* against vibriosis. J. Fish Shellfish Immunol .30, 128-134.
- Jawetz, E., Melnick and Adelberg. 1987. Review of Medical Microbiology. Translated: Gerard Bonang K. C. V. EGC. Medical Book Publishers. Jakarta. P. 846.
- Lightner, D.V. 1996. A Handbook of shrimp pathology and diagnostic procedures for diseases of cultured penaeid shrimp. World Aquaculture society. Louisiana. 157 p.
- Maldoni, B., 1991, alkaloids: Isolation and Purification, J. Chem. Educ. Vol. 68 (8): 700-707
- Moriarty., D.J.W. 1997. The role of microorganisms in aquaculture ponds. J. Aquaculture. (151). P. 333-349
- Sahan, A. and Duman, S. 2010. Influence of  $\beta$ -1, 3 / 1, 6 glucan applications on some non-specific cellular immune response and haematologic parameters of healthy Nile tilapia (*Oreochromis niloticus* L., 1758). Turk. J. Vet. Anim. Sci. Vol. 34 (1): 75-81
- Sakai, M. 1999. Current research status of fish immunostimulants Aquaculture. J. Aquaculture. Vol. 172: 63-92.
- Setyowati, A., D. Hidayati, P.D.N. Awik and Abdulgani, N. 2010. Histopathology Study of the Liver of the Belanak (*Mugil cephalus*) in the Estuary of Aloo Sidoarjo River. Institute of Technology Surabaya. 34 p.

## **Bacteria amount, protease enzyme activity, and protein energy retention of catfish (*Clarias gariepinus*) on Red Water System in different density.**

Mohamad Fadjar\*, Arning W. Ekawaty, Dhiannita Siskharini, Sherly S.T. Merdekawati, and Arif Udin

Aquaculture Dep, Fac. Of Fisheries and Marine Science, University of Brawijaya, Jl. Veteran, Malang 65145, Indonesia

\*Corresponding Author: [f4dj4r\\_02@ub.ac.id](mailto:f4dj4r_02@ub.ac.id), [f4dj4r\\_02@yahoo.com](mailto:f4dj4r_02@yahoo.com)

### **ABSTRACT**

The use of probiotics in the catfish culture with Red Water System (RWS) serves as a live microbial feed additive that affects the host by improving the balance of microorganisms in the digestion so as to help improve the digestive system of fish, because it produce extracellular protease that can help hydrolyze the protein in the fish. The purpose of this research was to identify the effect of RWS technique towards the amount of bacteria in the gut, protease activity, and retention of protein and energy of *C. gariepinus* on different density. The research method was experimental using completely randomized design (CRD) with 3 treatments and 3 replications of 250, 500, and 750 fish/m<sup>3</sup> stocking density. The results obtained wasn't significantly give different effect on the retention of protein and energy of (*C. gariepinus*). but the highest results was found on treatment B (500 fish/m<sup>3</sup>) which 44.94%, and 39.70%. The highest average of bacteria growth in treatment C with 152 x 10<sup>5</sup> cfu/ml, the lowest growth in treatment A (64.67 x 10<sup>5</sup> cfu/ml). Protease activity was not significantly difference between treatments. Protease activity in treatment A was 55.93 ± 10.59 U/ml, treatment B was 60.08 ± 3.05 U/ml, and treatment C was 75.15 ± 9.91 U/ml. Based on the result suggested that stocking densities of 750 ind/m<sup>3</sup> was economically better in catfish (*C. gariepinus*) culture using *Red Water System* (RWS).

**Keyword:** catfish, red water system, probiotic, protease, protein.

### **1. Introduction**

Catfish (*Clarias gariepinus*) is the most popular commodity and cultivated by the community in Indonesia, this is reinforced by statistic fishery data of Indonesia in 2014 which indicate that catfish ranked first freshwater fish production in Indonesia and followed by carp (Anonymous, 2014).

Because of the large demand of catfish then the current cultivation is done intensively. Intensive aquaculture brings an unfavorable impact on the preservation



and environmental health.

Utilization of bacteria in cultivation still revolves around the biofloc technique, which is on the application requires an aeration supply for sustains the oxygen demand of the organism inside it. Use of aeration requiring electrical power sometimes it becomes constraints for the cultivators. So there are ones trying application of bacteria utilization without using aeration, using a density below 250 fish / m<sup>3</sup>. This is the basic for Red Water System (RWS), which is still requires in-depth related studies about the amount of optimal stocking density.

Red water cultivation system is a development of biofloc cultivation system utilizing lactic acid bacteria (LAB) to improve fish digestibility. Yulvizar *et al.* (2014), said that acidic bacteria in the form of probiotics bacteria have the ability to produce compounds that can inhibit pathogenic bacteria growth.

Utilization of probiotics in RWS is expected to help improve the digestive system of fish, because on the use of RWS techniques utilizes facultative anaerobic bacteria which produce protease, extracellular enzymes that can help hydrolyze the protein in the fish body. Extracellular protease-producing enzyme bacteria will increase the concentration of enzymes. So it is expected the addition of probiotics can increase the enzyme protease inside digestion (Ahmadi *et al.*, 2012). Other than addition of enzyme, bacteria is also affected by stocking density, because it can increase fish body temperature.

The purpose of this research was to identify the effect of RWS technique towards the amount of bacteria in the gut, protease activity, and retention of protein and energy of *C. gariepinus* on different density

## **2. Methods**

### **2.1 Fish**

Juvenile Catfish (*C. gariepinus*) that used was 5-7 cm length. Feed with commercial catfish feed in the form of fermented pellets.

### **2.2 Probiotics**

A commercial probiotics was used for the water i.e. SGF BIOLIZER<sup>®</sup> contained  $7,6 \times 10^7$  CFU/ml *Bacillus subtilis*, *Agrobacterium tumefeciens*. and *Lactococcus lactis*

### **2.3 Red Water System**

Creating media in RWS, water to be used coupled with fermented manure. Fermentation of manure is done using one liter molasses plus 10 ml of commercial probiotics, then wait for one month. Dosage of manure given as much as 5 kg / m<sup>3</sup>. Other ingredients were agricultural lime (dolomite) with dose of 700 g / m<sup>3</sup>

### **2.4 Total Bacteria**

Bacteria identification was done three times, before treatment, 15 and 30 days after treatments; using biochemical identification and total plat count method. Amount of bacteria was counted using this formula (cfu/ml/day):

$$\frac{(\sum \text{bacteria Hn}) - (\sum \text{bacteria H0})}{t \text{ (time)}}$$

which :

$\sum$ bacteria Hn = amount of bacteria in H day

$\sum$ bacteria H0 = amount of bacteria in 0 day

Biochemical tests performed include oxidase and catalase, gram, TSIA, Indol, Motility, MR-VP, Simon citrate, urease, O / F, Gelatin, Nitrogen, Malonate, KCN (Potassium Cyanide Test), Lysin decarboxylase, Ornithin, Arginine, salt resistance, carbohydrate fermentation, and DNase test.

#### 2.4 Protease activity

After maintenance within 30 days, Dumbo catfish (*C. gariepinus*) is taken throughout the digestive tract and smoothed using mortar and pestle. The fine sample was inserted into the labeled film bottle and added with 5 ml aquades then homogenized, after which 1 ml was taken into the measuring tube mixed with 1 ml of 5% casein solution with 0.5 ml and phosphate buffer (pH 4) then it incubated at 37°C for 10 minutes. The sample was then added with a 4% TCA solution of 2.5 ml and incubated at room temperature (27°C) for 30 min, the sample was centrifuged at 4,000 rpm for 10 min for filtrate separation and precipitate. The filtrate was taken 1 ml and gave 5 ml aquadest and then measured the value of absorption on the length of 200-350 nm wave using spectrophotometer.

#### 2.5 Protein energy retention

Protein energy retention was counted based on Buwono (2004) *in* Hendrawati (2011) using:

$$RP = \frac{(\text{JPS final} - \text{JPS early}) \text{ g} \times 100\%}{\text{JPB (g)}}$$

Information :

Final JPS: Number of final body proteins

Early JPS: Amount of initial body protein

JPB: The amount of feed protein given

According to Yuwono (2011) *in* Kristanti, (2014) energy retention can be formulated as follows:

$$RE = \frac{(\text{E end} - \text{E early}) \text{ kkal} \times 100 \%}{\text{E feed (kkal)}}$$

Which:

E end: initial body energy (kkal / kg of meat)

E Early : End-body energy (kcal / kg of meat)

E feed: Feed energy (kcal / kg of feed)

## 2.6 Data Analysis

Data obtained from the results of the study were analyzed statistically by using diversity analysis (ANOVA) in accordance with the design used was RAL consisting of 3 treatments and 3 repetitions

## 3. Result and Discussion

### 3.1 Total Bacteria

The result of total bacteria can be read on Table 1

**Tabel 1.** Data Rata-Rata Pertambahan jumlah Koloni Bakteri Lambung Ikan Lele Dumbo (*C. gariepinus*)

Treatment	Repetition (10 <sup>5</sup> cfu/ml)			Total	Average ± 1 2 3 Deviation standard
	1	2	3		
A	63	77	54	194	194 ± 11,59
B	150	133	101	384	384 ± 24,88
C	136	167	153	456	456 ± 15,52

Increasing growth of bacterial colonies in the stomach of dumbo catfish (*C. gariepinus*) may be affected by the addition of probiotic bacteria added through feed. Anto (2012) in his research is the addition of probiotic bacteria in the feed, all probiotic bacteria added to the feed is found in the hull of the treated fish. The result of dumbo catfish (*C. gariepinus*) gastric bacteria identification showed that four genera of bacteria added to feed in RWS technique only *Bacillus* sp. was found in the hull. This happens allegedly because only *Bacillus* sp. can survive in pH conditions in the stomach. According to Setijaningsih (2011), several factors that caused bacteria can not grow in an environment are levels of nutrients, temperature, and environmental pH. According to Fukamizo *et al.* (1994), bacteria were found in the digestive system was *Bacillus pumilus* sp. In addition to the condition of gastric pH, suspected to inhibit the growth of other probiotic bacteria is quorum sensing conducted by *Bacillus* sp., where between bacterial cells occur coordination of activity to become a colony with a high density that can inhibit the growth of other bacteria. According to Setiawati (2013), the role of quorum sensing in bacteria is regulating survival in the environment and avoiding colonization by antagonistic bacteria. The growth rate of bacterial colonies in the stomach of catfish (*C. gariepinus*) will increase as the amount of bacterial stomach density increases.

Increasing the amount of density is influenced by several factors, including the availability of feed for bacteria and environmental pH. In addition to the condition of



the fish body, which affects the increase of bacterial colony growth rate in the stomach is the addition of fermentative bacteria that exist in the fermentation diet. By no means the direct probiotic bacteria that exist in the fermentation feed can maintain the balance of growth of other bacteria in the stomach. Verschuere *et al.* (2000), states that the development of bacterial communities influenced by the amount and quality of the feed given, and the opportunity that an organism has to be in the right time and time to enter proliferate in a supportive environment

### 3.2 Protease activity

The result of protease enzyme activity on catfish (*C. gariepinus*) digestion in treatment A got an average of  $55,93 \pm 10,59$  U / ml, B  $60,08 \pm 3,05$  U / ml, and C  $75,15 \pm 9,91$  U / ml. it showed no significant difference ( $p > 0,05$ ). According to Poedjiadi and Supriyanti (2006), factors affecting enzyme activity include temperature, pH, inhibitor, enzyme concentration and substrate concentration. According to Wang (2007), the use of probiotics with photosynthetic bacteria types and *Bacillus* sp. gave effects to the activity of digestive enzymes (protease, amylase, and lipase) in the white shrimp intestine. Not significantly different were also caused by the addition of proteins as protease enzyme activators of each treatment, ie 5% per biomass of catfish (*C. gariepinus*) maintained. According to Zairin and Handayani (2003), the greater feed protein feeding the greater activity of protease enzymes in the digestion of Gurame fish.

### 3.3 Protein Energy Ratio

The average value of protein retention in catfish seeds can be seen in Table 2 below.

Table 2. Average data of protein retention of Dumbo catfish (*C. gariepinus*)

Treatment	Repetition			Total	Average $\pm$ 1 2 3 Deviation standard
	1	2	3		
A	36.63	47.18	39.33	123.14	$41.05 \pm 5.48$
B	49.48	38.48	46.86	134.82	$44.94 \pm 5.75$
C	33.18	41.09	38.87	113.14	$37.71 \pm 4.08$

Based on the results of the data of protein retention Contained in Table 3, showed protein retention value in catfish seed Dumbo (*C. gariepinus*) at each treatment is not differs markedly. Average protein retention value between treatments are relatively the same. It means the use of RWS technique with different stockings density didn't affect the value protein retention in catfish seed (*C. gariepinus*). This was because the type of feed was given for each treatment was the same.

According to Supriyanto (2010), granting probiotics in the diet, affecting speed of fermentation of feed in the gastrointestinal tract, so it will be very helpful the

process of food absorption in the digestion of fish. Giving probiotics to the pellet can leads to fermentation of the pellets and improves digestion speed. Setiawati *et al.* (2013), adds that probiotics can regulate the microbial environment of the intestine, blocking pathogenic microorganisms in the intestine by releasing enzymes that aid food digestion. One of the bacteria that is believed to be able to increase digestibility in fish is *Bacillus* sp. *Bacillus* sp. has the ability to express protease enzymes, lipases, and amylases

### 3.2 Energy retention

The average value of energy retention in catfish (*C. gariepinus*) can be seen on Table 3.

Table 3. Average data of energy retention of catfish (*C. gariepinus*)

Treatment	Repetition			Total	Average $\pm$ Deviation standard
	1	2	3		
A	33.86	44.19	33.98	112.03	37.34 $\pm$ 5.93
B	43.46	32.85	44.46	120.77	40.26 $\pm$ 6.43
C	28.37	37.68	34.39	100.44	33.48 $\pm$ 4.72

Based on the results of the varied prints contained in Table 3 showed that energy retention value on catfish (*C. gariepinus*) in each treatment was not differs markedly. Average energy retention value between treatments are relatively similar. This was because of the type of feed given to fish at each treatment equally, where in this feed have the same nutritional content, besides the amount of feeding on the same fish although densely stocked fish differently on each treatment.

Average energy retention both showed that feed energy can be utilized efficiently to compose body proteins. According to Buwono (2010), the main function of food is as a provider of energy for the activity of body cells. Carbohydrates, fats and proteins are nutrients in the diet that serves as a source of energy body. Proteins, along with mineral and water are the main ingredients in the formation of body cells and tissues, while proteins together with minerals and vitamins, function in regulation of body temperature, pressure settings osmotic body fluids, as well as process settings metabolism in the body. Fish takes energy to process metabolism, body care (maintenance), physical activity, growth and reproduction (Haetami *et al.*, 2012). If there is excess energy will be used for growth. Energy was needed mostly filled by non-protein nutrients, such as fat and carbohydrates (Santoso and Agusmansyah, 2011).

### 4. Conclusion

The results obtained wasn't significantly different on protease activity, retention of protein and energy, and total bacteria in gut of *C. gariepinus*. The highest average of bacteria growth was in treatment C with  $152 \times 10^5$  cfu/ml,

Stocking densities of 750 ind/m<sup>3</sup> was economically better in catfish (*C. gariepinus*) culture using *Red Water System* (RWS).

### Acknowledgement

We would like to thanks CV Nelayan Indonesia which gave funding for this research.

### References

- Anto, Mohammad Tri. 2012. Studi komposisi bakteri pada usus benih ikan gurami (*Osphronemus gouramy*) setelah penambahan probiotik dengan dosis yang berbeda dalam pakan pellet. Skripsi. Universitas Brawijaya. Malang. 24 hlm.
- Buwono, I. D. 2002. Kebutuhan Asam Amino Esensial dalam Ransum Ikan. Kanisius. Yogyakarta. 56 hlm.
- Fukamizo, T., O. Takeshi, I. Yusuo, and G.Sachio. 1994. Specificity of chitosanase from *Bacillus pumilus*. *Biochimica et Biophysica Acta*. **1205**:183-188
- Haetami, K. 2012. Konsumsi dan efisiensi pakan dari ikan jambal siam yang diberi pakan dengan tingkat energi protein berbeda *Jurnal Akuatika*. **3** (2): 146-158.
- Poedjiadi, A., dan F.M.T. Supriyanti. 2006. Dasar-Dasar Biokimia. *Universitas Indonesia (UI-Press)*. Jakarta. 476 hlm.
- Santoso L. dan H. Agusmansyah. 2011. Pengaruh substitusi tepung kedelai dengan tepung biji karet pada pakan buatan terhadap pertumbuhan ikan bawal air tawar (*Colossoma macropomum*). *Berkala Perikanan Terubuk*. **39** (2): 41- 50.
- Setiawati, J. E., Tarsim, Y. T. Adiputra, dan S. Hudaidah. 2013. Pengaruh penambahan probiotik pada pakan dengan dosis berbeda terhadap pertumbuhan, kelulushidupan, efisiensi pakan dan retensi protein ikan patin (*Pangasius hypophthalmus*). *Jurnal Rekayasa dan Teknologi Budidaya Perairan*. **1** (2): 151-162.
- Supriyanto. (2010). Pengaruh pemberian probiotik dalam pellet terhadap pertumbuhan lele sangkuriang. *Jurnal Perikanan*. **8** (1): 17-25
- Verschuere L., G. Rombaut, P. Sorgeloos and W. Verstraete. 2000. Probiotic bacteria as biological control agents in aquaculture. *Microbiol. Mol. Biol. Rev.* **64** : 655–671.
- Wang, Y.B. 2007. Effect of probiotic on growth performance and digestive enzyme activity of the shrimp *Panaeus vanammei*. *Aquaculture* **269** : 259-264.
- Zairin, M. dan S. Handayani. 2003. Pola Perubahan Enzim-Enzim Pencernaan dan Enzim Metabolic sebagai respon terhadap Substrat pada Ikan Gurame (*Osphronemus gouramy* Lac.). Abstrak LPPMIPB : 1-2.

## Simulation Research on Speed Control of Permanent Magnet Direct-driven System for Mining Scraper Conveyor

En Lu, Wei Li\* and Xuefeng Yang

School of Mechatronic Engineering, China University of Mining and Technology,

No. 1 University Road, Xuzhou, China

\*Corresponding Author: liweicumt@163.com

### ABSTRACT

The simulation research on speed control based on the load characteristic of the permanent magnet direct-driven system is investigated in this paper. Firstly, the mathematical model of permanent magnet synchronous motor (PMSM) is established based on the coordinate transformation theory. Subsequently, the closed loop speed controller of permanent magnet direct-driven system is designed on the basis of the motor model and adaptive global fast non-singular terminal sliding mode control (SMC). The chain characteristics of scraper conveyor are described by Kelvin-Vogit model, and the dynamic model of the mining scraper conveyor is established with distinct element method. Then, according to the coupling relationship between the permanent magnet direct-driven system and the scraper conveyor, the electromechanical coupling model of the overall mining scraper conveyor system is established by using MATLAB/Simulink. The simulation results demonstrate that the speed controller of the permanent magnet direct-driven system can realize smooth starting of scraper conveyor, and the global fast non-singular terminal SMC controller has shorter response time and better robustness when the scraper conveyor has random load.

**Keyword:** Sliding Mode Control, Permanent Magnet Synchronous Motor, Scraper Conveyor, Electromechanical Coupling.

## **Position Sensorless Control for Short Range Cutting Interior Permanent Magnet Synchronous Motor of Shearer Based on a New Sliding Mode Observer**

**Abstract:** For the low reliability and poor adaptability of existing drum shears cutting part, this paper presents a permanent magnet short range cutting transmission system (PMSRCTS) with low-speed and high-torque internal permanent magnet synchronous motor(IPMSM) as the driving source and a position sensorless control strategy based on a new sliding mode observer(SMO). In order to increase the robustness of the observer and reduce the error caused by the chattering in the traditional SMO, the phase locked loop (PLL) technique is used instead of the traditional arctangent function estimation, and the sigmoid function is introduced to replace the traditional sign function, then the sliding mode gain is adjusted through the fuzzy control algorithm in the new SMO. The scheme effectively improves the problems that the high failure rate caused by the long transmission chain of the shearer cutting section and the environmental impact for the mechanical sensor measurement results. Finally, the mathematical model of IPMSM based on the two-phase rotating coordinate system and end cutting load are established for verifying the effectiveness and feasibility of the program. The results show that the new observer can accurately realize the speed and position estimation of the shearer cutting motor, and has good dynamic response performance, observation accuracy and robustness.

**Key words:** Internal permanent magnet synchronous motor; Short range cutting transmission system; Sliding mode observer; Position sensorless control; Lyapunov stability

## Stepwise Regression Model and Prediction of Retardance in Citric Acid Coated Ferrofluids

Jing-Fung Lin<sup>a\*</sup>, Xin-Rong Qiu<sup>b</sup>

<sup>a</sup>Department of Industrial Design, Far East University,

No.49, Zhonghua Rd., Xinshi Dist., Tainan City 74448, Taiwan

<sup>b</sup>Graduate School of Mechanical Engineering, Far East University,

No.49, Zhonghua Rd., Xinshi Dist., Tainan City 74448, Taiwan

\*Corresponding Author: jacklin@mail.feu.edu.tw

### ABSTRACT

Citric acid (CA) coated Fe<sub>3</sub>O<sub>4</sub> ferrofluids (FFs) have been conducted for biomedical application. The magneto-optical retardance of CA coated FFs was measured by a Stokes polarimeter. Optimization and multiple regression of retardance in FFs were executed by Taguchi method and Microsoft Excel previously, and the *F* value of regression model was large enough. However, the model executed by Excel was not systematic. Instead we adopted the stepwise regression to model the retardance of CA coated FFs. From the results of stepwise regression by MATLAB, the developed model had highly predictable ability owing to *F* of 1.70875e+6 and correlation coefficient of one. The average absolute error of predicted retardances to measured retardances was just 0.019%. Using genetic algorithm (GA) via MATLAB, the optimized parametric combination was determined as [5.499 0.12 39.369 90] corresponding to the pH of suspension, molar ratio of CA to Fe<sub>3</sub>O<sub>4</sub>, CA volume, and coating temperature. The maximum retardance was found as 42.411°, close to that obtained by the evolutionary solver in Excel and a relative error of -0.047%. Above all, the stepwise regression method was successfully used to model the retardance of CA coated FFs, and the maximum global retardance was determined by the GA method.

**Keyword:** Retardance, Stepwise Regression, Genetic Algorithm.

### 1. Introduction

It has been known that citric acid (CA) coated Fe<sub>3</sub>O<sub>4</sub> ferrofluids (FFs) may have biomedical applications such as magnetic resonance imaging (MRI) and hyperthermia (heat treatment of tumor). The surface of the magnetic nanoparticles (MNPs) can be stabilized in an aqueous dispersion by the adsorption of CA. This process, as described by Sahoo et al., occurs by the CA being coordinated via the carboxylate functionalities [1]. Srivastava et al. synthesized CA coated Fe<sub>3</sub>O<sub>4</sub> MNPs of 6 nm particle size, which exhibits excellent magnetic properties [2]. Effect of synthesis

conditions on the properties of CA coated iron oxide nanoparticles was discussed in [3].

In the present investigation,  $\text{Fe}_3\text{O}_4$  MNPs were prepared by an improved co-precipitation of  $\text{Fe}^{3+}/\text{Fe}^{2+}$  salts and then the MNPs were stabilized against agglomeration by surfactant encapsulating of CA [4]. Afterwards, the CA coated  $\text{Fe}_3\text{O}_4$  MNPs were used as the precursor of water-based FFs, and the retardance (magneto-optical property as the phase retardation of linearly birefringent medium, such as quartz and certain liquid crystals) of FFs were measured by a developed Stokes polarimeter [5]. It is known that Taguchi orthogonal design method may provide a powerful and efficient ways to find an optimal combination of factor levels that may achieve optimum. Hence, Taguchi method with range analysis was employed to find the parametric combination for CA coated FF with high retardance readily [4].

Optimization and multiple regression of retardance in FFs were executed by Taguchi method and Microsoft Excel, and the  $F$  value of regression model was large enough [6]. However, the model of retardance executed by Excel was not in a systematic way. Further, using Taguchi-based measured retardances as the training data, an artificial neural network (ANN) model was developed for the prediction of retardance in CA coated FF. Based on the well-trained ANN model, the predicted retardance at excellent program from Taguchi method showed less error of 2.17% compared with a multiple regression (MR) analysis of statistical significance [7].

The aim of this study was to use the stepwise regression for modeling the retardance of CA coated FFs. The stepwise regression via MATLAB was executed to model the retardance of CA coated FFs successfully. The regression model had highly predictable ability and had a high correlation coefficient of one. Moreover, two optimization techniques, including the evolutionary algorithm (in Microsoft Excel) and the genetic algorithm solver (in MATLAB® Optimization Toolbox), were used to find the global maximum retardance value. Then the CA coated FFs could be more useful in practical applications.

## 2. Method

In this study, the methods including Taguchi orthogonal design method, stepwise regression method, evolutionary algorithm and genetic algorithm were briefly described.

### 2.1 Taguchi Method

Taguchi method is straightforward and easy to apply to many engineering situations, making it a powerful yet simple tool. Subsequently, the optimal synthetic condition of

CA coated  $\text{Fe}_3\text{O}_4$  FFs with high retardance was determined by the Taguchi orthogonal design method- $L_9(3^4)$ , i.e. four parameters with three levels, respectively, and nine tests of FFs with 1000 g/L, correspondingly [4]. Influence parameters were (A) pH value of suspension after coating (4.5, 5, 5.5), (B) molar ratio of CA to  $\text{Fe}_3\text{O}_4$  MNPs (0.03, 0.06, 0.12), (C) CA volume (10 ml, 20 ml, 40 ml), and (D) coating temperature (70 °C, 80 °C, 90 °C). Procedure of the chemical co-precipitation method for producing CA coated FFs could be found in [4]. The retardance of FF was measured by a Stokes polarimeter with a feasible algorithm [5]. Results of the retardance under 64.5 mT were as shown in Table 1 [4]. Moreover, the influence sequence between these parameters on the retardance and the excellent program (parametric combination) of maximum retardance were decided by a simple range analysis. Above all, before the performance of Taguchi method, two single-parameter tests including pH value of suspension after coating and double centrifugations were executed; the appropriate values of parameters in the middle level were determined [4].

Table 1. Orthogonal design and test results of retardance.

No	A	B	C	D	Retardance (deg.)
A1	1	1	1	1	7.8228
A2	1	2	2	2	11.9872
A3	1	3	3	3	29.3618
A4	2	1	2	3	4.0525
A5	2	2	3	1	23.6294
A6	2	3	1	2	18.1662
A7	3	1	3	2	-0.4628
A8	3	2	1	3	4.5877
A9	3	3	2	1	20.2021

## 2.2 Stepwise Regression

While dealing with large number of independent variables, it is of significant importance to determine the best combination of these variables to predict the dependent variable [8]. Stepwise regression method is a routine statistic technique used for variable selection and is a combination of forward and backward procedures. The method starts with an initial model which includes a subset of all the candidate variables. And then, a so-called stepping procedure which iteratively altering the model established at the previous step by adding or removing variables in accordance with the stepping criteria is used in order to add significant variables or remove insignificant variables.

The stepping procedure terminates when the model has been optimized, or when a specified maximum number of steps have been reached. The obtained model can be



tested for validity through a variety of statistical methods. Usually, the evaluation of the model is made by using some criteria: correlation coefficient ( $R$ ), adjusted square of correlation coefficient (adjusted  $R^2$ ), standard error (SE), and  $F$  statistic [9]. The details on the use of stepwise model-building procedure could be found [8, 10].

In our previous study, optimization and multiple regression of retardance in FFs were executed by Taguchi method and Microsoft Excel, and the  $F$  value of regression model was large enough [6]. However, the model of retardance executed by Microsoft Excel was not in a systematic way, and the execution is time-consuming. Therefore, the stepwise regression method (or called as the optimized regression) can be used to model the retardance of CA coated FFs precisely and efficiently.

### 2.3 Evolutionary Algorithm in Microsoft Excel

We can use the evolutionary solver in Microsoft Excel to solve optimization problems [11]. A genetic or evolutionary algorithm applies the principles of evolution found in nature to the problem of finding an optimal solution. In a “genetic algorithm,” the problem is encoded in a series of bit strings that are manipulated by the algorithm; in an “evolutionary algorithm,” the decision variables and problem functions are used directly.

Most commercial solver products are based on evolutionary algorithms. The evolutionary solver combines genetic algorithm methods such as mutation, crossover, and natural selection with classic methods drawn from linear programming, nonlinear optimization, and pattern search, to find better solutions in less time. Further, on smooth nonlinear problems where the GRG (Generalized Reduced Gradient) solver can find only a locally optimal solution, the evolutionary solver can often find a better solution or even a globally optimal (or close to globally optimal) solution, which is described by Frontline System [11]. Therefore, the optimized parametric combination and the maximum retardance of CA coated FFs could be obtained by the use of evolutionary algorithm in Microsoft Excel, which is capable of solving smooth and non-smooth global optimization problems.

### 2.4 Genetic Algorithm

The genetic algorithm (GA) technique is based on the natural process of evolution to solve optimization and search problems. There are three main operators in GA which are reproduction, crossover and mutation [12]. GAs were pioneered by Holland in the 1960s and 70s [13] and have emerged as a highly effective technique for solving a wide variety of optimization problems [14].

Figure 1 presents a simple flowchart representation of a typical GA solution procedure [14]. As shown, the process commences by creating an initial population of

random solutions to the problem of interest. Each potential solution is then evaluated using a fitness function, i.e. an objective function which quantifies the optimality of each solution such that it can be ranked against that of all the other potential solutions. If the termination criteria are not satisfied, multiple candidate solutions are selected for modification via reproduction, crossover and mutation operations in order to create a new population pool. The optimality of each member of the population pool is then re-evaluated using the fitness function.

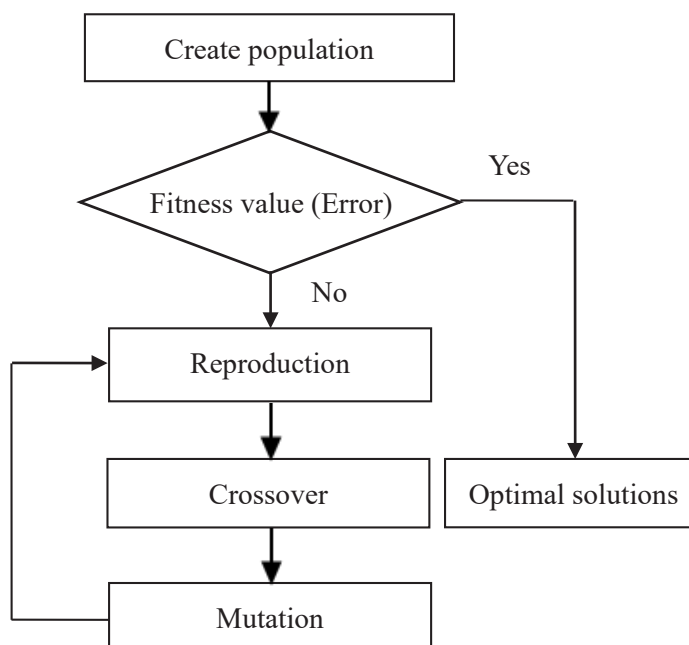


**Figure 1:** Flowchart of genetic algorithm.

### 3. Results

Based on the Taguchi-based measured retardances and the retardance obtained under the double-centrifugation test of CA coated FFs, the results of stepwise regression (the first order and the second order) are provided below. And the optimized parametric combination and the maximum retardance of CA coated FFs are obtained by the genetic algorithm, which are compared with those results obtained by the evolutionary solver in Microsoft Excel.

#### 3.1 Results of Stepwise Regression

Regression model is based on the Taguchi-based measured retardances (as shown in Table 1, the retardance value of the A7 sample is not considered due to the possible error) and the retardance of 15.24° obtained under the double-centrifugation test with parametric combination of [5 0.06 20 80], corresponding to the pH of suspension, molar ratio of CA to Fe<sub>3</sub>O<sub>4</sub>, CA volume, and coating temperature. The results of the

first order stepwise regression executed by MATLAB are as shown in Figure 2. We can see the meaningfulness degrees of input variables. This degree of meaningfulness is determined via being value of  $p$ -val ( $P$  value,  $P$  represents probability) below 0.05. Thus meaningfulness ranking of input variables is determined as variable 2 and variable 3, i.e. molar ratio of CA to  $\text{Fe}_3\text{O}_4$  MNPs and CA volume, respectively. The variable 2 (molar ratio of CA to  $\text{Fe}_3\text{O}_4$  MNPs) involved in this model represents the most significant influencing factor for the retardance of CA coated FFs. Based on the results obtained; equation of the first order stepwise regression model is given by equation (1):

$$\text{Retardance} = 29.3825 - 3.25319X_1 + 150.45X_2 + 0.42055X_3 - 0.227538X_4 \quad (1)$$

From the results of Figure 2, the  $R^2$  value is 0.967851. This indicates that the current equation is able to describe 96.7851 percent of the variation in the response variable; this doesn't guarantee the appropriateness of the first order model. In addition,  $t$  statistic ( $t$  Stat) in Table 2 is equal to the ratio of respective standard error to the coefficient value and tests the significance of individual regression coefficients for a confidence interval as 95%. Under the normality assumption, for  $n$  number of observations,  $t$  statistic follows student's  $t$  distribution with  $(n-2)$  degrees of freedom (DF), and critical value of  $t$  can also be found out by using TINV function in Microsoft Excel which comes out to be 2.3646. As can be seen that  $X_2$  coefficient ( $6.7298 > t$  critical value of 2.3646) has the strongest effect on the regression model followed by the  $X_3$  coefficient.  $P$  value in Table 2 is the probability that for a particular confidence level as 95%, a random variable having a student's  $t$  distribution is greater than absolute value of observed  $t$  statistic and hence significant. It is noted that the probability is 0.2033 and 0.065 for parameter  $X_1$  and parameter  $X_4$ , respectively, is higher than 0.05.

For testing whether the simple stepwise regression model gives any useful information about the response variable or not, as shown in Figure 2.  $F$  statistic is the ratio of mean squares due to regression model and error, and is used to test the significance of regression model for a confidence level. The  $F$ -test is executed by comparing the observed  $F$  statistic with the appropriate critical value obtained from the standard  $F$  distribution table. Critical value of  $F$  for the current regression model can be found out from standard  $F$  distribution table by  $F(7, 1, 0.05)$  or by using FINV function in Microsoft Excel, which comes out to be 236.7684. As can be seen that the observed  $F$  value of  $30.1056 < 236.7684$ , it implies the regression model is not significant enough. Figure 2 also shows the corresponding probability value as  $P(F)$ . It can be deduced that the regression model is not statistically significant although  $P$  value (0.003034, chance of 0.3034% that such model  $F$ -value could occur due to

noise) is less than 0.05 (i.e. 95% confidence level).

Compared to the results obtained by multiple linear regression in Microsoft Excel for Taguchi-based measured retardances of 9 samples [6], the determination coefficient  $R^2$  and the observed  $F$  value of the first order stepwise regression model as shown in Figure 2, are larger than those of 0.888 and 7.954, respectively [6]. It is seen that the first order stepwise regression is more reliable than the multiple linear regression. However the first order stepwise regression model is not statistically significant enough (the  $F$  value of 30.1056 is not high enough). Next, we will perform the second order stepwise regression.

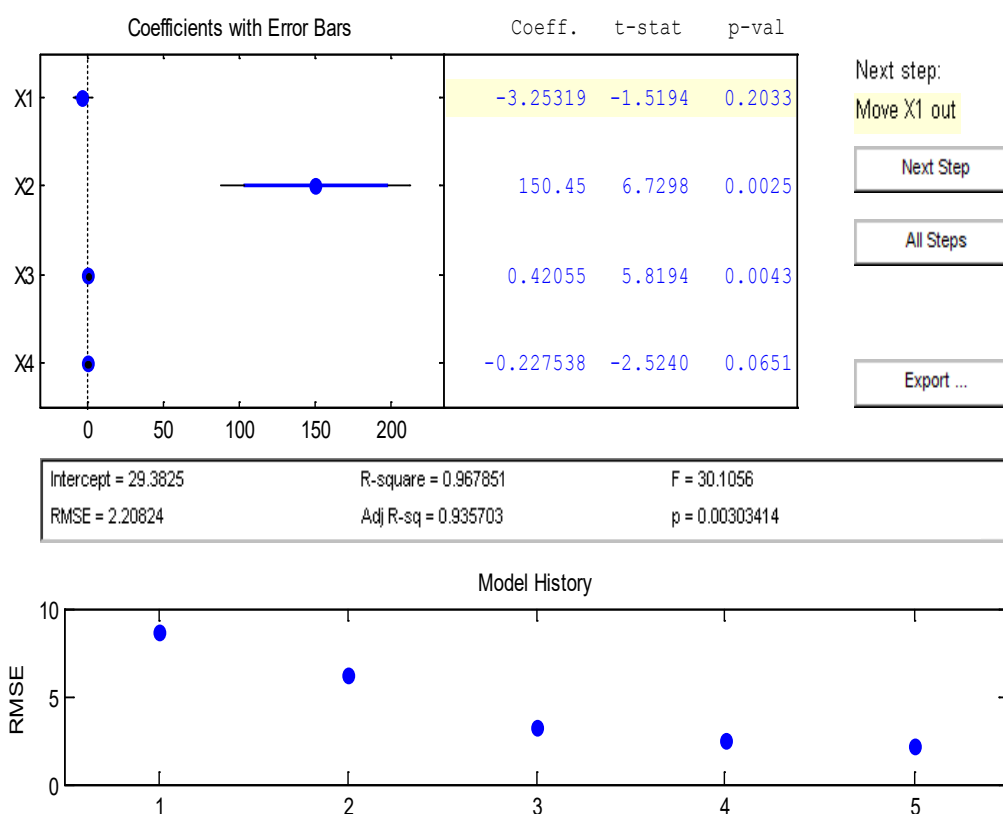


Figure 2: Results of stepwise regression (the first order).

Table 2. Results of stepwise regression (the first order).

	Coefficient	Standard Error	$t$ Stat	$P$ value
Intercept	29.3825	13.0136	2.2578	0.0869
$X_1$ (pH)	-3.25319	2.1411	-1.5194	0.2033
$X_2$ (Molar Ratio)	150.45	22.3557	6.7298	0.0025
$X_3$ (CA Volume)	0.42055	0.0723	5.8194	0.0043

$X_4$ (Temperature)	-0.227538	0.0902	-2.5240	0.0651
	$R^2=0.967851$		$R^2_{adj}=0.935703$	

Subsequently, we aim to increase the precision of regression model and precede the second order stepwise regression. The results of stepwise regression by MATLAB are shown in Figure 3, the model has highly predictable ability owing to the  $F$  value of  $1.70875e+6$  and has a high correlation coefficient  $R$  of one, which is suggested that this regression model is statistically significant and gives useful information about the response variable. In addition, as shown in Figure 3, the corresponding probability value  $P(F)$  (0.000589, chance of 0.0589% that such model  $F$ -value could occur due to noise) is much less than 0.05 (i.e. 95% confidence level).

The average absolute error of predicted retardances is less just as 0.019%. The equation for the second order stepwise regression model is given by equation (2):

$$\text{Retardance} = 37.1582 - 1298.73X_2 + 872.578X_2^2 - 0.0188368X_3^2 - 0.00796541X_4^2 + 0.326095X_1X_3 - 2.75515X_2X_3 + 17.0993X_2X_4 \quad (2)$$

As shown in Figure 3 and Table 3, we can see the meaningfulness degrees of input variables. This degree of meaningfulness is determined via being value of  $p$ -val below 0.05. Thus meaningfulness ranking of input variables is determined as  $8(X_4^2)$ ,  $13(X_2X_4)$ ,  $2(X_2)$ ,  $10(X_1X_3)$ ,  $7(X_3^2)$ ,  $12(X_2X_3)$ , and  $6(X_2^2)$ . As shown in Figure 3, the RMSE (Root Mean Square Error) value is 0.0071221 and is much lower than that of 2.20824 in the first order stepwise regression as shown in Figure 2. Further, the  $R^2$  value is determined as one and is higher than 0.967851 in the proposed first order stepwise regression (in Figure 2) and 0.9999998 in the multiple nonlinear regression model [6]. It is indicated that the ability of prediction in the second order stepwise regression model is excellent.

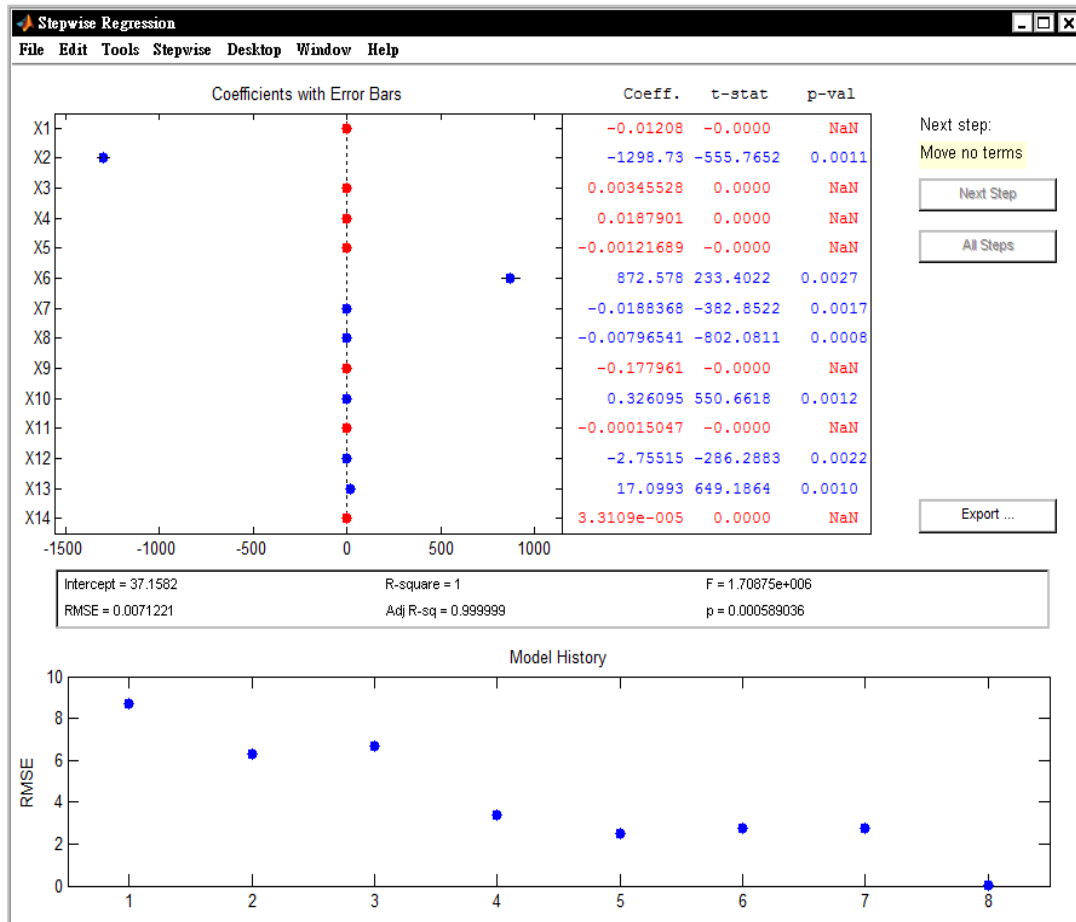


Figure 3: Results of stepwise regression (the second order).

Table 3. Results of stepwise regression (the second order).

	Coefficient	Standard Error	t Stat	P value
Intercept	37.1582	0.046098017	806.0696	0.0008
$X_2$	-1298.73	2.336825771	-555.7652	0.0011
$X_2^2 (X_6)$	872.578	3.738517427	233.4022	0.0027
$X_3^2 (X_7)$	-0.0188368	4.92012E-05	-382.8522	0.0017
$X_4^2 (X_8)$	-0.00796541	9.93093E-06	-802.0811	0.0008
$X_1X_3 (X_{10})$	0.326095	0.000592187	550.6618	0.0012
$X_2X_3 (X_{12})$	-2.75515	0.009623698	-286.2883	0.0022
$X_2X_4 (X_{13})$	17.0993	0.026339539	649.1864	0.0010
	$R^2= 1$		$R^2 adj= 0.999999$	

The significance *t*-test of each variable is listed in Table 3. It is seen that the significant influence of each term on the retardance of CA coated FFs is given by:  $X_4^2 > X_2X_4 > X_2 > X_1X_3 > X_3^2 > X_2X_3 > X_2^2$ . This indicates that the effect of the molar ratio of CA to Fe<sub>3</sub>O<sub>4</sub> ( $X_2$ ) on the retardance is the most significant, and the effect of CA

volume ( $X_3$ ) on the retardance is of the least significance ( $X_2 > X_4 > X_1 > X_3$ ). The influence sequence for these four parameters is different from that ( $X_2 > X_1 > X_4 > X_3$ ) obtained by the range analysis of Taguchi orthogonal method with 9 samples (the possible error of the retardance in the A7 sample was included in the range analysis) [6].

In addition, the cross correlation of the molar ratio of CA to  $\text{Fe}_3\text{O}_4$  and coating temperature ( $X_2X_4$ ) is more significant than the other cross correlations of two parameters such as pH value of suspension and CA volume ( $X_1X_3$ ) and as molar ratio of CA to  $\text{Fe}_3\text{O}_4$  and CA volume ( $X_2X_3$ ). The relative influence of cross correlations on the retardance of CA coated FFs (from examining the magnitude of the  $P$  value or from  $t$  Stat checking the significance level of the cross items) is given by:  $X_2X_4 > X_1X_3 > X_2X_3$ . In addition, factors at higher order (i.e.  $X_2^2$ ,  $X_3^2$  and  $X_4^2$ ) in equation (2) denote positive and negative quadratic relationships, respectively. Therefore, the effect of each factor on the experiment indices must be taken into account during the experiment.

### 3.2 Results of Optimization using Genetic Algorithm

Based on equation (2), the evolutionary solver in Microsoft Excel is used to solve optimization problem firstly. The optimized parametric combination and the maximum retardance of CA coated FFs are obtained as [5.499997 0.12 38.8397 89.99992], corresponding to the pH of suspension, molar ratio of CA to  $\text{Fe}_3\text{O}_4$ , CA volume, coating temperature, and  $42.431^\circ$ , respectively. Also, the GA in MATLAB is used to solve the optimization problem. As shown in Figure 4, the optimized parametric combination and maximum retardance of CA coated FFs are determined as [5.499 0.12 39.369 90] and  $42.411^\circ$ , close to those obtained by the evolutionary solver in Microsoft Excel and a relative error of -0.047%. Above all, we successfully model the retardance in CA coated FFs by the stepwise regression and the maximum global retardance is determined by the use of GA method.

It is noted that the fitness function as @FitFun425 is obtained by changing the sign of equation (2) and is used to find the minimum value. The results obtained by twelve times of executions of GA in MATLAB are listed in Table 4, and Figure 4 is corresponding to the results of the seventh execution of GA. It is noted that the lowest retardance was obtained as  $37.787^\circ$  in the tenth execution and the corresponding molar ratio of CA to  $\text{Fe}_3\text{O}_4$  is just 0.106.

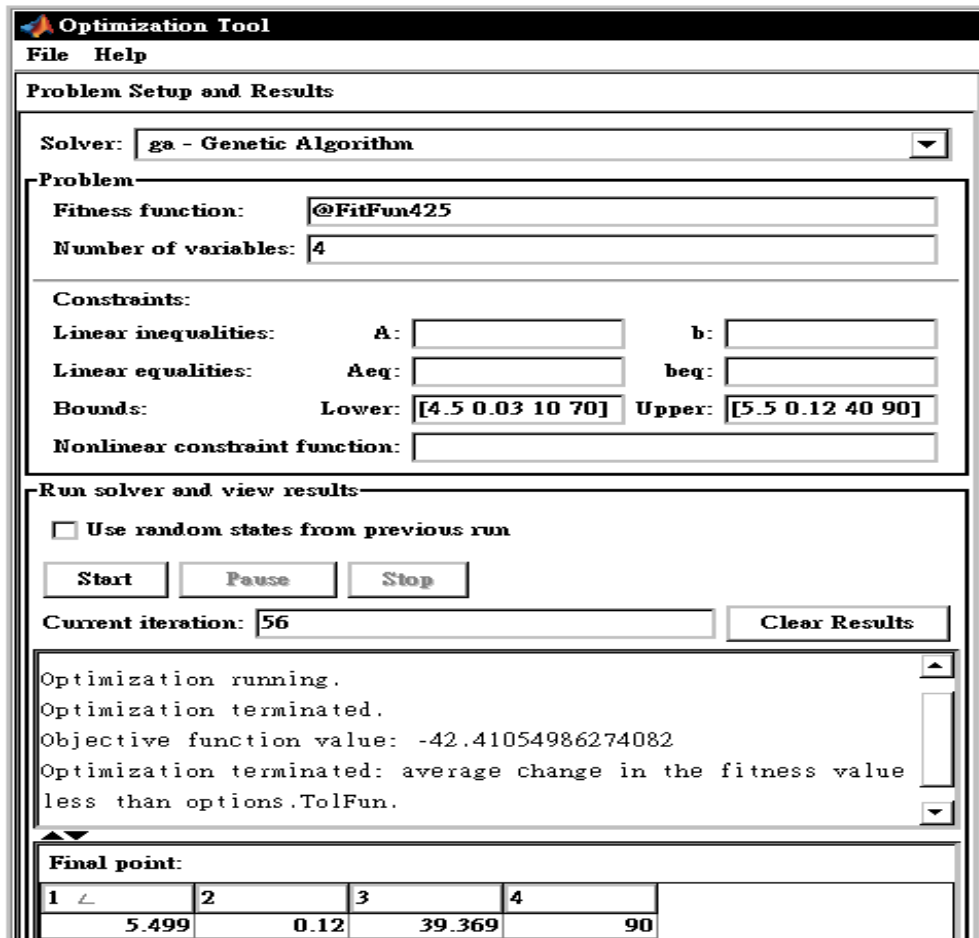


Figure 4: A graph output using the GA in MATLAB® optimization.

Table 4. Optimized parametric combination and maximum retardance.

No	pH	Molar Ratio	CA Volume	Coating Temp.	Retardance (deg)
1	5.498	0.118	38.917	89.992	41.627
2	5.5	0.12	38.555	89.993	42.390
3	5.498	0.12	38.821	89.999	42.392
4	5.498	0.12	32.385	89.99	41.612
5	5.498	0.12	34.824	89.991	42.091
6	5.498	0.12	38.814	89.996	42.300
7	5.499	0.12	39.369	90	42.411
8	5.5	0.118	38.942	89.847	41.739
9	5.494	0.112	39.378	89.993	39.744
10	5.496	0.106	39.832	89.976	37.787
11	5.5	0.12	38.682	89.985	42.390
12	5.5	0.117	39.346	89.975	41.550



In overall, Taguchi method is a discontinuous optimization approach, which can only obtain the local discontinuous optimal solution of pre-selected parameter level value, and cannot find out the global optimal solution [4]. The integration of Taguchi method with various approaches including numerical simulation, principal component analysis (PCA), artificial neural network (ANN), response surface methodology (RSM), and genetic algorithm (GA) could be used to enhance the efficiency of the optimization process. In addition, it is noted that GA based on a neural network model has been applied successfully to optimize complicated bioprocesses [4].

In future work, the predicted retardance value obtained by the trained ANN model [7] could be adopted as the fitness value, further, the GA operation such as select, crossover, and mutation are executed to find the global retardance of CA coated FFs. Moreover, the multiple-objective optimization including maximum retardance and low dichroism of CA coated FFs [4] or in other double-layer coated FFs is supposed to be performed in future. Therefore, the practical biomedical applications such as hyperthermia (magnetic inductive heating of cancer tumour) and magnetic resonance imaging (MRI) could be executed.

#### 4. Conclusion

The stepwise regression method was used to model the retardance of CA coated FFs precisely and efficiently. According to the MATLAB results of the second order stepwise regression, the  $F$  value was obtained as high as  $1.70875e+6$  and had a correlation coefficient of one; the developed regression model had highly predictable ability. Therefore, the retardance value, corresponding to each parametric combination, built by four parameters with three levels in Taguchi method, could be precisely determined by the stepwise regression equation. Also, using the genetic algorithm in MATLAB, the optimized parametric combination was determined as [5.499 0.12 39.369 90]. The maximum retardance was found as  $42.411^\circ$ , close to that obtained by the evolutionary solver in Microsoft Excel and a relative error of -0.047%.

#### REFERENCES

- [1] Sahoo, Y., Goodarzi, A., Swihart, M. T., Ohulchanskyy, T. Y., Kaur, N., Furlani, E. P., Prasad, P. N. 2005. Aqueous ferrofluid of magnetite nanoparticles: fluorescence labeling and magnetophoretic control, *Journal of Physical Chemistry B*, 109, 3879-3885.
- [2] Srivastava, S., Awasthi, R., Gajbhiye, N. S., Agarwal, V., Singh, A., Yadav, A., Gupta, R. K. 2011. Innovative synthesis of citrate-coated superparamagnetic  $Fe_3O_4$  nanoparticles and its preliminary applications, *Journal of Colloid and Interface Science*, 359, 104-111.

- [3] Li, L., Mak, K. Y., Leung, C. W., Chan, K. Y., Chan, W. K., Zhong, W., Pong, P. W. T. 2013. Effect of synthesis conditions on the properties of citric-acid coated iron oxide nanoparticles, *Microelectronic Engineering*, 110, 329-334.
- [4] Lin, J. F., Tsai, C. C. and Lee, M. Z. 2014. Linear birefringence and dichroism in citric acid coated Fe<sub>3</sub>O<sub>4</sub> magnetic nanoparticles, *Journal of Magnetism and Magnetic Materials*, 372, 147-158.
- [5] Lin, J. F. and Lee, M. Z. 2012. Concurrent measurement of linear birefringence and dichroism in ferrofluids using rotating-wave-plate Stokes polarimeter, *Optics Communications*, 285, 1669-1674.
- [6] Lin, J. F., Wu, J. S. and Sheu, J. J. 2015. Modeling of retardance in ferrofluid with Taguchi-based multiple regression analysis, *Proceedings of SPIE*, 9302, 930229-1-6.
- [7] Lin, J. F., Sheu, J. J. 2016. Modeling and prediction of retardance in citric acid coated ferrofluid using artificial neural network, *Journal of Magnetism and Magnetic Materials*, 404, 201-208.
- [8] Cevik, A., Gog̃us, M. T., Guzelbey, I. H., Filiz, H. 2010. A new formulation for longitudinally stiffened webs subjected to patch loading using stepwise regression method, *Advances in Engineering Software*, 41, 611-618.
- [9] Jiao, L. and Li, H. 2010. QSPR studies on the aqueous solubility of PCDD/Fs by using artificial neural network combined with stepwise regression, *Chemometrics and Intelligent Laboratory Systems*, 103, 0-95.
- [10] Hsieh, K. L. and Lu, Y. S. 2008. Model construction and parameter effect for TFT-LCD process based on yield analysis by using ANNs and stepwise regression, *Expert Systems with Applications*, 34, 717-724.
- [11] Frontline System, 2016.  
<http://www.solver.com/genetic-evolutionary-introduction>.
- [12] Yusup, N., Zain, A. M. and Hashim, S. Z. M. 2012. Evolutionary techniques in optimizing machining parameters: Review and recent applications (2007-2011), *Expert Systems with Applications*, 39, 9909-9927.
- [13] Holland, J. H. 1975. *Adaptation in Natural and Artificial Systems*, Cambridge, MA: MIT Press.
- [14] Lin, W. L., Yu, T. C., Lo, Y. L., Lin, J. F. 2009. A hybrid approach for measuring the parameters of twisted nematic liquid crystal cells utilizing the Stokes parameter method and a genetic algorithm, *IEEE Journal of Lightwave Technology*, 27, 4136-4144.

## **A design of inter-vehicle communication system using software-defined radio**

Wen-Tzu Chen and Jen-Yu Wu

Institute of Telecommunications Management, National Cheng Kung University,  
Tainan, Taiwan

Corresponding Author: wtchen@mail.ncku.edu.tw

### **ABSTRACT**

One of the primary technologies for connected vehicle network is vehicle ad hoc network (VANET). The VANET can be divided into four parts; 1) vehicle to vehicle (V2V), 2) vehicle to roadside (V2R), 3) vehicle to infrastructure (V2I), 4) vehicle to human (V2H). Through the use of V2V technology, vehicle identification information and emergence messages can be automatically delivered among vehicles and can help drivers make right decision to increase road usage efficiency and avoid traffic accident. The VANET technology provides broadband network service and allows high rate transmission for multimedia. However, it uses microwave band, i.e. 5.8 GHz, and such high carrier frequency can be easily blocked and attenuated by nearby buildings. Also, the volume of vehicle identification information and emergency message is small and just needs a small bandwidth to transmit to each other. The primary information may include vehicle ID, speed, position, owner, etc. The main objectives of this paper include 1) designing an automatic identification and safety message transmission system for connected vehicles based on software-defined radio (SDR) technology, 2) building V2V transmission platform through the use of lower carrier frequency, 160 MHz, to overcome the obstacle of nearby buildings, 3) implementing self-organized time division multiple access (SOTDMA) technology to avoid interference among vehicles, 4) measuring system performance of the proposed inter-vehicle communication system. The main software-defined radio device we used is USRP B200 mini with frequency range from 70 MHz to 6 GHz. To reduce the size of our design, we adopt Raspberry Pi embedded with a WiFi network as the computation server. In fact, both USRP B200 and Raspberry Pi are credit-card-sized devices. The open-source development platform GNU Radio is employed to design the inter-vehicle communication system. With the prototype system, we can exchange important information of vehicles. Also, our proposed system is more extensible than traditional hardware-based design due to the flexible implementation of SDR technology.

**Keyword:** VANET, GNU Radio, Raspberry Pi, self-organized time division multiple access, software-defined radio

# Energy Planning Framework Based on a Multi-objective Optimization Approach for University Campus Buildings

Aumnad Phdungsilp<sup>a\*</sup>

<sup>a</sup>Graduate Program in Engineering Management

College of Innovative Technology and Engineering, Dhurakij Pundit University

Bangkok, Thailand

\*Corresponding Author: aumnad@dpu.ac.th

## ABSTRACT

Energy planning plays an important role for the development or retrofitting of university campuses towards sustainability. University campuses offer a great potential for testing innovative energy concepts at both the demand and supply sides. University campus usually comprises of a group of buildings, so-called building clusters. Energy management at the building cluster level enhances improving energy efficiency, reducing primary energy use, increasing renewable energy sources, and reducing CO<sub>2</sub> emissions in the building sector. This paper presents a framework of energy planning for university campus buildings based on a multi-objective optimization approach for providing energy planning strategies. This paper focuses on the development of a tool for campus-wide energy planning. Building clusters in university campus offer synergies for optimized energy supply system and the demand of energy services can exchange among buildings with a different pattern of energy requirements. The paper describes a framework and model for multi-objective approach in energy systems planning. This framework can be served as a tool to managing energy services and efficient use of resources in the development and planning of sustainable university campuses.

**Keyword:** Building Clusters, Energy Planning, Multi-objective Optimization, University Campus.

## 1. Introduction

The built environment has been recognized for implementing energy management strategies and CO<sub>2</sub> emission reduction actions. There are many attempts to integrate sustainability into university campus operations, for example the International Sustainable Campus Network. The development of university campuses presents many opportunities to investigate the options that can minimize the inefficient use of energy resources, as well as to explore new ideas to improve energy efficiency, and to reduce primary energy sources while providing the same energy services.

University campus buildings can provide a living laboratory for testing innovative energy concepts at both the demand side (the building) and supply side (the energy system), for example energy matching between supply and demand based on the quality of energy (Kilkiş et al., 2017; Wang et al., 2017). Also, there is a need for future university campus development or retrofitting to plan for utilizing local energy sources and maximizing the use of renewable energy resources. The energy use in any building type is usually during the operation stage of the building's life-cycle. Many initiatives and efforts have been taken to reduce energy use and to increase energy efficiency on a single building basis. It is clearly that the energy-related issues are the area of strategic for sustainable development (Kilkiş et al., 2017).

In the literature, existing studies involve various aspects of energy-related issues in university campus buildings. Various publications have conducted the studies from the equipment and building levels to the energy system level in university campuses. The analysis at the equipment level is mainly for heating, ventilation and air-conditioning (HVAC) equipment, such as Escrivá- Escrivá et al. (2010) and Dong et al. (2014). At the building level, the analysis involves the evaluation of measures for promoting more efficient buildings, energy-saving potential, and simulation the gaps between real and estimated energy usage (Chung and Rhee, 2014 and Herrando et al., 2016). There is a growing research with the analyses involving energy system level at university sites, and to develop efficient models and application, as well as to propose new concepts for the university campuses, for example Kilkiş et al., 2017 and Wang et al., 2017. The abovementioned studies highlight that university campus buildings can provide effective testing grounds for assessing energy-related issues at various levels.

Thus, innovative and systematic solutions are required to support the transition towards sustainability and to minimize the impact of climate change and environmental footprints. Many studies have developed methods and tools for optimizing and reducing the energy use in buildings (Dong et al., 2017). The design methods have been developed over the years with the focus on developing both low-emissions and energy efficient buildings (Fesanghary et al., 2012; Evins, 2013). However, in the case of campus buildings that comprise of a group of buildings, few studies have been performed the design of energy systems and services through building cluster modeling (Han et al., 2013; Rees et al., 2014).

Analysis of energy systems and services at the building cluster level provides high potential of energy sharing between buildings in a cluster. Energy management in

campus buildings is possible in energy exchange, distribution, and collective production. In the published work, a limited study was used optimization analysis for energy systems at the building cluster level. Some investigations limited their optimization on the building scale (Chantrelle et al., 2011; Fesanghary et al., 2012) but some applied for a city level (Sampaio et al., 2013) and industrial area (Buoro et al., 2013). Energy planning is an important task for managing university campuses. However, in many cases energy use data availability and insufficient data is a significant barrier for energy planning. On the other hand, most energy system planning models focus on a single objective, for example minimization of total cost. The energy planning objectives are naturally conflicting. Hence, a multi-objective approach helps to identify compromise solutions that benefit all stakeholders.

The primary objective of this paper is to propose and describe a conceptual framework for energy planning from both the demand side (the building) and the supply side (the energy system) based on simulation-based optimization approach. The multi-objective optimization (MOO) is proposed to find the optimal mix of energy conversion technologies to cover the energy requirements at the building cluster level (university campus buildings). The framework can be used to facilitate the testing of potential strategies for energy planning in university campus areas.

## **2. Multi-objective Optimization Approach in Building Energy Planning**

Energy planning is predominantly to find the least cost solution or a single objective. In recent years, there is a growing need to incorporate sustainability concern in energy systems planning, which results in the increased application of multi-criteria approaches. The energy planning is a multi-objective problem in nature. The solution to this kind of problem must be solved by the method that provides an optimal or near optimal solution to generate useful results. MOO is a scientific area that offers various methods with large potential for the solution of complicated problems.

A large number of MOO techniques have been developed over the past decades. Some techniques convert the problem to a single objective problem. This is referred to as a classical approach to MOO. A new group of MOO techniques have been developed based on the principles of natural evolution. They are often referred to as multi-objective evolutionary algorithms. They handle groups of possible solutions and able to find several solutions of the Pareto set in a single run (Deb, 2001). They are powerful methods for problems with discrete and integer variable, such as building materials and energy systems designs.

The evolutionary MOO algorithm becomes an established field of research and application with many dedicated books, for example Deb (2001). Several algorithms have been proposed and applied to engineering problems, including energy studies (Deb, 2001; Alarcon-Rodriguez, 2010). The primary reason is the ability to deal with a set of possible solutions and finding Pareto optimal solutions. Applying optimization problem to energy systems planning is the structured process of optimization energy technology types, sizes, and locations to achieve a set of objective(s) and subject to a set of constraint(s). MOO enables to address the issue of conflicting objective functions, for example the life cycle cost, the life cycle CO<sub>2</sub> emissions, the indoor thermal comfort level, and the structural design analysis. The approach finds a set of solutions by varying the impact of each objective function in the global optimum. A generic MOO problem can be expressed as follows:

$$\min F(x) = \min([f_1(x), f_2(x), \dots, f_m(x)]) \quad (1)$$

Subject to

$$x \in \Omega \quad (2)$$

$$g_j(x) = 0, \quad j = 1, 2, \dots, p \quad (3)$$

$$h_k(x) \leq 0, \quad k = 1, 2, \dots, p \quad (4)$$

where  $F_{(x)}$  is a vector of  $m$  objective functions  $f_i(x)$ . All objectives are expressed as minimization. A maximization objective can be formulated by minimizing the negative of the objective function as  $\min -f_i(x)$ , where  $x$  is the decision vector, such as technology types and envelop-related variables that includes a set of decision variables  $[x_1, x_2, x_3, \dots, x_n]$ . The decision domain ( $\Omega$ ) is defined by the possible values that the decision variables can take or the search space. The optimization problem is also bounded by equality constraints ( $g_j$ ) and inequality constraints ( $h_k$ ). A problem with conflicting objectives has no single solution, but a set of optimal solutions that satisfies the objectives at an acceptable level without being dominated by any other solution (Deb, 2001).

The optimization procedure finds a set of decision variables that allow the minimization of objective functions. The optimization determines the values of variable  $x$  in Eq. 1–4. In the context of building energy system modeling, these variables are often focused on the design of energy technologies to supply energy services, such as heating, cooling, lighting, hot water, and electrical appliances. The constraint functions reduce the variability of the design variables. The equality and inequality constraints in Eq. (3) and (4) can be involved in design characteristics and operating parameters.



The goal of MOO is to identify solutions in the Pareto optimal set. A practical approach is to investigate a set of solutions that represent the Pareto optimal set by means of computational algorithms, such as genetic algorithm (GA) (Deb, 2001; Konak et al., 2006). MOO problems have a large number of solutions defined by the Pareto front. Finding all Pareto solutions is practically impossible. Therefore, a subset of the Pareto set is usually looked for. Previous studies, such as Deb (2001), Konak et al. (2006), and Alarcon-Rodriguez et al. (2010), suggested that solving MOO problems involve satisfying three areas: (i) accuracy finding a set of solutions as close to the real Pareto front as possible; (ii) diversity finding a set of solutions as diverse as possible; and (iii) spread finding a set of solutions that capture the whole spectrum of the true Pareto front.

Finding the optimal solution can be done with various state-of-the-art optimization tools that coupling with the energy performance simulation tools and energy systems models. With regard to the optimization algorithms in the literature, it is found that four algorithms, namely NSGA-II (non-dominated sorting genetic algorithm), MOPSO (multi-objective particle swarm optimization), MOGA (multi-objective genetic algorithm), and MODE (multi-objective differential evolution), are the most widely used for building performance optimization problems (Li et al., 2017).

### **3. Proposed Framework**

#### **3.1 Framework for Optimizing Energy Planning**

There is a growing concern in improving building performance in terms of energy and environmental perspectives. In the context of university campus buildings which can be characterized as building clusters, the energy use profiles are the fundamental information for energy planning. Also, there is a need for some tools that offer a holistic integration of sustainability aspect in energy systems planning and optimizing the energy planning strategies.

Having identified the research gap, this paper proposes a generic framework of MOO energy planning for university campuses to find energy planning strategies for university campus. The system boundary can be seen as building clusters. A number of studies have been developed the simulation-based optimization tools for a building scale. But few studies have been developed for a building cluster level (Phdungsilp et al., 2013). Therefore, this paper focuses on developing tool for building cluster scale or university campus in particular. The proposed framework is based on techniques of



three modules: building energy modeling; energy systems modeling; and simulation-based optimization. A generic framework is presented in Figure 1.

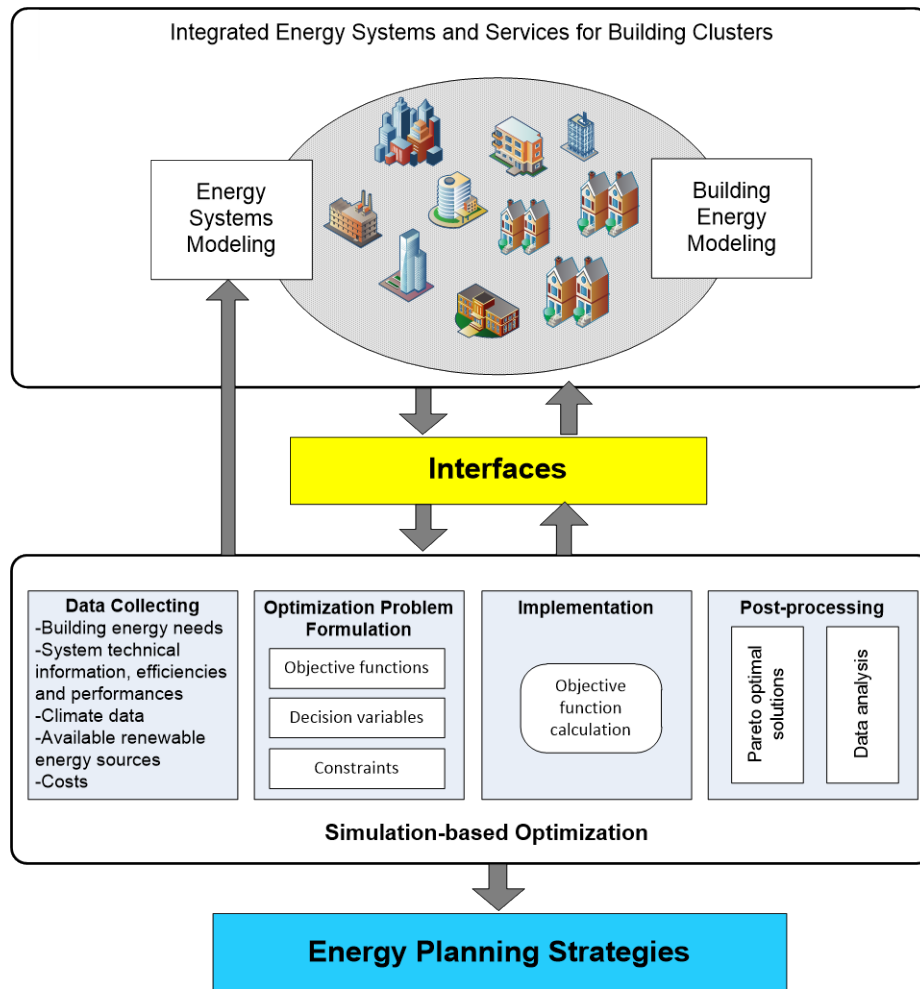


**Figure 1.** The proposed framework for optimizing energy planning strategies (Adapted from Phdungilp et al., 2013; Magny et al., 2014)

The building energy performance module can be modeled with various building energy performance programs, for example EnergyPlus, IDA ICE, ESP-r, and TRNSYS (Chantrelle et al., 2011; Hamdy et al., 2012; Evins, 2013; Phdungilp et al., 2013; Li et al., 2017). These tools can provide hourly load profiles for heating, cooling, hot water, and electricity. All of the load profiles are taken as the inputs to the energy system simulation and optimization. In the proposed framework, EnergyPlus will be used for testing the framework and modeling building energy performance. Similarly to building energy modeling, there are some sophisticated tools for preliminary design and assessment of the energy system configurations, such as RETScreen. The tools can also help to identify the potential of available energy

sources for the local areas, as well as energy conversion technologies.

The interfaces or data interactive module reads input and output files with simulation models and optimization tool, such as MATLAB, MOBO, and GenOpt (Phdungsilp et al., 2013; Magny et al., 2014; Wang et al., 2017). At the beginning of each iteration during the searching procedure, the interface module reads variables from optimization tool and passes the data to simulation model. Then, the module reads the results from the simulation model and passes the data to optimization tool to evaluate the objective functions. The processes work with the data by text files.

Having identified the energy conversion technologies, the simulation-based optimization model uses the energy conversion technologies as the design variables. These variables can be continuous and discrete or binary. Continuous design variable are the size of energy technologies. Discrete or binary variables are the number of energy technologies. Then, the optimization process finds a set of design variables that minimize the desired objective functions. In addition, the proposed framework can apply to optimize the demand side. Building design variables can be used into the optimization framework and can also be optimized together with energy conversion technology variables.

The energy planning often involves conflicting objectives between different stakeholders involved in the processes, for example the life-cycle cost, life-cycle CO<sub>2</sub> emissions, and non-renewable primary energy use. The proposed framework employs MOO technique based on GA to find a set of optimal solutions. This can be solved using several customized or generic optimization tools.

### **3.2 Towards Application of the Framework**

The proposed framework will be applied to a case study of university campus in Bangkok, Thailand. The campus consists of office buildings, lecture buildings, and student apartments. The energy systems that connect with various energy supply technologies to provide building energy services will be determined by means of energy system model to provide energy planning strategies. The hourly energy use profiles for each building will be obtained through a building energy performance modeling tool (EnergyPlus). The objective functions are calculated by the developed MATLAB script that models and simulates the energy system. A generic optimization software (MOBO) is used to solve the MOO problem.

The case study will be tested using the research question: what are the measures to achieve low emissions and high energy efficiency campus development under the sustainability criteria? Regarding solution strategy, it is expected to find the optimal mix of energy technologies to cover the energy requirements of the case study. The framework presented in this paper could provide new strategies to achieve sustainable campus development. The application would allow other researchers to test their strategies to identify campus-wide sustainability measures.

#### 4. Conclusion and Future Work

This paper proposes and describes a generic framework based on a MOO approach for energy planning at the building cluster level. The study focuses on the development of a tool for campus-wide to achieve low emissions and high energy efficiency. The proposed framework is based on techniques of three modules, namely building energy modeling, energy systems modeling, and simulation-based optimization to select the optimum energy planning strategy. The framework can be applied to optimize the energy system from both supply and demand side. For the supply side, the energy conversion technologies and corresponding energy resources are optimized, and on the demand side, building design parameters are optimized together with energy technology parameters. The framework is also flexible to allow addition, deletion, and modification of new energy supply and demand technologies for other cases. The proposed framework can support the realization of energy planning for university campuses and enhance urban sustainability because university campuses can be considered as downscaled versions of cities. In addition, the proposed framework can be further developed by connecting with information systems for visualizing the results. The integrating with visualization platform can potentially serve as a tool for decision-making. The performance of the MOO algorithms and case studies will be conducted in the future work.

#### REFERENCES

- Alarcon-Rodriguez, A., Ault, G., and Galloway, S. 2010. Multi-objective planning of distributed energy resources: A review of the state-of-the-art, *Renewable and Sustainable Energy Reviews*, 14, 1353-1366.
- Buoro, D., Casisi, M., Nardi, A.D., Pinamonti, P., and Reini, M. 2013. Multicriteria optimization of a distributed energy supply system for an industrial area, *Energy*, 58, 128-137.
- Chantrelle, F.P., Lahmidi, H., Keilholz, W., Mankibi, M.E., and Michel, P. 2011. Development of a multicriteria tool for optimizing the renovation of buildings, *Applied Energy*, 88, 1386-1394.

- Chung, M., and Rhee, E., 2014. Potential opportunities for energy conservation in existing buildings on university campus: A field survey in Korea, *Energy and Buildings*, 78, 176-182.
- Deb, K. 2001. *Multi-Objective Optimization using Evolutionary Algorithms*. John Wiley and Sons.
- Dong, B., O'Neill, Z., Luo, D., and Bailey, T. 2014. Development and calibration of an online energy model for campus buildings, *Energy and Buildings*, 76, 316-327.
- Dong, L., Wang, Y., Scipioni, A., Park, H-S., and Ren, J. 2017. Recent progress on innovative urban infrastructures system towards sustainable resource management, *Resources, Conservation and Recycling*, (Article in press), <http://dx.doi.org/10.1016/j.resconrec.2017.02.020>.
- Escrivá- Escrivá, G., Álvarez-Bel, C., and Valencia-Salazar, I. 2010. Method for modeling space conditioning aggregated daily load curves: Application to a university building, *Energy and Buildings*, 42, 1275-1282.
- Evens, R. 2013. A review of computational optimization methods applied to sustainable building design, *Renewable and Sustainable Energy Reviews*, 22, 230-245.
- Fesanghary, M., Asadi, S., and Geem, Z.W. 2012. Design of low-emission and energy-efficient residential buildings using a multi-objective optimization algorithm, *Building and Environment*, 49, 245-250.
- Hamdy, M., Palonen, M., and Hasan, A. 2012. Implementation of Pareto-Archive NSGA-II Algorithms to a Nearly-Zero-Energy Building Optimisation Problem, In: *Proceedings of the 1st Building Simulation and Optimization Conference (BSO12)*, 10-11 September 2012, Loughborough, UK.
- Han, X., Pei, J., Liu, J., and Xu, L. 2013. Multi-objective building energy consumption prediction and optimization for eco-community planning, *Energy and Buildings*, 66, 22-32.
- Herrando, M., Cambra, D., Navarro, M., Cruz, L., Millán, G., and Zabalza, I. 2016. Energy Performance Certification of Faculty Buildings in Spain: the gap between estimated and real energy consumption, *Energy Conversion and Management*, 125, 141-153.
- Kilkiş, Ş., Wang, C., Björk, F., and Martinac, I. 2017. Cleaner energy scenarios for building clusters in campus areas based on the Rational Exergy Management Model, *Journal of Cleaner Production*, 155, 72-82.
- Konak, A., Coit, D.W., and Smith, A.E. 2006. Multi-objective optimization using genetic algorithms: A tutorial, *Reliability Engineering and System Safety*, 91, 992-1007.

- Li, K., Pan, L., Xue, W., Jiang, H., and Mao, H. 2017. Multi-Objective Optimization for Energy Performance Improvement of Residential Buildings: A Comparative Study, *Energies*, 10, 245-268.
- Magny, A., Martinac, I., and Phdungsilp, A. 2014. Optimization of energy supply systems for a sustainable district in Stockholm using genetic algorithms, In: Proceedings of the 2014 World Sustainable Building Conference, 28-30 October 2014, Barcelona, Spain.
- Phdungsilp, A., Martinac, I., and Ngo, T. 2013. A framework for integrated energy systems, infrastructure, and services optimization with visualization and simulation platform for low-carbon precincts, In: Proceedings of the International Symposium for Next Generation Infrastructure, 30 September-4 October 2013, Wollongong, Australia.
- Rees, M.T., Wu, J., Jenkins, N., and Abeysekera, M. 2014. Carbon constrained design of energy infrastructure for new build schemes, *Applied Energy*, 113, 1220-1234.
- Sampaio, H.C., Dias, R.V., and Balestieri, J. 2013. Sustainable urban energy planning: The case study of a tropical city, *Applied Energy*, 104, 924-935.
- Wang, C., Kilkiş, Ş., Tjernstrom, J., Nyblom, J., and Martinac, I. 2017. Multi-objective optimization and parametric analysis of energy system designs for the Albano university campus in Stockholm, *Procedia Engineering*, (Article in press), urn:nbn:se:kth:diva-192952.

## A Novel Q-Learning Approach for Early-Termination Algorithm for HEVC Coding Unit Partition

Yih-Chuan Lin\* and Yi-Sheng Lin

Department of Computer Science and Information Engineering, National Formosa University, Yunlin, Taiwan 63201.

\*Corresponding Author: lyc@nfu.edu.tw

### ABSTRACT

HEVC (High Efficiency Video Coding) is the newest video compression standard, and when comparing with the former compression standard H.264/AVC (Advanced Video Coding), it can make over 50% increase of compression ratio under the almost equivalent perceptual reconstruction quality. The cost of raising compression ratio comes at a drastic increase on the encode time. To speed up the HEVC standard encoder, the early termination and early skip-mode coding unit quad-tree partition schemes have been proposed in literature, whose performance is solely dependent on the thresholds chosen to early terminate the coding unit partition process. Nonetheless, these thresholds are usually selected according to empirical or heuristic data analysis; leading to a manual choice of thresholds from case to case. With regards to this issue, an adaptive threshold selection scheme that can determine the threshold values depending to the incoming video data should be more suitable for the development of speeding up HEVC encoder. We define the HEVC quad-tree partition process as a MDP (Markov Decision Process) problem, and try to use the reinforcement learning to decide the adaptive early termination threshold for the varying video data distribution. In the coding unit quad-tree partition process, one needs to partition each coding unit down to the maximum depth, and then uses the pruning process to make the final split decision. With the proposed method, the encoder needs only to get the RDCost (Rate-Distortion Cost) of current coding unit and its children blocks for making the action of selecting a termination threshold for avoiding the unnecessary computation of prediction and transform process in HEVC encoder. Current experimental results show that the purposed method is able to gain 15% of average time savings with only 0.05%'s PSNR (Peak Signal-to-Noise Ratio) degradation when comparing to the HEVC standard encoder.

**Keyword:** High Efficiency Video Coding, Early Termination, Machine Learning, Reinforcement Learning, Quad-Tree Partition.

# **Development of surface assembly of Immunostimulatory Gelatin Nanoparticle Carriers for Mucosal Antigen Delivery**

**Shen-Fu Lin<sup>1</sup>, Jeng-Shiang Tsai<sup>3</sup>, I-Hsiu Liu<sup>4</sup>, Yun-Huan Liu<sup>4</sup>, Shyr-Yi Lin<sup>\*,2</sup> and Der-Zen Liu<sup>\*,1</sup>**

**<sup>1</sup> Graduate Institute of Biomedical Materials and Tissue Engineering, College of Biomedical Engineering, Taipei Medical University, Taipei, Taiwan**

**<sup>2</sup> Department of General Medicine, Taipei Medical University, and Department of Primary Care Medicine, Taipei Medical University Hospital, Taipei, Taiwan.**

**<sup>3</sup> Institute of Biomedical Engineering, National Taiwan University, Taipei, Taiwan**

**<sup>4</sup> School of Dental Technology, College of Oral Medicine, Taipei Medical University, Taipei, Taiwan**

## **Abstract**

Mucosal vaccine induces both mucosal (secretory IgA) and systemic immune responses and is considered an ideal vaccination strategy for prevention of infectious diseases. One important point to be considered in mucosal vaccination is effective antigen delivery system which can effective delivery of antigen to antigen-presenting cells (APCs) of mucosal. In the present study, cationic gelatin nanoparticles (GNPs) were prepared as ideal carriers for more efficient antigen delivery. The average diameter of cationic gelatin nanoparticle was approximate 165 nm, and the zeta potential was about +35 mV, then ovalbumin (OVA) was physically absorbed onto cationic gelatin nanoparticle. The OVA absorption rate was near 95% the zeta potential was about +25 mV. The results that cationic gelatin nanoparticle effectively facilitated antigen uptake of macrophage cell line and mice bone marrow-derived dendritic cells (BMDCs). It also induced higher levels of pro-inflammatory cytokines and higher expression of co-stimulatory molecules of BMDCs. C57BL/6 mice twice immunized intranasally with OVA-absorbed cationic gelatin nanoparticle induced high levels of OVA-specific IgA in their in the nasal and lung wash fluid.

**Key words:** Antigen delivery, Antigen-presenting cells, Gelatin nanoparticle, Cationic modification, Mucosal vaccine



## **The synthesis of sex steroid hormones is dysregulated in the placenta of preeclampsia women**

Min Jae Kim<sup>a</sup>, Ye Young Shin<sup>a</sup>, Mee-Na Park<sup>a</sup>, Jae-Eon Lee<sup>a</sup>, Beum-Soo An<sup>a\*</sup>

<sup>a</sup>Department of Biomaterials Science, College of Natural Resources & Life Science/Life and Industry Convergence Research Institute, Pusan National University, Republic of Korea

\*Corresponding Author: anbs@pusan.ac.kr

### **ABSTRACT**

Preeclampsia (PE) is a pregnancy-specific hypertensive syndrome that results in substantial maternal and fetal morbidities and mortalities. The exact cause of PE has not been fully demonstrated, but abnormal formation of the placenta has been considered. The placenta connects the developing fetus to the uterine wall, producing a large amount of steroid hormones to maintain pregnancy. Steroid hormones, especially progesterone (P4) and estrogen (E2), have been widely studied in PE serum. However, steroidogenesis by steroidogenic enzymes in the placenta of PE women has not well been established. In this study, we compared concentrations of steroid hormones such as pregnenolone (PG), P4, dehydroepiandrosterone (DHEA), testosterone (T), and E2 in serum and placenta of PE women. PG, P4, DHEA, and E2 concentrations tended to decrease in PE serum and placenta, and the results were significant for P4 and E2 in the serum. Quantification of genes related with steroidogenesis in the placenta was examined, and expression of P4- and E2-synthesizing enzymes, HSD17B3 and HSD3B1, was reduced in PE placenta compared with normal placenta. Interestingly, CYP19A1, an enzyme critical for production of E2, was up-regulated in PE placenta, suggesting steroidogenic enzymes are dynamically regulated and could affect symptoms of PE. To evaluate the regulatory mechanism, human placental bewo cells were exposed to hypoxia, and expression of steroidogenic proteins was determined. The results show opposite expression patterns of those enzymes, meaning placenta cells synthesize more steroid hormones under hypoxic conditions. In summary, our results suggest that the levels of steroid hormones such as P4 and E2 in serum and placenta of PE women are down-regulated, which is mediated by regulation of steroidogenic enzyme expression in the PE placenta. This physiological symptom suggests that placenta cells stimulate expression of steroidogenic enzymes when cells are under hypoxic conditions.

**Keyword:** Preeclampsia, Steroid hormone, Placenta



## Hospital Wastewater Treatment Using Aerated Fixed Film Biofilter (AF2B)

Prayitno<sup>1\*</sup>, Hadi Saroso<sup>2</sup>, Sri Rulianah<sup>3</sup>, Hardjono<sup>4</sup>

\*Department of Chemical Engineering, State Polytechnic of Malang, Jl. Soekarno Hatta 9, Malang, Indonesia

\*Corresponding: prayitno\_polmal@yahoo.com

### ABSTRACT

In Indonesia, biological processes such as Activated Sludge, Anaerobic-Aerobic Biofilter, and Fluidized Bed Biofilm Aeration process have been used but still less effective which meet the water quality standards are only 52%. The purpose of this experiment was to investigate the capability of Aerated Fixed Film Biofilter (AF2B) reactor as an alternative process in reducing pollutants discharged from hospital wastewater. This study used AF2B reactor consisting biofilter shaped Honey comb as a medium for the growth of microorganisms. The microorganisms used were endogenous bacterial consortium obtained from the isolated bacteria in hospital wastewater. The hospital wastewater used discharge from some hospital. The research conducted with flowing an hospital wastewater into the AF2B reactor with circulation flow and through a number of biofilter. Experiment data were obtained through measuring the concentration of BOD<sub>5</sub>, fecal coli, phenol, and Pb at influent- effluent reactor that using APHA method. Results showed that AF2B reactor could remove BOD<sub>5</sub>, fecal coli, phenol and Pb were 91.59 %, 85.42 %, 62.5 %, 60 %, respectively. Thus it can be concluded that AF2B process has large capability of pollutants removal in hospital wastewater such as BOD, fecal coli, phenol, Pb.

**Keywords:** Hospital wastewater, Honey comb, Biofilter, Circulation flow

### 1. Introduction

Hospital wastewater is wastewater discharged from all hospital activities, both medical and non-medical activities, including activities at health care rooms, health check rooms, laboratories, radiology rooms, kitchens, and laundry rooms (Nasr and Yazdanbakhsh, 2008). Hospital wastewater contains hazardous pollutants such as pathogenic microorganisms (bacteria, viruses), the remaining of medicine and laboratory chemicals (antibiotics, antitumor, phenol, and chloroform), chemicals toxic (Pb), and biodegradable organic materials such as protein, fat, and carbohydrate (Al-Ajlouni *et al.*, 2013; Altin *et al.*, 2003; Nasr and Yazdanbakhsh, 2008; Prayitno *et al.*, 2013). In Indonesia, the processing and management of hospital wastewater are very worrying, where only 36% of hospitals have a Wastewater Treatment Plant (WWTP) and 64% of wastewater is discharged directly into receiving water bodies or using infiltration wells (Altin *et al.*, 2003). The materials pollutant that exceeds the quality standards and was mixed into an aquatic environment can cause pollution and health problems for humans being (Acharya *et al.*, 2014; Al-Ajlouni *et al.*, 2013; Nasr and Yazdanbakhsh, 2008; Sarafraz *et al.*, 2007).

Some pollutants that often exceed quality standards, among others: BOD<sub>5</sub>, Pb, phenol, fecal coli, ammonia free, orthophosphate, and chlorine free (Prayitno *et al.*, 2013). Several biological processes have been used in HWWTP, namely the Activated Sludge Biological Contactor (ASBC) (Rodgers, 1999), Submerged Membrane Bioreactor (SMB) (Wen *et al.*, 2004), Anaerobic Aerobic Fixed Film Bioreactor (A2F2B) (Rezaee *et al.*, 2005) and Anaerobic - Aerobic Biofilter (A2B) (Rezaee *et al.*, 2005). Low quality of discharges on HWWTP especially toxic pollutants (Pb, phenol) can be caused by not-yet-optimal biological process. In biological process, pollutants removal is affected by the temperature, pH, kinds of microorganism, time contact, the type of reactor, and the presence of inhibitors (Dhokpande and Kaware, 2013; Nair *et al.*, 2008; Tchobanoglous *et al.*, 2003; Wiesmann *et al.*, 2007). Furthermore, several kinds of microorganisms are proven effective to reduce heavy metal compounds (example: Pb) contained in wastewaters (Chaalal *et al.*, 2005; Farooqi *et al.*, 2008; Tchobanoglous *et al.*, 2003; Wiesmann *et al.*, 2007).

Thus, process of toxic pollutant removal in hospital wastewater can be done through using selected microorganisms (Mixed Bacterial Culture, MBC) and increasing contact time in biological process by using circulation flow in the biofilters. The purpose of this research was to investigate the capability of Aerated Fixed Film Biofilter (AF2B) process in reducing BOD<sub>5</sub>, fecal coli, phenol and Pb pollutants discharged from hospital wastewater.

## 2. Materials and Methods

### 2.1 Materials

The pilot system which consists of Aerated Fixed Film Biofilter Reactor (AF2B reactor) was designed as given in Fig.1. AF2B reactor is divided into 3 equal parts where each part contains biofilter which is made of plastic and shaped like a Honey comb. pH controller is fitted on the inlet of AF2B reactor while the submerged pump is fitted on the sedimentation tank to recycle some of the sludge into each biofilter. A diffuser is placed at the bottom of the biofilter which is connected to a blower that supplies air for the growth of microorganisms and for the perfection of the mixing process.

The characteristic of biofilter is material (plastic), density (0.125 g/cm<sup>3</sup>), volume (2,160 cm<sup>3</sup>), specific surface area (150 - 240 m<sup>2</sup>/m<sup>3</sup>), and number (3). While wastewater was taken from hospitals in Malang City which had characteristics as follow: Temperature: 30 C, pH: 8, BOD<sub>5</sub>: 240.25 mg/L, phenol: 0.04 mg/L, fecal coli: 2,400 MPN/100 ml, Pb: 0.025 mg/L. The microorganisms used were bacterial consortium (Mixed Bacterial Culture, MBC) obtained from the isolated bacteria in hospital wastewater (bacterial endogenous) by Central of Biotechnology Research – ITB, Bandung which MCB consists of several types of bacteria, such as: *Pseudomonas capica*, *Pseudomonas diminuta*, *Bacillus sp1*, *Bacillus sp2*.

### 2.2 Methods

The experiment was conducted by flowing the hospital waste water into the AF2B reactor by using the submerged pump (Type: Voss SN 3500). Influent flow rate of wastewater was set by using a flow meter of 0.1 L/min or Hydraulic Residence Time (HRT) of AF2B reactor was maintained constant for 3 hours. Wastewater flowed from the top of the biofilter towards the bottom and then moved circulation in every part of biofilter and flowed to the sedimentation part where the sludge were formed and partly recycled while the overflow flowed into tank. Each biofilter contained MBC derived

from the results of the acclimatization process that had been adapted to the hospital wastewater.

The sample were taken from effluent of the AF2B reactor on every 2 hours for 24 hours and followed every 12 for 120 hours. Furthermore, the samples were analyzed by using APHA methode where the parameters analyzed, among others: BOD5, phenol, fecal coli and Pb. Determination of test parameters based on the results of the research where the parameters often exceed the quality standard.

Pb was measured using Atomic Absorption Spectrophotometry (AAS) (Type: Perkin-Elmer AA900), fecal coli was measured using the Most Probable Number (MPN) method, phenol was measured using a UV-Vis (Type: Hitachi-U900), BOD5 was measured using the modified Winkler method, and Mixed Liquor Suspended Solid (MLSS) was measured using a Gravimetric method.

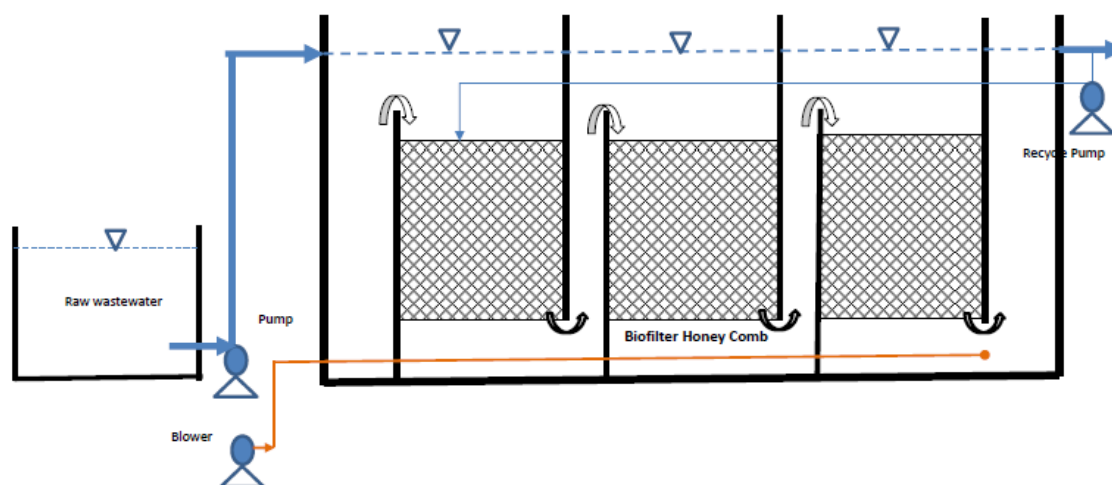


Figure 1. Schematic view of AF2B Reactor

### 3. Results and Discussion

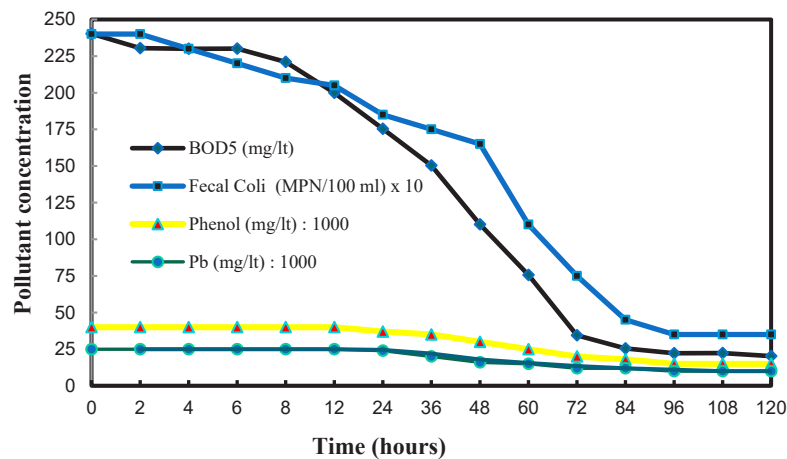
This research used real hospital wastewater as feed which hospital wastewater contained pollutants in different concentrations and AF2B reactor's performance was measured based on the initial concentration of pollutants in the feed.

The results of acclimatization and adaptation MBC in hospital wastewater media showed that MLSS concentration increased continuously until 1,500 mg/L. These conditions indicated that the MBC had grown and adapted to fit well with its surroundings and was ready for use in the biodegradation of pollutants. The pollutants concentration (BOD5, fecal coli, phenol, Pb) in the effluent AF2B reactor was measured at each period (Fig.2). The concentration of BOD5 and fecal coli decreased at the first 4 hours and reached a maximum decrease at 96 hours with the percentage of pollutant removal of 91% (Fig. 2). The largest decrease of the concentration of pollutants occurred in the period of 2 - 96 hours when BOD5, fecal coli, phenol, Pb were 74.01%, 67.6%, 62%, 60%, respectively. This happened because at the first 4 hours, microorganisms (MCB) were still adapting to the environment so the growth of MCB was not maximized, and it was indicated on the little slime formed on the surface of the biofilter. While, at time of 4-12 hours, the MCB began to adapt so the growth of MCB and the biodegradation process began to take place, and it was shown by the increased thickness of the slime on the surface of the

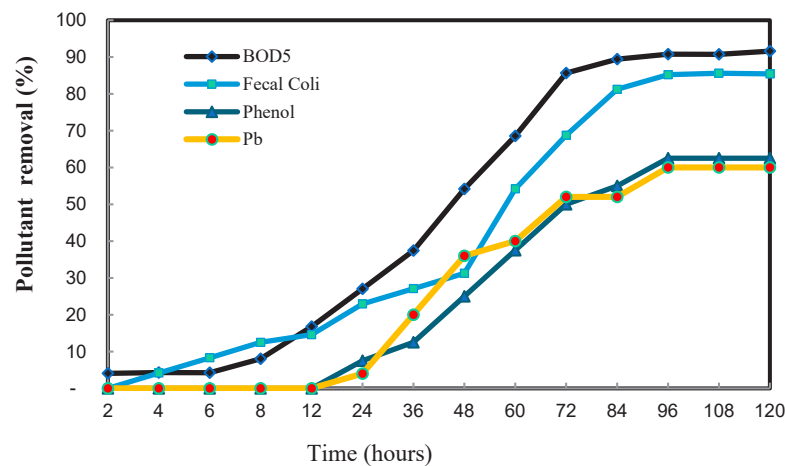
biofilter. Biofilm formation in a submerged biofilter takes place in five stages: initial attachment, irreversible attachment, maturation 1, maturation 2 and dispersion (Kaplan *et al.*, 2003).

AF2B reactor is composed of several biofilter shaped like a Honey comb that has a large specific surface area (150-240 m<sup>2</sup>/m<sup>3</sup>) where microorganisms grow and are in contact with wastewater (Rezaee *et al.*, 2005). At the time of 12-96 hours, MCB growth is increasing, in line with the increasing consumption of substrate (pollutant) by MCB which causes all surface of biofilter covered by the MCB to increase the speed of biodegradation process. On the other hand, by making the flow circulation in the reactor, supplies of air uniformly and continuously will increase the contact time in the Biofilter, causing biodegradation processes of pollutants going on rapidly (Dhokpande and Kaware, 2013; Rezaee *et al.*, 2005; Wiesmann *et al.*, 2007). At time 96-120 hours, stationary phase was reached where the rate of growth was proportional with rate of death of MCB in the biofilter so that the biodegradation of pollutants in stayed in steady state. These conditions reduced BOD<sub>5</sub> and fecal coli up to 91.59% and 85.42%, respectively.

In the aerobic biological process, biodegradation rate of organic material and phenol by microorganisms were affected by the temperature, initial concentration, pH, type of microorganism, HRT, the type of reactor and the presence of inhibitors (Dhokpande and Kaware, 2013; Nair *et al.*, 2008; Wiesmann *et al.*, 2007).



(a)



(b)

Figure 2. Performance of AF2B reactor for The HWW ( $Q_{\text{influent}}$ : 0.1 L/min, HRT:3 hour)  
 (a). Reduction of pollutant concentration (b). Percentage of pollutant removal

Furthermore, Bioremoval of Pb by microorganisms in the AF2B reactor had the same pattern with phenol biodegradation, where biodegradation was running slow and low. Increasing initial concentration of Pb may cause a decrease in the removal of BOD5. However, BOD5 removal re-increased by microorganisms acclimation to changes (Naja *et al.*, 2009).

At time 36 - 96 hours, the largest removal of Pb was 40%, and it was followed with the achievement of steady state. Bioremoval of Pb is affected by initial concentration of Pb and the number of microorganisms at pH 7-8 while aeration time at 48 hour and the initial concentration of Pb (30 mg/L) can reduce Pb concentration by 93.3% (Chojnacka, 2010). This experiment was with HRT :3 hours, pH 8, biodegradation time at 120 hours and initial concentration of Pb (0.01 mg/L) had decreased the removal of Pb (60%).

Phenols are aromatic organic compounds and Pb are the toxic substance (inhibitor) for microorganisms, making the biodegradation of phenol and Pb by microorganisms slower than that of BOD5 and fecal coli in the AF2B reactor. So Phenol and Pb concentrations began to reduce at 12 hours and reached a maximum decrease at 96 hours with the removal percentage up to 62% (Fig. 2). The biggest decrease of phenol and Pb occurred in a period of 24 - 84 hours which were 55 % and 52 %, respectively. Then they reached steady state at 96 hours with the percentage of pollutants phenol and Pb were 62.5% and 60%, respectively.

Phenol biodegradation by microorganisms is influenced by the shape of phenol compound, HRT, initial concentration and form of the enzyme (Farooqi *et al.*, 2008). The Biodegradation of phenol by mixed cultures is more efficient than that by pure cultures with biodegradation of phenol produce simple compounds such as carboxylic acids, CO<sub>2</sub> (Sridevi *et al.*, 2012). This research used mixed cultures (MCB) so that biodegradation of phenol was faster than the other, and biodegradation period of HTR was 3 hours. This made biodegradation time of 120 hours could reduce phenol by 62.5%. MCB consists of *Pseudomonas capica* and *Bacillus spl* that has the ability to degrade organic compound such as phenols and lead in aerobic / anaerobic (Sridevi *et al.*, 2012; Varghese *et al.*, 2012). UASB reactor with HRT of 40 days was able to reduce phenol by 80 % while SBR reactor with HRT of 30 days was able to reduce phenol by 95% (Dey and Mukherjee, 2010).

The ASBC process was able to decrease the concentration of COD and coliform up to 87.8% and 99.98%, respectively (Rodgers, 1999). The combination of the Up flow Anaerobic Fixed Bed (UAF-B), Suspended Aerobic Reactor (SAR) with the Membrane (Micro Filtration, MF) can reduce the concentration of COD (94-98%) (Kocadagistan *et al.*, 2005). Submerged Membrane Bioreactor (SMB) can reduce the BOD5 (47.7-70%) and coliform (50-75%) (Wen *et al.*, 2004). A2F2B process can reduce the concentration of pollutants in the hospital wastewater, namely BOD5, COD and coliform up to 89%, 82%, and 90%, respectively (Rezaee *et al.*, 2005).

The AF2B reactor was able to reduce of BOD5, fecal coli, phenol and Pb, with the biggest pollutant removal capability at 96 hours when it could reduce BOD5, fecal coli, phenol, and Pb up to 91.59%, 85.42%, 62.5%, and 60%, respectively (Table.1). This means that AF2B reactor began operating optimally at 96 hours.

**Table. 1. Total removal of pollutants in AF2B reactor**

Parameters	Quality Standard	AF2B Reactor		
		Inlet	Outlet	% Removal
BOD5 (mg/L)	30	240.25	20.2	91.59
Fecal coli (MPN/100 ml)	4,000	2,400	350	85.42
Phenol (mg/L)	0.01	0.04	0.015	62.5
Pb (mg/L)	0.01	0.025	0.01	60

#### 4. Conclusions

It can be concluded that The Aerated Fixed Film Biofilter (AF2B) process has a large capability of pollutants removal in hospital wastewater such as BOD5, fecal coli, phenol, and Pb up to 91.59%, 85.42%, 62.5%, and 60%, respectively.

#### Acknowledgments

The authors would like to thank to Ministry of Research, Technology and Higher Education – Indonesia has funded this research.

#### REFERENCES

- Acharya, A, Gokhale, V A, Joshi, D. 2014. Impact of Biomedical Waste on City Environment: Case Study of Pune, India. *IOSR Journal of Applied Chemistry*, 6 (6), 21-27.
- Al-Ajlouni, K, Shakhathreh, S, Ibraheem, N A-, Jawarneh, M. 2013. Evaluation of Wastewater Discharge from Hospitals in Amman - JORDAN. *International Journal of Basic & Applied Sciences IJBAS-IJENS*, 13 (4), 44-50.
- Altin, A, Altin, S, Degirmenci, M. 2003. Characteristics And Treatability Of Hospital (Medical) Wastewaters. *Fresenius Environmental Bulletin*, 12 (9), 1098-1108.
- Chaalal, O, Zekri, A Y, Islam, R. 2005. Uptake of Heavy Metals by Microorganisms. *Energy Sources*, 27 (1-2), 87-100.
- Chojnacka, K. 2010. Biosorption and Bioaccumulation – the Prospects for Practical Applications. *Environment International*, 36 (3), 299-307.
- Dey, S, Mukherjee, S. 2010. Performance and Kinetic Evaluation of Phenol Biodegradation by Mixed Microbial Culture in a Batch Reactor. *International Journal of Water Resources and Environmental Engineering*, 2 (3), 40-49.
- Dhokpande, S R, Kaware, J P. 2013. Biological Methods for Heavy Metal Removal-A Review. *International Journal of Engineering Science and Innovative Technology*, 2 (5), 304-309.



- Farooqi, I H, Basheer, F, Ahmad, T. 2008. Studies on Biodegradation of Phenols and *m*-Cresols by Upflow Anaerobic Sludge Blanket and Aerobic Sequential Batch Reactor. *Global NEST Journal*, 10 (1), 39-46.
- Kaplan, J B, Rangunath, C, Ramasubbu, N, Fine, D H. 2003. Detachment of *Actinobacillus actinomycetemcomitans* Biofilm Cells by an Endogenous  $\beta$ -Hexosaminidase Activity. *J. Bacteriol.*, 185 (16), 4693-4698.
- Kocadagistan, B, Kocadagistan, E, Topcu, N, Demircioğlu, N. 2005. Wastewater Treatment with Combined Upflow Anaerobic Fixed-Bed and Suspended Aerobic Reactor Equipped with a Membrane Unit. *Process Biochem.*, 40 (1), 177-182.
- Nair, C I, Jayachandran, K, Shashidhar, S. 2008. Biodegradation of Phenol. *African Journal of Biotechnology*, 7 (25), 4951-4958.
- Naja, G M, Murphy, V, Volesky, B, Flickinger, M C. 2009. "Biosorption, Metals" in *Encyclopedia of Industrial Biotechnology*, John Wiley & Sons, Inc.
- Nasr, M M, Yazdanbakhsh, A R. 2008. Study on Wastewater Treatment Systems in Hospitals of Iran. *Iranian Journal of Environmental Health, Science and Engineering*, 5 (3), 211-215.
- Prayitno, P, Kusuma, Z, Yanuwadi, B, Laksmono, R W. 2013. Study of Hospital Wastewater Characteristic in Malang City. *Research Inventy: International Journal of Engineering and Science*, 2 (2), 13-16.
- Rezaee, A, Ansari, M, Khavanin, A, Sabzali, A, Aryan, M M. 2005. Hospital Wastewater Treatment Using an Integrated Anaerobic Aerobic Fixed Film Bioreactor. *American Journal of Environmental Sciences*, 1 (4), 259-263.
- Rodgers, M. 1999. Organic Carbon Removal using a New Biofilm Reactor. *Water Res.*, 33 (6), 1495-1499.
- Sarafraz, S, Khani, M R, Yaghmaeian, K. 2007. Quality and Quantity Survey of Hospital Wastewaters in Hormozgan Province. *Iranian Journal of Environmental Health, Science and Engineering*, 4 (1), 43-50.
- Sridevi, V, Lakshmi, M V V C, Manasa, M, Sravani, M. 2012. Metabolic Pathways for the Biodegradation of Phenol. *International Journal of Engineering Science & Advanced Technology*, 2 (3), 695-705.
- Tchobanoglous, G, Burton, F L, Stensel, H D. 2003. *Wastewater Engineering: Treatment and Reuse*. 4th ed., McGraw-Hill New York, United States.
- Varghese, R, P., K M, V., A B, Hatha, A A M. 2012. Biological Removal of Lead by *Bacillus sp.* Obtained from Metal Contaminated Industrial Area. *Journal of Microbiology, Biotechnology and Food Sciences*, 2 (2), 756-770.
- Wen, X, Ding, H, Huang, X, Liu, R. 2004. Treatment of Hospital Wastewater using a Submerged Membrane Bioreactor. *Process Biochem.*, 39 (11), 1427-1431.
- Wiesmann, U, Choi, I S, Dombrowski, E-M. 2007. *Fundamentals of Biological Wastewater Treatment*. Wiley-VCH, Weinheim, Germany.

## **Auranofin, a Thioredoxin Reductase Inhibitor, Induces ER stress and PI3K/Akt pathways-mediated Apoptosis in Human Breast Carcinoma Cells**

Hyun Hwang<sup>a,b</sup>, Jin Woo Jeong<sup>a</sup>, Cheol Park<sup>c</sup>, Su Hyun Hong<sup>d</sup>, Jae-Hun Cheong<sup>b</sup>,  
Yung Hyun Choi<sup>a,d\*</sup>

<sup>a</sup>Anti-Aging Reserch Center, Dongeui University, Eomgwang-ro, Busan, Republic of Korea

<sup>b</sup>Department of Molecular Biology, Pusan National University, Busandaehak-ro, Busan, Republic of Korea

<sup>c</sup>Department of Molecular Biology, Dongeui University, Eomgwang-ro, Busan, Republic of Korea

<sup>d</sup>Department of Biochemistry, Dongeui University College of Korean Medicine, Yangjeong-ro, Busan, Republic of Korea

\*Corresponding Author: choiyh@deu.ac.kr

### **ABSTRACT**

As thioredoxin reductase (TrxR) is overexpressed in various cancers, several studies suggested that TrxR is an important target for anti-cancer therapy. Auranofin is an inhibitor of TrxR that has potential anticancer effects. In the present study, we demonstrated that auranofin induces cell death in MDA-MB-231 cells, which was associated with the inhibition of TrxR activity and induction of ER stress-mediated apoptosis. Our results indicated that auranofin induced apoptosis as evidenced by the increased population of annexin-V positive cells and loss of MMP ( $\Delta\psi_m$ ). Auranofin also increased the protein levels of ER stress-related proteins that CHOP, Bip and p-eIf2 $\alpha$ . In addition, auranofin enhanced the generation of reactive oxygen species (ROS). However, pretreatment with ROS scavenger completely blocked auranofin-induced apoptosis in MDA-MB-231 cells. Moreover we explored the roles of the PI3K/Akt pathways in apoptotic effects of auranofin. Consequently auranofin decreased phosphorylated Akt form and inhibition of PI3K/Akt enhanced apoptosis. The results indicate that the inhibition of TrxR activity contributes to apoptosis by auranofin, amplifying ROS generation, ER stress and PI3K/Akt pathway-medicated apoptosis in MDA-MB-231 cells.

**Keyword:** Auranofin, apoptosis, ER stress, TrxR, ROS



## Baicalein Protects the Schwannoma Cells against Hydrogen Peroxide-induced Cellular Damage and Apoptosis *via* Activation of the Nrf2 Signaling Pathway

Eun Ok Choi<sup>a,b</sup>, Jin-Woo Jeong<sup>a</sup>, Cheol Park<sup>c</sup>, Su Hyun Hong<sup>b</sup>, Hye-Jin Hwang<sup>a,d</sup> and Yung Hyun Choi<sup>a,b\*</sup>

<sup>a</sup>Anti-Aging Research Center, Donggeui University, Eomgwang-ro, Busan, Republic of Korea

<sup>b</sup>Department of Biochemistry, Donggeui University College of Korean Medicine, Yangjeong-ro, Busan, Republic of Korea

<sup>c</sup>Department of Molecular Biology, College of Natural Sciences and Human Ecology, Donggeui University, Eomgwang-ro, Busan, Republic of Korea

<sup>d</sup>Department of Food and Nutrition, College of Natural Sciences and Human Ecology, Donggeui University, Eomgwang-ro, Busan, Republic of Korea

\*Corresponding Author: [choiyh@deu.ac.kr](mailto:choiyh@deu.ac.kr)

### ABSTRACT

Baicalein, a polyphenol presents in *Scutellaria baicalensis* Georgi, displays antioxidant and cytoprotective effect in brain pathologies associated to oxidative stress, but its neuroprotective mechanisms have not been clearly established. This research aims to detect the effects of baicalein against hydrogen peroxide (H<sub>2</sub>O<sub>2</sub>)-induced neuronal damage using two Schwann cell lines (HEI 193 human Schwann and RT4-D6P2T rat Schwann cells) and to investigate the molecular mechanisms in this process. The results showed that baicalein effectively suppressed H<sub>2</sub>O<sub>2</sub>-induced growth inhibition and reactive oxygen species (ROS) production in both cell lines. Baicalein also attenuated the H<sub>2</sub>O<sub>2</sub>-induced  $\gamma$ H2A.X phosphorylation and changes of apoptosis-related protein expression, which suggest that baicalein prevents the cellular DNA damage and apoptosis induced by H<sub>2</sub>O<sub>2</sub>. Furthermore, baicalein effectively induced not only heme oxygenase-1 (HO-1) but also nuclear factor erythroid 2-related factor 2 (Nrf2) expression. Moreover, the protective effects of baicalein against H<sub>2</sub>O<sub>2</sub>-induced DNA damage and apoptosis were significantly reversed by HO-1 inhibitor. In addition, the cytoprotective effects were abolished by transient transfection with Nrf2-specific small interfering RNA. These results indicate that baicalein has protective activity against oxidative stress-induced neuronal damage through the inhibition of ROS generation and activation of the Nrf2 signaling pathway, thus baicalein has an important role for protection of Schwann cells against oxidative stress.

**Keywords:** Baicalein, Schwannoma cells, Antioxidant, ROS, Nrf2.

## Electrochemistry evaluation of ferrocene in organic solvents for high-performance non-aqueous organic redox flow electrolyte

Yongbeom Kim<sup>a</sup>, Joonhyeon Jeon<sup>a\*</sup>

<sup>a</sup>Department of Electronic & Electrical engineering, Dongguk University,  
Pildongro-1gil street, Seoul, Republic of Korea

\*Corresponding Author: [memory@dgu.edu](mailto:memory@dgu.edu)

### ABSTRACT

Non-aqueous organic redox flow batteries are attractive energy storage devices because of their high energy densities. Ferrocene, which is an organometallic compound with the formula  $\text{Fe}(\text{C}_5\text{H}_5)_2$ , is usually considered as high performance non-aqueous redox flow electrolyte. However, its performance has lagged far behind its inherent capability due to one major limitation of low electrochemical properties of the redox species, which are solubility, conductivity and reversibility of ferrocene in on organic solvent. Thus, best electrochemistry properties of ferrocene in organic solvent are needed for high-performance non-aqueous organic redox flow batteries. This paper deals with electrochemistry properties of the ferrocene in various organic solvents and allows an electrochemistry-property parameter to characterize its redox properties. Electrochemical experiments are carried out, respectively using ferrocene in ten kinds of organic solvents as follows: (1) Dioxolane, (2) Tetrahydrofuran, (3) N N-dimethylformamide, (4) Benzene, (5) Hexane, (6) Toluene, (7) Heptane, (8) Acetonitrile, (9) Propylene carbonate, (10) N-methyl-2-pyrrolidinone (NMP). Then, cyclic voltammetry (CV) is measured with 10mV/s of scan rate, where Graphite Foil, standard calomel electrode and Pt-wire are used as a working electrode, reference electrode and counter electrode respectively. Experimental results show that (7) Heptane has highest solubility of ferrocene, while NMP (10) provides highest conductivity (Table 1 and 2). In addition, it appears that in the CV experiment, as shown in Fig.1, (2) N N-dimethylformamide has the peak potential and suitable reversibility. Consequently, some kind of solvents shows that good reversibility and standard potential, but there is a disadvantage of giving low solubility or low conductivity. Based on these results, a redox parameter can be defined as

$$p = \frac{\text{solubility} \times \text{conductivity}}{||V_{PC}| - |V_{PA}||}$$

where  $V_{pc}$  and  $V_{pa}$  are peak cathode voltage and anode cathode voltage, respectively. This redox parameter can be used as an electrochemistry-property parameter to choose a best organic solvent with high solubility, conductivity and reversibility of ferrocene. Using the formula potentially leads to (8) Acetonitrile as a best organic solvent for

ferrocene, and the experimental results are also indicated. This paper provides a new insight into the performance improvement of non-aqueous redox flow electrolyte using ferrocene in organic solvent.

Table1. Solubility of ferrocene according to organic solvents.

Solvent	1	2	3	4	5
Solubility(g/ml)	0.146	0.161	0.087	0.174	0.134
Solvent	6	7	8	9	10
Solubility(g/ml)	0.128	0.201	0.053	0.055	0.113

Table2. Conductivity of ferrocene according to organic solvents.

Solvent	1	2	3	4	5
Conductivity( $\mu\text{S}/\text{cm}$ )	0.000	0.000	0.236	0.000	0.000
Solvent	6	7	8	9	10
Conductivity( $\mu\text{S}/\text{cm}$ )	0.000	0.000	0.318	0.121	0.344

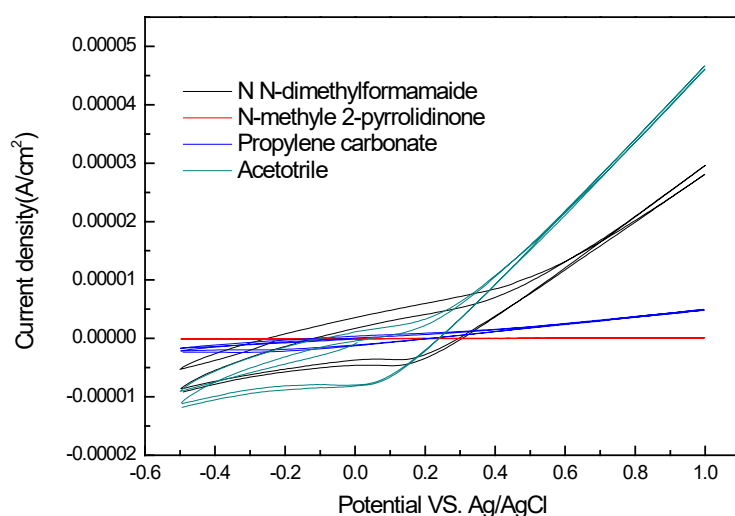


Figure 1. Cyclic voltammograms of ferrocene resolved in organic solvents.

### Acknowledgement

This work was supported by the Industrial Strategic technology development program (20162020107050) funded by the Ministry of Trade, industry & Energy (MI, Korea)

**Keyword:** flow battery, electrolyte material, electrochemical character, ferrocene, organic solvent

## Greenhouse Monitoring system using Arduino Yún and Blynk Framework

Meena Momand<sup>a</sup>, Chika Yoshida<sup>b</sup>

Department of Information Technology, Kobe Institute of Computing,  
650-0001 Hyogo Prefecture, Kobe, Chuo Ward, Kanocho, -2-7

\*Corresponding Author Meena Momand: [s15124@st.kic.ac.jp](mailto:s15124@st.kic.ac.jp)

### ABSTRACT

Since the advent of greenhouse technology there has been a rapid increase in basic production and being independent of specific seasons compared to the open areas. Protected cultivation in greenhouses, it's highly consistent atmosphere and desirable environmental conditions has encouraged most farmers to invest in making greenhouses. Greenhouses form an important part of the agriculture and horticulture sectors in our country as they can be used to grow plants under controlled climatic conditions for optimum produce. Current method for greenhouse climate control and monitoring is the traditional way of farming. As the farmer have to visit greenhouse continuously which is time consuming and require lots of effort. However in recent years, greenhouse technology in agriculture is to automation, information technology direction with the IoT (internet of things) with rapid development and wide application. It is now possible for Afghan farmers to equip their greenhouse with wireless sensor network due to their low-cost, simplicity and mobility. The project discussed in this paper focus on a wireless greenhouse monitoring system using Arduino Yún as server, Blynk framework web and mobile apps as client. The project aims at solving traditional greenhouse monitoring problems faced by Afghan farmers.

**Keywords**— Afghanistan Agriculture, Greenhouse Monitoring ,IoT, Blynk ,Arduino Yún

### 1. INTRODUCTION

Greenhouse is a limited agriculture area covered by plastic or transparent materials to grow late off season crops such fruits and vegetables. A Greenhouse monitoring system controls the temperature, humidity, light, CO<sub>2</sub> and other environmental changes inside a greenhouse. Tomato and cucumber are the main products which are highly consumed in the markets. [1] IoT can be used for various applications in agriculture, such as smart agriculture and smart animal farming. Smart agriculture focuses on soil and environmental condition monitoring for maximizing the yield and ensuring the product quality. [2]

The rapid development of greenhouse in all provinces of Afghanistan in recent years led to increased employment opportunity for many farmers in rural area. Greenhouse main crops are Tomato, chili and cucumber, which are largely grown in the greenhouses. Current method of monitoring is the traditional method of farming. Farmers are required to visit the greenhouse to check the humidity level, temperature level and soil moisture. Afghan farmers do not possess any technology to control and monitor greenhouse. However, due to increasing number of greenhouses, this type of continuous monitoring is apparently time consuming, labor-intensive and needs a lot

of work and effort which is difficult a job on a daily bases. When the farmers are in remote area less or no information are available about crops nutrition. In addition winter is critical for agriculture in Afghanistan. Most of the farmers in Afghanistan make little or no income during the winter months. Furthermore, the high start-up costs for cold storage to boost farmer income is not feasible for the average small and medium-scale farmer. In Herat province, the approximately 1.5 million inhabitants must consume imported fresh fruit and vegetables from Iran or Pakistan at high prices during winter.[3] Due to environmental factors and lack of the technology to grow late-season or off-season fruits and vegetables, greenhouse productivity drops to zero in winter season. Above mentioned factors are causes that agriculture is difficult to be stable throughout the year with large demand of the country.

This study present a wireless greenhouse monitoring system using Arduino Yún as server, DHT11 sensor for getting real-time temperature and humidity and grove sensor for Soil Moisture changes. The system sends data to two different clients a web server and a Mobile App that uses Blynk framework to request for the latest data using an HTTP request to the Yún server.

## 2. RESEARCH PURPOSE

Majority of Afghans rely on agriculture for their livelihoods and their family's sustenance. However Agriculture sector is highly dependent on manual and labour work, less effective, time-consuming and expensive. In addition Agriculture plays a critical role to the economies in Afghanistan. Our country is a large agricultural nation, the stand or fall of agricultural development is key factors which are effect on our country's economic development and social harmony, greenhouse, taken as the important content of facilities agriculture, where agricultural needs to move toward modernization. ICT has been defined as a tool which contributes agricultural development, poverty alleviation, speed-up agriculture, adds value to people live and income, Therefore this research aims to:

- To Design a Greenhouse Environment Monitoring system using IOT Technology
- To improve crop quality and reduce farmers workload.
- To introduce tools for creating the first statistical data of greenhouse production in Afghanistan

Research Questions:

1. What kind of infrastructure are affordable for Greenhouse Monitoring, what is their knowledge on the ICTs facilities?
2. What are the available ICT solution and what are barriers with the existing system?
3. How to develop a need-base system to improve productivity and quality of crops for greenhouse in Afghanistan?
4. Finding out how a combination of Arduino Yun, Blynk framework and web, mobile application could affect greenhouse productivity and reduce farmers workload?

### 3. METHODOLOGY

In order to verify research hypotheses quantitative approach was applied to gain a deep insight and understanding of the government and agriculture experts views on greenhouse automation in Afghanistan. The approach also helped us to be more specific and concise in our research objectives.

### 4. SURVEY

An online survey was conducted using Google Forms and the link was shared through email with government officials and agriculture experts on social media platforms such as Facebook for the public to respond. This method was selected because the responses are automatically saved in a spreadsheet making analysis of results easier. From the survey results 75% agreed that using greenhouse monitoring system will increase productivity. Fig. (1) and 80% are interested to use the system in the future. Fig. (2)

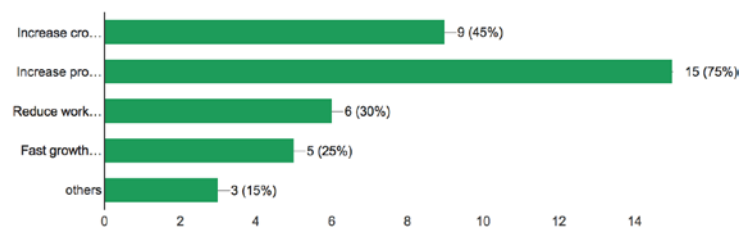


Figure 1. Opinions of agriculture experts on effect of Automatic monitoring on productivity

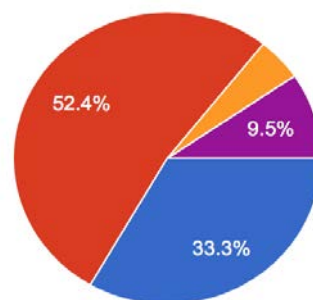


Figure 2. Number of people agreed to replace current manual monitoring with the proposed system

### 5. RELATED WORK

Sustainable improvements in farmers' incomes are linked to sustained production. However, with the improvement of smart greenhouses, IoT based wireless greenhouse monitoring system are developed and tested in many countries[8]. Smart greenhouses using IoT have been rapidly developed and widely applied in various industries particularly in environmental monitoring and agriculture. IoT deployment

in agriculture is a proven solution to many challenges and increase in quality, quantity, and cost-effectiveness of agricultural production. [4]

Zhaing Qain (2007) developed and tested a greenhouse monitoring and control system using wireless solution based on ZigBee technology[5]. Izzatdin Abdul (2009) developed a temperature remote monitoring and alerting system which utilizes wireless sensor for temperature level detection, as well as GSM and SMS technologies for sending alert notification message to farmers.[6] The use of sensors in a greenhouse as a Wireless Sensor Networks System, is an efficient method of technology used in agricultural development by sending data to the cloud and controlling values such as temperature, humidity, soil moisture levels, etc.[9] Therefore rural competitiveness in Afghanistan requires a significant improvement by involving ICT in greenhouses to stabilize the productivity throughout the year. Agriculture has always been a high-risk, labor-intensive, low-reward industry in Afghanistan. However IoT based wireless greenhouse monitoring system is a concrete answer to the challenges due to its liability, simplicity, and low cost in both installation and maintenance.[5]

## 6. SOLUTION OVERVIEW

The developed system in this study is a wireless greenhouse monitoring system using Arduino Yún as server which has built in WiFi and Web application, Mobile app as clients. The Arduino Yún server is wired to temperature and humidity sensor (DHT11) and soil moisture sensor (ER-SPM32100S). The Yún server receives and stores sensors data and sends it to the clients upon request. The mobile app uses Blynk framework to receive Temperature, humidity and soil moisture levels from the Yún server. When the condition is abnormal, the application alerts and informs farmer of the greenhouse condition. The web application can be accessed by any website browser of any local PC in the same LAN using YUN server IP. Wi-Fi is chosen to improve system security (by using secure Wi-Fi connection), and to increase system.

## 7. HARDWARE DESIGN

The system architecture consists of two major parts: software and hardware design. Hardware configuration involves arranging microprocessor, micro controller, sensors and the software portion encloses programming that is written and uploaded in each of the micro controllers and microprocessor. Fig (3) shows the hardware and software overall interaction. The specifications and information regarding various components are described below.



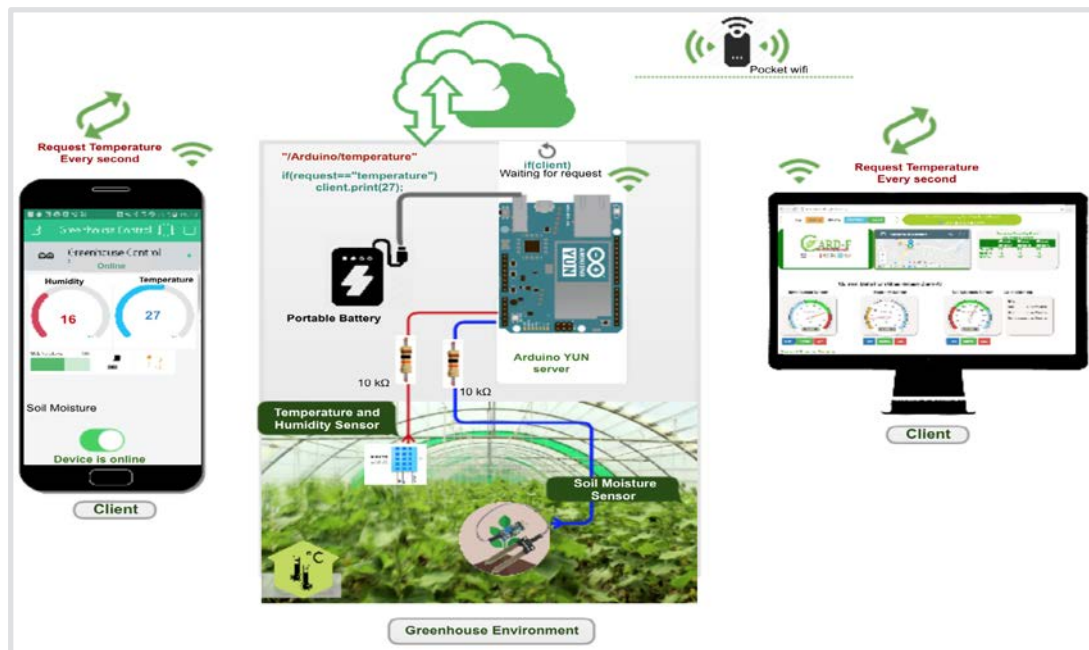


Figure 3. System Architecture components used in this system are descriptively explained below.

## 7.1 .Microcontroller Unit - Arduino Yún

**Arduino Yún:** is a micro-controller board based on the ATmega32u4 and the Atheros AR9331[8]. The Atheros processor supports a Linux distribution based on OpenWrt named Linino OS. The board has built-in Ethernet and WiFi support, a USB-A port, micro-SD card slot, 20 digital input/output pins (7 of them can be used as Pulse Width Modulation(PWM) outputs and 12 as analog inputs), a 16MHz crystal oscillator, a micro USB connection, an ICSP header, and 3 reset buttons. In this project, a 4GB SD card is used to store the sensor's data and exchange with the client upon request. Arduino Yún can be used as a server. This means that once the Yún is configured to connect via WiFi, a client web page will be uploaded smoothly on the SD card (plenty of space) and user can access it from any browser in the same LAN. In the connection part, all the regular Arduino pins can be controlled from a web page using Javascript. Arduino Yún can be used via USB like a regular Arduino board, even though in this project it is used via WiFi.[8]

The power supply is 5VDC which is connected to a portable battery as shown in the system architecture in Figure 3.

## 7.2 Sensor Unit

- DHT11 is a digital temperature and humidity sensor. It is a composite sensor which contains a calibrated digital signal output of the temperature and humidity. DHT11 is cheap, has a long-term stability, relative humidity and temperature measurement, excellent quality, fast response, strong anti-interference ability, long distance signal transmission, digital signal output, and precise calibration. DHT11 has four pins VCC connected to (5V power) of Yún Board. Data output is connected to digital pin7 on Arduino Yún, the third pin can be left as Not connected it is not used and



Ground(GND) is connected to the ground on the Arduino board. A 10K resistor between VCC and the data pin, acts as a medium-strength pull up on the data line.

- Soil Moisture Sensor (ER-SPM32100S) is used to detect the moisture of soil or plant's water level. The Interface is very easy to use with power of V4.0. In this system A 10k resistor is used to maintain the power.

- Pocket Wifi (ZTE) pocket wifi is used in this project as a communication protocol to exchange data between clients and server. Pocket wifi can be carried anywhere in the greenhouse area and is reliable and highly secure. The device can access the Internet in two ways and it allows multiple clients to surf on the Internet at the same time. All appliance and sensors in this project are connected must be in the same LAN.

- Portable battery is used to keep the Arduino Yún Power stable. Portable battery regulate the 5V connectivity to the Yún. The portable battery is easy to use and be carried out anywhere with the Yún.

### 7.3 User Interface

The graphical interfaces is divided into two parts.

1. Mobile Application: The app was built using Blynk for smartphone and tablet application in the form of android design. The application consists of a gauge for temperature and another gauge for humidity. A Level H control is designed to display soil moisture level and Even handler with push notification is added in the App, graph-plotter, LCD and sensor-value display.

The user can simply download the app, log in and then monitor and control greenhouse temperature, humidity and soil moisture. The application was designed in a way that when the temperature goes across the normal temperature, Figure 4. System Architecture a notification will be pushed to the user whether the temperature become warm or cold. Similarly, when the humidity and soil moisture changes the farmer will be notified until the farmer confirm the notification. The farmer can check at the real-time data received from the greenhouse.

2. The second part of the user interface is a web application[7] developed using HTML5, CSS, JSON, and JavaScript. For accessibility and data exchange between Yún and clients the Arduino IDE is used by adding the bridge library. Yún is configured to connect via WiFi, the Web Application created uploads on the SD card each time by running the source code on Arduino IDE and sending the request through Yún IP or name which is selected from the port .The client web page will update automatically every 2 seconds to receive the real-time data from the Yún server.

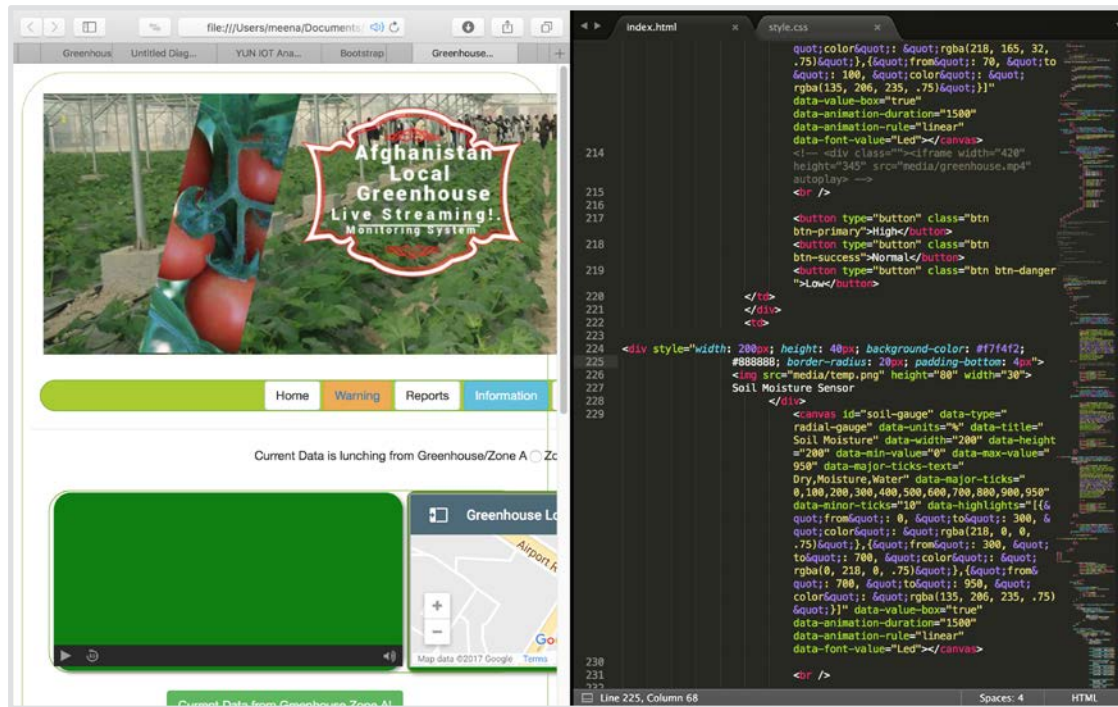


Figure 4. Application interface view

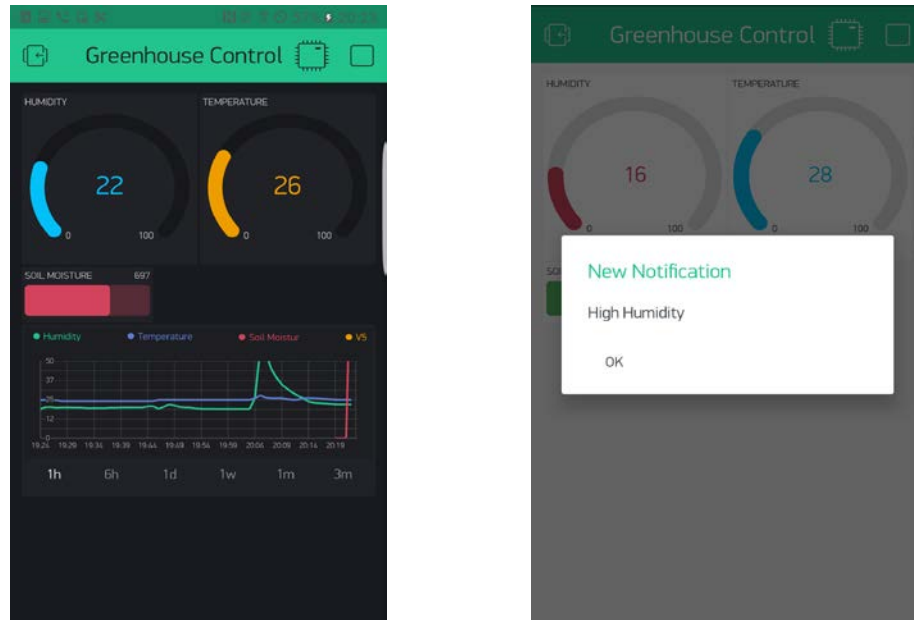
Each time Arduino IDE is uploading, HTML files will be automatically stored on SD card of the Yún. The webpage can be accessed using the Yún dedicated IP address for inspecting the status from desktop PCs and laptops. The user can monitor real-time data coming from the greenhouse, generate reports for specific range of date, read list of warnings and notifications. Arduino Yún can be accessed using its IP address or the name given by the developer in the WiFi setup procedure.

### 8. RESULTS AND APPLICATION

The proposed prototype consist of Three different parts : i) The Arduino Yún server with sensors controlled ii) Mobile application iii) Web Application. Through the mobile app the user can access current greenhouse temperature and humidity as shown in Figure 5.

DHT11 detects temperature and humidity and send the updates to the mobile application. The soil moisture measure the soil moisture level and send to the application. The screenshots of the results of the designed system obtained on android application are shown in Figure 5.

Figure 5. Screenshot of the Mobile Application show current temperature , humidity and soil moisture. The second screenshot shows a pop-up screen alert for high humidity.



When the temperature, humidity and soil moisture is not normal the user will be notified by an alert pop-up on the screen. The alert will be stopped when the user confirms it. The application can be shared with more than one farmer and can also be used as a stand alone application for greenhouse management. The second part of the UI is a web application which displays temperature, humidity and soil moisture shown in the figure 6.

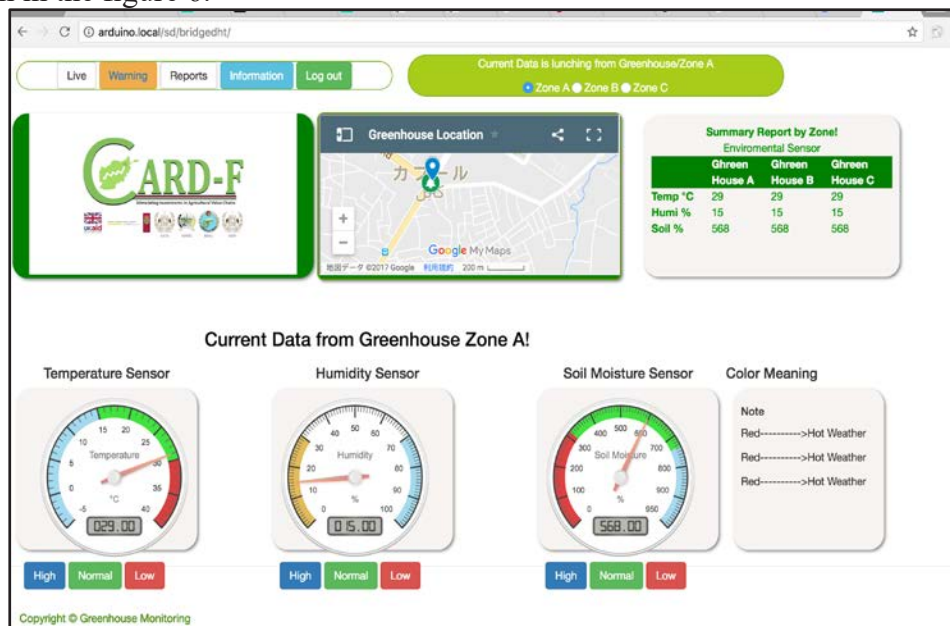


Figure 6. Screenshot of web application interface

Home page: in this page, the overall data received from the sensors are displayed using gauges which is very user friendly.

Warnings: The second tab is a list of warnings that a user will receive during the day for any abnormal changes taking place in the greenhouse.

Report: this page displays the overall history of data (soil moisture level, temperature and humidity). The user can also specify a range of date and generate a report for what happened during past weeks in the greenhouse.

Three gauge are designed for simplicity which clearly shows the temperature, humidity and soil moisture.

## 9. CONCLUSION AND FUTURE WORK

In this study, we discussed the wireless solution of greenhouse monitoring and control system based on Arduino Yún and Blynk framework.

This paper mainly focused on overcoming everyday problems faced by farmers in Afghanistan. Currently, the greenhouse is controlled as traditional farming which is highly time consuming and require lots of effort. The system is capable of receiving real-time data from the greenhouse environment and send to the users such farmers or monitoring officer within two seconds. The system also notify farmers of any abnormal condition when occurring in the greenhouse.

The system has been smoothly running after lab testing which proved its accessibilities and reliabilities. We, therefore, conclude that the Yún-based monitoring system can be a good solution for greenhouse monitoring and control.

For The future work, we will move the system from LAN to WLAN where the users will be able to control the greenhouse when they are not in the city by adding more actuators to be activated and make possible remote control.

## ACKNOWLEDGMENT

This research is sponsored by Japan International Cooperation Agency (JICA). We express our heartfelt gratitude to JICA and Kobe Institute of Computing (KIC) for their endless support and assistance to make this project a reality. We are also thankful to all lab members.

## REFERENCE

1. Agriculture growth report by Card-f , page No .3 Available at website

- (referred 15.05.2016):  
<http://cardf.gov.af/images/Multimedia/2013%20Annual%20Report.pdf>
2. K. Priyanka Gandhi, Dr. P. Thimmaiah, Dr. B. Rama Murthy, March 2017) "Design and Implementation of Embedded System for Monitoring and Automatic Controlling a Greenhouse in a Field", International Conference on Emerging trends in Engineering Science and Management Computing, India, 2017
  3. USAID, "Afghan Farmers Adopt Greenhouse Techniques", Available [online]: <https://www.usaid.gov/results-data/success-stories/afghan-farmers-adopt-greenhouse-techniques>
  4. Teemu Ahonen, Reino Virrankoski and Mohammed Elmusrati "Greenhouse Monitoring with Wireless Sensor Network" Mechatronic and Embedded Systems and Applications, 2008. MESA 2008. IEEE/ASME International Conference
  5. Q. Zhang, X. Yang, Y. Zhou, L. Wang, X. Guo, July 23 2007, "A wireless solution for greenhouse monitoring and control system based on ZigBee technology", Zhang et al. / J Zhejiang Univ Sci A 2007 8(10):1584-1587, China
  6. Ab. Izzatdin, M. Hilmi Hasan, M. Jimmy Ismail, M. Mehat, N. Samiha, Malaysia, "Remote Monitoring in Agricultural Greenhouse Using Wireless Sensor and Short Message Service (SMS)" International Journal of Engineering & Technology IJET Vol: 9 No: 9
  7. Introduction to the YUN web server: Available [online]: [http://aaronscher.com/Arduino\\_tutorials/Arduino\\_WiFi\\_Tutorial/documents/Arduino\\_Yn\\_Intro\\_to\\_web\\_server.pdf](http://aaronscher.com/Arduino_tutorials/Arduino_WiFi_Tutorial/documents/Arduino_Yn_Intro_to_web_server.pdf)
  8. John M. Wachira, Patience M. Mshenga and M. Wanyarusi Saidi, March 25 2014, "Comparison of the Profitability of Small-scale Greenhouse and Open-field Tomato Production Systems in Nakuru-North District, Kenya" Asian Journal of Agricultural Sciences 6(2): 54-61, 2014, ISSN: 2041-3882; e-ISSN: 2041-3890, Maxwell Scientific Organization, 2014
  9. Ji-chun Zhao, Jun-feng Zhang, Yu Feng, Jian-xin Guo, September "The study and application of the IOT Tech in Agri" Computer Science and IT (ICCSIT), 2010 3rd IEEE International Conference on, DOI:10.1109/ICCSIT.2010.5565120

## Study on new control system design of PV cell emulating system in the stand alone mode

Kirian Guiller<sup>a,b</sup>, Vu Minh Phap<sup>a,c</sup>, N. Yamamura<sup>a</sup>, M. Ishida<sup>a</sup>, J. Hirai<sup>a</sup>

<sup>a</sup>Department of Electrical and Electronic Engineering, Faculty of Engineering, Mie University, Japan

<sup>b</sup>Ecole Normale Supérieur des Arts et Metiers  
151 Bd de l'Hopital, Paris, France

<sup>c</sup>Institute of Energy Science, Vietnam Academy of Science and Technology,  
Hanoi, Vietnam  
kiriangu@gmail.com

### ABSTRACT

In recent decades, generation of electricity from photovoltaic (PV) arrays has been increased to meet the world's growing energy demand. However, the utilization rate of the power conditioner system in the grid-tied solar power system is low because the operation of solar panels is dependent on sunlight. So, we pair to the solar panel a wind power plant for increasing the utilization rate of the PCS. However, the power conditioner of the PV cell cannot control optimally the wind turbine because the output characteristics of the solar panel and the wind power plant are different. Thus, in previous research [1], we studied the method that the small scale wind power generating system can be connected to the grid-tied power conditioner of the solar power system by emulating technical characteristic of PV cell with 2 model equations. In this paper, we propose a new model with 3 equations to improve the accuracy of the existing system. The simulation results verify that this new design is functional and permit the output characteristic of the PV Cell Emulating system in the stand alone mode to be more stable.

**Keyword:** PV Cell Emulating System, Power Converter Circuit, Control System.

### 1. Introduction

Nowadays, solar power generation systems for home scale application are more and more widely used in many countries in the world. For converting produced energy in available energy, a power converter system (PCS) has been introduced at the output of the PV cell. However, the power production of the PV cell depending on the sunlight and the weather condition is not regular, so the utilization rate of the PCS is low as can be seen in Figure 1.

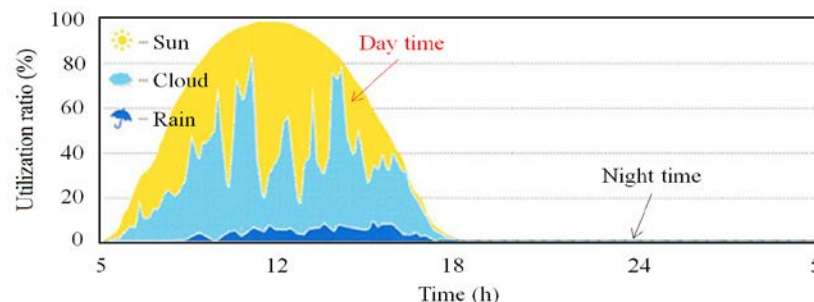


Figure 1: Utilization ratio of the power conditioner in the grid-tied PV system



We can connect the small scale wind power system to the existing solar power generation system to improve the utilization rate of the PCS because the small scale wind turbine utilizes possibly the PCS at night and also can use the remaining capacity of the PCS during the daytime. Therefore, we proposed the solution [1] that the small scale wind turbine could be connected to the grid-tied PCS of the solar power system by emulating characteristic of the solar panel with 2 model equations. However, 2 equations make the system output having more fluctuation because the operating point will switch between the equations. In this research, the efficiency of new control system design with 3 model equations for PV cell emulating system is analyzed in detail.

## 2. PV Cell Emulating system in the stand alone mode

### 2.1. System configuration

The typical grid-tied solar power system is shown in Figure 2. This system includes the PCS composed of a DC/DC converter and a grid-tied DC/AC inverter. The PV array is then linked to the boost-type DC/DC converter which uses the P&O (Perturb & Observe) method [2] for performing the maximum power point tracking (MPPT). The grid-tied DC/AC inverter converts the electrical power from the output terminals of the PV array in a suitable power to the utility grid.

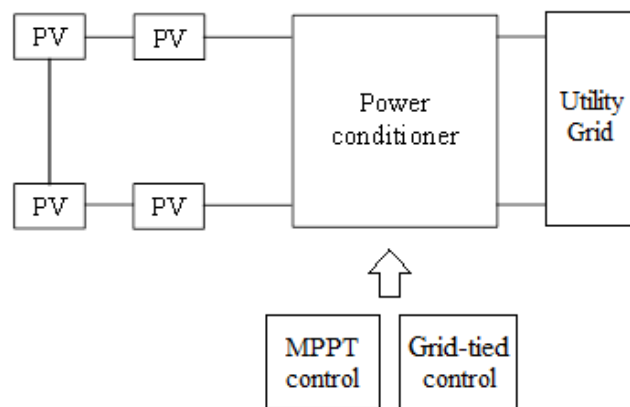


Figure 2 : Grid-Tied Solar Power System

The PV cell emulating system comprises the small scale wind power generating system, a battery and the power converter circuit. The battery is charged by the small scale wind power generating system. The power converter circuit converts the output voltage and output current of the battery thanks to the control system.

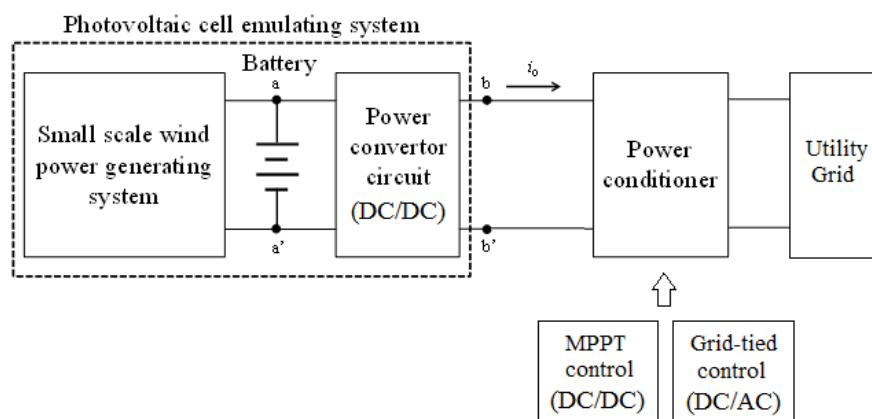


Figure 3: PV Cell Emulating system in the stand alone mode



When the sunlight is nonexistent, the PV cell is not functional and the PV cell emulating system is called in the stand-alone mode (Figure 3). Thus, in this mode, the PV cell is bypassed to avoid that it becomes the load, .

### 3. Control System of the Power Converter Circuit

#### 3.1. Old model of Stand-alone mode using 2 equations

In the stand-alone mode, the power converter circuit emulates the technical output characteristic of the PV cell. Figure 4 shows the real behavior of the output current and output voltage of the PV cell. The old configuration modeled the PV cell characteristic by two linear equations joining at the maximum power point as can be seen in Figure 5.

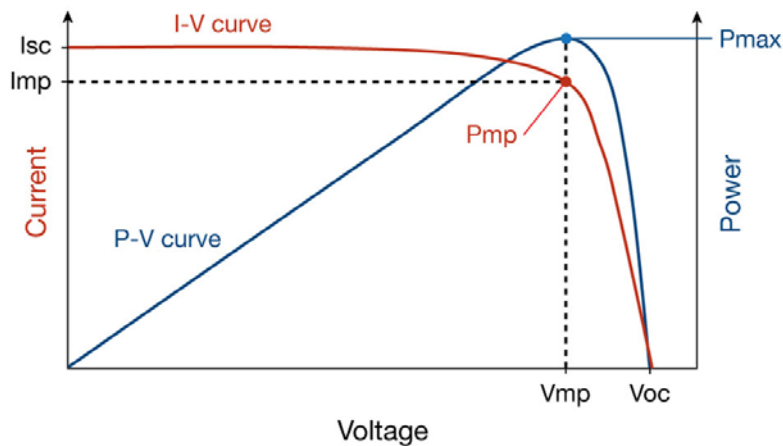


Figure 4: PV cell technical characteristics

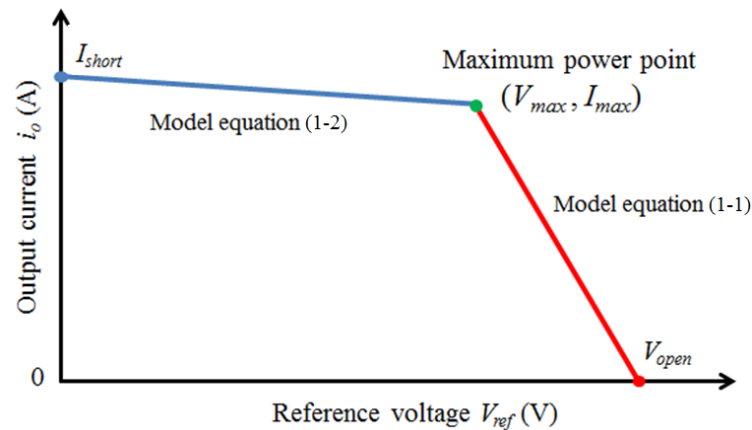


Figure 5: 2 model equations of PV cell technical characteristic

The maximum power point current  $I_{max}$  is determined by dividing generated power from the small scale wind turbine by the maximum power point voltage  $V_{max}$  while the maximum power point voltage  $V_{max}$  is calculated considering the operating voltage of the PCS. The open voltage and the short current are computed by multiplying correlative constant factors by the maximum power point voltage and the maximum power point current respectively. The two linear equations (1-1) and (1-2) are determined as follows:

$$V_{ref} = -\frac{V_{open} - V_{max}}{I_{max}} i_o + V_{open} \tag{1-1}$$

$$V_{ref} = -\frac{V_{max}}{I_{short} - I_{max}} i_o + \frac{V_{max} I_{short}}{I_{short} - I_{max}} \quad (1-2)$$

with  $V_{max}$  and  $I_{max}$  are the maximum power point voltage and the maximum power point current respectively;  $V_{open}$  is the open voltage;  $I_{short}$  is the short current;  $V_{ref}$  calculated by the linear model equations is the reference voltage to PI controller;  $i_o$  is the output current of the PV cell emulating system.

### 3.2. New model of Stand-alone mode using 3 Equations

The two model equations are connected at the maximum power point. So, when operating in the steady state, the maximum power point will continuously permute between 2 reference equations. Therefore, the output current of the PV cell emulating system can be strongly fluctuated and it leads to reduce the quality of the output power. We propose a new model with 3 equations including 4 parameters (Figure 6) to solve the disadvantage of the old model as the operating point will be moving on a linear equation and not fluctuating around the intersection of linear equations. The parameters of the new model are:

- The maximum power point  $P_{max}$  ( $V_{max}$ ,  $I_{max}$ ),
- The open circuit voltage ( $V_{oc}$ , 0),
- The short circuit current (0,  $I_{sc}$ )
- And a voltage width  $V_h$  (which will determine the width of the center equation).

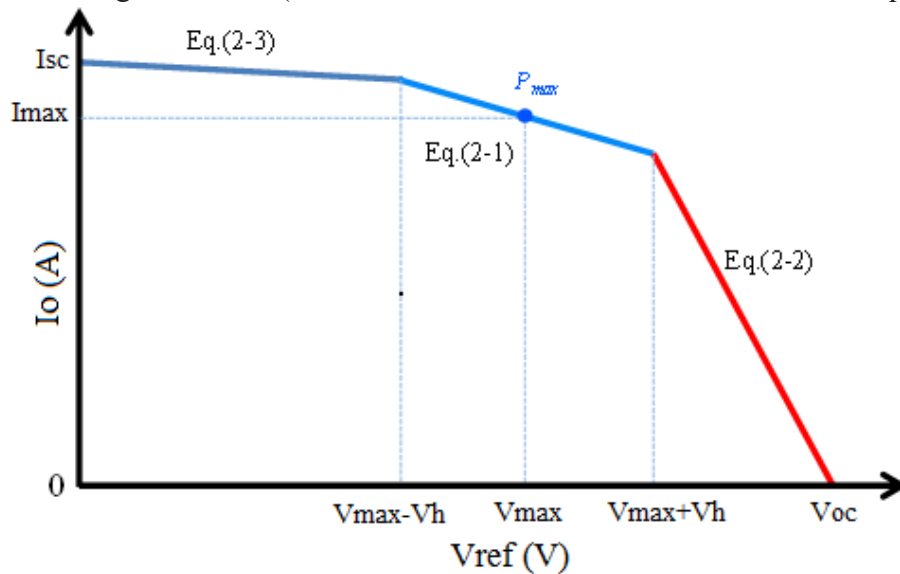


Figure 6: 3 model equations of the PV Cell technical characteristic

After resolving the system, we have the following equations:

$$V_{ref} = -\frac{V_{max}^2}{P_{max}} i_o + \frac{V_{max}^2}{P_{max}} i_{max} + V_{max} \quad (2-1)$$

$$V_{ref} = \frac{V_{max} + V_h - V_{oc}}{-\frac{P_{max}}{V_{max}^2} V_h + i_{max}} i_o + V_{oc} \quad (2-2)$$

$$V_{ref} = \frac{V_{max} - V_h}{\frac{P_{max}}{V_{max}^2} V_h + i_{max} - i_{sc}} (i_o - i_{sc}) \quad (2-3)$$

In this paper, an example of 3 linear model equations is used in Figure 7 with the parameters in table 1.

Table 1: Parameter of the 3 linear model equations

Parameter	Value
Maximum power point voltage $V_{max}$	100 V
Maximum power point current $I_{max}$	1 A
Open voltage $V_{oc}$	171 V
Short current $I_{short}$	1.5 A
Voltage Width $V_h$	7 V

### 3.3. Power converter circuit

First of all, the small scale wind power generating system is connected to the battery and charges it. When the battery is completely charged, it disconnects from the small scale wind turbine and connects to the power converter which will convert the power suitable for the power conditioner.

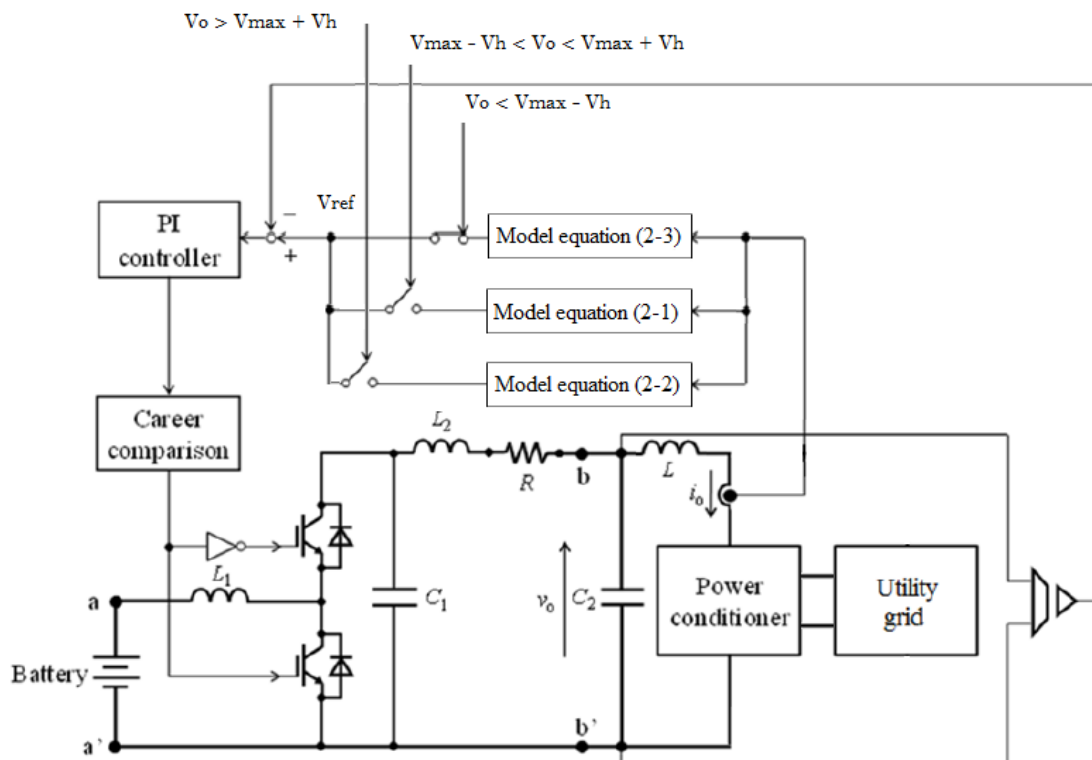


Figure 7: 3 model equations of the PV cell technical characteristic

Figure 7 presents the configuration of the power converter circuit in the stand alone mode. A bi-directional chopper circuit is used, as a boost chopper, for increasing the battery voltage to the operating voltage of the power conditioner. The current  $I_o$  coming into the power conditioner and the voltage  $V_o$  are measured for the control system.

The PV emulator control block determines the used model equation to calculate the voltage reference  $V_{ref}$  by comparing the output voltage value with  $V_{max}-V_h$  or  $V_{max}+V_h$ . Then, a PI controlled PWM compares the reference voltage with the output

voltage  $V_o$  for determining the duty factor. The power is then converted by the two switches and smoothed by the inductor  $L2$  and the capacitor  $C2$ .

**4. Simulation result**

Figure 8 shows the circuit of the grid-tied PV system in the stand-alone mode. including three main parts are the PV cell emulating system, the DC/DC bi-direction converter and the grid-tied DC/AC inverter. The parameters of the different component are written in the table below.

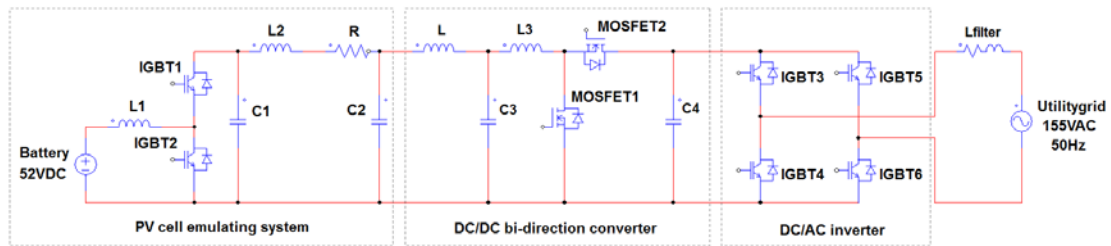


Figure 8: PSIM Circuit of Grid-Tied PV System

Table 2: Parameter of the components

Parameter	Value
Voltage of battery	52 VDC
Inductor L1, L2	10 mH, 2 mH
Capacitor C1, C2	13.2 $\mu$ F, 15 $\mu$ F
Input capacitor C3	400 $\mu$ F
DC bus capacitor C4	300 $\mu$ F
Inductor L, L3	1 mH, 2 mH
Peak grid voltage	155 VAC
Grid frequency	50 Hz
Filter Inductor Lfilter	150 mH

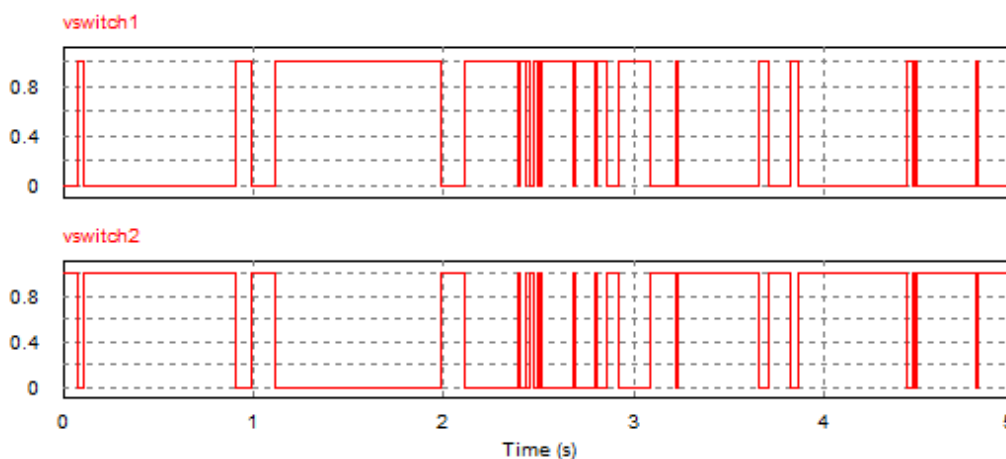


Figure 9: State Switches of 2 old Model equations

In the old topology, the two switches of the power converter circuit were permuting continuously in Figure 9 but we can see with the new model, the state of the switches are more stable as can be seen in Figure 10.

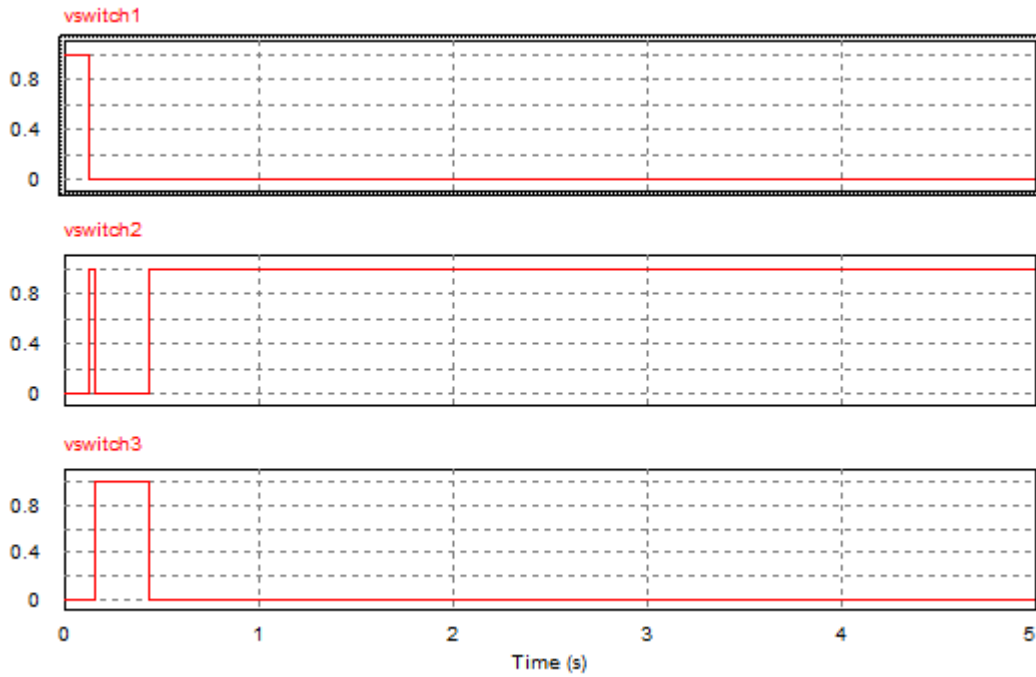


Figure 10: State Switches of 3 new Model equations

To validate this new model, we need to compare the value of the output characteristics of the PV cell emulating system in both configurations.

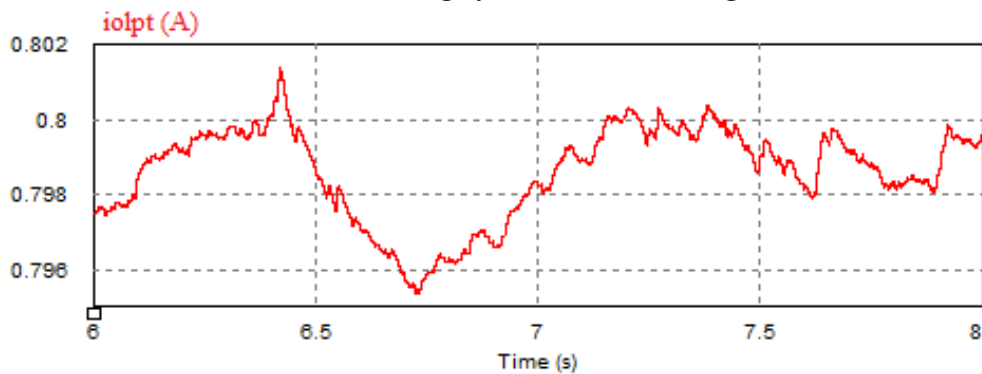


Figure 11: Fluctuations of the output current for the old model equations

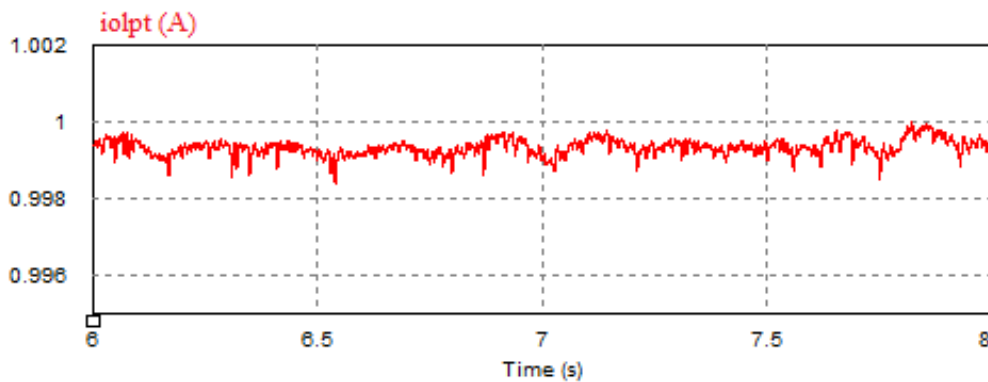


Figure 12: Fluctuations of the output current for the new model equations

Figure 11 and Figure 12 show that the value of the current of the new model

equation is more stable than the value of the old model equation. Through the calculation of the different gap, we find that there is a fluctuation of the output current of about  $0.7\%I_{max}$  for the old model equation and only  $0.15\%I_{max}$  for the new model equation. That's mean the new model is about 4.5 times more steady than the old one.

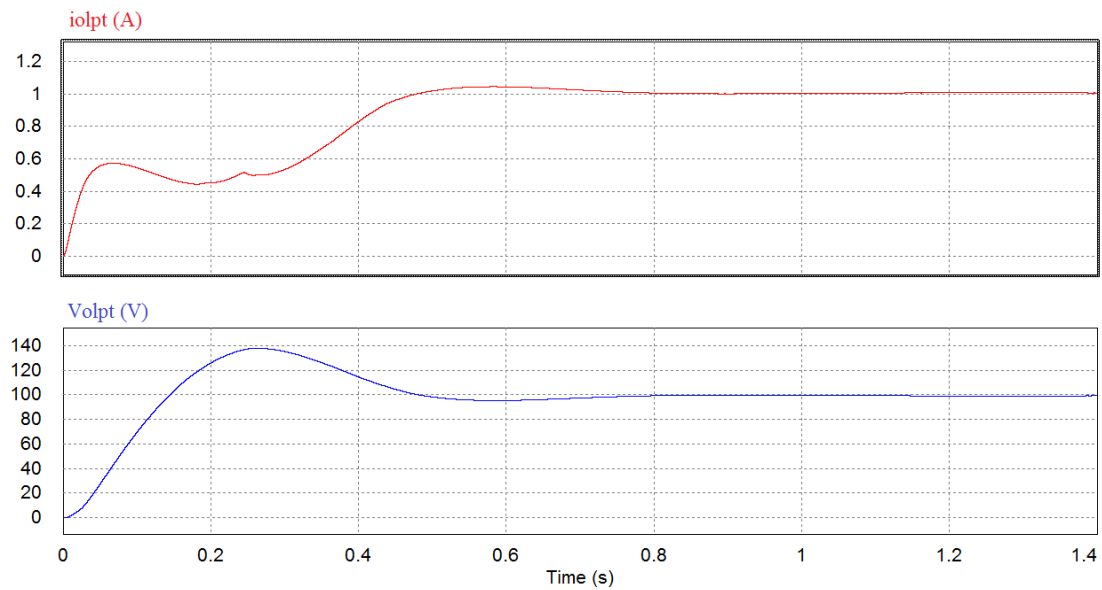


Figure 13: Output characteristics for new model equations

Figure 13 presents the simulation result of the output voltage  $V_{olpt}$  and the output current  $I_{olpt}$  of the PV cell emulating system. The simulation results match with maximum power point characteristics (MPP voltage of 100V, MPP current of 1A) of the linear model equations. Hence, the PV cell emulating system can connect to the PCS.

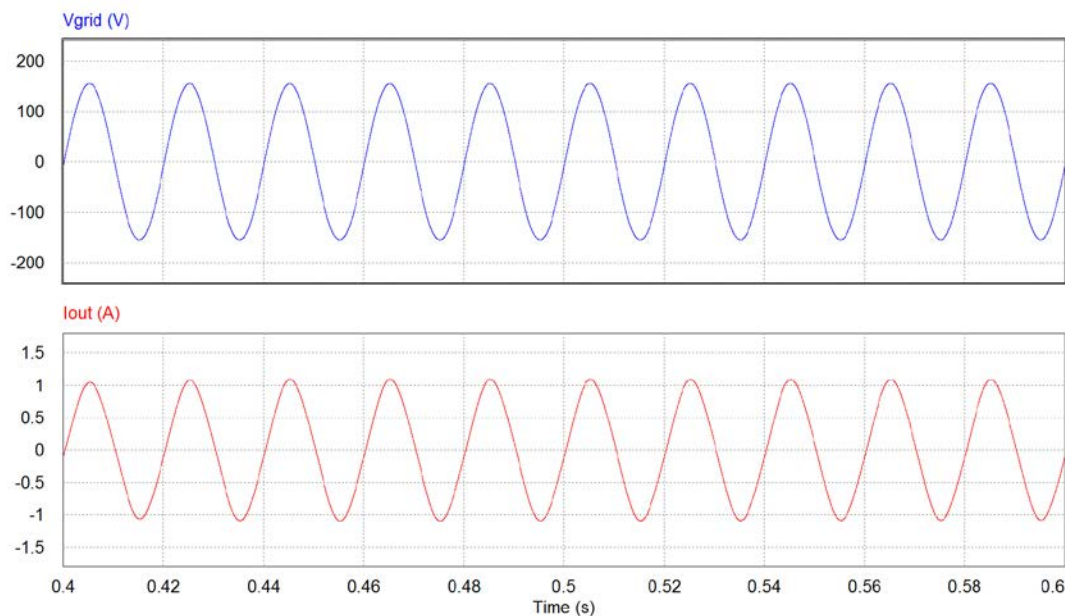


Figure 14: Grid-tied results of the PCS

Simulation result of output current after the low pass filter of grid tie DC/AC inverter and grid voltage is shown in Figure 14. The PV cell emulating system can

connect and supply the power to the utility grid by the grid tie PCS because the magnitude and frequency of the output current is sinusoidal and in phase with the grid voltage.

## 5. Conclusion

In this paper, emulating more accurately the technical characteristics of an PV array in adding one more equation allow the whole system to not switch between the different reference equation which bring a more accurate behavior of the value of the output current and output voltage of the PV cell emulating system. The output current fluctuation of the PV cell emulating system using new model equations is about 4.5 times smaller than the old model equations and the state of the switches are more stable. Therefore, the quality of the output power is increased by using the new model equations.

## REFERENCES

- [1] Vu Minh Phap, N. Yamamura, M. Ishida, J. Hirai, K. Natakani. 2016. Development of Novel Connection Control Method for Small Scale Solar – Wind Hybrid Power Plant, *International Journal of Engineering Research*, Volume No.5, Issue No.8, 731-735.
- [2] Vu Minh Phap, N. Yamamura, M. Ishida, J. Hirai, and N. T. Nga. 2016. Design of Novel Grid-tied Solar - Wind Hybrid Power Plant Using Photovoltaic Cell Emulating System, *Proc. IEEE, 4th International Conference on Sustainable Energy Technologies (ICSET)*, Hanoi, Vietnam, Nov. 168–171.
- [3] S. Masashi, N. Yamamura, M. Ishida. 2012. Development of Photovoltaic Cell Emulator using the Small Scale Wind Turbine, *Proceeding of 15th International Conference on Electrical Machines and Systems (ICEMS)*, 1–4.
- [4] Nicola Femia et al 2013. Power Electronics and Control Techniques for Maximum Energy Harvesting in Photovoltaic Systems, *CRC Press Taylor & Francis Group*.
- [5] Fernando Lessa Tofoli, Dênis de Castro Pereira, Wesley Josias de Paula. 2015. Comparative Study of Maximum Power Point Tracking Techniques for Photovoltaic Systems, *International Journal of Photoenergy*, 1–10.
- [6] Adham Makki et al. 2015. Advancements in hybrid photovoltaic systems for enhanced solar cells performance, *Renewable and Sustainable Energy Reviews*, 658–684.
- [7] Ioulia T. Papaioannou, Minas C. Alexiadis, Charis S. Demoulias, Dimitris P. Labridis, and Petros S. Dokopoulos. 2011. Modelling and Field Measurements of Photovoltaic Units Connected to LV Grid. Study of Penetration Scenarios, *IEEE Trans. Power Delivery*, 979–987.
- [8] F. Freijedo et al. 2009. Grid synchronization methods for power converters, in *Proc. IEEE, 35th Industrial Electronics Conference (IECON)*, Porto, Portugal, 522–529.
- [9] M. G. Villalva, J. R. Gazoli, E. Ruppert F. 2009. Comprehensive approach to modeling and simulation of photovoltaic arrays,” *IEEE Transactions on Power Electronics*, Vol. 25, No. 5, 1198-1208.
- [10] R. J. Wai, and W. H. Wang. 2009. Grid-Connected Photovoltaic Generation System, *IEEE Transactions on circuits and systems*, Vol. 55, No. 3, 953-964.



## The Viscoelastic Behavior of Alginate Hydrogels for Cartilage applications

Hussein Mishbak<sup>a</sup>, Dhurgham A. Kadhim<sup>b</sup>, Roberto Donno<sup>c</sup>, \*Paulo Bartolo<sup>d</sup>

<sup>a,d</sup> School of Mechanical, Aerospace and Civil Engineering, University of Manchester, Manchester, UK

<sup>a,b</sup> School of Engineering, University of Thi-Qar, Thi-Qar, Iraq

<sup>b</sup>The university college of Humanities

<sup>c</sup> School of Health Sciences, Faculty of Biology, Medicine and Heal, Stopford building, Manchester, UK

Dhurgham.alshakarchi@uch.edu.iq

Roberto.donno@manchester.ac.uk

paulojorge.dasilvabartolo@manchester.ac.uk

\*Corresponding Author: Hussein.al-hasani@postgrad.manchester.ac.uk

### ABSTRACT

The design of proper materials to create tissue replacements is a key topic of research. This paper investigates suitable photopolymerizable alginate hydrogels for bioprinting cartilage replacements. Alginate, chemically-modified with methacrylate groups containing different photoinitiator concentrations, was crosslinked using ultraviolet (UV) radiation (10 mW/cm<sup>2</sup>). Photo-rheology was used to assess the curing (crosslinking) reaction. The viscoelastic behaviour of the polymerized hydrogels is presented and its printability characteristics discussed. Results shown that alginate-methacrylate hydrogels exhibit a shear thinning behaviour making them good candidates for 3D bioprinting applications. Findings also show that gelation time depends on alginate concentration and photoinitiator type and concentration. It was also possible to observe that the reaction conditions are of paramount importance to control the extent of methacrylation and rheological properties, which are critical to design bioinks with appropriate properties for bioprinting applications.

**Keywords-** Alginate polymers; hydrogels; Rheological characterization; Cartilage applications

### 1. Introduction

Bioprinting comprises a group of additive biofabrication technologies developed to precisely printing biocompatible materials, cells and biochemical factors in predefined spatial positions (Pereira & Bártolo, 2015). Photocrosslinkable hydrogels are attractive materials for bioprinting as they provide fast polymerization under cell-compatible conditions and exceptional spatiotemporal control over the

crosslinking process. Hydrogels are polymeric materials widely investigated for several biomedical applications due to their potential use in a wide variety of applications such as, scaffolds for tissue engineering applications, drug delivery, contact lenses, corneal implants and wound dressing (Bashir et al., 2016)(Bertassoni et al., 2014)(Ren et al., 2015)(Catanzano et al., 2015)(Caló & Khutoryanskiy, 2014). Photocrosslinkable hydrogels can be synthesized according to specific requirements in terms of mechanical stability and degradation properties (Bonino et al., 2011). Additionally, hydrogels synthesized from natural materials are biodegradable and low toxic materials (Bonino et al., 2011).

Alginate is one of the most used natural hydrogel due to its relatively low cost, natural origin and easy handling. Alginate gels are currently being explored for cell encapsulation, drug delivery and cartilage replacements (Lee et al., 2012)(Bidarra et al., 2014). This paper reports on the synthesis of methacrylate-functionalized alginate hydrogels aimed to be used as bioinks for bioprinting of cartilage constructs. This hydrogel can be tailored to have different degree of reticulation and mechanical properties to replicate the different layers of cartilage (see Fig (1)). Moreover, these hydrogels must also present adequate printability characteristics, which strongly depends on the rheological properties, allowing the printing process to occur at low stress levels and providing a proper microenvironment to embedded cells. These characteristics strongly depend on the level of unsaturation of the functionalized hydrogels.

This paper investigates different alginate-methacrylate materials. Alginate was primarily reacted with methacrylic anhydride (MA) for different reaction times in order to assess the effect of reaction time on the degree of functionalization and rheological properties. Additionally, photo-rheological tests were performed to investigate the crosslinking properties of hydrogels containing different photoinitiator concentrations.

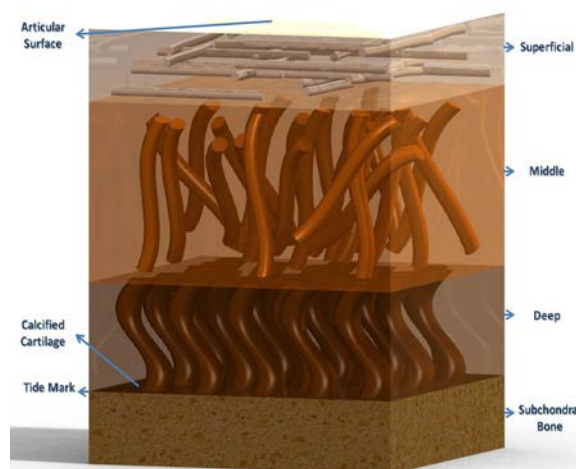


Figure .1 Cartilage layers' structure

## 2. METHODS AND MATERIALS

### 2.1 Synthesis of methacrylated alginate

Alginate was functionalized with methacrylate groups according to a published protocol (Lee et al., 2012). Low molecular weight sodium alginate 2% (w/v) (Sigma-Aldrich, UK) was dissolved in Dulbecco's Phosphate Buffered Saline (DPBS) (Sigma-Aldrich, UK) and then mixed with methacrylate anhydride (MA) (Sigma-Aldrich, UK) at 15 mL MA/g of alginate under vigorous stirring. The pH of the solution was kept around 7.5-8.0 during the reaction time by adding of 5M NaOH. Different reaction times (8, 12 and 24 hours) were used to assess the effect of the reaction time. After the chemical modification, the polymeric solution was precipitated with cold ethanol, dried in an oven overnight at 50 °C and purified through dialysis membranes SnakeSkin™ Dialysis Tubing, 10K MWCO, 22 mm (Thermo Fisher Scientific, UK) for 4 days. The solution was freeze at -80°C and the polymer recovered by lyophilization. Photo-polymerization tests were performed by heading different amounts of two photo-initiators (PI): Irgacur2959 a 2-Hydroxy-4'-(2-hydroxyethoxy)-2-methylpropiophenone initiator (Sigma Aldrich, UK) and VA-086 a 2,2'-Azobis[2-methyl-N-(2-hydroxyethyl) propionamide azo initiator (Wako Pure Chemical Industries, USA). The photo-polymerization process of alginate-methacrylate with PI is a radical polymerization process started by the absorption of UV light by the PI.

The Photopolymerization mechanism is briefly presented in Fig (2).

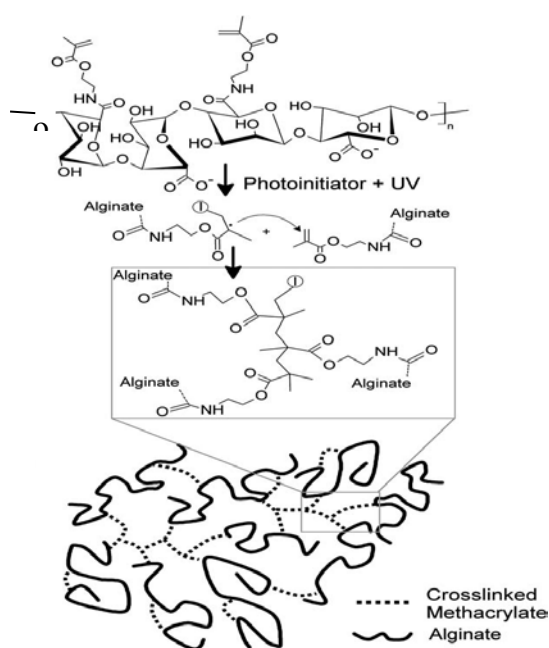


Figure .2 Photo-polymerization process of alginate-methacrylate. Adapted from (Bonino et al., 2011).

## 2.2 Characterization of chemical modification through $^1\text{H}$ NMR

The chemical structure of functionalized alginate was assessed through Nuclear Magnetic Resonance Spectroscopy ( $^1\text{H}$ NMR), using the B400 Bruker Avance III 400 MHz. Polymeric materials were dissolved in Deuterium oxide ( $\text{D}_2\text{O}$ ), transferred to NMR tubes and the spectra acquired with 128 scans.

## 2.3 Rheological characterisation

The rheological analyses were carried out using the Bohlin Gemini (Malvern Instruments) system. Oscillation tests were considered. It is assumed that the material flows by applying a stress being the response measured. A controlled stress was applied and the resulting movement measured. Small strain oscillations have been used to measure viscoelastic properties without destroying the sample structure. The oscillatory test provides a mechanical spectrum for the material. The rotational speed depends on viscosity computed by means of stress and shear rate. Photo-rheology was performed using the OmniCure® S1000 curing system, irradiating in the range of 254-450 nm wavelength. The light intensity was  $10 \text{ mW}/\text{cm}^2$ .

# 3. Result and discussion

## 3.1 Chemical modification through $^1\text{H}$ NMR

The alginate functionalization with methacrylate anhydride was performed under standard conditions, allowing the introduction of photoreactive methacrylate groups into the polymer backbone, as confirmed by  $^1\text{H}$ NMR analysis (Fig 3). After alginate functionalization, results show the appearance of new characteristic peaks of methacrylate (MA) at 5.63 ppm and 6.09 ppm attributed to the methylene group in vinyl bond, and a peak at 1.82 ppm assigned to the methyl group (Fig. 3b), which are not present in the non-modified polymer (Fig. 3a). The results presented in (Fig 3) are related to hydrogels obtained considering 8,12 and 24 hours of reaction time between alginate and methacrylate.

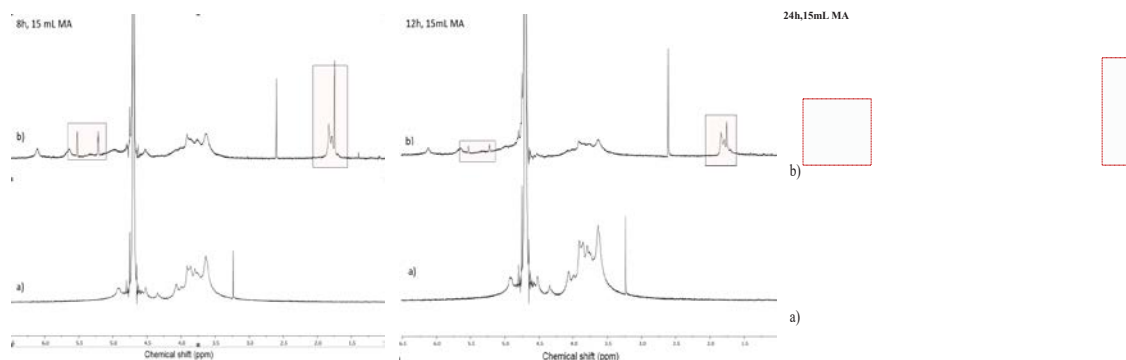


Figure. 3 Representative  $^1\text{H}$  NMR spectra of a) pure alginate and b) methacrylated alginate after 8, 12 and 24 hours of reaction.

### 3.2 Prepolymerised alginate hydrogels characterisation

Stress versus shear rate analysis indicates that functionalized alginate exhibits a shear-thinning behaviour (Fig. 4). This behaviour characterized by a decrease in the viscosity as a function of increased shear rate, is crucial for bioprinting applications, since less extrusion force is required during the deposition or extrusion process. These results are particularly relevant as the nozzles used by most bioprinters are small in diameter to control macro-porosity.

It is also possible to observe that the reaction time has a significant impact on the viscosity of the hydrogels being investigated. Results show that polymers modified with the highest reaction time (24 hours for AlgMA) present lower viscosity at low shear rates, but the viscosity decrease with the shear rate is less pronounced. Since the polymers exhibit a shear-thinning behaviour, a power law model can be used to fit the experimental data.

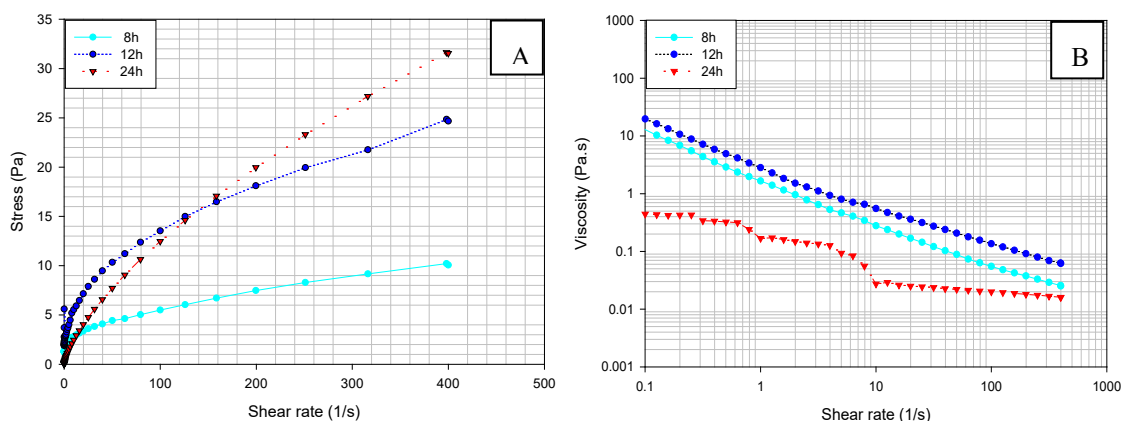


Figure. 4 Rheological behavior of 2% alginate prepared with different reaction times. a) Stress versus shear rate; b) Viscosity versus shear rate

According to this model, the rheological behaviour of the material is described by the following equation

$$\tau = \eta \cdot \dot{\gamma}^n \quad (1)$$

where  $\tau$  is the shear stress (Pa),  $\dot{\gamma}$  the shear rate (s<sup>-1</sup>),  $\eta$  the consistency index (Pa s) and  $n$  is the power law index (dimensionless).

Table I, presents the results of both the power law index and the effect of reaction time on the modification degree of alginate, showing a good approximation ( $R^2$  around 0.98) between the power law and experimental, showing that all hydrogels present a shear-thinning behaviour. The increase of reaction time leads to an increase

on the power law index, resulting in reduced printability properties. The alginate reaction time was varied between 8 and 24 hours, and the degree of modification was determined by dividing the relative integrations of methylene to carbohydrate protons (Smeds et al., 2001). Results show that the degree of modification increases with increased reaction time, reaching a maximum value of 33 % at 24 hours.

Table I: shows the power law index and degree of modification of alginate methacrylated for three different reaction time

Reaction time between alginate and methacrylate	n	R <sup>2</sup>	Degree of modification (%)
8 h	0.30	0.9635	21
12 h	0.38	0.9687	27
24 h	0.68	0.9999	33

### 3.3 Photopolymerized alginate hydrogels characterisation

The elastic or storage modulus ( $G'$ ) and the viscous or loss modulus ( $G''$ ) were measured at room temperature through a controlled frequency of 1Hz to provide quantitative information on viscoelastic properties of different polymeric samples. Photo-rheology was used to characterise the curing (photopolymerization) process of functionalised alginate polymers. In this case, alginate methacrylate (2%ALG-15 mL of MA) obtained through a 24-hour reaction time was mixed with different concentrations of two photoinitiators: 0.5%, 1% and 1.5% of VA-086; 0.05%, 0.075% and 0.1% of Irgacure 2959. The curing kinetics was assessed by monitoring the variation of  $G'$  and  $G''$  along time. Results are presented in Figures 5 and 6. During the polymerization process, the polymer becomes less viscous increasing the mechanical properties.

For all investigated polymeric formulations, it was possible to observe that increasing the curing time, increases  $G'$ , which becomes significantly higher than  $G''$ . The increase of the elastic behaviour seems also to be strongly dependent on the type of photoinitiator and its concentration. As observed, Irgacure 2959 is more efficient than VA-086. Therefore, relatively small concentrations of Irgacure 2959 are required for the curing reaction (the polymerization process requires less irradiation time), while polymeric solutions containing VA-086 require long irradiation times, high photoinitiator concentration or high light intensities.

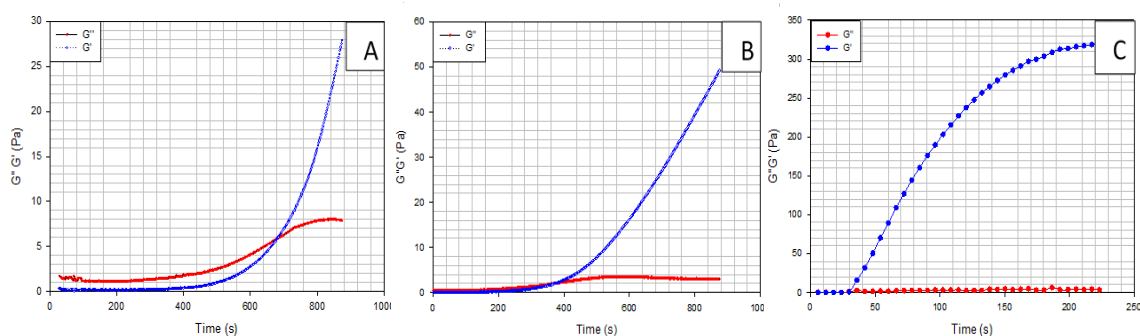


Figure. 5 2% alginate methacrylated, 24 h was the functionalization time A) 0.5% VA-086 B) 1% VA-086 C) 1.5% VA-086

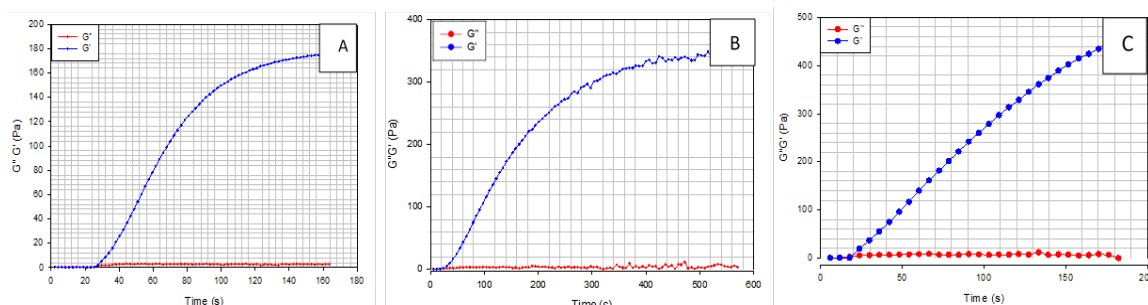


Figure. 6 2% alginate methacrylated, 24 h was the functionalization time A) 0.05% Irgacure 2959 B) 0.075% Irgacure 2959 C) 0.1% Irgacure 2959

From (Fig 5 and 6) it is also possible to observe that by increasing the photoinitiator concentration the gelation time, which corresponds to the time point where the  $G'$  curve crosses the  $G''$  curve, decreases. From Figure 6, the crosslinking density increases by increasing the photoinitiator concentration. In the case of alginate-methacrylate containing 0.075% of Irgacure 2959,  $G'$  reaches a plateau which corresponds to a vitrification stage of the curing process, i.e., from a chemical point the polymerization process stopped. However, the same behaviour is not observed in (Fig 6c), which corresponds to the curing process of alginate-methacrylate containing 0.1% of photoinitiator. The possible explanation for this observation is that, for the layer thickness considered in this study ( $\sim 100 \mu\text{m}$ ), a critical concentration of initiator was already been achieved. This means that by increasing photo-initiator concentration above the critical values, the polymerisation occurs very fast at the polymer surface, reducing light penetration and, consequently, the overall polymerisation reduces.



#### 4. Conclusion

Alginate hydrogels can be tailored for bioprinting applications by reacting them with methacrylate solutions. Results show that the reaction time plays a key role on the functionalization process. It was possible to observe that by increasing the reaction time, the polymeric solutions become less shear-thinning and consequently easy to process. In order to use alginate-methacrylate polymeric solutions for photo-curing based additive bioprinting applications, photoinitiators must be added. Two types of photo-initiators were considered (Irgacure 2959 and VA-086). Results show that the most suitable formulations are obtained with Irgacure 2959, which allows fast photo-polymerization with higher mechanical properties (viscoelastic characteristics) in comparison to VA-086. The results reported in this paper are particularly important to prepare future alginate-based bioinks for cell encapsulation, as long irradiation times or high light intensity values might cause cell death.

#### ACKNOWLEDGMENTS

The authors wish to acknowledge the support of the government of Iraq for supporting a PhD studentship through a grant provided by the Higher Committee for Development Education Iraq (HCED).

#### REFERENCES

- Bashir, S., Teo, Y. Y., Ramesh, S., & Ramesh, K. 2016. Synthesis, characterization, properties of N-succinyl chitosan-g-poly (methacrylic acid) hydrogels and in vitro release of theophylline. *Polymer*, 92: 36–49.
- Bertassoni, L. E., Cardoso, J. C., Manoharan, V., Cristino, A. L., Bhise, N. S., et al. 2014. Direct-write bioprinting of cell-laden methacrylated gelatin hydrogels. *Biofabrication*, 6(2): 24105.
- Bidarra, S. J., Barrias, C. C., & Granja, P. L. 2014. Injectable alginate hydrogels for cell delivery in tissue engineering. *Acta Biomaterialia*, 10(4): 1646–1662.
- Bonino, C. a., Samorezov, J. E., Jeon, O., Alsberg, E., & Khan, S. a. 2011. Real-time in situ rheology of alginate hydrogel photocrosslinking. *Soft Matter*, 7(24): 11510.
- Caló, E., & Khutoryanskiy, V. V. 2014. Carvacrol and trans-cinnamaldehyde reduce *Clostridium difficile* toxin production and cytotoxicity in vitro. *International Journal of Molecular Sciences*, 15(3): 4415–30.

- Catanzano, O., D'Esposito, V., Acierno, S., Ambrosio, M. R., De Caro, C., et al. 2015. Alginate-hyaluronan composite hydrogels accelerate wound healing process. *Carbohydrate Polymers*, 131: 407–414.
- Lee, K. Y., Mooney, D. J., & Manuscript, A. 2012. Alginate: properties and biomedical applications. *Progress in Polymer Science*, 37(1): 106–126.
- Pereira, R. F., & Bártolo, P. J. 2015. 3D bioprinting of photocrosslinkable hydrogel constructs. *Journal of Applied Polymer Science*, 132(48): n/a-n/a.
- Ren, K., He, C., Xiao, C., Li, G., & Chen, X. 2015. Injectable glycopolymer hydrogels as biomimetic scaffolds for cartilage tissue engineering. *Biomaterials*, 51(1): 238–249.
- Smeds, K., Pfister-Serres, A., Miki, D., Dastghieb, K. A., Inoue, M., et al. 2001. Novel Photocrosslinkable Polysaccharides for In Situ Hydrogel Formation. *J. Biomed. Mat. Res.*, 54(July): 115–121.

## Heat Conduction Analysis of Wall Materials

Sirikul Siriteerakul<sup>a,\*</sup>, Teera Siriteerakul<sup>b</sup>

<sup>a</sup>Department of Mathematics, Faculty of Science, King Mongkut's Institute of Technology Ladkrabang, Chalongkrung Street, Bangkok, Thailand

<sup>b</sup>Department of Computer, Faculty of Science, King Mongkut's Institute of Technology Ladkrabang, Chalongkrung Street, Bangkok, Thailand

\*Corresponding Author: yok.math@ gmail.com

### ABSTRACT

The temperature distributions into a building depends on several factors. One of those is wall material. Simulation of transient heat conduction into a model house through the different kinds of wall materials is presented in this research. To investigate the effect of temperature distribution within the materials, two-dimension heat conduction equation in Cartesian coordinates system was utilized. This is under the assumption of homogeneous materials, no convection nor radiation effects. Finite element method (FEM) under Taylor Galerkin principle with iterative technique was created as a software using C language. The results demonstrate the temperature distributions passing through the wall of each material type and temperature distribution within the building. It seems that the temperature variety significantly, especially with the temperature near the wall. The heat can pass into the building built using yellow pine harder than those built using adobe brick, autoclaved aerated concrete (AAC), common brick and glass, respectively.

**Keyword:** Heat Transfer, Finite Element Method.

### 1. Introduction

Several buildings were constructed and designed according to necessity and usability. For example, brick house, Thai house, clay house, and igloo. In addition, the temperature inside the building is one of the things to pay attention.



Fig.1 Example of buildings

Home designers are interested in choosing the right building materials. In terms of materials used to make the roof, various materials and the colors used to paint buildings. In addition, home style is one of the things to consider. For example, Thai homes are elevated to protect against floods and animals as well as there are also many windows for easy air circulation. Brick houses are sturdy and weather resistant. The clay house is made of easily accessible materials and reduces the cost of moving raw materials as well as being cheap. On the other side, a number of researches are trying to study and devise ways to build a building for maximum benefit.

In 1998, P. Taksatian [1] studied roof slopes and three materials (Cpacmonier tiles, Asbestos tiles and Ceramic tiles) in order to conserve energy. After many years, P.Chitsakul and S.Siriteerakul [2] simulated heat transfer within three geometric shape buildings. Their simulation illustrated that octagon, the heat through is less than hexagon and rectangle respectively. Moreover, they [3] compared thermal distribution pass plain glass and filmed glass. In 2012, S. Siriteerakul et.al [4] simulated thermal distribution as well as did an actual physical experiment on three different types of roof tiles (smooth, CPAC Monier and double wave) to find out how they affected heat transfer into the model houses. In later years, S. Siriteerakul and S. Thenissara [5] studied the effect of arrangement of wall to heat transfer with building. They found that the more glass divided by heat, the more difficult to pass. A few years ago, S. Siriteerakul et.al [6, 7] simulated heat transfer in model houses with the different roof angle and roof geometries by using finite difference method and finite element software (Easy FEM) which created by P. Dechaumpai and S. Phongthanapanich[8]. Moreover, they presented steady-state temperature distributions of three model triangular tent,

each with windows of different position. Recently, Nongrat et.al [9] investigated transient heat conduction in kitchenware materials.

In this study, we divided the calculation into two parts. First, transient heat conduction through the different kinds of wall materials were investigated by using the finite element method in two-dimensional rectangular coordinate system. Second, we gave examples of the temperature distribution at steady state in each model house at selected period by using finite different method. The assumptions made were that each material was homogeneous and smooth surface. The building was of closed space. Convection and radiation were not considered.

## 2. Governing Equation

In this paper, the transient heat transfer in five materials of wall were illustrated and example of the distribution of temperature in the model houses with different wall materials. They were solved by using a heat equation under the assumptions of no convection and nor radiation.

The governing equation of heat conduction in two-dimensional rectangular coordinate system can be expressed as:

$$\frac{\partial^2 T}{\partial x^2} + \frac{\partial^2 T}{\partial y^2} = \frac{1}{c^2} \frac{\partial T}{\partial t} \quad (1)$$

where  $T$  is the temperature and  $c^2$  is the thermal diffusivity. At steady state, the equation becomes Laplace equation.

## 3. Methodology

To determine the solution, numerical methods which consists of finite difference method, finite element method and iterative technique were used as follows

### 3.1 Finite difference method

Finite difference method (FDM) is one of an introductory method to solve engineering problems which are in term of differential equations. Domains of the problems should be simple. In 1980, this method has been used by Runge [10]. After that this method was famous and popular in research groups around the world. Many researchers take this method to solve the problem of thermal conductivity [11]. Moreover, some researchers applied this method with elastics and fluid dynamics problems [12-14].

For solving any problem, domain was separated by uniform grid point which shown in Fig.1. Therefore, solution of the problem with complicated domains is not as precise as it should be. Most problems are in term of differential equations so FDM was

used approximate their derivatives at any point of domain. There are three schemes to approximate the derivatives as forward difference, backward difference and central difference schemes. For this problem, the numerical solution based on central difference or Crank-Nicolson scheme.

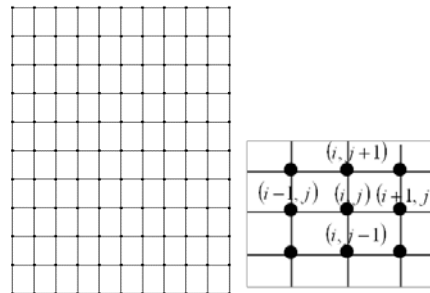


Fig.2 Generating grid points

From Governing equation, the heat equation was estimated the derivatives by using Taylor series expansion as follows:

$$\frac{\partial^2 T}{\partial x^2} = \frac{T_{i+1,j} - 2T_{i,j} + T_{i-1,j}}{h^2}$$

$$\frac{\partial^2 T}{\partial y^2} = \frac{T_{i,j+1} - 2T_{i,j} + T_{i,j-1}}{k^2} \quad (2)$$

After that, we substituted and rearranged the equation and given  $h=k$ . It becomes

$$T_{i+1,j} + T_{i-1,j} - 4T_{i,j} + T_{i,j+1} + T_{i,j-1} = 0 \quad (3)$$

Then, the equations for each unknown point were obtained. Then, they were written in a linear system. This system of equation ( $Ax=b$ ) was solved numerical technique such as direct technique (Gauss Elimination, LU Factorization, or Cholesky decomposition LDL<sup>t</sup>) and iterative technique (Jacobi iterative method, Gauss-Seidel iterative technique, or Successive Over-Relaxation).

### 3.2 Finite element method

Finite element method is one of the method developed from finite different method for solving boundary value problems. It can be obtained the accuracy solutions while the domains are complex shapes. In 1965, Zienkiewicz and Cheung [15] has been used first. Then, many researchers applied and developed this method to various problems, for example, beam, truss, and heat transfer. In addition, the finite element method can be solved the complex problems such as vibration problem and continuum fluid dynamics [16,17]. Our group and other groups attempted create software program to solve the problems. Some group created software by Fortran, some group created by visual basic. Our group created software by visual C program which used the scheme of finite

element method under Galerkin principle and iterative technique.

In this paper, the structured meshes were consider. Therefore, each element was considered in linear rectangular mesh and transform to major axis as shown in Fig 2.

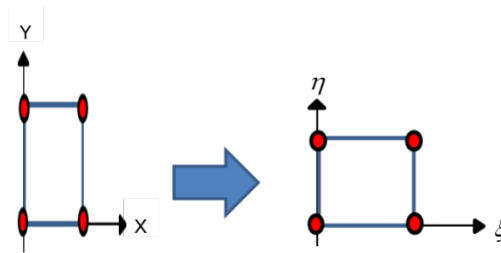


Fig. 3 linear rectangular mesh

Their linear shape functions and their derivative are following

Table 1

Shape functions	Derivative of $\xi$	derivative of $\eta$
$N_1(\xi, \eta) = \frac{1}{4}(1-\xi)(1-\eta)$	$\frac{\partial}{\partial \xi} N_1(\xi, \eta) = -\frac{1}{4}(1-\eta)$	$\frac{\partial}{\partial \eta} N_1(\xi, \eta) = -\frac{1}{4}(1-\xi)$
$N_2(\xi, \eta) = \frac{1}{4}(1+\xi)(1-\eta)$	$\frac{\partial}{\partial \xi} N_2(\xi, \eta) = \frac{1}{4}(1-\eta)$	$\frac{\partial}{\partial \eta} N_2(\xi, \eta) = -\frac{1}{4}(1+\xi)$
$N_3(\xi, \eta) = \frac{1}{4}(1+\xi)(1+\eta)$	$\frac{\partial}{\partial \xi} N_3(\xi, \eta) = \frac{1}{4}(1+\eta)$	$\frac{\partial}{\partial \eta} N_3(\xi, \eta) = \frac{1}{4}(1+\xi)$
$N_4(\xi, \eta) = \frac{1}{4}(1-\xi)(1+\eta)$	$\frac{\partial}{\partial \xi} N_4(\xi, \eta) = -\frac{1}{4}(1+\eta)$	$\frac{\partial}{\partial \eta} N_4(\xi, \eta) = \frac{1}{4}(1-\xi)$

### 3.3 Iterative technique

The system of linear equation ( $Ax=b$ ) can be solve by direct technique or iterative technique. Although, some problem can be solved by direct technique which it comfortable and it would deliver an exact solution, several problems which in the algebraic equations should be determined by iterative technique.

The iterative technique is a mathematical procedure that generates a sequence of improving approximate solutions for a class of problems, in which the n-th approximation is derived from the previous ones. This technique need to uses an initial guess to generate successive approximations to a solution. Then, good initial solution effect to good final solution. The iterative technique consists of several methods as follows:

**Jacobi method** is a basic method of solving a matrix equation that has no zeros along its main diagonal. Each diagonal element is solved for, and an approximate value plugged in. The process is then iterated until it converges.



For each  $k \geq 1$ , generate the components,  $x_i^{(k)}$  of  $x^{(k)}$  from  $x^{(k-1)}$  by

$$x_i^{(k)} = \frac{1}{a_{ii}} \left[ \sum_{\substack{j=1, \\ j \neq i}}^n (-a_{ij}x_j^{(k-1)}) + b_i \right] \quad (4)$$

where  $i = 1, 2, \dots, n$

The definition of the Jacobi method can be expressed with matrices as

$$\mathbf{x} = D^{-1}(L + U)\mathbf{x} + D^{-1}\mathbf{b} \quad (5)$$

where the matrices D, -L, and -U represent the diagonal, strictly lower triangular, and strictly upper triangular parts of A, respectively.

**Gauss-Seidel method** is a developing method of Jacobi method but it uses previously computed results as soon as they are available.

For each  $k \geq 1$ , generate the components,  $x_i^{(k)}$  of  $x^{(k)}$  from  $x^{(k-1)}$  by

$$x_i^{(k)} = \frac{1}{a_{ii}} \left[ - \sum_{j=1}^{i-1} (a_{ij}x_j^{(k)}) - \sum_{j=i+1}^n (a_{ij}x_j^{(k-1)}) + b_i \right] \quad (6)$$

where  $i = 1, 2, \dots, n$

In terms of matrices, the definition of the Gauss-Seidel method can be expressed as

$$\mathbf{x}^{(k)} = (D - L)^{-1}U\mathbf{x}^{(k-1)} + (D - L)^{-1}\mathbf{b} \quad (7)$$

This paper used Gauss-Seidel to computed the temperature at each time.

#### 4. Problem Specification

In this paper, the problem was separated in 2 problems as shown in Fig. 2. First, the transient heat conduction along each material were computed. Next, the output of first problem became input of second problem as display in Fig. 4. Second problem, the example of steady state temperature distribution within the model houses with materials. We chose 5 popular materials to shown in this case. Autoclaved aerated concrete(AAC), common brick, adobe brick, yellow pine, and glass were chosen. Materials parameter which obtained by Wikipedia are shown in Table 2:

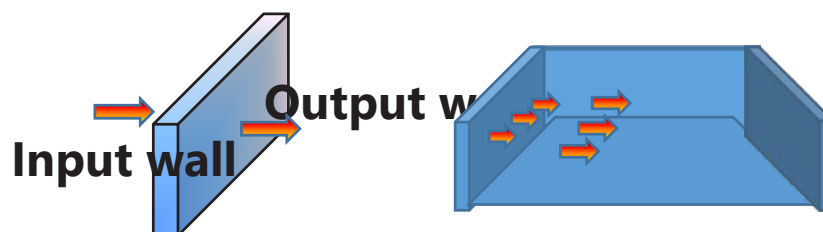




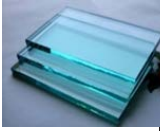


Fig.4 Diagram shown heat pass from outside to inside of house

Table 2 Materials parameter

Parameters/ Materials	ACC	Common brick	Adobe brick	Yellow pine	Glass
Pictures					
Cross section size (cm.)	20 x 12.5	6.2 x 3	8 x 4	10.16 x 5.08	4 x 1
Thermal diffusivity (m <sup>2</sup> /s)	2.48 x 10 <sup>-6</sup>	5.2x10 <sup>-7</sup>	2.7 × 10 <sup>-7</sup>	8.2 × 10 <sup>-8</sup>	3.4 × 10 <sup>-7</sup>
Grid number	10 x 10	5 x 5	10 x 10	10 x 10	5 x 5

In this paper, initial temperature of first problem obtained by Meteorological Department since January 2009 to December 2014. Outer wall is the average temperature which is 33.97778. Texture in the wall is a minimum temperature which is 25.25417. Grid points of each material are showed in table 3:

For the governing equation, it was discretized to algebraic equation by using finite element method under Taylor Galerkin principle and Crank-Nicolson scheme as follow:

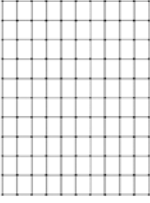
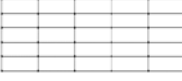
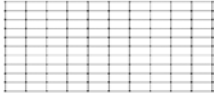
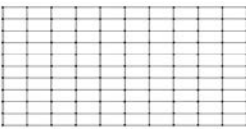
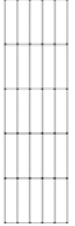
$$\left( [A] + \frac{1}{2} \Delta t^{n+1} C^2 [B] \right) (T_j)^{n+1} = \left( [A] - \frac{1}{2} \Delta t^{n+1} C^2 [B] \right) (T_j)^n \tag{8}$$

where each element  $A_{ij}^e, B_{ij}^e$  can write in term of  $\xi, \eta$  as following equations

$$A_{ij}^e = \iint_{\Omega} N_i N_j |J| d\xi d\eta \tag{9}$$

$$B_{ij}^e = \iint_A \left[ \frac{\partial N_i}{\partial x} \quad \frac{\partial N_i}{\partial y} \right] \begin{bmatrix} \frac{\partial N_j}{\partial x} \\ \frac{\partial N_j}{\partial y} \end{bmatrix} |J| d\xi d\eta \tag{10}$$

Table 3 Grid points of each material

ACC	
Common brick	
Adobe brick	
Yellow pine	
Glass	

### 5. Results

The results demonstrate that each material that effects the temperature distribution passed into the building. The heat can be through into the building of yellow pine less than adobe brick, autoclaved aerated concrete (AAC), common brick and glass, respectively. It can be shown as in Fig.5.

From the results, heat from outside can be through into the building of yellow pine less than adobe brick, autoclaved aerated concrete (AAC), common brick and glass, respectively.

The glass can heat pass rapidly. It used less time to the outside and inside temperatures equal. Autoclaved aerated concrete and common brick gave the similar result. The heat entering the building of these two materials is about 2 times slower than the glass. Adobe brick is a good choice because it can reach temperatures about 2 times slower than conventional bricks. For the case of yellow pine, it is the building block material that brings the least heat. Moreover, when we considered that round at 90000, average temperature within materials and temperature at the outlet are shown below:

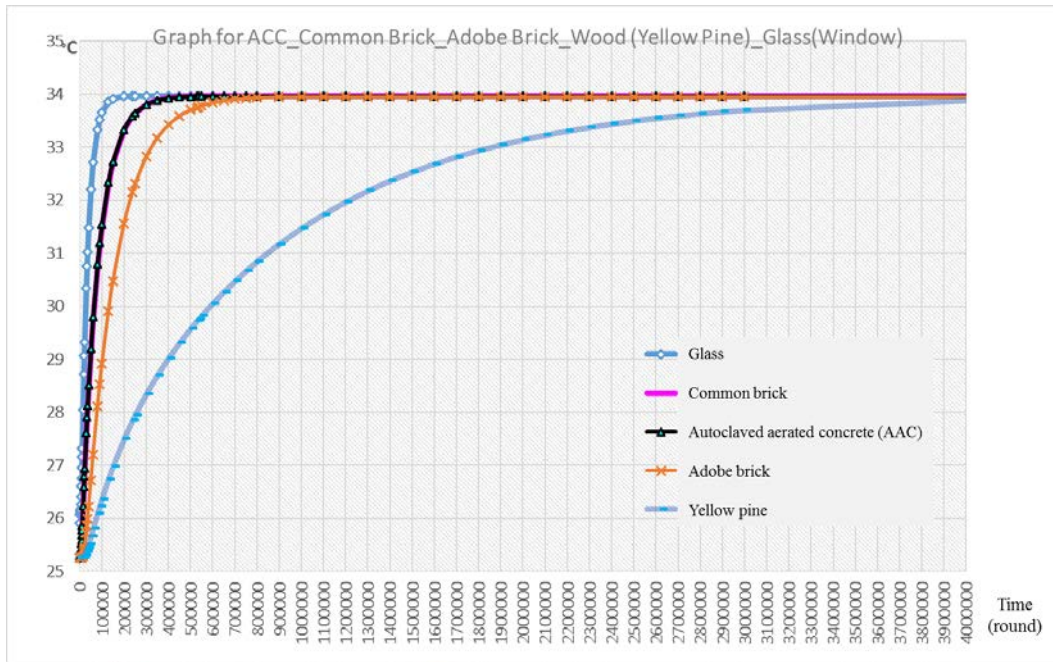


Fig. 5 Comparison of temperature of each material

Table 4

Materials	ACC	Common brick	Adobe brick	Yellow pine	Glass
Average temperature	31.56253	31.63738	30.04627	26.75563	33.64208
Temperature at the outlet	31.15452	31.14589	28.52591	25.56644	33.63167

Temperature distributions of each material at this time were illustrated in Fig.6

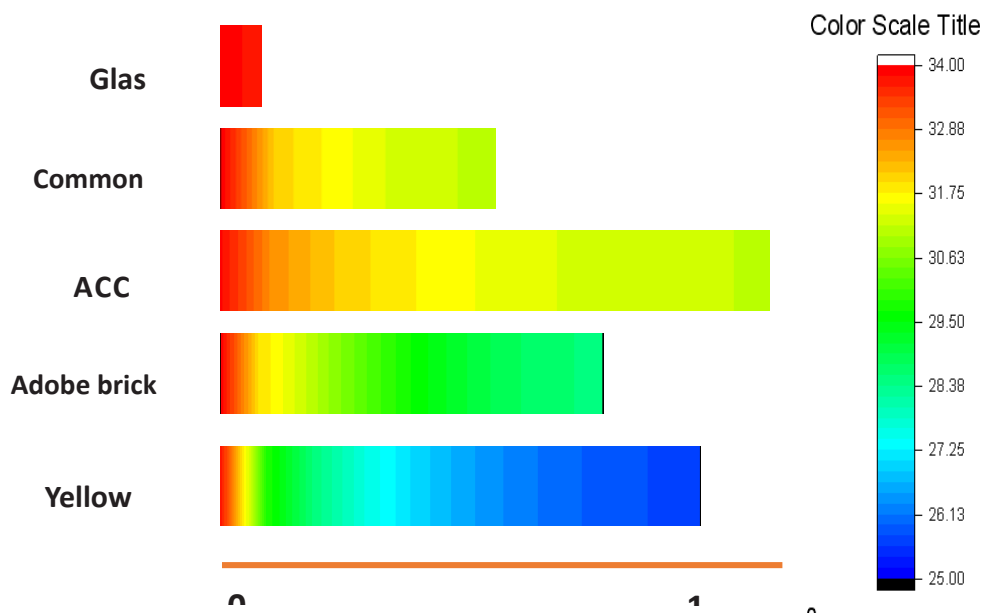


Fig.6 Temperature distributions of each material

After the passing temperatures were known, they became input temperature of the model houses in the second problem.

This following is the example of model houses with different wall materials. All model was similar shape. The outside temperatures were the outlet temperature of each material which received from first problem. Domain and grid point of the model house as shown in Fig.7

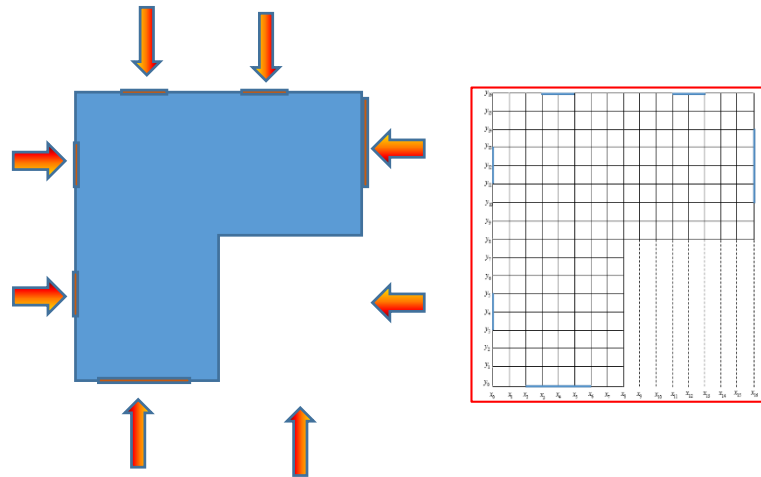


Fig.7 Domain and grid point of the model house

The temperature distribution within these model houses as below:

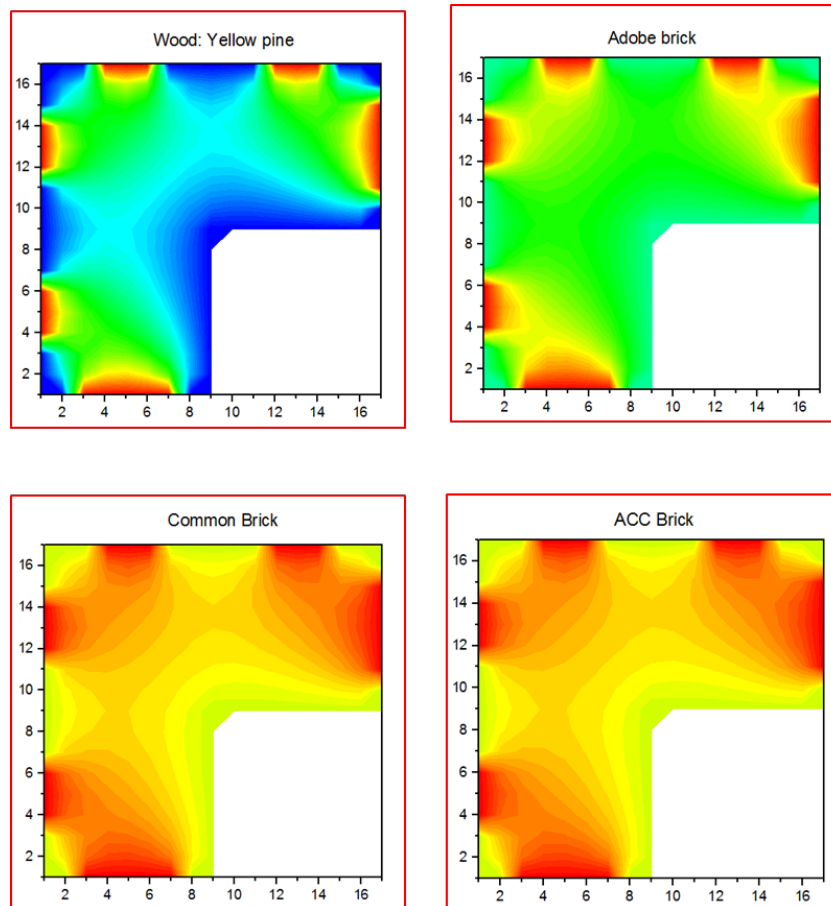


Fig.8 The temperature distribution within these model houses  
The different of materials effect to the temperature distribution passed into the building and the temperature inside the residence significantly, especially with the temperature near the wall.

## 6. Conclusion

Type of materials effect to the temperature distribution passed into the building and the temperature inside the residence significantly, especially with the temperature near the wall. The heat can be through into the building of yellow pine less than adobe brick, autoclaved aerated concrete (AAC), common brick and glass, respectively.

Therefore, yellow pine is the best material for the person who need the building less heat pass. However, bringing wood to build houses is destroying the forest which is the reason for global warming. Another good way, clay house (house made from adobe brick) is a good choice for saving energy. Moreover, adobe brick is a cheap material and it is an inherently natural material with no boundaries. By the way, The material selection depends on consumer necessity and usability.

## REFERENCES

- [1] P. Taksatain, “Comparative Study Of Roofing Design And Materials To Support Energy Conservation”, M.Sc. Mahidol University, University of Thailand, 1998.
- [2] P.Chitsakul and S.Siriteerakul, Simulation of heat transfer within Geometry Shape Symmetry Building, TJIA 2009.
- [3] S.Siriteerakul and P.Chitsakul, Simulation of heat transfer within a room with plain and filmed glass, TJIA 2011.
- [4] S. Siriteerakul et.al, “A study on heat diffusion of Tile”, *TJIA*, 2012
- [5] S. Siriteerakul and S. Thenissara, “Glass Arrangement Effect on Heat Transfer in rectangular Building”, WASET, 2013
- [6] S. Siriteerakul et.al, Simulation of Heat Transfer in Model Houses with the different Roof Angles, TJIA 2013
- [7] S. Siriteerakul et.al, Temperature distribution in three model houses with different roof geometries, 2013
- [8] P. Dechaumpai and S.Phongthanapanich, “Easy Finite Element Method with Software”, 2005.
- [9] Nongrat et.al, The study of how materials and surface shape of kitchenware affect heat conduction, GCEAS, 2016.
- [10] C. Runge, *Z. Math. Phys.*, 56 (1908): 255.
- [11] R.D. Richtmyer and K.W. Morton, “Difference Method for Initial Value Problems”, John Wiley and Sons, 2<sup>nd</sup> Eds., New York, 1967.
- [12] L.F.Richardson, “The approximate arithmetical solution by finite element of physical problems involving differential equations, with an application to the stress in a masonry dam”, *Philos. Trans. Roy. Soc. London, ser. A*, 210 (1910): 307-357.
- [13] P.J. Roache, “Computational Fluid Dynamics”, (Hermosa, Albuquerque, NM), 1976.
- [14] M.J. Crochet, A.R. Davies and K. Walters, “Numerical Simulation of Non-Newtonian Flow”, Elsevier, London, 1984.
- [15] O.C. Zienkiewicz and Y.K. Cheung, “Finite Element in the Solution of Field Problems”, *The Engineer*, (1965): 507-510.
- [16] J.T. Oden, “Finite Element of Nonlinear Continua”, McGraw-Hill, New York, 1972.
- [17] A.J. Baker, “Finite Element Computational Fluid Dynamics”, McGraw-Hill Book company(UK) Limited, USA, 1985.



## Text Localization based on Multiple Features and Recognition Techniques

Teera Siriteerakul<sup>a\*</sup> and Sirikul Siriteerakul<sup>a</sup>

<sup>a</sup>Faculty of Science, King Mongkut's Institute of Technology Ladkrabang,  
Ladkrabang, Bangkok, Thailand

\*Corresponding Author: teera.si@kmitl.ac.th

### ABSTRACT

Identify text location in images is one of the fundamental tasks in image understanding. There are so many applications to this task such as traffic direction sign understanding for autonomous vehicle or people with limited vision. This paper combined two of the state of the art methods for text localization, Stroke Width Transform (SWT) and Maximally Stable Extremal Regions (MSER) by searching for connected neighboring pixels in image and color space.

**Keyword:** Text Localization, Maximally Stable Extremal Regions, Component-based Method, Stroke Width Transform.

### 1. Introduction

Although an image can worth a thousand words, sometime, a single sentence in an image can be crucial information that we want to identify. For example, it would be easy for us to travel to places, if we have a system which at identify and read the sign for location or direction. In order to understand text in image, first we have to identify its location (Karatzas et al, 2013). This paper proposes a method to correctly identify text location based on combination of the two state of the art methods, Stroke Width Transform (SWT) and Maximally Stable Extremal Regions (MSER).

### 2. Relevant Theories and Methods

Text localization is one of the popular field of research. There are two major approaches to this problem: region based approach and component based approach. The region based methods typically applies sliding windows to an image and try to identify if that window contains text information or not. The accuracy of this approach lies on the quality of the classification features extracted from the image (although it can be helped by Deep Learning). However, this approach can be slow since the size and the number of sliding windows in an image can be large.

On the other hand, the component based methods rely on identify components which are likely to be a part of text. This approach can group pixels together based on chromatic information as in Maximally Stable Extremal Regions (MSER) based

method (Forsen and Lowe, 2007) or characterize each pixel as belonging to a certain stroke width and group pixels with similar stroke width together as in Stroke Width Transform (SWT) based method (Epshtein et al, 2010). After identifying the components, these methods group them together according to text-like properties. Methods using this approach can be faster than those using region-based approach. However, the component detection can be effected severely by noise and local light.

### 3. Text Localization Framework

This paper couples two component-based methods to create an accurate text-detection framework. First, Maximally Stable Extremal Regions – MSER is a way to form a component based on similar chromatic information. Then, these components are group together if they become more likely to be a character. Matas et al. (2002) and Forsen and Lowe (2010) utilized this approach with good results. This approach has also adopted by Neumann and Matas (2015) with addition information such as base-line information to improve detection accuracy. We utilize MSER-based components finding with relaxing parameter to find candidate component with good recall.

Then, Stroke Width Transform – SWT (Epshtein et al, 2010) is performed to examine the stroke width of the candidate regions. The SWT is done by first detecting edges using Canny method (Canny, 1986). Then, stroke width is done by measuring distance between edge to edge in gradient direction. If the component is a text region, there must be enough pixel with similar stroke width. Our proposed framework can be summarized as in fig. 1.

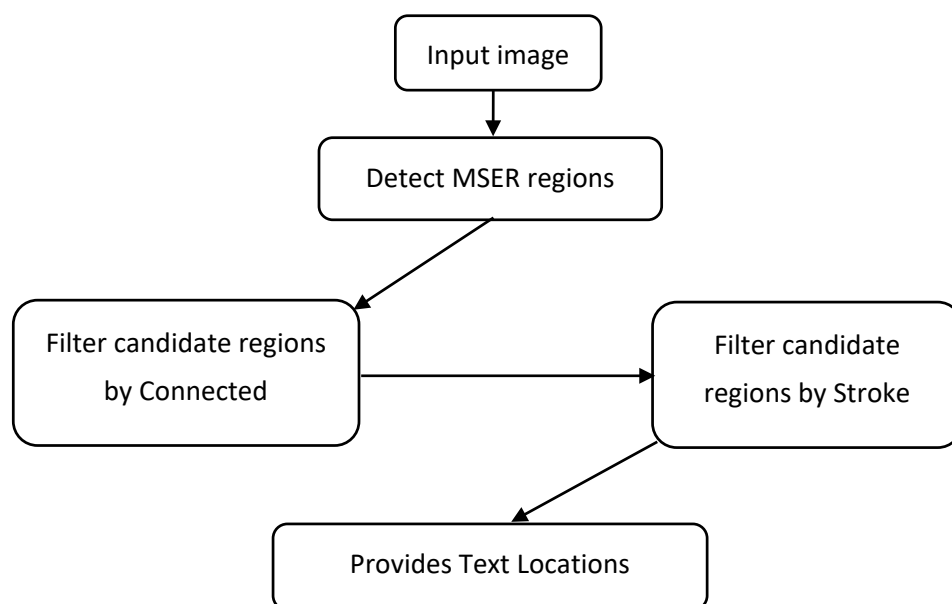


Fig. 1: Text detection framework

## 4. Experimental Setup and Results

This section describes experimental setup such as dataset and results with discussion.

### 4.1 Dataset

Images used for testing our proposed was taken from a competition, Text Location Detection Contest (BEST 2015), in Thailand from Benchmark for Enhancing the Standard for Thai language processing (BEST) organized by National Electronics and Computer Technology (NECTEC), Thailand. There are 29 images in the final round of the competition (see fig.2 for image examples). The images are taken from uncontrol natural scene. They vary in light, text size, color, font, and direction. The scenes also contain component which is similar to character which make the detection very challenging.



Fig.2: Example image from the testing dataset

### 4.2 Experimental Result

Results from testing our approach on 29 images are shown in table 1. The average of precision recall and F-score are 0.385, 0.655, and 0.436 accordingly. Our F-score is the second best in the BEST 2015 competition. The best F-score achieve by the winner was 0.713 which taken Deep Learning approach which require much higher computational power.

From table 1, our approach failed to detect text location in image 5 and 20 which resulted non-horizontal orientation of image 5 (Fig.3 left) where our system has not been prepared for. On the other hand, in image 20 (Fig.3 right), our system produced some error which result in fail to detect. Even though our system can detect the text fairly well.

In the other images, there are some of which that can be hard to identify which components are text. For example, images in Fig.4 contain components with similar stroke width within the component but are not text regions.

image	precision	recall	F-score	image	precision	recall	F-score
1	0.42	0.59	0.49	16	0.27	0.67	0.38
2	0.21	1.00	0.35	17	0.27	0.85	0.41
3	0.18	0.67	0.28	18	0.50	1.00	0.67
4	0.36	0.80	0.50	19	0.40	0.67	0.50
5	0.00	0.00	0.00	20	0.00	0.00	0.00
6	0.26	0.8	0.4	21	0.50	1.00	0.67
7	0.75	0.75	0.75	22	0.33	0.25	0.28
8	0.4	0.5	0.44	23	0.20	0.50	0.28
9	0.5	0.5	0.5	24	0.67	1.00	0.80
10	0.25	1.00	0.4	25	0.62	1.00	0.76
11	0.15	0.42	0.23	26	1.00	0.6	0.75
12	0.2	1.00	0.33	27	0.21	0.8	0.33
13	0.27	0.6	0.37	28	0.57	0.30	0.40
14	0.67	0.67	0.67	29	0.21	0.83	0.34
15	0.75	0.2	0.31	<b>Avg</b>	<b>0.38</b>	<b>0.65</b>	<b>0.43</b>

Table 1: Experimental result



Fig. 3: Images with fail detection result

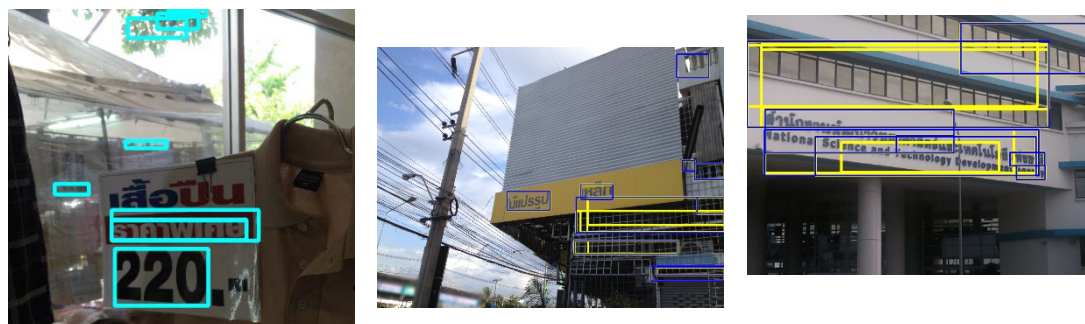


Fig. 4: Images with bad detection result

Images with good detection results are displayed in Fig. 5. The left image shows that our approach can detect text written on a transparent surface such as glass. The right images demonstrated that text can be detected even in a low contrast environment.

## 5. Conclusion

This paper demonstrates performance of a detection framework which combines MSER and SWT approach. The system can sufficiently localize text in images even in a transparent surface or a low contrast environment. However, the system can confuse region with similar stroke width with text region.

## REFERENCES

- Karatzas, D., Shafait, F., Uchida, S., Iwamura, M., Bigorda, L., Mestre, S., Mas, J., Mota, D., Almaz'an, J., and Heras, L. 2013. "ICDAR 2013 Robust Reading Competition." In Proceedings of ICDAR 2013 1115-1124
- Forssen, P. and Lowe, D. 2007. "Shape Descriptors for Maximally Stable Extremal Regions". In Proceeding of ICCV.
- Epshtein, B., Ofek, E., and Wexler, Y. 2010. "Detecting text in natural scenes with stroke width transform". In Proceedings of CVPR.
- Matas, J., Chum, O., Urban, M., and T. Pajdla. 2002. "Robust wide baseline stereo from maximally stable extremal regions." Proc. of British Machine Vision Conference, pages 384-396
- Neumann, L., & Matas, J. 2015. Efficient scene text localization and recognition with local character refinement. In Document Analysis and Recognition (ICDAR), 2015 13th International Conference on (pp. 746-750). IEEE.
- Canny, J. 1986, A Computational Approach to Edge Detection, IEEE Trans. Pattern Analysis and Machine Intelligence, 8(6):679-698.

## The Shift in Generations of Computing Platforms and the Impact on Information Technology Solutions

Mehdi Asgarkhani<sup>a\*</sup>, Eduardo Correia<sup>a</sup> and Bernard Otinpong<sup>a</sup>

<sup>a</sup>Department of Computing, Ara Institute of Canterbury

Christchurch, New Zealand

[\\*Mehdi.Asgarkhani@Ara.ac.nz](mailto:Mehdi.Asgarkhani@Ara.ac.nz)

### ABSTRACT

Information Technology (IT) has been recognised as a key business enabler. Throughout the last decade, IT alongside other technology and engineering solutions have transformed organisations and communities to make use of technology to revolutionise practices and services achieving significant productivity gains. This study examines the shift in generations of information technology platforms, solutions, and applications to identify the possible impact on both the nature of solutions and strategies for solution deployment. The preliminary results suggest that there are potentially significant shifts in platforms, infrastructure, solutions, the use of solutions, and deployment strategies.

**Keyword:** Generations of Computing Platforms, Information Technology Solutions, New Generation Information Technology, Cloud Services, SCADA, Internet of Things, Impact of New Generation Technologies.

### 1. Introduction

Since the establishment of the philosophy, practices, and standards of managing and deploying Information Technology solutions and Information Technology Governance (in the 1990s), the IT industry has undergone significant changes. Most of the changes experienced in the sector originate from rapid advancement of networking technologies, including mobile networks. The advancements have resulted in a significant shift in computing platforms, the use of IT in businesses and the social and economical of the impact of IT and engineering solutions. The shift in generations of technology platforms and solutions have also transformed how solutions are deployed and managed (Asgarkhani 2005, Asgarkhani 2013).

One of the most significant developments in the recent times has been advancements in technologies that support the practice of Cloud Computing. The advancements have resulted in increased uptake of Cloud Services resulting in a major paradigm shift in the management of applications and infrastructure of IT (Chinyao, Ychsueh & Mingchang 2011; Venkata, Reddy & Chandra 2012).



Moreover, rapid network technology advancements have made it possible to manage complex systems remotely via complex network solutions. For instance, Supervisory Control and Data Acquisition (SCADA) systems are deployed to manage critical systems (such as the electricity grid) remotely through complex networks (Asgarkhani & Sitnikova 2014; Nicholson, Webber, Dyer, Patel & Janicke 2012).

This paper examines the most significant changes in technology platforms and the impact on technology solutions and the management and deployment of technology solutions. The paper presents the work-in-progress results of the study. The study is based on an exploratory, descriptive approach. It is a qualitative study based on analysis of the literature on generations of technology platforms and solutions.

## **2. An Overview of Cloud Services**

In 1969, Leonard Kleinrock, one of the chief scientists of the original Advanced Research Projects Agency Network (ARPANET), said: “As of now, computer networks are still in their infancy, but as they grow up and become sophisticated, we will probably see the spread of computer utilities’ which, like present electric and telephone utilities, will service individual homes and offices across the country”. This vision of the computing utility based on the service provisioning model anticipates the massive transformation of the entire computing industry in the 21st century whereby computing services will be readily available on demand, like other utility services available in today’s society (Bhagyashree & Vaishali 2012; Buyya, Yeo & Venugopal 2008).

The term Cloud originated from a telecommunications term in the 1990s when service providers began using virtual private network (VPN) services for data communication (Buyya, Yeo & Venugopal 2008). VPNs maintained the same bandwidth as fixed networks with considerably less cost: these networks supported dynamic routing, which allowed for a balanced utilisation of the network and an increase in bandwidth efficiency, and led to the coining of the term telecom cloud. Cloud computing’s premise is very similar in that it provides a virtual computing environment that’s dynamically allocated to meet user needs. Cloud computing is defined as “ A model for enabling convenient, on-demand network access to a shared pool of configurable computing resources (e.g. networks, servers, storage, applications, and services) that can be rapidly provisioned and released with minimal management effort or service provider interaction”. The term Cloud Computing is a general term for IT solutions and services that involve delivering hosted services over the Internet (Jaimin, N. &



Shah, UA. 2012; Kaufman 2009). Cloud computing encompasses a range of services that can be hosted in a variety of approaches.

Typical services offered via Cloud are (Jaimin, N. & Shah, U. a. N. 2012; Mandala, Bhaskar & Marepalli 2012):

- Infrastructure-as-a-Service (IaaS) - Delivers computer infrastructure as a utility service, typically in a virtualized environment. Also, provides enormous potential for extensibility and scale.
- Platform-as-a-Service (PaaS) - Delivers a platform or solution stack on a cloud infrastructure. It also sits on a top of the IaaS architecture and integrates with development and middleware capabilities as well as database, messaging and queuing functions.
- Software-as-a-Service (SaaS) - Delivers the application over the Internet or Intranet via a cloud Infrastructure. It is built on underlying IaaS and PaaS Layer.

Cloud platforms such as Infrastructure as a Service, Platform as a Service and Software as a Service are dynamically built through virtualisation with provisioned hardware, software, networks, and datasets. Cloud Computing is comprised of virtual services being delivered through a virtualized environment. Cloud customers can access their data anywhere in the world on demand. For that reason, the Cloud is seen as a single point of access to the computing needs of its customers delivering a robust and readily available infrastructure (Jaimin and Shah 2012). Alongside providing effective solutions, Cloud Computing also introduces challenges and concerns. Some of these challenges impact on specific domains of ITG (for instance in the area of risk management). Cloud service delivery by companies offering Cloud solutions requires new standards and regulatory requirements (Ramgovind, Eloff & Smith 2015; Wen & Hsu 2012). New Zealand Institute of IT Professional (IITP) developed and put in place a set of regulatory requirements known as Cloud Code of Practice (<https://cloudcode.nz/>).

Adopting cloud solutions in organisations require governance models to ensure a secure cloud computing environment and to comply with all relevant organisational information technology policies. Some governance models have been developed to facilitate the adoption of cloud solutions. Governance of cloud solutions will need to be acknowledged and may impact on upon current ITG standards (Stieningera, Nedbala, Wetzlingera, Wagnera & Erskineb 2014; Luftman & Derksen 2012, Mandala, Bhaskar & Marepalli 2012).

### 3. SCADA Systems

Recent technological advancements have evolved the Internet into a complex global network that has resulted in both higher risks and new opportunities for network-based management of critical systems and infrastructures (Wen, Hsi & Hsu, Lydia 2012). Deployment of complex solutions implemented on global networks may benefit from review and changes in ITG standards and frameworks.

Critical systems such as Supervisory Control and Data Acquisition (SCADA) systems were originally designed to operate stand-alone. The advancements in networking technologies have made it possible to connect SCADA systems to networks via the Internet for more efficient communication of signals and information (Asgarkhani & Sitnikova 2014; Chinyao, Yahsueh & Mingchang 2011; Nicholson, Webber, Dyer, Patel & Janicke 2012).

SCADA systems are used to automate complex processes where human interference to collect data in assessing the overall performance of systems is not possible.

Alternatively, SCADA systems can be deployed to increase efficiencies significantly via automation of data gathering and transmission processes. Cases of SCADA in managing electricity generation and distribution or in managing water resources are examples of SCADA as strategic technology system with benefits that reach beyond an organisation or one community (Dickman 2011; NSW Government 2015; Vale, Morais & Faria 2010; WaterWorld 2011).

Traditionally, SCADA was seen as being a technical engineering tool to automate complex processes. However, soon it was realised that what SCADA systems achieve benefit not only engineers but also decision makers within organisations. In recent times, SCADA has moved from being an engineering solution to become as a key corporate system for management decision making (Asgarkhani & Sitnikova 2014; Chinyao, Yahsueh & Mingchang 2011; Luftman & Derksen 2012).

SCADA solutions are complex strategic solutions. They represent all characteristics of a typical IT solutions. However, they introduce significant differences from common IT solutions. More specifically, SCADA solutions deal with highly critical data (measurements by sensors) that play a vital role in automated decision making. SCADA is not only connected to the internal networks within the organisation but also to the Internet. Therefore, security management (governance) of SCADA should involve:

- a) the risk management domain of a typical standard ITG framework
- b) the specialist network security management frameworks

Some of the standards developed for managing risk and security in SCADA solutions could include (Von Solms 2005; Kaufman 2009; European Network and Security Agency 2012; Nicholson, Webber, Dyer, Patel & Janicke 2012):

- ISO27001 – This standard looks at the requirements for establishing, implementing, operating, monitoring, reviewing, maintaining and improving documented Information Security Management Systems (ISMS) within an organisation.
- PCIDSS - The Payment Card Industry Data Security Standard (PCIDSS) is an internally adopted standard defined by the Payment Card Industry Security Standards Council. It was created to help an organisation that process credit card transactions to prevent credit card fraud by implementing strict data controls.
- ISO27002:2007/ISO17799:2005 – ISO27001 was discussed earlier as an information security management standard. The ISO27002 series builds on the old ISO17799 standard which in turn built on the old British standard BS7799.
- ANSI/ISA-99.02.01-2009 - In 2008 NIST released a comprehensive guidance on securing SCADA systems in the special paper 800-82, Guide to Industrial Control Systems (ICS) Security. This document addresses issues ranging from an outline of SCADA systems, security program development and technical controls and network architecture.
- Generic SCADA Risk Management Framework for Australian Critical Infrastructure (ITSEAG).
- Critical Infrastructure Resilience Strategy (TISN).

#### **4. Internet of Things: An Overview**

Alongside major developments resulting in the new generation of technologies and solutions known as *Cloud Services* and *Remote Sensor and Data Acquisition systems*, we have been witnessing another development that has resulted from advancements in networking technologies. Internet of Things (IoT) is known as the interconnection of objects in day-to-day life equipped with sufficient intelligence to give objects the ability of presence anytime and anywhere (referred to as ubiquity). Consequently, IoT will enable the Internet to provide an environment where every object can interact (via embedded systems and a highly distributed network of devices) and communicate with human and other devices.

Rapid developments in underlying technologies, IoT is opening tremendous opportunities for applications that can potentially improve the quality of lives and a more effective management critical resources.

It should be noted that overall the literature does not indicate a universally agreed definition for IoT. In simple terms and to sum up, what was outlined above, IoT is the upcoming generation of the Internet where objects with sensors are connected to the Internet so they can gather, send and get data, facilitate smarter solutions. For instance, wearables are connected and enable us to send and receive data; vehicles get connected, home appliances, industrial assets, street lights, etc. (Source: i-Scoop). Figure 1 outlines the basic aspects of IoT.

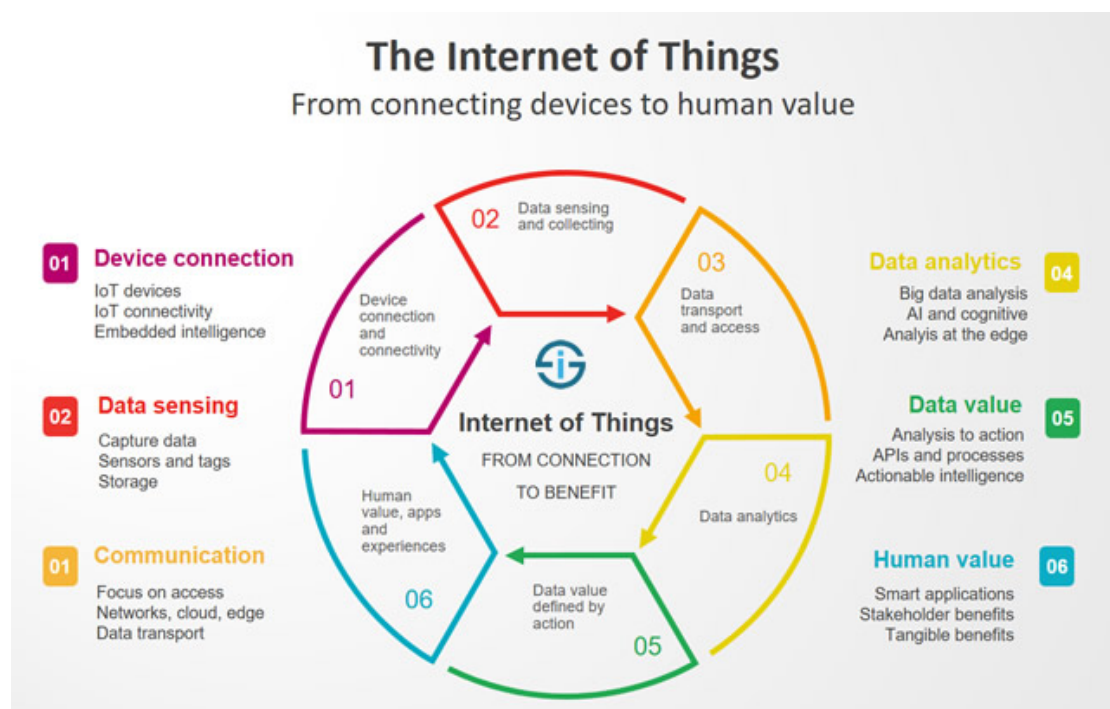


Figure 1. The Internet of Things (Source: i-Scoop)

### 5. Potential Implications of the New Generations of Technology Solutions

Previous sections outlined a broad overview of potential new generations of technology solutions. The emergence of cloud, Remote Sensory Solutions, and IoT have transformed the landscape of technology solutions.

The use of new generation of solutions heavily reliant on networking technology have implications on both solutions and the practices of solution deployment strategies. Preliminary results of the study identify some of the implications to be as follows.

- Increased volume of data stored and made available – The new technologies and related solutions make it possible for communities greater access to data than ever before. Similarly, companies can start taking advantage of increased availability of data to gain data-based insights to develop more effective methods of developing solutions and connecting with clients. At the same time, organisations face increased complexities and challenges of managing risks to security and privacy of information.
- Flexible hours of working or remote working – Increased use of networked solutions creates an opportunity for some organisations to rethink the concept of office and workspace. The concept of a physical space and a desk may no longer be the only method of conducting work. Employees can potentially work and be in communication from any location any time.
- Increased accessibility and timely access to information - the speed of access to information – Timely access to information through interconnected networks of devices will speed up the decision-making process.
- Increased efficiency and productivity – In addition to the speed of access to information, the new generation of solutions should make it possible to increase the number of tasks performed in a certain unit of time. The latest Cloud and IoT developments are likely to make it possible to accomplish tasks faster and with greater precision making use of more effective data analysis and data management solutions.
- Changed client expectations and needs – Increased access to more data is likely to change customer expectations. They are likely to expect more advanced solutions and faster (and easier) access to data.
- Changed skills and competency needs – Accessing, analysing and making sense of data in organisations to facilitate better decision making requires skills beyond traditional It skills. Employees need skills in IoT and Cloud technologies and skilled workers in integrating IoT devices into current procedures and data analysis.

## 6. Conclusion

Computing platforms have undergone major developments throughout the last two decades. Technology platforms have evolved from centralised computing and storage to large data centres, commodity hardware and portable devices.

Alongside changes in platforms, advances in networking technologies have made it possible for new generations of computing and IT Solutions (such as Cloud Services, IoT, and other remote sensors and control technologies) transforming how technology is deployed and used in organisations.

The preliminary findings of the study indicated that the change in computing platforms is likely to impact on various aspects of day to day use of It in communities

and organisations. Some of the implications included:

- Increased availability of large volumes of data
- Flexible hours of working or remote working
- Increased accessibility and timely access to information
- Increased efficiency and productivity
- Changed client expectations and needs
- Changed skills and competency needs
- The need for new management of data including risk and security management

## REFERENCES

- Asgarkhani, M 2005, 'Digital government and its effectiveness in public management reform: A local government perspective', *Public Management Review*, vol. 7, no. 3, pp. 465-87.
- Asgarkhani, M 2012, 'The effectiveness of E-service in local government: A case study', in F Bannister (ed.), *Case Studies in E-Government*, Academic Publishing International Ltd., pp. 22-41.
- Asgarkhani, M 2013, 'Corporate ICT Governance: A Tool for ICT Best Practice', in *International Conference on Management, Leadership and Governance*, ACL, Bangkok, pp. 1-8.
- Asgarkhani, M & Sitnikova, E 2014, 'Developing a Strategic Framework for Managing Security in SCADA Systems', *Journal of Information Warfare*, vol. 13, no. 4, pp. 70-84.
- Bhagyashree, A & Vaishali, B 2012, 'Data Mining in Cloud Computing', [faratarjome.ir](http://faratarjome.ir), viewed 4 8, <[http://faratarjome.ir/u/media/shopping\\_files/store-EN-1428394761-6932.pdf](http://faratarjome.ir/u/media/shopping_files/store-EN-1428394761-6932.pdf)>.
- Buyya, R, Yeo, CS & Venugopal, S 2008, 'Market-Oriented Cloud Computing: Vision, Hype, and Reality for Delivering IT Services as Computing Utilities', *International Conference on High-Performance Computing and Communications*, 2008., pp. 5-13, <<http://arxiv.org/ftp/arxiv/papers/0808/0808.3558.pdf>>.
- Chinyao, L, Yahsueh, C & Mingchang, W 2011, 'Understanding the Determinants of Cloud Computing Adoption', [www.seu.ac.lk](http://www.seu.ac.lk), viewed May 4, <<http://www.seu.ac.lk/students/freedownload/Understanding%20the%20determinants%20of%20cloud%20computing%20adoption.pdf>>.
- Dickman, F 2011, 'SCADA security for municipal water', <<https://www.phoenixcontact-cybersecurity.com/data/downloads/success-stories/united-water-scada-security-municipal-water.pdf>>.
- European Network and Security Agency 2012, 'Shortlisting network and information security standards and good practices', <<https://resilience.enisa.europa.eu/article->

13/shortlist-of-networks-and-information-security-standards>.

- Jaimin, N & Shah, UA 2012, 'Cloud Computing for Business', citeseerx.ist.psu.edu, viewed April, <<http://citeseerx.ist.psu.edu/viewdoc/download?doi=10.1.1.417.444&rep=rep1&type=pdf>>.
- Kaufman, L 2009, 'Data Security in the World of Cloud Computing', viewed August, <<file:///C:/Users/Andrea/Downloads/NDU-2.pdf>>.
- Luftman, J & Derksen, B 2012, 'Key issues for IT executives 2012: Doing more with less', MIS Quarterly Executive, vol. 11, no. 4, pp. 207-18.
- Mandala, V, Bhaskar, R & Marepalli, C 2012, 'Cloud Computing Organisational Benefits A Managerial Concern', www.bth.se, viewed January, <[http://www.bth.se/fou/cuppsats.nsf/all/ad7847243c12eb23c1257aba004e8a24/\\$file/BTH2012BhaskarReddy.pdf](http://www.bth.se/fou/cuppsats.nsf/all/ad7847243c12eb23c1257aba004e8a24/$file/BTH2012BhaskarReddy.pdf)>.
- NSW Government 2015, 'ISMAART: Integrated surveillance, monitoring, automation and remote telemetry', <<http://www.waternsw.com.au/projects/efficiency/ismart>>.
- Nicholson, A, Webber, S, Dyer, S, Patel, T & Janicke, H 2012, 'SCADA security in the light of Cyber-Warfare', Journal of Computers & Security, vol. 31, no. 1, pp. 418-36.
- Ramgovind, S, Eloff, M & Smith, E 2015, 'The Management of Cloud Security in Cloud Computing', uir.unisa.ac.za, viewed August 16, <<http://uir.unisa.ac.za/xmlui/bitstream/handle/10500/3883/ramgovind.pdf?sequence=1>>.
- Stieningera, M, Nedbala, D, Wetzlingera, W, Wagnera, G & Erskine, MA 2014, 'Impacts on the organisational adoption of cloud computing: A reconceptualization of influencing factors', in 2014 Conference on ENTERprise Information Systems, ELSEVIER, USA, pp. 85-93.
- Vale, Z, Morais, H & Faria, P 2010, 'Distributed energy resources management with cyber-physical SCADA in the context of future smart grids', in 2010 15th IEEE Mediterranean Electrotechnical Conference, <http://ieeexplore.ieee.org/document/5476239/>>.
- Von Solms, B 2005, 'Information security governance: COBIT or ISO 17799 or both?', Computers & Security, vol. 24, no. 2, pp. 99-104.
- Venkata, M, Reddy, B & Chandra, M 2012, 'Cloud Computing Organisational Benefits A Managerial Concern', www.bth.se, viewed January, <[http://www.bth.se/fou/cuppsats.nsf/all/ad7847243c12eb23c1257aba004e8a24/\\$file/BTH2012BhaskarReddy.pdf](http://www.bth.se/fou/cuppsats.nsf/all/ad7847243c12eb23c1257aba004e8a24/$file/BTH2012BhaskarReddy.pdf)>.
- WaterWorld 2011, SCADA system monitors water transport, distribution, treatment, <<http://www.waterworld.com/articles/print/volume-27/issue-8.html>>.



Wen, H & Hsu, L 2012, Conceptual Framework of Cloud Computing Governance Model- An Educational Perspective, 16 October 2015, <<http://itee-edsoccom.com/index.php/itee/article/viewFile/240/225>>.

## Co-doping effect on structural, morphological and optical properties of ZnO thin films

Ahmed MAACHE<sup>a</sup> and Mokhtar BOUDISSA<sup>a\*</sup>

<sup>a</sup>ENMC Laboratory, F. ABBAS SETIF-1 University,  
SETIF, Algeria

\*Corresponding Author: boudi44@yahoo.fr

### ABSTRACT

Thin pure ZnO films, Lanthanum doped La (3%), and Lanthanum-lithium co-doped La (3%) - Li (1-3-5-10-%) were successfully prepared by dip coating method. The effect of lithium atom as an element of co-doping was investigated. X-ray diffraction (XRD) has shown that all films were highly *c*-axis oriented, with hexagonal wurtzite structure. Due to the reduced ionic radius of Li (0.68Å<sup>o</sup>) compared to those of Zn (0.74Å<sup>o</sup>) and La (1.16Å<sup>o</sup>), Li ions had been easily incorporated in the ZnO matrix and may be the responsible for tensile stress in the lattice, which increases with the rate of Li. The estimated crystallite size of the samples decreased from pure ZnO to La 3% - Li 1% co-doped samples, then increases linearly with the increase of Li concentration. The UV-VIS-NIR spectroscopy showed over 90% transmission for all samples and the energy gap was enhanced with Li co-doping percentage of 5%Li.

**Keyword:** ZnO, co-doping, Lanthanum, Lithium, X-ray diffraction, UV-VIS-NIR.

### 1. Introduction

Zinc oxide, (ZnO), a typical n-type compound semiconductor with its wide and direct band gap (3.37 eV) in the near-UV spectral region, its high exciton binding energy (60 meV), crystallizes according to hexagonal wurtzite crystal structure. ZnO thin films are polycrystalline, with a strong *c*-axis (002) oriented perpendicular to the surface, are used in various applications such as optical and magnetic memory devices, light emitting diodes, solar cells... Doping ZnO thin films with the proper elements can enhance their properties. Different methods to obtain doped ZnO materials have been studied. The incorporation of rare- earth elements such as La make efficient donors for producing an *n*-type ZnO material with low resistivity but substitution creates a charge imbalance, as La<sup>3+</sup> ions substitutes the Zn<sup>2+</sup> sites in the ZnO. La serves as an electron donating group to ZnO. The charge compensation from the local defect sites results in lattice deformation, thus it is necessary to provide a charge compensating material such as, Li for the formation of a stable compound. Lithium may behave both as a donor and as an acceptor in ZnO. when lithium occupies an

interstitial position in the ZnO matrix. Indeed, due to its small ionic radius Li can easily occupy interstitial positions; in that case, the donor behavior of Li arises when lithium substitutes on a Zn site it acts as donor [1-6; 12].

In this paper, pure; La doped and lithium-Lanthanum co-doped ZnO films have been deposited by sol gel technique at low temperature. We mainly studied effects of Li and La co doping on structural and optical properties of the ZnO films.

## 2. Experimental details

### 2.1. Films preparation

In this experiment, zinc acetate dihydrate ( $\text{Zn}(\text{CH}_3\text{COO})_2 \cdot 2\text{H}_2\text{O}$ , Merck, N99.5%) and lanthanum nitrate hexahydrate ( $\text{La}(\text{NO}_3)_3 \cdot 6\text{H}_2\text{O}$ , Merck, N99.00%) are used as starting material and dopant sources, respectively. Moreover, absolute ethanol ( $\text{C}_2\text{H}_5\text{OH}$ , Merck, N 99.9%) and monoethanolamine (MEA) ( $\text{C}_2\text{H}_7\text{NO}$ , Merck, N99.8%) are used as solvent and stabilizer, respectively. In a typical preparation procedure, for La-ZnO thin films, Zinc acetate dihydrate is first dissolved in a mixture which was composed of ethanol and MEA at 60 °C. The molar ratio of MEA to zinc acetate dihydrate maintained at 1.0 and the concentration of zinc acetate was 0.6 mol/L. The mixed solution was stirred at 60 °C for 1 h and, then, ethanolic solutions of lanthanum nitrate hexahydrate with optimized [ La/Zn; Li/Zn] ratio at [3% ;0-1-3-5-10%] was added to it. The final solution was stirred for an additional two hours. After stirring, the solution became clear and homogeneous and was used as the coating solution after cooling to room temperature and allowed to age for 24 h before initiating deposition. The films were obtained by a dip-coating procedure. The deposition process was performed by dipping cleaned microscope slide glass into the prepared solution for 60 s, and pulling them out at a rate of 12 mm/s. After the coating step, the films were dried at 225 °C for 10 min. Then, they finally were annealed at 550 °C in air for 1 h.

### 2.2 Characterization techniques

The structural studies were performed using an X-ray diffractometer (XRD; PANalytical with Cu  $K\alpha$  radiation, 40 kV, 30mA). The optical properties were studied using an UV-VIS-NIR Spectrophotometer (Varian 5000).

## 3. Results and discussion

### 3.1 Structural analysis

For comparison of the structural quality of undoped and La doped and Li-La co-doped ZnO films on glass substrate, XRD measurements were taken from 5° to 90° with a

0.050° step size.

It can be seen from the DRX spectra pattern on figure 1, that two peaks at  $\theta = 34^\circ$  and  $\theta \simeq 63^\circ$  appeared in both Li and La-doped and pure ZnO samples, assigned to (002) and (103) reflection of hexagonal wurtzite ZnO structure respectively (JCPDS card no.89-0510) [9]. No extra peaks of lanthanum oxide or other materials were observed, which reveals that there is no detectable additional phase present in the samples. This suggests that the rare earth ions have been incorporated in the  $Zn^{2+}$  sites of the ZnO lattice. The (002) peak is much more intense than the other peaks which indicates that all films have a preferential growth with the c-axis perpendicular to the film plan.

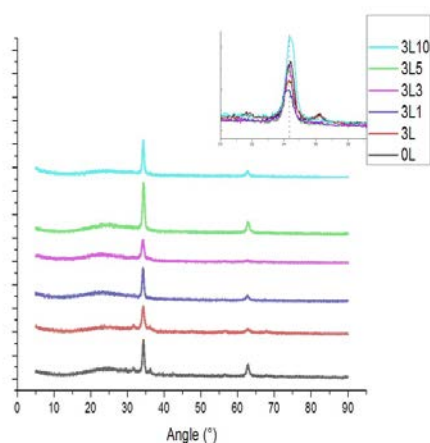


**Figure 1.** XRD patterns of undoped and Li-La co-doped ZnO films with doping concentrations

- (a) Undoped ZnO films (0L); (b) 3 mol%-La(3L); (c) 3 mol%La -1 mol% Li(3L1); (d) 3 mol% La -3 mol% Li(3L3); (e) 3 mol% La- 5 mol% Li(3L5); (f) 3 mol% La- 10 mol% Li(3L10).

Compared to pure ZnO, as shown in the inset of Figure 1, there is a slight shift of the (002) peak, into lower position ( $34,4269^\circ$  to  $34,2289^\circ$ ) for 3% La doping, but slight shift into higher position will appear with respect to Li co-doping for main diffraction peaks and reaches the maximum value at 5% Li content (table1). This lead to dramatic intensity decrease of (002) peak for 3% La doping, this intensity gradually improves and reaches the highest value at 5% Li doping.

On table 1, we have reported, for different  $2\theta(002)$ , the calculated values of the full width at half-maximum (FWHM), the lattice constants c and a, the crystallite grain

size  $G$ , the in-plane stress  $\sigma$ , the Zn–O bond length of ZnO thin films,  $L(A^\circ)$

The interplanar distances of the diffracting planes  $d$  were identified using the Bragg equation:

$$n\lambda = 2d \sin \theta,$$

Where  $n$  is the order of the diffracted beam,  $\lambda$  is the wavelength of the X-ray and  $\theta$  is the angle between the incoming X-ray and the normal of the diffracting planes. The grain sizes of the crystallites were determined from X-ray diffraction data. The crystallite grain size  $G$  can be estimated using the Scherrer Formula [7]:

$$G = \frac{0.9\lambda}{\beta \cos\theta} \quad (1)$$

The lattice constants  $c$  and  $a$ , for ZnO films are estimated for  $2\theta(002)$  orientation, by using the following relation [8]:

$$c = \frac{\lambda}{\sin\theta} \quad (2)$$

$$a = \sqrt{\frac{1}{3} \frac{\lambda}{\sin\theta}} \quad (3)$$

The volume of the unit cell ( $V$ ) of the hexagonal ZnO, the internal parameter ( $u$ ) and the Zn–O bond length ( $L$ ) are determined using the following equations [12]:

$$\begin{cases} V = \frac{\sqrt{3}}{2} a^2 c \dots\dots\dots (5) \\ u = \left(\frac{1}{3}\right) \left(\frac{a^2}{c^2}\right) + \frac{1}{4} \dots\dots\dots (6) \\ L = \sqrt{\left(\frac{a^2}{3} + \left(\frac{1}{2} - u\right)^2 c^2\right)} \dots (7) \end{cases}$$

For hexagonal crystals with a highly c-axis preferred orientation, the in-plane stress of

the films can be calculated using the biaxial stress–strain model [10]:

$$\sigma = 4.5 \times 10^{11} \frac{c_0 - c}{c_0} N/m^2 \quad (4)$$

where  $c_0$  is the corresponding value for bulk ZnO (5.2054Å).

**Table 1:** Values of  $2\theta(002)$ , full width half-maximum (FWHM), The lattice constants  $c$  and  $a$  for The crystallite grain size  $G$ , the in-plane stress  $\sigma$  the Zn–O the Zn–O bond length of ZnO thin films,  $L(A^\circ)$ .

	$2\theta(002)$ ( $^\circ$ )	FWHM(002) ( $^\circ$ )	$a$ ( $A^\circ$ )	$C$ ( $A^\circ$ )	$G$ (nm)	$\sigma$ ( $N/m^2$ )* $10^9$	$L(A^\circ)$
Pure	34,4269	0,5412	3,2461	5,2039	25,268	0,1297	1,9759
3L	34,2289	0,246	3,2576	5,2331	15,451	-2,3946	1,8808
3L1	34,4154	0,4428	3,2699	5,2056	15,8535	-0,0173	1,8879
3L3	34,4217	0,1968	3,2685	5,2046	25,009	0,0692	1,8871
3L5	34,5800	0,1476	3,2894	5,1815	33,038	2,0661	1,8991
3L10	34,4153	0,3936	3,2522	5,2056	16,941	-0,0173	1,8776

From table, we have plotted the evolution of  $2\theta$  and FWHM for all samples (figure 2-a) (undoped and doped thin films) and the grain size evolution with doping rate (figure 2-b). The FWHM decreases at first from undoped ZnO (0%La) to (3.0%La), then increases for 1%Li doping, then decreases swiftly again with the incorporation of Li atoms into the ZnO host matrix, till 5.0% Li doping. The grain size estimated by using the Scherrer formula, decreases gradually from 25,268 nm to 15,451 for (3.0%La), then increases gradually to 33,038 nm for for 5.0% Li doping. For 10.0% Li doping, we observe a dramatic change: crystallinity is destroyed: The incorporation of Li atoms into the ZnO host matrix results in better crystal quality for the Li+ doping till the limit of 5%Li. For 10%Li, there a saturation phenomena. In higher doping levels, the excess Li atoms occupy the interstitial sites and lead to the formation of electrically inactive LiZn–Lii pairs leading to reduced crystallinity [1-2].

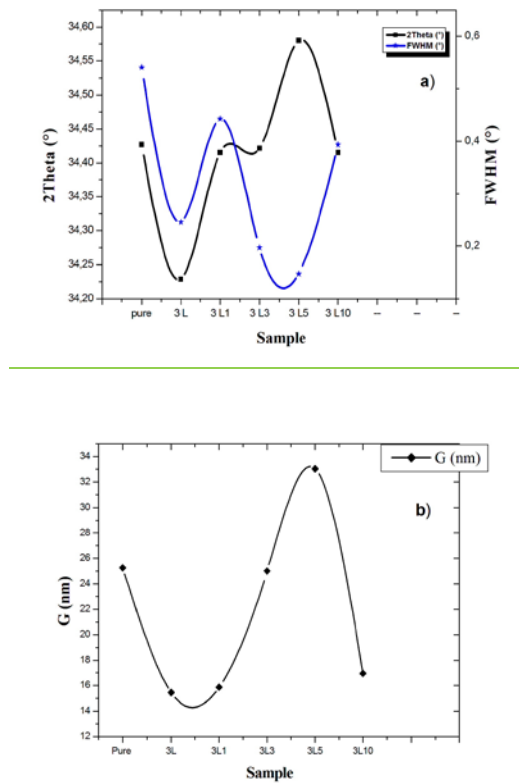


**Figure 2.** a)-2θ vs FWHM for undoped and doped thin films.  
 b)- grain size evolution with doping rate

From table 1, we have plotted the evolution stress values and lattice parameter  $c$ , figure 3, for undoped and co-doped thin films. We observe that the crystallites change state from compressive for 3%La doping to tensile with increase of Li doping level of 5.0% Li doping. the lattice parameters ( $c$ ) consequently diminishes: it decreases to  $5,1815\text{\AA}$  for 5% Li content as shown in Table 1. This reduction indicates an amelioration of the quality of cristallinity [11]. For 10% Li co-doping, here too we observe the saturation phenomena: the atoms in excess occupy Zn interstitial positions and the effect of La doping is annihilated [10].

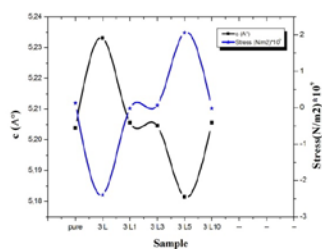


**Figure 3.** stress values vs  $c$  lattice parameter for undoped and doped thin films.



On figure 1, we have plotted, from table 1, the evolution of the bond length Zn-O, L, and a/c ratio. We observe a decrease of L with La doping; this is in accord with the increase of compressive stress for 3%La doping; then L reaches higher values when co-doping with  $\text{Li}^+$ . This Zn-O bond stretching may be attributed to the difference in ionic radii of  $\text{Li}^+$ ,  $\text{Zn}^{2+}$  and  $\text{La}^{+2}$  atoms. With the concentration of Li further increasing, Li ions entered into the grain boundaries destroying cristallinity.

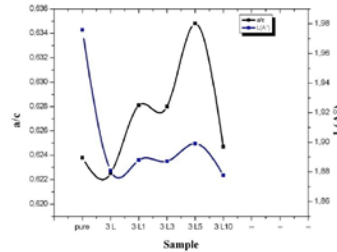


**Figure 4.** Evolution a/c ratio and bond length of ZnO thin films with La-Li doping

## 3.2 Optical properties

### 3.2.1 Transmittance spectra

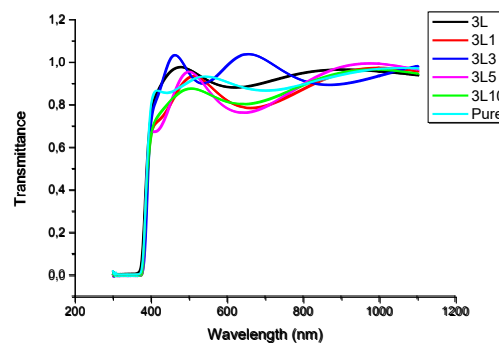


**Figure 5.** The transmittance spectrum of undoped and La doped ZnO thin films

On figure 5, are reported the transmittance spectra of undoped and La doped ZnO thin films. The spectra show a high transmittance of all thin films, higher than 90% except for pure ZnO and 3L10 samples. This phenomenon can be attributed to less scattering effects, structural homogeneity and an improvement of the crystalline state for doping of Li less than 5% (3L5). Besides, the presence of the interference phenomenon indicates a smooth and homogeneous surface of all observed films. An increase of The transmittance had also been observed when the crystallite size is smaller due to decreased optical scattering [13]. With the concentration further

increasing, to saturation, the doping Li ions may occupy interstitial sites and even entered into the grain boundaries, inducing scattering centers increase by enhancement in roughness of surface morphology resulting in reduction of transmittance [10].

### 3.2.2 Band gap energy calculation

In order to estimate the optical band gaps of the films, the first derivative of the optical transmittance is calculated. The curves of  $(dT/d\lambda)$ , vs.  $(E = \frac{hc}{\lambda})$  were plotted as shown in Figure 6. The Optical band gaps can be obtained through the maximum photon energy [14]. These values are reported on table 2 and plotted on figure 7.

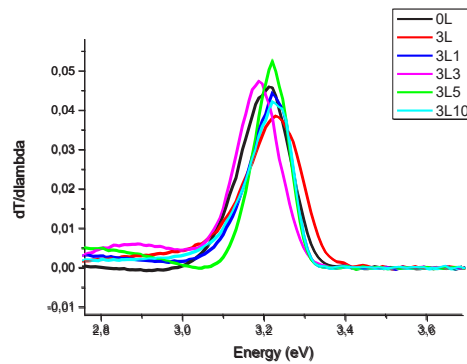


Figure 6. Plot of the derivate of transmittance with respect to energy.

Table 2 Values of optical optical band gaps deduced from measurements

	Pure	3L	3L1	3L3	3L5	3L10
<b>Eg (eV)</b>	3,21	3,23	3,22	3,19	3,22	3,22

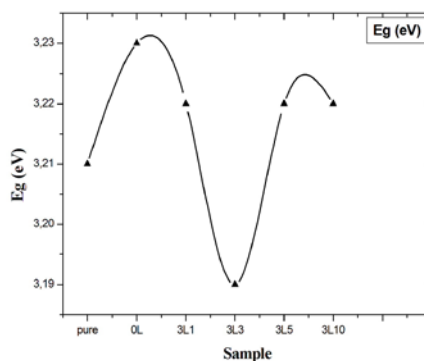


Figure 7. Evolution of optical band gaps with La-Li doping

The measured optical band gap values increased from 3.21 eV (0%La) to 3.23 eV (3.0%La), which explained that it can be attributed to the band gap broadening phenomenon described by Burstein and Moss [15,16], which states that the increase in the Fermi level in the conduction band leads to the band gap energy broadening as a result of increase in carrier concentration; then decreased to 3.22 eV with Li codoping. The band gap broadening occurring with the increase of La concentration from 0 to 3 at.% was mainly related to the shrinkage of the average particle size (from 25,268 nm to 15,451 nm) and the obvious decrease in the  $E_g$  value may be due to the increase in defects such as the oxygen vacancies [17].

#### 4. Conclusion

Thin pure ZnO films, Lanthanum doped La (3%), and Lanthanum-lithium co-doped La (3%) - Li (1-3-5-10-%) were successfully prepared by dip coating method.

-The effect of lithium atom as an element of co-doping was investigated. X-ray diffraction (XRD) has shown that all films were highly c-axis oriented, with hexagonal wurtzite structure.

-Li ions had been easily incorporated in the ZnO matrix and may be the responsible for tensile stress in the lattice, which increases with the rate of Li.

-The estimated crystallite size of the samples decreased from pure ZnO to La 3% - Li 1% co-doped samples, then increases linearly with the increase of Li concentration.

-For 10%Li doping there is a saturation phenomena. In higher doping levels, the excess Li atoms occupy the interstitial sites leading to reduced crystallinity

-We observe a decrease of Zn-O bond length,  $L$ , with La doping, for 3%La doping.  $L$  reaches higher values when co-doping with  $Li^+$ .

-The UV-VIS-NIR spectroscopy showed over 90% transmission for all samples and the energy gap was enhanced with Li co-doping percentage. The measured optical band gap values increased from 3.21 eV (0%La) to 3.23 eV (3.0%La), then decreases with Li Co-doping.

#### REFERENCES

1. Anderson Janotti and Chris G Van de Walle, Fundamentals of zinc oxide as a semiconductor, Rep. Prog. Phys. 72 (2009) 126501 (29pp)
- 2.- OlegMaksimov, RECENT ADVANCES AND NOVEL APPROACHES OF P-TYPE DOPING OF ZINC OXIDE, Rev.Adv.Mater.Sci. 24(2010) 26-34
3. D. SRIDEVI, K. V. RAJENDRAN, Enhanced optical properties La doped ZnO nanoparticles, OPTOELECTRONICS AND ADVANCED MATERIALS – RAPID COMMUNICATIONS Vol. 4, No. 10, October 2010, p. 1591 – 1593

4. Li-Wei Sun, Han-Qiao Shi, Wan-Nan Li, Hong-Mei Xiao , Shao-Yun Fu, Xing-Zhong, Cao and Zhuo-Xin Li Lanthanum-doped ZnO quantum dots with greatly enhanced fluorescent quantum yield, Electronic Supplementary Material (ESI) for Journal of Materials Chemistry, This journal is © The Royal Society of Chemistry 2012
5. Y. J. Zeng, Z. Z. Ye, W. Z. Xu, D. Y. Li, J. G. Lu, L. P. Zhu, and B. H. Zhao, Dopant source choice for formation of *p*-type ZnO: Li acceptor, APPLIED PHYSICS LETTERS 88, 062107 (2006)
6. C. Rauch, W. Gehlhoff, M. R. Wagner, E. Malguth, G. Callsen, R. Kirste, B. Salameh, A. Hoffmann, S. Polarz, Y. Aksu, and M. Driess, Lithium related deep and shallow acceptors in Li-doped ZnO nanocrystals, JOURNAL OF APPLIED PHYSICS 107, 024311 (2010)
7. K.N. Harish, H.S. Bhojya Naik, P.N. Prashanthkumar, R. Viswanath, ACS Sustain. Chem. Eng. 1, 1143 (2013).
8. C. Amutha, A. Dhanalakshmi, B. Lawrence, K. Kulathuraan, V. Ramadas, B. Natarajan, Progress in Nanotechnology and Nanomaterials, Jan. 2014, Vol. 3 Iss. 1, PP. 13-18.
9. Mohamed Shaban a, A.M.ElSayed. Materials Science in Semiconductor Processing. 41(2016) 323–334.
10. Olfa Bechambi, Azza Touati, Sami Sayadi, Wahiba Najjar. Materials Science in Semiconductor Processing 39 (2015) 807–816.
11. Yuan-Hua Lin, Jingnan Cai, and Ce-Wen Nan, Journal Of Applied Physics 99, 056107 (2006).
12. J.A.Mary, J.J.Vijaya, J.H.Dai, M.Bououdina, L.J.Kennedy, Y.Song, Mater.Sci.Semicond. Process. 34(2015) 27–38
13. Mohd Firdaus Malek, Mohamad Hafiz Mamat , Mohd Zainizan Sahdan, Musa Mohamed Zahidi, Zuraida Khusaimi, Mohamad Rusop Mahmood, Thin Solid Films 527 (2013) 102–109.
14. S.A. Kamaruddin, K.Y. Chan, H.K. Yow, M.Z. Sahdan, H. Saim, D. Knipp, Applied Physics A 104 (2011) 263.
15. E. Burstein, Phys. Rev. 93, 632 (1954); T.S. Moss, Proc. Phys. Soc. London Sect. B 67, 775 (1954).
16. T.S. Moss, Proc. Phys. Soc. Lond. Sect. B 67, 775 (1954).
17. Sumetha Suwanboona, Pongsaton Amornpitoksuk, Phuwadol Bangrak, Nantakan Muensit, Ceramics International 39 (2013) 5597–5608

## Spatial Relationship Between Hydro Oceanography Parameters And Phytoplankton Potentially Habs In Bali Strait

Endang Yuli Herawati <sup>1\*</sup>, Mohammad Mahmudi <sup>1</sup>, Fani Fariedah <sup>1</sup>, Ruly Isfatul Khasanah<sup>2</sup>

<sup>1</sup> Faculty of Fisheries and Marine Sciences, Universitas Brawijaya. Jl. Veteran, 65145. Telp./ Fax. 0341-553512, Malang - Indonesia  
Email: eyulih@yahoo.co.id

<sup>2</sup> Post Graduate Program of Fisheries and Marine Sciences - Faculty of Fisheries and Marine Sciences, Universitas Brawijaya. Jl. Veteran, 65145. Telp./ Fax. 0341-553512, Malang - Indonesia

### Abstract

Harmful Alga Blooming (HABs) has a negative impact in ecological, economic, and health. Many cases occurred vary by environmental factors or species adaptability. The research conducted in January 2017 aims to find out the relationship between hydro oceanography parameter and the presence of potentially HABs phytoplankton in Bali Straits. There were five sampling locations and hydro oceanography parameter measurement was conducted in each locations. Samples were taken from two different water layers, which were the surface layer and in the depth under metalimnion layer. Hydro oceanography parameter including temperature, brightness, current, pH, salinity, dissolved oxygen (DO), BOD, ammonia, nitrate and phosphate, and plankton. The analysis method used was statistic correlation to find out the relationship between hydro oceanography parameter spatially with the structure of phytoplankton which potentially HAB. From 23 identified genera, there were 8 genera (2%) which potentially causing HABs, they were *Ceratium fusus*, *Ceratium macroceros*, *Ceratium pulchellum*, *Dinophysis acuminata*, *Gonyaulax polygramma*, *Gonyaulax triacantha*, *Noctiluca scintillans*, *Protocentrum sp*, *Chaetoceros compressus*, *Chaetoceros lacinosus* and *Nitzschia closterium*. Species *Nitzschia closterium* was found in all station and had the highest total abundance of all stations, which was 17,892 cells/liter (46.20%). The statistical test result showed that the temperature and DO of the water has a significant positive correlation with abundance, diversity index and uniformity of HAB phytoplankton in Bali Strait.

**Key word:** Spatial, HABs, Phytoplankton, Hydro Oceanography, Bali Strait

### INTRODUCTION

The coastal area of Bali Strait, especially the area of Muncar, has many industrial activities, including fish processing industries and fishing ports. Disposal of fish processing industrial waste and fishing ports increase nutrients in the water such as nitrate and phosphate. Nutrients concentration of nitrate and phosphate in coastal water in Muncar was reported 1.6 mg/L and 1.5 mg/L (Choirun, 2014). The value was far beyond the required standard of sea water quality by the government in Ministry of Environment Decree number 51 the year 2004.

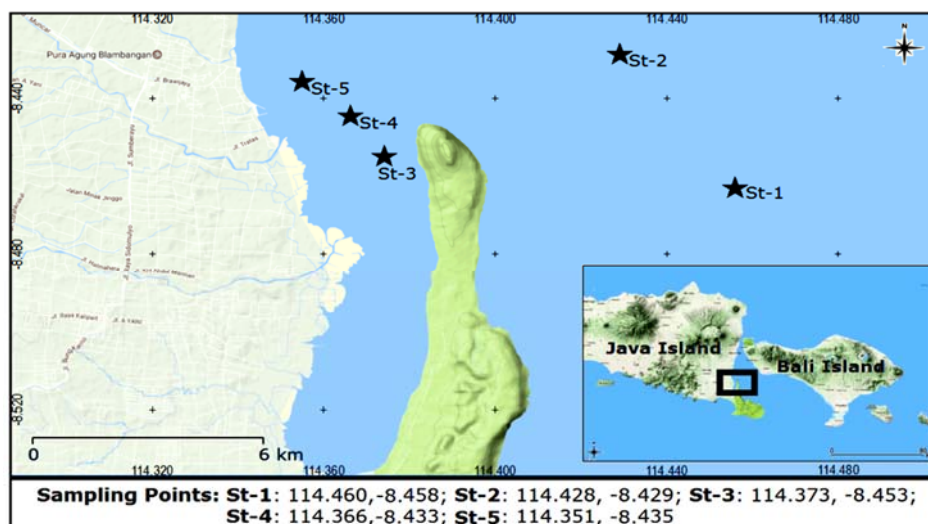
Effendi (2003) mentioned that nitrate was the most dominant nitrogen compound in the natural water and was very important for plant and algae growth. This compound

was a result from a complete oxidation process of nitrogen in the water. Beside nitrate, abundant phosphate in the water environment gives the positive impact that is an increase in production of phytoplankton and fish production. However, abundant phosphate could also cause a negative impact in high concentration, which is a population blooming of toxic phytoplankton known as Harmful Algae Bloom (HAB). The effect of HAB event is the decreasing of the oxygen level in the water that may cause a mass death of water biota (Risamasu and Prayitno, 2011). A decreasing in phytoplankton abundance was very much influenced by eutrophication process. The water with high numbers of nutrients was also caused by oceanography factors, such as upwelling process (Anderson *et al.*, 2008). The phytoplankton group which has the potential of blooming was Dinoflagellate, such as *Alexandrium spp.*, *Gymnodinium spp.*, *Dinophysis spp.*, and from Diatom group like *Pseudonitzschia spp.* (Aunorohim, 2009).

The high potential of fisheries in the coastal water of Muncar needs more studies and further research to identify the potential of HAB phytoplankton. It is also supported by the condition of coastal water that receives anthropogenic waste which increases the nutrients in that water. This research aimed to know the relationship between the characteristics of hydro oceanography parameters with the presence of phytoplankton potentially HAB in Bali Strait. This study was also covering the abundance and community structures aspect of phytoplankton with HAB in this area which aimed to provide quantitative data of phytoplankton with HAB compared to phytoplankton without HAB, and their relationship with environmental factors as an effort to generally evaluate the environment condition in the coastal water of Bali Strait.

## RESEARCH METHOD

The research was conducted in January 2017 during west monsoon season. The phytoplankton samples were taken in Bali Strait. There were five sampling locations, and hydro oceanography parameter measurement was performed in each location. Samples were taken from two different layers, which were water surface layer and in the depth under metalimnion layer. Hydro oceanography parameter measured include temperature, brightness, current, pH, salinity, dissolved oxygen (DO), BOD, ammonia, nitrate, phosphate, and plankton. Phytoplankton samples were collected at five sampling stations by applying purposive sampling method. Then, samples were identified in the Water Environment and Biotechnology Laboratory, at the Faculty of Fishery and Marine Science, Barawijaya University, Malang. Research location and sampling stations are shown in Picture 1.



Picture 1. Map of Sampling Location

Instruments used in the research were 100 ml sample bottles, Winkler bottles, DO Meter, salinometer Atago s/mill-e, GPS Map 76 CSX Garmin, pH Meter, Secchi disk, washing bottles, digital cameras, cool boxes, spectroquant NOVA 60, rectangular cells, funnels, burette and stative, droppers/ pipettes, measuring cylinders, cuvette, stationery, current balls, water quality checker, scale bar, plankton net no. 25, plankton identification book, sedgewick rafter, microscope and 10 L plastic bucket. Materials used were sea water samples, phytoplankton samples, Lugol iodine, label paper, aquadest, tissue paper,  $MnSO_4$  solution,  $NaOH+KI$ ,  $H_2SO_4$ , Amylum, and  $Na_2S_2O_3$ .

Samples of phytoplankton were taken using plankton net vertically at 9-10 o'clock in the morning because it was the best time for phytoplankton to metabolize and do the photosynthesis in the water. Phytoplankton samples were taken by dropping plankton net with some weight until  $\pm 10$  meters deep to the sampling spot determined by a metalimnion layer measurement that was done in advance. Then, the plankton net was pulled vertically to get phytoplankton from every column of water to the surface. The sifted phytoplankton from the water was then put in the 30 ml plastic sampling bottles and a label was given to every bottle according to the sampling station. After that, 2-3 drops of 4% potassium iodide was dropped to preserve phytoplankton samples. Phytoplankton samples were then kept in the container in low temperature before they were observed in the laboratory. Phytoplankton species observations were performed off-site (*ex situ*) in the laboratory using a microscope and guided by identification book (Yamaji, 1966), to analyze toxic species that potentially cause HAB.

Water quality parameters measured in this research were temperature, brightness, and current, while the chemical parameters were salinity, pH, DO, BOD, ammonia ( $NH_3$ ), nitrate ( $NO_3$ ) and phosphate ( $PO_4$ ). The number of phytoplankton was counted to know the abundance of individuals in the cell per volume unit (litter), and further, the phytoplankton density level was known to determine the water ecosystem balance index. The number of plankton cells in one liter of water was calculated using repetition method twice which shown in the following formula:



$$N = n \times \frac{V_t}{V_{cg}} \times \frac{1}{V_d} \quad (1)$$

Where:

- N = Total number of phytoplankton (cells/liter)  
 ni = Numbers of phytoplankton species observed  
 Vd = Volume of sifted water =  $(\pi \times r^2) \times$  length of rope or depth (liter)  
 Vt = Volume of sample (30 ml)  
 Vs = Volume of sample under the covering glass (1 ml)

Diversity index was a mathematic description which depicted community structure of phytoplankton to analyze any information about the species and numbers of the plankton. Phytoplankton diversity index was calculated using Shannon-Wiener Index, that is:

$$H' = \sum_{i=1}^s p_i \ln p_i \quad (2)$$

Where:

- H' = diversity index  
 pi = ni/N  
 ni = numbers of the i<sup>th</sup> individuals  
 N = Total numbers of individuals.

Grouping was done based on the condition of diversity/biota community, and classified as follow:

- H' < 2,30 = low diversity and low community stability  
 2,30 < H' < 6,91 = average diversity and average community stability  
 H' > 6,91 = high diversity and high community stability

Uniformity index was used to show the distribution of phytoplankton in a community. Uniformity index was calculated using the following formula:

$$E = \frac{H'}{H_{max}} = \frac{H'}{\ln s} \quad (3)$$

Where:

- E = Uniformity Index  
 H' = *Shannon-Wiener* Diversity Index  
 Hmaks = ln s (maximum diversity index)  
 s = numbers of genus found

Index value ranges between 0-1, where diversity index value between 0 - 0.5 indicating that the distribution between genera is low, meaning that individual wellness of every genera is much different. If diversity index is 0.6 - 1, it shows that the distribution of genera is relatively uniform or a number of every individual is relatively same.

Domination index is used to know if there is a certain species dominates in a population. The index was calculated using Simpson's domination index formula:

$$D = \sum \left[ \frac{n_i}{N} \right]^2 \quad (4)$$

Where:

D = domination index

$n_i$  = number of the  $i^{\text{th}}$  individual

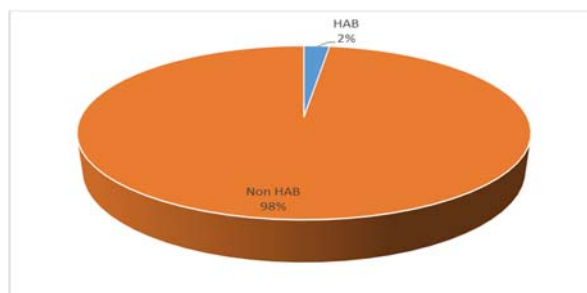
N = Total number of individual

Domination index ranges between 0-1, where the domination index value which  $<0.5$  indicating that there is not any kind dominates, while the domination index values which  $>0.5$  meaning that there is a certain kind dominates. A correlation test was used to know the relationship between environment parameter with community structure of phytoplankton that causes HAB. Environment parameter that becomes variable (demand) are temperature, salinity, pH, DO, BOD, ammonia ( $\text{NH}_4$ ), nitrate ( $\text{NO}_3$ ), and phosphate ( $\text{PO}_4$ ). Correlation test used *Statistical Product and service Solutions* (SPSS) version 16.0.

## RESULT AND ANALYSIS

### HAB Phytoplankton composition di Bali Strait

Picture 2 shows the comparison between HAB phytoplankton and non-HAB phytoplankton. It is shown by the picture that the ratio of non-HAB is 98% with the total abundance is 1,637,068 cells/liter. The ratio of HAB phytoplankton during tide is 2% with the total abundance is 35,444 cells/liter. Percentage of the abundance of HAB phytoplankton from every class found during the research in Bali Strait is 97.43 % of Bacillariophyceae, 1.52 % of Cyanophyceae, and 1.05% of Dinoflagellate.



Picture 2 The ratio between HAB phytoplankton and non-HAB phytoplankton in Bali Strait during West Monsoon

Toxic phytoplanktons that cause Harmful Algal Bloom (HAB) in Bali Strait during the research were the species from the class of Dinophyceae and Bacillariophyceae. From Dinophyceae class, there were 8 species found, namely *Ceratium fusus*, *Ceratium macroceros*, *Ceratium pulchellum*, *Dinophysis acuminata*, *Gonyaulax polygramma*, *Gonyaulax triacantha*, *Noctiluca scintillans* and *Protocentrum sp.* From Bacillariophyceae class there were 3 species found, namely *Chaetoceros compressus*, *Chaetoceros lacinosus* and *Nitzschia closterium*. Those species also found in other Indonesian waters and were categorized into phytoplankton that causes HAB, and have a negative effect on the people's health and water ecosystem (GEOHAB, 2001). The potential effect that caused by HAB species found in the research location according to GEOHAB (2001) is shown in Table 1.

Table 1. Potential effect caused by HAB species

Species	Potential impact of HAB
<i>Ceratium spp.</i>	<i>Hypoxia, anoxia</i>
<i>Chaetoceros spp.</i>	Mechanical effect on the fish gill (respiration)
<i>Dinophysis spp.</i>	<i>Diarrhetic Shellfish Poisoning (DSP)</i>
<i>Gonyaulax polygramma</i>	<i>Red tide</i> , cause biota osmoregulatoric effect
<i>Gonyaulax triacantha</i>	Hemolytic, hepatotoxic, osmoregulatoric effect.
<i>Nitzschia sp.</i>	<i>Amnesic Shellfish Poisoning (ASP)</i>
<i>Noctiluca scintillans</i>	<i>Red tide</i> , produce foam, mucous, and allelopathic substance, <i>hypoxia</i> and <i>anoxia</i>
<i>Protocentrum sp.</i>	<i>Red tide</i> , toxic on biota, reduce water quality

The number of species of Dinophyceae class was found more than Bacillariophyceae class. The possible reason is that Dinophyceae can form *cysta* as a rest phase. This *cysta* was then settled on the seabed and rested until the environment condition was good enough to grow. Commonly, species from Dinophyceae group were known as the group that has the biggest in numbers of toxic species. One of disadvantageous HAB phenomena in Indonesia happened in June 2005 at Ancol Beach, Marina. The blooming of *Noctiluca scintillans* caused a massive death of fish and other biotas. Great blooming phenomena of species *Pyrodinium bahamense* from Dinophyceae caused 240 people got poisoned and 4 people died after consuming fish and sea shells in Lewtobi Strait, East Flores (Praseno, 2000).

The Blooming of phytoplankton species is indicated by a rapid growth and happens in 1-2 weeks of time. There is no standard for the limit of phytoplankton cell density that can be considered as blooming and harmful or toxic. Some kinds of phytoplankton in low-density level are harmful without making any change in water color. The abundance of some toxic and harmful species of *Alexandrium sp.*, which has PSP toxin, can be detected as dangerous in  $10^3$  cells/liter. *Gymnodinium sp* of mollusk can kill fish and other water organisms on abundance concentration of more than  $10^7$  cells/liter. The abundance of phytoplankton reaches  $10^9$  cells/liter can be considered as red tide phenomena. If the abundance more than  $10^9$  cells/liter, we can consider the condition as the extreme red tide (Asriyana and Yuiana, 2012). Blooming phenomena of toxic phytoplankton are very dangerous. There are about 4000 species of toxic phytoplankton and there are only 200 species that have been identified or about 6% of the total number of species. In Indonesia, there are at least 30 species of phytoplankton that potentially cause HAB (GEOHAB, 2011). Composition and abundance of HAB phytoplankton in Bali Strait are shown in Table 2.

Table 2. Abundance (cells/liter) of HAB phytoplankton in Bali Strait

Phytoplankton species	St 1	St 2	St 3	St 4	St 5	Percentage
<i>Ceratium fusus</i>	278	0	0	0	152	1.11
<i>Ceratium macroceros</i>	0	0	308	0	152	1.19
<i>Ceratium pulchellum</i>	502	0	0	96	0	1.54
<i>Chaetoceros compressus</i>	2,155	0	1,967	0	0	10.64
<i>Chaetoceros lacinosus</i>	1,133	0	0	867	2114	10.62
<i>Dinophysis acuminata</i>	0	0	502	0	0	1.30
<i>Gonyaulax polygramma</i>	352	0	0	0	0	0.91

<i>Gonyaulax triacantha</i>	0	0	0	454	225	1.75
<i>Nitzschia closterium</i>	5,673	3,222	3,602	2,701	2,694	46.20
<i>Noctiluca scintillans</i>	578	0	1,401	502	258	7.07
<i>Protocentrum sp</i>	578	844	502	1,331	3,587	17.67

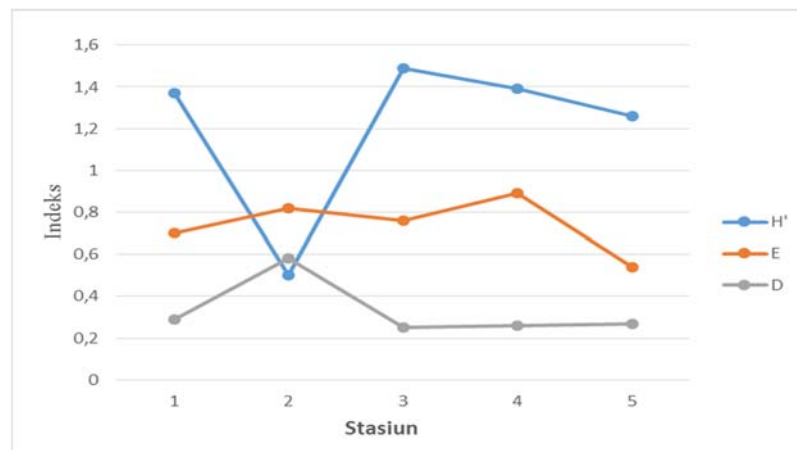
Based on data in the table above, the abundance of HAB phytoplankton is between 326 – 5625 cells/liter. Species *Nitzschia closterium* was found in all stations and had the highest total of abundance, that reaches 16,550 cells/liter. On the other hand, *Gonyaulax polygramma* has the lowest abundance level in all observed stations, which was 326 cells/liter. The blooming of *Nitzschia closterium* in Bali Strait is ecologically disadvantageous because this species cause *Amnesic Shellfish Poisoning* (ASP) illness that releases domoic acid toxin. The produced toxin enters food chain to the human bodies through seashells. Seashell is a suspended feeder that sifts the abundant plankton in the water column (Aunurohim *et al.*, 2008). Domination of *Nitzschia closterium* can increase ammonia concentration in the water so that it is accumulated in the fish cells. *Nitzschia closterium* is a species from Bacillariophyceae class that has a high tolerance to the change of environmental parameters so that this species is abundant in every station.

#### Community Structure of HAB Phytoplankton

Diversity, uniformity and domination index of HAB phytoplankton in Bali Strait is shown in Picture 3. Diversity index value ( $H'$ ) from five research station was between 0.52 – 1.49. The highest value was in station 3, which was 1.49. And the lowest value was in station 2, which was 0.52. The diversity index obtained in the research indicated that Bali Strait has a relatively low diversity and unstable community (Basmi, 2000).

Uniformity index value ( $E$ ) that was obtained during the research showed the similar uniformity between species. The value was between 0.69-0.84, meaning that the distribution between genera was relatively uniform or the numbers of each genera was relatively the same (Fachrul, 2007). The highest value of uniformity index was in station 4, which was 0.84 and the lowest was in station 5, which was 0.69.

The result of domination index value ( $D$ ) calculation from 5 observation station was between 0.23 – 0.59. The obtained domination index value showed that there was no species dominating in average at every station. Only in station 2, domination index value showed that there was a species dominating, which was *Nitzschia closterium*, one of the species from Bacillariophyceae class. Station 2 was in an estuary so that it might get nutrients from land which was brought by the river current and affected domination of species from Bacillariophyceae class. This is in accordance with Wulandari's (2009) statement that the class dominates an estuary is generally Bacillariophyceae class. The highest domination in this research was 0.59 in station 2, and the lowest was 0.23 in station 3. The domination index is  $<0.5$ , meaning that there are no dominating species. Diversity, uniformity, and domination index of HAB Phytoplankton in Bali Strait is shown in Picture 3.



Picture 3. Diversity, Uniformity, and Domination Index of HAB Phytoplankton in Bali Strait.

### Hydro Oceanography of Bali Strait

The result of environmental factors measurement or hydro oceanographic parameters is shown in Table 3. The temperature ranges from 29.7 – 31.1 °C, the brightness ranges from 0.28 – 0.68 m, and the current velocity is from 0.74 – 0.91 m/s. pH level ranges from 8.57 – 8.83 with average level at 8.70. Salinity ranges from 21.7 – 31.1 ‰, the DO ranges from 8.18 – 9.16 mg/L, while the BOD was from 3.08-4.42 mg/L. The average ammonia level in the strait is 0.198 mg/L, while the average of nitrate and phosphate concentration is 3.16 and 0.088 mg/L. Overall, the parameters which are over the quality requirement standards are the ammonia and nitrate. The hydro oceanography parameters measured in Bali Strait is shown in Table 3.

Table 3. Hydro Oceanography of Bali Strait

Station	Tempa rature (°C)	Brightness (m)	Tides (m/s)	pH	Salinity (‰)	DO (mg/L)	BOD (mg/L)	NH3 (mg/L)	NO3 (mg/L)	PO4 (mg/L)
1	30,4	0,67	0,84	8.83	29.6	8.36	4.09	0.18	2.61	0.05
2	29.7	0.28	0.91	8.65	21.7	9.17	3.08	0.22	3.32	0.13
3	31.1	0.57	0.81	8.57	30.2	9.01	4.42	0.16	2.83	0.08
4	30.2	0.58	0.74	8.65	30.8	8.18	3.37	0.19	3.31	0.06
5	29.8	0.68	0.82	8.82	31.1	9.16	4.36	0.24	3.73	0.12
Average	30.24	0.556	0.824	8.70 4	28.68	8.776	3.864	0.198	3.16	0.088

### Correlation between HAB Phytoplankton and Hydro Oceanographic Parameter

The correlation analysis result of hydro oceanographic parameters with the structure of HAB phytoplankton community in Bali Strait is shown in Table 4. Based on the correlation analysis, temperature and abundance of HAB phytoplankton are positively correlated (0.61\*) with 0.02 significance score, while temperature and the diversity of HAB phytoplankton are also positively correlated (0.58\*) with significance score 0.02. It means that the temperature is closely related and has significant effect to the abundance and diversity of HAB phytoplankton during the high tide. The rising of temperature can affect phytoplankton directly by improving the chemical reaction. Therefore the photosynthetic rate is improved by the rising of temperature in the range between 10° C – 20° C (Mulyanto, 2006). The rising of temperature accelerates the

phytoplankton photosynthesis which later affects the abundance of the phytoplankton, but the rising temperature should not over the normal water temperature. In the high abundance of HAB phytoplankton, there is a high average level of diversity, so there is a real correlation between temperature and the diversity of HAB phytoplankton. The correlation analysis result between hydro oceanography parameters and HAB phytoplankton community structure is shown in Table 4.

Table 4. Correlation Analysis between Hydro Oceanographic Parameter and HAB Phytoplankton Community Structure

Variable		N (Abundance)	H' (Diversity)	E (Uniformity)	D (Dominance)
temperature	Correlation	0.61*	0.58*	0.27	-0.28
	sig. (2-tailed)	0.02	0.02	0.33	0.31
Brightness	Correlation	0.07	-0.03	-0.03	-0.13
	sig. (2-tailed)	0.81	0.93	0.93	0.65
Current	Correlation	-0.39	-0.27	0.06	0.26
	sig. (2-tailed)	0.16	0.33	0.83	0.34
pH	Correlation	-0.03	-0.21	0.15	0.43
	sig. (2-tailed)	0.92	0.45	0.59	0.11
Salinity	Correlation	0.46	0.38	0.22	0.05
	sig. (2-tailed)	0.08	0.16	0.42	0.86
DO	Correlation	0.64*	0.72*	0.54*	0.04
	sig. (2-tailed)	0.01	0.00	0.04	0.89
BOD	Correlation	0.35	0.38	0.19	-0.41
	sig. (2-tailed)	0.20	0.16	0.51	0.13
Ammonia	Correlation	-0.25	-0.28	-0.21	-0.25
	sig. (2-tailed)	0.36	0.30	0.45	0.36
Nitrate	Correlation	-0.36	-0.23	0.04	0.41
	sig. (2-tailed)	0.19	0.40	0.89	0.13
Phosphate	Correlation	-0.44	-0.36	-0.29	-0.30
	sig. (2-tailed)	0.10	0.19	0.30	0.28

\*Significance ( $p < 0.05$ )

The correlation analysis result of DO with the abundance of HAB phytoplankton showing a positive correlation (0.64\*) with significance score 0.01, while DO correlation with the diversity of HAB phytoplankton is positive (0.72\*) with significance score 0.00, and DO correlation with the uniformity of HAB phytoplankton is positive (0.54\*) with significance score 0.04. The positive correlation shows that DO parameter is closely related to the abundance, diversity, and uniformity of HAB phytoplankton. During the day when the sun shines, the dissolved oxygen in the intensive process of photosynthesis on the euphotic surface layer was greater than the oxygen needed for the respiration process (Effendi, 2003). It means that the increase of oxygen level in the water during the day is an indicator of phytoplankton abundance which happens during the tide. Therefore this research shows the significant correlation between DO and the abundance of HAB phytoplankton during the high tide. In the abundance of HAB phytoplankton during the high tide, there is high average diversity and uniformity level from HAB



phytoplankton, so there is a real close correlation between DO and the diversity and the uniformity of HAB phytoplankton. There is no significant correlation found between the nutrients (nitrate dan phosphate) and the abundance of HAB phytoplankton, but it does not mean that those nutrients do not play their roles as the food for phytoplankton. The nutrients variability and a number of samples are not believed enough to show the correlation clearly (Soedibjo 2007).

## CONCLUSION

The comparison between HAB phytoplankton and non-HAB phytoplankton composition is 2% and 98%. Species of phytoplankton which potentially causes HAB in Bali Strait are *Ceratium fusus*, *Ceratium macroceros*, *Ceratium pulchellum*, *Dinophysis acuminata*, *Gonyaulax polygramma*, *Gonyaulax triacantha*, *Noctiluca scintillans*, *Peridinium claudicans*, *Chaetoceros compressus*, *Chaetoceros lacinosus* and *Nitzschia closterium*. *Nitzschia closterium* is the species with the highest abundance level at 17,892 cells/liter (46.20 %). The temperature and DO of the water area also have positive correlation which is significant to the abundance, diversity and uniformity index of HAB phytoplankton in Bali Strait.

## REFERENCES

- Effendi, H. 2003. **Telaah uji kualitas air bagi pengelolaan sumberdaya dan lingkungan perairan**. Penerbit Kanisius, Yogyakarta: 258 hlm. Risamasu, Fonny J.L, dan H. B. Prayitno. 2011. **Kajian Zat Hara Fosfat, Nitrit, Nitrat dan Silikat di Perairan Kepulauan Matasiri, Kalimantan Selatan**. Pusat Penelitian Oseanografi-LIPI. 16 (3): 135- 142.
- Anderson, D.M., J.M, Burkholder., W,P, Cochlan., P,M, Gilbert., C,J, Gobler., C,A, Heil., R,M, Kudela., M,L, Parsons., J,E, Jack Rensel., D,W, Townsend., V,L, Trainer., G,A, Vargo.,. 2008. **Harmful algal blooms and eutrophication: Examining linkages from selected coastal region of the United Stated, Harmful Algae**
- Aunurohim. Saptarini, Dian. Yanthi, Devie. 2008. **Fitoplankton Penyebab Harmful Algal Bloom (HAB) di Perairan Sidoarjo**. Institut Teknologi Sepuluh Nopember-Surabaya.
- GEOHAB. 2011. **Global ecology and oceanography of harmful Algal blooms science plan**. SCOR and IOC, Paris: Vol 84.
- Praseno. D.P. 2000. **Red tide di perairan Indonesia**. LIPI, Jakarta: hal. 82
- Basmi , J. 2000. **Planktonologi: Bioekologi Plankton Alga**. Fakultas Perikanan dan Ilmu Kelautan. IPB. Bogor: 44 hal
- Fachrul, M.F, H. Haeruman & A. Anggraeni, 2006. **Distribusi Spatial Nitrat, Fosfat, dan Ratio N/P di Perairan Teluk Jakarta**. Makalah Seminar disampaikan pada Seminar Nasional Penelitian Lingkungan di Perguruan Tinggi, IATPI - Teknik Lingkungan ITB, Bandung, 17-18 Juli 2006.
- Wulandari, D. 2009. **Keterikatan Antara Kelimpahan Fitoplankton dengan Parameter Fisika dan Kimia di Estuari Sungai Brantas (Porong), Jawa Timur**. Bogor. Institut Pertanian Bogor. Soedibjo, B.S. 2007. **Fenomena kehadiran Skeletonema Sp. di Perairan Teluk Jakarta**. Ilmu Kelautan, 12(3): 119-124.